Towards the modelling of recrystallization phenomena in multi-pass conditions: application to 304L steel

Ke Huang

▶ **To cite this version:**

Ke Huang. Towards the modelling of recrystallization phenomena in multi-pass conditions: application to 304L steel. Materials. École Nationale Supérieure des Mines de Paris, 2011. English. NNT : 2011ENMP0079 . pastel-00682138

HAL Id: pastel-00682138
https://pastel.hal.science/pastel-00682138

Submitted on 23 Mar 2012

HAL is a multi-disciplinary open access archive for the deposit and dissemination of scientific research documents, whether they are published or not. The documents may come from teaching and research institutions in France or abroad, or from public or private research centers.

L'archive ouverte pluridisciplinaire **HAL**, est destinée au dépôt et à la diffusion de documents scientifiques de niveau recherche, publiés ou non, émanant des établissements d'enseignement et de recherche français ou étrangers, des laboratoires publics ou privés.

ParisTech
INSTITUT DES SCIENCES ET TECHNOLOGIES
PARIS INSTITUTE OF TECHNOLOGY

MINES ParisTech

École doctorale n° 364 : Sciences Fondamentales et Appliquées

Doctorat ParisTech

T H È S E

pour obtenir le grade de docteur délivré par

l'École nationale supérieure des mines de Paris

Spécialité " Sciences et Génie des Matériaux "

présentée et soutenue publiquement par

Ke HUANG

15/12/2011

Towards the modeling of recrystallization phenomena in multi-pass conditions - Application to 304L steel

~ ~ ~

Vers la modélisation des phénomènes de recristallisation en conditions multi-passes - Application à l'acier 304L

Directeur de thèse : **Roland LOGÉ**

Jury

M. Frank MONTHEILLET,	Directeur de recherche CNRS, SMS Center, ENSM-SE	**Rapporteur**
M. Knut MARTHINSEN,	Professor, Department of MSE, NTNU	**Rapporteur**
M. Paul DUVAL,	Directeur de recherche CNRS émérite, LGGE	**Examinateur**
Mme. Astrid PERLADE,	Docteur, Arcelor Mittal	**Examinateur**
Mme. Nathalie BOZZOLO,	Chargée de Recherches, CEMEF, Mines ParisTech	**Examinateur**
M. Roland LOGÉ,	Chargé de Recherches, CEMEF, Mines ParisTech	**Examinateur**
M. Rémy BESNARD,	DAM, CEA / Valduc	**Invité**

T H È S E

MINES ParisTech
CEMEF UMR CNRS 7635
1,rue Claude Daunesse – BP 207
06904 Sophia Antipolis Cedex - France

Acknowledgments

This work is supported by the French National Research Agency (ANR) as part of "Thermide" project, I want to thank all the academic and industrial partners of this project, it has been a great honor for me to work with them. I am very grateful to the Centre for Material Forming (CEMEF), Mines ParisTech, for providing me world-class facility to complete this thesis work. This work would not have been possible though, without the different kinds of contributions of a lot of people.

First of all, I would like to express my deepest sense of gratitude to my Ph.D thesis supervisor, Roland Logé, for recruiting me and giving me the opportunity to achieve this work. The many invaluable discussions, his patient gudidance and the nice way he supervisored me are greatly appreciated, without which I would not have been able to overcome all the hurdles on the road of my study at CEMEF.

I would like to thank the members of the jury of this thesis. In particular, thanks for Dr. Frank Montheillet and Prof. Knut Marthinsen for taking time to read carefully my manuscript and giving back their constructive advice. Dr.Paul Duval, Dr. Astrid Perlade, Dr. Nathalie Bozzolo, Dr. Rémy Besnard are greatfully thanked, who also served on my thesis committee and provided many valuable suggestions on both the manuscript and the future work of this project.

I am very greatful to all the members of the MSR group, who nourished my work. I would like to thank Pierre Bernard and Swarup Bag for their help as a post doctoral researcher at CEMEF. My appreciation also goes to the mean field model users, Christophe, Sébastien, Oscar who also contributed a lot to the Thermide project. My sincere thanks go to Nathalie and Marc, who answered my numerous questions on microstructure and numerical simulation. Thanks also go to Suzanne, Gilbert and Bernard who helped me enormously on torsion tests and microstructure characterization.

I would also like to express my gratitude to all the CEMEF staff. Special mention to CEMEF's administrative director Patrick Coels, who provided valuable help when I first arrived in France from China. I would also like to thank my fellow graduate students and friends at CEMEF. In particular, I want to thank my officemates Anne and Tommy for their patient help. Special mention is made here to the Chinese team in CEMEF, with whom I had the pleasure to work and share some outdoor activities.

Last but not least, I would like to take this opportunity to thank the dearest people to my heart, my wife, my parents and the rest of the family, who provided love and support during my study in France, I wouldn't have made it without them.

List of symbols used

The following notation is generally used in the text. On rare occasions, especially in the graphs from literature, where different symbols are used for the same meaning, it is specifically stated.

b	Burger's vector (m)
b_g	Constant related to nucleation
τ	Energy per unit dislocation length (N)
m	Grain boundary mobility ($m^3\ s^{-1}\ N^{-1}$)
d_0, D_0	Initial average grain diameter (m)
d_{ss}	Steady state grain size
d_{drx}	Dynamically recrystallized grain size
d_{pdrx}	Post-dynamically recrystallized grain size
$D_{\max}$	Initial maximum grain diameter (m)
$\overline{D}_{RX}$	Average grain diameter of recrystallized grains (m)
K_1	Parameter related to strain hardening (m^{-2})
K_2	Parameter related to dynamic recovery
K_s	Parameter related to static recovery
K_3	Parameter related to grain boundary mobility (m^3s^{-1}), $K_3 = m\ \tau$
K_g	Probability parameter related to nucleation ($m^{-2}s^{-1}$)
K_p	Pinning effect constant
K_j	Relative value of K parameters
t_{50}	Time for 50% of recrystallization/softening
t_0	Incubation time
M	Taylor factor
N_p	Number of potential nucleation sites
$\dot{N}_{nucl}$	Total number of activated nuclei per unit time (s^{-1})
M_i	Number of data points for i^{th} objective function
O_i	i^{th} objective function
q	Parameter related the type of nucleation (surface or volume)
r	Grain radius (m)
c_1, c_2	Principal radii of curvature

η	Constant for grain growth
n	Grain growth exponent
r_{RX}	Recrystallized grain radius (m)
r_u^{DRX}	Radius of a DRX nucleus (m)
r_u^{SRX}	Radius of a SRX nucleus (m)
r_{HEM}	Radius of homogeneous equivalent media (m)
ω	Scaling constant for SRX/DRX nucleus
ΔE	Driving force for grain boundary migration
E_z	Grain boundary migration pinning
S_{cr}	Surface area of all grain boundaries satisfying $\rho > \rho_{cr}$ (m^2)
Δt	Time step (s)
t^{tot}	Total time of thermomechanical processes
V_{nucl}	Total nucleated volume (m^3) in a time step
V_{ext}	Extended nucleated volume (m^3)
$V_{RX/NR}$	Recrystallized volume (m^3)
$V_{NR/RX}$	Non recrystallized volume (m^3)
X , X_V	Recrystallized volume fraction
ρ_i	Dislocation density of representative grain i (m^{-2})
ρ_0	Initial average dislocation density (m^{-2})
$\rho_{\max}$	Initial maximum dislocation density (m^{-2})
ρ_{cr}^{DRX} , ρ_{cr}	Critical dislocation density for DRX (m^{-2})
ρ_{HEM}	Dislocation density for the homogenous equivalent media
ξ	Constant to relate ρ_{cr}^{DRX} and ρ_{cr}^{SRX}
ρ_{cr}^{SRX}	Critical dislocation density for SRX (m^{-2})
ρ_{ss}^{SRV}	Minimal dislocation density for static recovery (m^{-2})
ρ_{cr}^{Dis}	Critical dislocation density for re-defining RX and NR grains (m^{-2})
β	Constant to relate ρ_{cr}^{Dis} and ρ_{cr}^{SRX}
ε	Strain or deformation
ε_p	Peak strain
ε_{cr}^{DRX} , ε_{cr}	Critical strain for DRX
ε_{cr}^{SRX}	Critical strain for SRX
ε_T	Transition strain

σ_i	Flow stress of representative grain i (MPa)
σ^0	Dislocation free yield stress (MPa)
$\bar{\sigma}$	Macroscopic flow stress (MPa)
μ	Shear modulus (MPa)
E	Elastic modulus (MPa)
ν	Poisson's ratio
α	Constant related to flow stress
γ_b	Grain boundary energy per unit area (J m^{-2})
v	Grain boundary velocity (m s^{-1})
$\dot{\varepsilon}$	Strain rate (s^{-1})
γ^{RX}	Mobile surface fraction of a recrystallized representative grain
γ^{NR}	Mobile surface fraction of non-recrystallized representative grain
δ	Constant limiting the dislocation density change within a time step
θ	Work-hardening rate
Z	Zener-Hollomon parameter $\mathrm{Z} = \dot{\bar{\varepsilon}} \exp(\mathrm{Q}/\mathrm{RT})$
γ_{SFE}	Stacking fault energy

Abbreviations

DRX	Dynamic recrystallization
SRX	Static recrystallization
PDRX	Post-dynamic recrystallization
RX	Recrystallized grains
NR	Non-recrystallized grains
CDRX	Continuous dynamic recrystallization
DDRX	Discontinuous dynamic recrystallization
GG	Grain growth
F.C.C	Face Centered Cubic
SIBM	Strain induced boundary migration
GB	Grain boundary
EBSD	Electron backscatter diffraction
SEM	Scanning electron microscope
OM	Optical microscope
ECD	Equivalent circle diameter
SFE	Stacking fault energy
CA	Cellular automata
CSL	Coincidence site lattice
GOS	Grain Orientation Spread
IPF	Inverse Pole Figure
FEM	Finite element method
JMAK	Johnson–Mehl–Avrami–Kolmogorov kinetic model
KM	Kocks-Mecking model

Table of contents

1. Introduction 13

1.1. Background of this project 13
1.2. Objective of the thesis 13
1.3. Thesis outline 14
1.4. French summary 14

2. Literature review 17

2.1. Scope of the literature review 17
2.2. Work hardening and recovery 17
2.2.1. Work-hardening 17
2.2.2. Recovery 18
2.2.3. Modelling of Work-hardening and recovery 20
2.3. Nucleation mechanism 21
2.3.1. Strain induced boundary migration (SIBM) 21
2.3.2. Nucleation by low angle boundary migration 22
2.3.3. Nucleation by subgrains coalescence 23
2.3.4. Nucleation by grain boundary sliding 24
2.3.5. Nucleation mechanism during the progress of DRX 24
2.4. Discontinuous dynamic recrystallization 25
2.4.1. Investigation of DRX through flow curves 25
2.4.2. Critical condition for the onset of DRX 26
2.4.3. Influence of temperature, strain rate and initial grain size 29
2.4.4. Microstructure changes associated with DRX 32
2.4.5. Modeling of dynamic recrystallization 35
2.4.5.1. Constitutive models 35
2.4.5.2. The JMAK model 35
2.4.5.3. The “old” theoretical models 36
2.4.5.4. The DRX model of Montheillet *et al*. 37
2.4.5.5. The model of Cram *et al.* 38
2.4.5.6. The model of Fan *et al.* 40
2.4.5.7. The models of DRX using other simulation methods 41
2.5. Recrystallization after deformation 42
2.5.1. Softening fraction 43
2.5.2. Four mechanisms during recrystallization after deformation 43
2.5.2.1. Introduction 43
2.5.2.2. Static recovery 44
2.5.2.3. Static recrystallization 44
2.5.2.4. Post dynamic recrystallization 45
2.5.2.5. Grain growth and twin formation 47
2.5.3. Factors affecting the recrystallization behavior after hot deformation 51
2.5.3.1. Effect of stop strain 51
2.5.3.2. Effect of temperature and strain rate 53
2.5.3.3. Effect of initial grain size 54
2.5.4. Modelling of recrystallization after deformation 55
2.5.4.1. JMAK modeling 55
2.5.4.2. Physically based models 57
2.6. Summary of existing investigation on recrystallization 60
2.6.1. Experimental investigation on recrystallization of austenitic stainless steel .. 60

2.6.2. Existing models for recrystallization 61
2.6.3. Focus of the thesis 62
2.7. French summary 62
3. Experimental methods 63
3.1. Introduction 63
3.2. 304L austenitic stainless steel 63
3.2.1. Chemical composition 63
3.2.2. Physical and mechanical properties 64
3.3. Hot torsion test 65
3.3.1. Introduction 65
3.3.2. Torsion test sample 65
3.3.3. Conversion of torsion test data to stress-strain curves 66
3.3.4. Hot torsion test 67
3.4. Microstructure characterization 68
3.4.1. Sample preparation 68
3.4.2. Characterization by SEM+EBSD and Optical microscope 69
3.4.3. The qualification of recrystallization 70
3.4.3.1. Grain size 70
3.4.3.2. Recrystallized fraction 72
3.5. Quasi in situ heating experiments 73
3.5.1. Introduction on quasi in situ heating experiments 73
3.5.2. Experimental set up 74
3.5.3. In situ heating experiments 74
3.6. French summary 75
4. Description of numerical model 77
4.1. Introduction 77
4.2. Material representation 78
4.3. Discontinuous dynamic recrystallization model 79
4.3.1. Strain hardening, recovery and flow stress 79
4.3.2. Grain boundary migration 79
4.3.3. Nucleation 80
4.3.4. Interaction with the surrounding HEMs 81
4.3.4.1. Migration of RX-NR interfaces 82
4.3.4.2. Migration of RX-RX and NR-NR interfaces 84
4.3.4.3. Overall volume change 84
4.3.5. Computational aspects of mathematical modeling 85
4.3.5.1. Time step management 85
4.3.5.2. Numerical implementation of the model 85
4.4. Static/Post dynamic recrystallization model 86
4.4.1. Introduction 86
4.4.2. Static recovery 86
4.4.3. Nucleation 87
4.4.4. Definition of RX and NR grain 88
4.4.5. Grain growth and Zenner pinning effect 90
4.4.6. Computational aspects of mathematical modeling 90
4.4.6.1. Continuity from dynamic to static conditions 90
4.4.6.2. Time step management 91
4.4.6.3. Numerical implementation of the SRX/PDRX/GG model 91

4.5. Conclusions 92
4.6. French summary 92

5. Discontinuous dynamic recrystallization 95

5.1. Introduction 95
5.2. Experiment 95
5.3. Influence of deformation temperature 96
5.4. Influence of strain rate 103
5.5. Influence of initial grain size 107
5.6. Application of the DDRX model to 304L steel 112
5.6.1. Identification of fitting parameters 112
5.6.1.1. From experimental results and literature data 112
5.6.1.2. Inverse analysis 114
5.6.2. Calibration of the DRX model 114
5.6.3. Qualitative grain size effect 115
5.6.4. Quantitative temperature effect 117
5.6.5. Quantitative strain rate effects 119
5.6.6. Quantitative initial grain size effect 121
5.7. Conclusions 126
5.8. French summary 126

6. Recrystallization after deformation 129

6.1. Introduction 129
6.2. Post dynamic recrystallization 129
6.2.1. Experiment 129
6.2.2. Influence of temperature 132
6.2.3. Influence of strain rate 137
6.2.4. Influence of applied strain 142
6.3. Static recrystallization 148
6.3.1. Experiment 148
6.3.2. Effect of temperature and strain rate 149
6.3.3. Effect of applied strain 154
6.4. Investigation of SRX/PDRX mechanisms by quasi in situ heating experiments .. 155
6.4.1. Experiment 155
6.4.2. Static recrystallization 156
6.4.3. Post dynamic recrystallization 158
6.4.4. Grain growth 160
6.5. Application of the post deformation model to 304L steel 161
6.5.1. Annealing twins during DRX and SRX/PDRX 161
6.5.2. Identification of fitting parameters for SRX/PDRX/GG model 163
6.5.2.1. From experimental results and literature data 163
6.5.2.2. Inverse analysis 164
6.5.3. Post dynamic recrystallization 164
6.5.3.1. Calibration of the PDRX/GG model 164
6.5.3.2. Effect of temperature 168
6.5.3.3. Effect of strain rate 170
6.5.3.4. Effect of applied strain 171
6.5.4. Static recrystallization 172
6.5.4.1. Calibration of the SRX model 172
6.5.4.2. Effect of temperature 177

6.5.4.3. Effect of strain rate 178
6.5.4.4. Effect of applied strain 179
6.6. Conclusions 181
6.7. French summary 181
7. Conclusions and future work 183
7.1. Conclusions 183
7.2. Suggestions for the future work 185
7.2.1. Experimental aspects 185
7.2.2. Numerical modeling aspects 185
7.3. French summary 186
8. References 187
Appendix A

1. Introduction

1.1. Background of this project

Many metallic parts are produced initially from large castings which are then further deformed by forging, extrusion, rolling, etc., to an intermediate or final product. These procedures, which may be carried out cold or hot, and which may involve annealing between intervals of deformation processes, are collectively termed thermomechanical processing. Most of the time, two or more thermomechanical processing steps are needed to obtain the final product. Recrystallization, which can occur dynamically or statically during these processing steps, is an important phenomenon causing microstructure changes on deformed metals and therefore affecting the properties of the material. It is possible for the deformed product to have partial recrystallisation after one pass, introducing a heterogeneous microstructure prior to the next pass. When multi-pass processes are envisaged, the history of the microstructure evolution has to be taken into account. It is hence difficult to control the microstructure evolution under multi-pass condition.

In response to this problem, researchers from both industry and academic institutions including Industeel, Institute Carnot de Bourgogne, Creusot Forge, CEA, Arts & Metiers ParisTech, together with materials processing centre (CEMEF) from Mines ParisTech, started the "Thermide" project launched by French National Research Agency (ANR) in 2007.

The objective is to understand the constitutive law of the material during deformation by following the geometry of the product, the grain size and its microstructure experimentally and predict these numerically. In order to achieve these objectives, this project needs to develop physically-based models to follow deformation and microstructure evolutions during the forming process as well as during heat treatment process, which are actually used by industrial practice. In the end, the numerical codes developed in this project will be implemented into a finite element code modeling the forming operations.

To a large extent the mechanical properties and behavior of a metal depend on the dislocation content and structure, the size of the grains. Of these, the dislocation content and structure are the most important: the mechanical properties depend primarily on the number of dislocations and their spatial distribution. The grain size is determined mainly by the recrystallization process, and there are numerous examples of the need to control grain size. So, the distribution of dislocation density and grain size were chosen to represent the microstructure in this work.

Before the start of this thesis, a post-doctorate (Pierre Benard) initiated the modeling of discontinuous dynamic recrystallization (DDRX). Another post-doctorate (Swarup Bag) mainly focused on the identification of model parameters by inverse analysis.

1.2. Objective of the thesis

My PhD work focuses on developing numerical models to predict microstructure evolution in 304L stainless steel, including phenomena like hardening, recovery and recrystallization. The approach is designed such as easy coupling is possible with finite element codes to model forming processes. These codes allow to compute the thermal/mechanical histories of a volume element, possibly in multi-pass conditions (Static recrystallization, dynamic recrystallization, post dynamic recrystallization). The proposed model follows distributions of grain sizes and dislocation densities (state variables), described by a set of differential equations which have a physical meaning. At the level of the finite element model, the equations are integrated at each time step. Experiments are conducted to validate the model and

identify the parameters: torsion tests plus heat treatment and analysis of the resulting microstructures in terms of recrystallized volume fraction and grain size.

1.3. Thesis outline

Recrystallization under multi pass condition, including work-hardening and recovery, dynamic recrystallization (DRX), static recrystallization (SRX), post-dynamic recrystallization (PDRX), grain growth (GG) are all studied in this thesis.

This thesis begins with a brief introduction (Chapter 1) on the background and objective of this project, which clarifies the importance of the current research and explains why physically-based model is chosen for the modelling of recrystallization.

In Chapter 2, a detailed literature review on recrystallization is presented. The physical phenomena occurs during recrystallization of stainless steels are carefully summarized, together with a review of available numerical models of recrystallization in the published literature with an emphasis on physically-based models.

The experimental methods and facilities for mechanical testing, preparation of metallography samples as well as microstructure characterization are described in Chapter 3. The properties of the analyzed material, 304L austenitic stainless steel, are also described in this chapter.

A two-site mean field recrystallization model is developed in Chapter 4, introducing improvements to the existing models examined in the literature review. This model is developed firstly for DDRX, but extensions to SRX/PDRX and GG are also presented in this chapter, which thus makes the modeling of multi-pass recrystallization possible. Emphasis has been made on the difference between SRX and PDRX, while GG after these two processes is treated the same way. Special attention is paid on the critical values of strain, which, together with other parameters, determines how the different types of recrystallization (DRX, SRX, PDRX) occur. All the necessary details of the model are discussed in this section.

In Chapter 5, the effects of deformation temperature, strain rate, stop strain as well as initial grain size on DRX are all studied experimentally. A full set of experimental data was collected including flow stress, recrystallized volume fraction and recrystallized grain size for each deformation condition. The tentative value of parameters of the DDRX model proposed in Chapter 4 are identified based on these experimental results, a further tuning by the inverse analysis is then performed to get the final value of the parameters. This section completes with the comparison between the experimental and numerical results.

The experimental investigation on SRX/PDRX/GG is first presented in Chapter 6, taking into account the effect of different deformation parameters and holding times, which sheds light on modeling issues and identification of fitting parameters. The role of annealing twins during nucleation and grain boundary migration after deformation is discussed. The application of the SRX/PDRX/GG model is then detailed.

Finally, major conclusions from all chapters of this thesis are presented in Chapter 7. Potential areas for further studies and future works are proposed.

1.4. French summary

Le travail développé dans ce projet de thèse a pour but le développement d'un modèle numérique capable de prédire l'évolution microstructurale de l'acier 304L, en prenant en compte les phénomènes d'écrouissage, restauration et recristallisation. Ce modèle a été conçu de façon à permettre un couplage facile avec des codes d'éléments finis afin de les utiliser pour la

modélisation de la mise en forme. Ces codes permettent de calculer l'historique thermique/mécanique d'un élément de volume en conditions multi passes (recristallisation statique, recristallisation dynamique et recristallisation post-dynamique). De plus, ce modèle permet un suivi de la distribution de taille de grain et de la densité de dislocations (variables d'état), décrites par un ensemble d'équations différentielles. Au niveau du modèle éléments finis, les équations sont intégrées à chaque pas de temps. Des expériences ont été réalisées afin de valider le modèle et d'identifier les paramètres d'entrée : tests de torsion avec traitements thermiques et analyses des microstructures en fonction de la fraction volumique recristallisée et de la taille des grains.

2. Literature review

2.1. Scope of the literature review

The research on recrystallization which occurs during thermomechanical processing of materials can date back to 150 years ago [1]. Considering that many aspects related to recrystallization are not fully understood until now, and experimental evidence is often poor and conflicting, a careful literature review is proposed here.

Among the vast body of literature, we focus on phenomena including work-hardening, recovery, grain boundary migration, nucleation and grain growth, which are related to dynamic recrystallization (DRX), static recrystallization (SRX) or post-dynamic recrystallization (PDRX) of low stacking fault energy materials.

An overview of the available numerical models of recrystallization is also presented in this chapter to the best knowledge of the author, with a favouritism to physically-based models. Emphases are also put on modeling of recrystallization in multi-pass conditions, as well as identification of model parameters.

Literature data on different kinds of recrystallization (DRX, SRX, PDRX) of austenitic stainless steel are also collected. The mechanisms of these recrystallization processes are explained, together with the analyses of the influence of deformation temperature, strain rate, strain, as well as initial grain size.

2.2. Work hardening and recovery

Microstructural control during hot working and subsequent static annealing is of great importance in the thermomechanical processing of steels in order to get the desired geometry and properties of the final product. In industrial practice, the final product is usually obtained under multi pass conditions, including sequences of the deformation passes, the intermediate heat treatments. Starting from cast products, the steels are usually deformed at high temperature, with concurrent work-hardening and dynamic recovery.

2.2.1. Work-hardening

The fact that work-hardening occurring means that it becomes difficult for dislocations to move as the strain increases. The mechanical properties and behaviour of metallic materials depend mostly on the dislocation content and structure, the grain size and the texture. Among these, the dislocation content and structure are the most important. The dislocation density of a typical annealed state is ~10^{11} m^{-2}, which increases to as much as ~10^{16} m^{-2} if the metallic material is heavily deformed, the yield strength is hence increased by up to 5-6 times and the ductility decreased [1]. These are perhaps the most outstanding changes during the deformation processes. Such changes are of great importance in industrial practice, because the rate at which the material hardens during deformation influences both the power required and the method of working in the various shaping operations. The hardness introduced by workhardening usually makes an intermediate annealing process necessary (always an expensive operation) to enable further working to be continued. Extensive investigation on work-hardening has been made since 1934 when Taylor put forward the basic idea of hardening: some dislocations become ‘stuck’ inside the crystal and act as sources of internal stress, which oppose the motion of other gliding dislocations [2]. The work-hardening behavior

in metals with a cubic structure is more complex than in most other structures because of the variety of slip systems available, and it is for this reason that much of the experimental evidence is related to these metals, particularly those with F.C.C structures. Progress on work-hardening can be found at Kocks and Mecking's excellent review on the strain hardening of F.C.C materials [3], as well as other review articles by McQueen *et al*. including [4,5].

As F.C.C crystals are capable of deforming in a complex manner on more than one slip system, these metals normally show a strong work-hardening behavior which is caused by the mutual interference of dislocations gliding on intersecting slip planes.

2.2.2. Recovery

The extensive early work on the recovery of deformed metals has been reviewed by Beck [6], Bever [7] and Titchener and Bever [8], but despite its obvious importance, recovery attracted little interest in later years. However, the current industrially driven move to produce quantitative physically-based models for annealing processes has resulted in renewed interest in recovery [9].

The deformed state of a material, which has a dislocation structure formed during deformation by the glide and interaction of dislocations, is usually not in thermodynamic equilibrium. At low deformation temperatures, however, the deformed state is conserved after deformation because the structure is mechanically stable. Once the temperature increases, however, this mechanical stability no longer exists, because thermally activated processes, i.e., climb of edge dislocations and cross slip of screw dislocations, become active. Through climb, dislocations can leave their glide planes to a lower-energy configurations, can mutually annihilate, or even leave the crystal altogether. These processes are subsumed under the term recovery, which is always associated with a decrease of the dislocation density and the formation of special dislocation patterns, i.e., networks of low-angle grain boundaries, also referred to as polygonization. It is important to notice that no migration of large angle boundaries is involved here.

During recovery the stored energy of the material is lowered by dislocation movement. There are two primary processes, these being the annihilation of dislocations and the rearrangement of dislocations into lower energy configurations. Both processes are achieved by glide, climb and cross-slip of dislocations.

Regarding the annihilation of dislocations, a schematic diagram of a crystal containing an array of edge dislocations is shown in Figure 2-1. Dislocations A and B are on the same glide plane, but with opposite sign, they may annihilate by gliding towards each other. Such processes are able to occur even at low temperatures, lowering the dislocation density during deformation and leading to dynamic recovery. When the two dislocations of opposite sign, e.g. C and D, are not on the same slip plane, a combination of climb and glide must first occur. As both climb and cross-slip requires thermal activation, they can only occur at high temperatures. A similar configuration of screw dislocations would recover by the annihilation of dislocations by cross-slip.

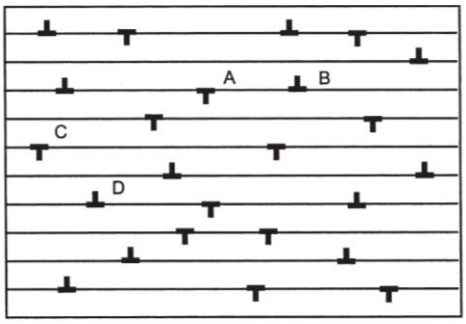

Figure 2-1 Schematic diagram of a crystal containing edge dislocations [1]

Another important recovery process which leads to a resultant lowering of the lattice strain energy is rearrangement of the dislocations into cell walls. This process is illustrated schematically in Figure 2-2, whereby dislocations all of one sign align themselves into walls to form small-angle or sub-grain boundaries. During deformation a region of the lattice is curved, as shown in Figure 2-2a, and the observed curvature can be attributed to the formation of excess edge dislocations parallel to the axis of bending. On heating, the dislocations form a sub-boundary by a process of annihilation and rearrangement. This is shown in Figure 2-2b, from which it can be seen that it is the excess dislocations of one sign which remain after the annihilation process that align themselves into walls. As shown in Figure 2-3, the energy of a tilt boundary increases with increasing misorientation and the energy per dislocation decreases with increasing misorientation. Therefore there is a driving force to form fewer, more highly misoriented boundaries as recovery proceeds.

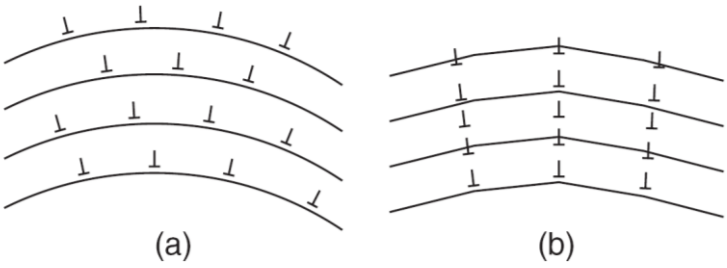

Figure 2-2 (a) Random arrangement of excess parallel edge dislocations. (b) Alignment into dislocation walls.

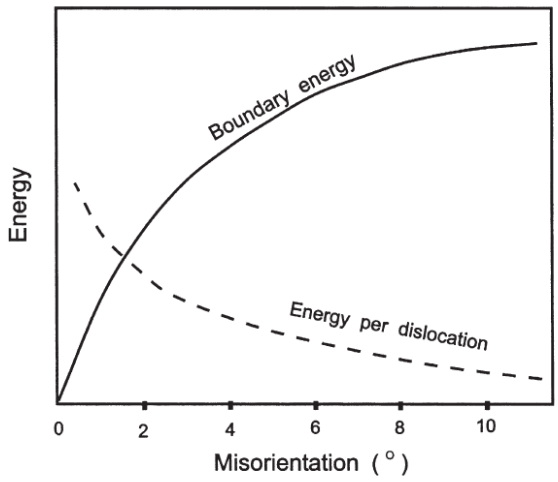

Figure 2-3 The energy of a tilt boundary and the energy per dislocation as a function of the crystal misorientation [1].

The recovery is usually increases with strain (before the onset of recrystallization), and with temperature. [1]. The stacking fault energy, which, by affecting the extent to which dislocations dissociate, determines the rate of dislocation climb and cross slip, also controls the rate of recovery. In metals of low γ_{SFE} such as 304L austenitic stainless steel, climb is difficult, and little recovery of the dislocation structure normally occurs prior to recrystallization. So, well developed subgrain structures are not usually observed in these materials.

2.2.3. Modelling of Work-hardening and recovery

According to Kocks and Mecking [10,11], the evolution equation for the dislocation density ρ can be described by two concurrent effects: storage and recovery. The well known Kocks-Mecking (KM) model considers that the dislocation density storage is represented by the term $K_1\sqrt{\rho}$, and dynamic recovery is assumed to be linear in ρ:

$$\frac{d\rho}{d\varepsilon} = K_1\sqrt{\rho} - K_2\rho \qquad \text{(Equation 2-1)}$$

Following the KM model, Estrin & Mecking [12] describe the evolution of dislocation density ρ as a function of the equivalent plastic strain ε by assuming that the mean free path is constant,

$$\frac{\partial\rho}{\partial\varepsilon} = K_1 - K_2\rho \qquad \text{(Equation 2-2)}$$

where K_1 and K_2 represent respectively the strain hardening and the recovery terms, similar equation has also been suggested by Bergstrom [13].

Less attention has been paid to static recovery, Fridel's model

$$\frac{d\rho}{dt} = -2M\tau\cdot\rho^2 \qquad \text{(Equation 2-3)}$$

Where τ is the liner dislocation energy, M is a dislocation mobility which, in a pure metal, is directly related to the self-diffusion coefficient:

$$M = M_0\exp(-Q_M/RT) \qquad \text{(Equation 2-4)}$$

Estrin [14] proposed a Bailey-Orowan type equation, in which a decrement of the dislocation density is proportional to the corresponding time (rather than strain as in the dynamic recovery case) increment, can be written as:

$$\frac{d\rho}{dt} = -r \qquad \text{(Equation 2-5)}$$

A reasonable phenomenological equation for the static recovery r would be:

$$r = r_0 \exp(-\frac{U_0}{k_B T}) \sinh(\frac{\beta\sqrt{\rho}}{k_B T}) \qquad \text{(Equation 2-6)}$$

implying that static recovery is driven by the stress determined by the square root of the current dislocation density and introducing the activation energy U_0, a constant β and a constant pre-exponential factor r_0: (k_B denotes the Boltmann constant)

2.3. Nucleation mechanism

Nucleation is the key concept in understanding of microstructural evolution in recrystallization. The classical homogeneous nucleation theories associated with solidification or phase transformation do not hold true for recrystallization, due to its low driving force and high grain boundary energies [1]. The dislocation free regions are unlikely formed by thermal fluctuations. It is now well known that a critical stored energy must be reached before the onset of recrystallization, and under most high temperature deformation conditions, nuclei mostly originate at, or near, the pre-existing grain boundaries.

Even though extensive investigation has been made, significant disagreements on the mechanism of nucleation still exists (and this may vary from one material to the other), the mostly accepted mechanisms are summarized below.

2.3.1. Strain induced boundary migration (SIBM)

SIBM is the most common mechanism of nucleation, it has been originally proposed by Beck and Sperry [15] based upon observations of Al using optical microscopy. It is worth to notice that different names are used to describe the same mechanism, including: bulging, migration of pre-existing grain boundaries etc. This mechanism considers the migration of a pre-existing grain boundary toward the interior of a more highly strained grain, leaving a dislocation-free region behind the migrating boundary as shown schematically in Figure 2-4. The characteristic feature of this mechanism is that the nuclei have similar orientations to the old grains from which they have grown.

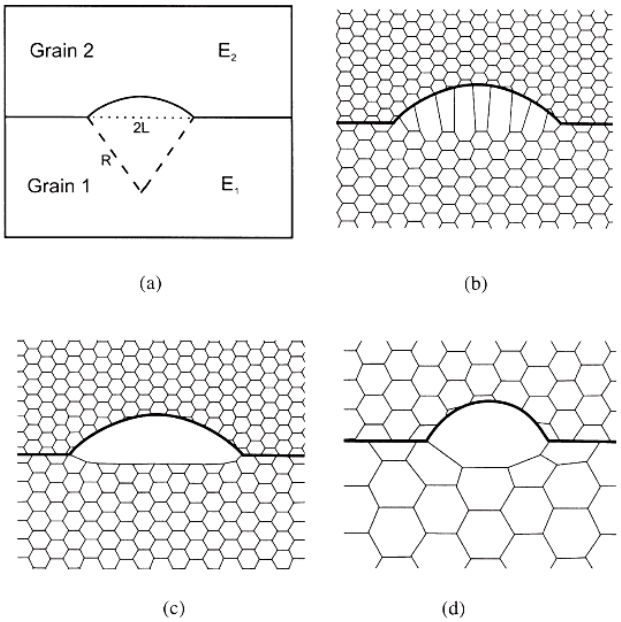

Figure 2-4 (a) SIBM of a boundary separating a grain of low stored energy (E1) from one of higher energy (E2), (b)dragging of the dislocation structure behind the migrating boundary, (c) the migrating boundary is free from the dislocation structure, (d) SIBM originating at a single large subgrain.

The condition for the process to occur should be favorable of energy-balance between the decrease of stored energy due to the elimination of dislocations in the region behind the migrating boundary and the increase in total grain boundary surface due to bulging. The growth condition is given by:

$$L > \frac{2\gamma_b}{\Delta E} \qquad \text{(Equation 2-7)}$$

where γ_b is the grain boundary surface energy per unit area and ΔE is the released energy associated with the decrease in defects, $2L$ is the initial length of the bulging boundary as shown in Figure 2-4a. Therefore, a critical stored energy difference is necessary for the initiation of nucleation.

This mechanism is believed to be particularly important after low strains up to 40%. More recent research has shown that SIBM is also very important during recrystallization after high temperature deformation of steels, when the deformation microstructures are more homogeneous than after lower temperature deformation [16,17]. Other types of nucleation also seem possible in association with existing grain boundaries. Beck and Sperry [15] also presented evidence for new recrystallized grains which did not share either of the parent grains' orientations. The same phenomenon has been observed in bicrystals of iron by Hutchinson [18].

2.3.2. Nucleation by low angle boundary migration

This model has been presented independently by both Beck [19] and Cahn [20] in the 1940s. The dislocation density around the low angle boundaries maybe relatively high, promoting their migration. During the migration of the sub boundaries, the dislocations are continuously absorbed and hence increase the low angle boundaries crystallographic orientation until it is finally transformed into a high angle boundary. The stored energy decreases during this process

since the microstructural defects behind the moving sub grain boundaries are removed or rearranged. The experimental evidences of nucleation by this mechanism were summarized by Riots *et al*. in a review paper [21]. Figure 2-5 illustrates schematically the mechanism of nucleation by sub-boundary migration.

It is believed that this mechanism usually occurs at high strains, large spread in the subgrain size distribution, relatively high annealing temperatures, and occurs preferentially in low-SFE metals [21].

Figure 2-5 The sequence shows the nucleation of a recrystallized grain starting from a subgrain: a) initial substructure; b) the larger (middle) subgrain growth over the other (smaller) ones; and c) an area free of defects associated to a large angle boundary that is being formed [21].

2.3.3. Nucleation by subgrains coalescence

The mechanism of subgrain coalescence was based upon the coalescence of two adjacent subgrains and which is equivalent to a rotation, causing the crystal lattices to coincide, as shown in Figure 2-6.

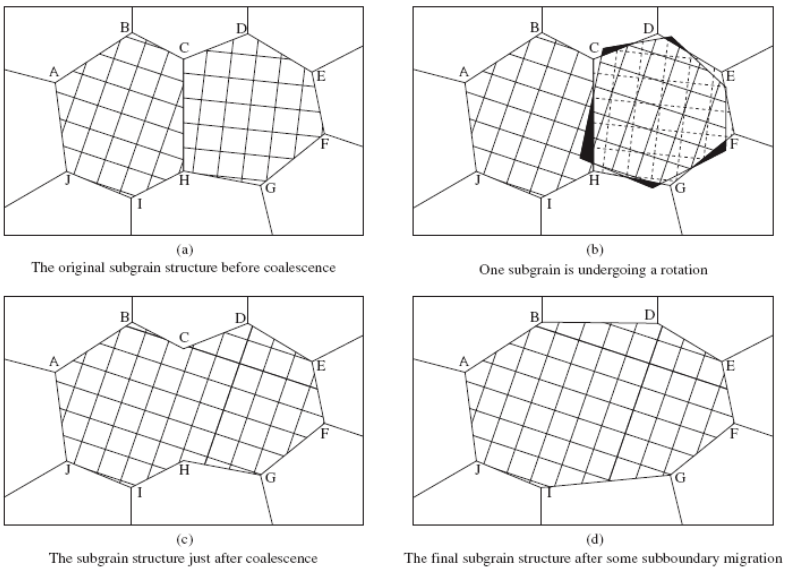

Figure 2-6 Coalescence of two subgrains by "rotation" of one of them: a) original structure prior to coalescence; b) rotation of the CDEFGH grain; c) subgrain structure subsequent to coalescence; and d) final structure after sub-boundaries migration.

This mechanism seems to be associated with transition bands (which consists of a cluster of long narrow cells or subgrains with a cumulative misorientation from one side of the cluster to the other [1]), large spread in the distribution of subgrain angles, moderate strains, regions next to grain boundaries, relatively low annealing temperatures, and metals with high SFE.

2.3.4. Nucleation by grain boundary sliding

The three nucleation mechanisms mentioned above were all proposed many decades ago, extensive investigations have been carried out since their first appearance, even though disagreements still exist. More recently, a new nucleation model for the DRX process has been proposed by Sakai and his cooperators [22,23], as shown schematically in Figure 2-7. First, grain boundary sliding or grain boundary zone shearing occurs at appropriate boundaries during hot forming. Dislocation accumulates and then subgrain boundaries form near the prior grain boundaries, followed by the development of the grain boundary serration (Figure 2-7a). Local concentration of strains is developed due to the continuous grain boundary shearing at these serrations (Figure 2-7b). Such boundary serrations should assist the operation of grain boundary bulging and so the bulging mechanism can operate much easier than that operating in cold deformed grain structures. Finally, DRX nucleus will form by the bulging of a part of the serrated grain boundaries (Figure 2-7c).

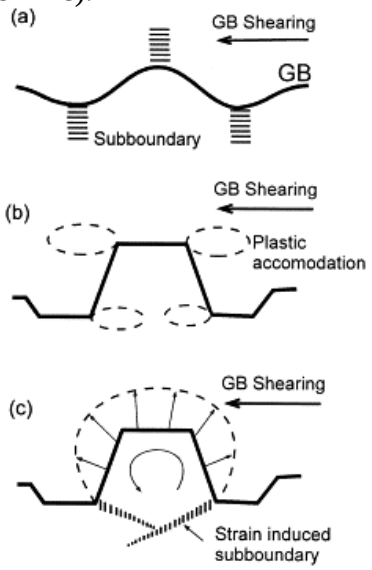

Figure 2-7 A schematic modified model for the nucleation of a DRX grain at a grain boundary (GB): (a) Boundary corrugation accompanied by the evolution of subboundaries; (b) Partial grain boundary shearing, leading to the development of inhomogeneous local strains; and (c) Bulging out of a serrated grain boundary and the evolution of strain induced subboundaries due to grain boundary shearing and/or grain rotation, leading to the formation of a new DRX grain [22].

2.3.5. Nucleation mechanism during the progress of DRX

While the mechanism by which the first recrystallized grains were formed at pre-existing grain boundaries seems to be well and widely investigated as presented above, there is an almost complete lack of knowledge on the nucleation mechanisms which are able to explain the progress of DRX after the prior grain boundaries were entirely decorated with new grains (necklace structure).

Gottstein and his co-workers [24,25,26] are among those few researchers who investigated the nucleation mechanism during the progress of DRX. By compressing austenitic steel alloy 800H to a strain of 0.49 at 1100 ℃, with constant true strain rates of $0.1s^{-1}$, Brunger *et al.*[25] observed fractions of 20% of twins at the interface between initial grains and dynamically recrystallized grains using TEM observation, which indicates the importance of twinning for the nucleation of DRX. Even though twinning seems to play an important role during the nucleation of DRX, their origin was not analyzed in details. Wang *et al.* [26] continued this

work, with the aim to investigate to what extent twinning contributes to the progress of DRX. When comparing the twin frequency at the front of the recrystallized regions to that in the center of such regions, they observed that the twin frequency was higher at the recrystallization front where the twins are most recently created and thus less affected by deformation. The mean twin frequency during DRX was found to be about 18%, which is not likely to originate from or is affected by statistical coincidence of twin rotations, since the mean twin frequency being formed by a random orientation distribution, is 2% only. It was concluded that twinning is an active nucleation mechanism during DRX process, the increase in DRX volume fraction occurred through the formation of multiple twinning chains drives the continuous progress of the recrystallization front.

An austenitic Ni-30% Fe model alloy was investigated within the DRX regime using hot torsion testing by Hodgson *et al*. [27]. They confirmed that the DRX nucleation mechanism of the first DRX layer was SIBM accompanied by the formation of large-angle sub-boundaries and annealing twins. And the subsequent DRX layers were formed through the repeated nucleation and growth of annealing twins on the migrating interface. This process continues until the deformed matrix becomes completely consumed by DRX grains.

2.4. Discontinuous dynamic recrystallization

When deformation at sufficiently high temperature exceeds a critical strain, ε_{cr}^{DRX}, DRX is initiated and increases with further deformation until a steady state where the microstructure is stable due to a dynamic equilibrium between softening by dynamic nucleation and work-hardening.

2.4.1. Investigation of DRX through flow curves

The early investigation on dynamic recrystallization modeling was mostly based on the existence of flow stress peaks (single or multi-peak) and the transition from cyclic to single peak recrystallization behavior, less attention was paid to the microstructral evolution within the material [28]. Many published articles have shown that low strain rates, high temperatures as well as small initial grain size promote multiple peaks recrystallization, and vice versa, at relatively high strain rates, low temperatures and coarse initial grain size, the flow curves are single peak type [29,30,31,32,33].

Several criteria have been proposed to analyze the transition from single to multiple peak flow curves. Luton and Sellars [32] studied the DRX of nickel and nickel-iron alloys and found that the transition from multiple to single peak behavior is associated with the peak strain ε_p and the strain close to full recrystallization ε_x. As shown in Figure 2-8, it is apparent that the peak strain is very close to critical strain ε_{cr}^{DRX} for the initiation of DRX. According to their model, when $\varepsilon_x < \varepsilon_c$, i.e. recrystallization in one cycle is mostly completed before new cycle of recrystallization is again initiated for the concurrently work hardened recrystallized grains, the flow curve will show multiple peaks. In contrast, the single peak behavior appears when $\varepsilon_x > \varepsilon_c$ where a subsequent cycle of recrystallization is started in the most work-hardened recrystallized grains in the previous cycle before the recrystallization of that cycle is complete.

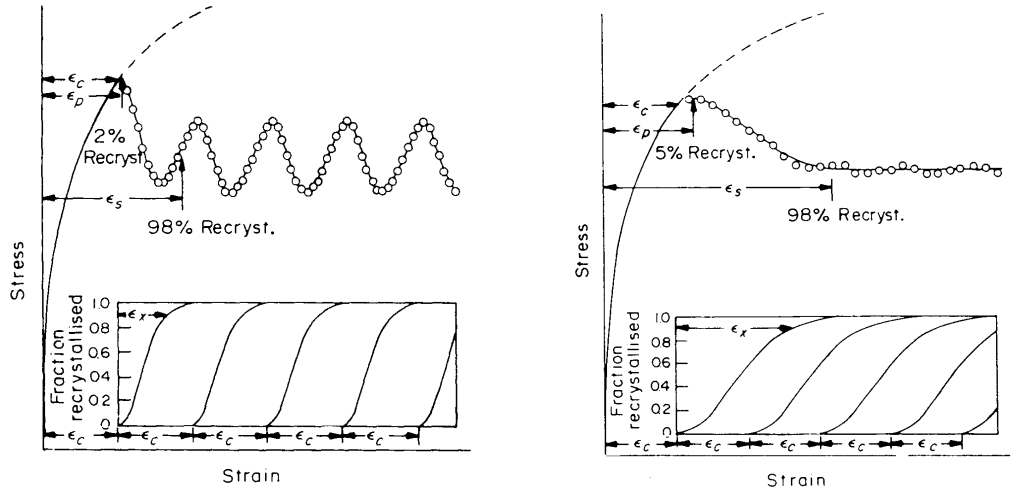

a) b)

Figure 2-8 Predicted stress-strain curves for DRX [32]

a) $\varepsilon_x < \varepsilon_c$ b) $\varepsilon_x > \varepsilon_c$

In the second criterion, proposed by Sakai and his co-workers both in Japan and Canada [28,34,35], suggested that the shape of flow curve depends on the ration of the initial (d_0) to steady state (d_{ss}) grain sizes. According to their model, the transition from multiple to single peak behavior corresponds approximately to a 2:1 reduction in the grain size. The single peak flow curve represents a growth controlled mechanism (i.e. grain refinement) and usually the initial grain size (d_0) is greater than twice the steady state DRX grain size (d_{ss}). The single peak behavior is usually associated with dynamic recrystallization based on the formation of a necklace structure. In contrast, the multi peak flow curve is related to a nucleation control and impingement mechanism (i.e. grain coarsening) and also $d_0 < 2\,d_{ss}$. However, the necklace mechanism cannot take place during grain coarsening and the growth of each new grain is stopped by grain boundary impingement with other recrystallizing grains [28]. Several different studies [36,37] have shown that this criterion is not always valid for all materials and the Luton and Sellars model can generally predict the flow curve behavior more accurately [38].

2.4.2. Critical condition for the onset of DRX

While it is well known that the onset of discontinuous dynamic recrystallization during hot deformation occurs when a critical strain ε_{cr} (or critical dislocation density ρ_{cr}), is reached, the identification of this exact value need to be clarified. The critical strain for initiation of DRX could be determined by metallography. However, this technique requires extensive sampling before and after the critical strain, and the newly created nuclei are usually too small to be detected. Moreover, the critical strain for DRX depends on the chemical composition of the material under consideration, the grain size prior to deformation, and the deformation conditions, i.e., temperature and strain rate [28,31,32], which add difficulties to metallography examination of critical strain.

One possible approach of identifying critical strain is to relate it to the peak strain, ε_p (the strain corresponding to the maximum stress in the flow curve) following relationships of the

type: $\varepsilon_{cr} = A\varepsilon_p$, where A is a constant. For different materials, values between 0.2 and 0.87 have been reported for this constant A [28,39,40,41]. The lower limit of the value was found in polycrystalline copper where the DRX grains are formed from the triple junctions or non-equilibrium grain boundary junctions [42,43], compared to the nucleation on serrated grain boundaries, which starts at a higher strain around 0.6-0.8 of the peak strain. As for stainless steel, the DRX of AISI 304 stainless steel was studied by Kim and Yoo [44] with torsion tests in the temperature range of 900–1100 ℃ and the strain rate range of 0.05–5.0 s^{-1}. The relationship between the critical and peak strain was expressed as follows: $\varepsilon_{cr} = 0.7\varepsilon_p$, which is close to that found by Dehghan-Manshadi [39], who obtained $\varepsilon_{cr} \approx 0.6\varepsilon_p$ using the same material.

Several attempts have been made to predict the initiation of DRX through the flow curve analysis. The basis of the flow curve analysis method is that DRX affects the flow curve shape by changing the rate of work hardening through the introduction of new dislocation free grains. The identification of critical strain by a serial of mathematical calculations on flow stress curves was firstly proposed by Kocks and Mecking [11] and then continued by McQueen and Ryan [45,46,47]. With this approach, the onset of DRX corresponds to a deviation in the work hardening curves($\theta = \partial\sigma/\partial\varepsilon$) versus stress ($\sigma$). However, it is difficult in this method to obtain the exact value for the inflection point in the work hardening curves, since the slope changes slowly and gradually [39]. Wray [48] was the first to point out that the critical strain corresponds to the application of the minimum amount of work, necessary for the initiation of DRX. Poliak and Jonas [49] have shown that the initiation of DRX is governed by both energetic and kinetic critical conditions. The former requires that the energy stored during a given deformation condition attains its maximum, while the latter requires the dissipative processes associated with deformation to decelerate to a critical level. The kinetic critical condition leads to a minimum value of $\left|-\partial\theta/\partial\sigma\right|$ when the critical state is attained and to the appearance of an inflection point in the $\theta - \sigma$ curve. It is important to note that ε_{cr} is not the strain at which the first nuclei appear, but is the strain at which a small fraction of recrystallzation (1-5%) takes place, this fraction are needed to have a detectable effect on the flow stress [50,51]. Furthermore, the approach of Poliak and Jonas was subsequently simplified by Najafizadeh and Jonas [52]. There are many other work on this topic, for example, Barnett *et al*. [53,54] have identified the critical strain for initiation of DRX using the kinetics of static recrystallization (SRX), Gottstein *et al*. [55] predicted the critical strain for initiation of DRX based on a dislocation density work hardening model.

In the context of numerical modeling of DRX, the notion of critical dislocation density is very often used instead of the critical strain. The critical dislocation density depends on deformation conditions, and can be determined from the energy changes in relation to the formation of a nucleus on a pre-existing grain boundary. Sandstrom and Lagneborg [56] proposed a semi-quantitative approach by assuming that DRX is only possible when the rate of boundary migration of the potential nucleus is high in relation to the rate of reaccumulation of dislocations behind it. Following their model, Roberts and Ahlblom [57] further analyzed the critical condition for DRX. As shown in Figure 2-9, the high angle boundary is moving from right to left into unrecrystallized material which has a high dislocation density of (ρ_0) with velocity of $\dot{x}$. The dislocation density of the potential nucleus behind the moving boundary drops to around zero, however, concurrent deformation of the material raises the dislocation density behind the boundary following some function $\rho(x)$, tending towards a value of ρ_0 at large distances.

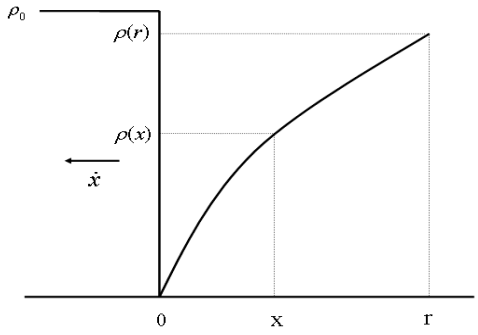

Figure 2-9 Schematic diagram of the dislocation density at a dynamic recrystallization front

A spherical nucleus of radius r is considered. The driving force is related to the dislocation density difference $\rho_0 - \rho(r)$. By taking the radial average of the dislocation density difference, the difference in stored energy is:

$$\Delta E = \frac{\tau}{r}\int_0^r (\rho_0 - \rho(x))dx \qquad \text{(Equation 2-8)}$$

where τ is the dislocation line energy. The net energy change resulting from the creation of a nucleation is calculated from the simple nucleation theory as follows:

$$\Delta G(r) = -\frac{4}{3}\pi r^3 \cdot \frac{\tau}{r}\int_0^r \rho_0 - \rho(x)\cdot dx + 4\pi r^2\gamma_b \qquad \text{(Equation 2-9)}$$

where γ_b is the grain boundary energy per unit area. Concerning $\rho(x)$, a simple equation was used by neglecting dynamic recovery. Dislocation density was assumed to increase due to work hardening, which is determined by a constant dislocation mean-free path (close to the subgrains size (l) developed during deformation):

$$\dot{\rho} = \frac{\dot{\varepsilon}}{bl} \qquad \text{(Equation 2-10)}$$

The moving velocity $\dot{x}$ of the high angle boundary is determined by driving force due to the stored energy difference in the vicinity of the boundary,

$$v = mP \qquad \text{(Equation 2-11)}$$

which gives:

$$\dot{x} = m\tau(\rho_0 - \rho(x=0)) \approx m\tau\rho_0 \qquad \text{(Equation 2-12)}$$

Combining the last two equations and ignoring the sign of x, we have the expression of $\rho(x)$:

$$\rho(x) = \frac{\dot{\varepsilon}}{blm\tau\rho_0}\cdot x \qquad \text{(Equation 2-13)}$$

The critical nucleation conditions can be established by maximizing the net free energy change in (Equation 2-9). After substitution of (Equation 2-13) into (Equation 2-9) and then differentiation, the turning points in $\Delta G(r)$ can be obtained according to:

$$\frac{2}{3}r_c^2\frac{\dot{\varepsilon}}{blm\tau\rho_0} - r_c\tau\rho_0 + 2\gamma_b = 0 \qquad \text{(Equation 2-14)}$$

which gives a real r_c only if:

$$\rho_0 \geq \left(\frac{16\gamma_b \dot{\varepsilon}}{3blm\tau^2} \right)^{1/3} = \rho_{cr} \qquad \text{(Equation 2-15)}$$

For the bulging nucleation mechanism, see Figure 2-10, which is a little different from the case above where spherical nuclei are considered, similar development can be conducted. The critical condition for the bulging nucleation mechanism is shown in (Equation 2-16). For the details of the calculation, the reader is referred to [57].

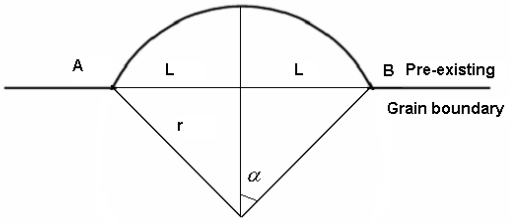

Figure 2-10 Schematic diagram of bulge mechanism

$$\rho_{cr} = \left(\frac{20\gamma_b \dot{\varepsilon}}{3blm\tau^2} \right)^{1/3} \qquad \text{(Equation 2-16)}$$

Comparing these two above equations, it is surprising that DRX nucleated by the bulging mechanism needs a dislocation density about 10% higher than when nucleation is 'homogeneous'. As previously mentioned, this model did not take into account dynamic recovery. Since in materials of lower stacking fault energy such as copper and stainless steel, recovery is slow, this assumption will not significantly affect the critical value. However, the reduction of the driving force due to capillarity effect related to the grain boundary energy and curvature was also neglected when calculating the grain boundary migration velocity in (Equation 2-12). If this term was taken into account, the beneficial effect of a pre-existing grain boundary (Figure 2-10) would be apparent.

2.4.3. Influence of temperature, strain rate and initial grain size

As shown in Figure 2-11, the shape of the flow curve changes from multi-peak type to single peak when the strain rate is increased, see Figure 2-11a. On the other hand, the same transition can be observed when the temperature is decreased (Figure 2-11b).

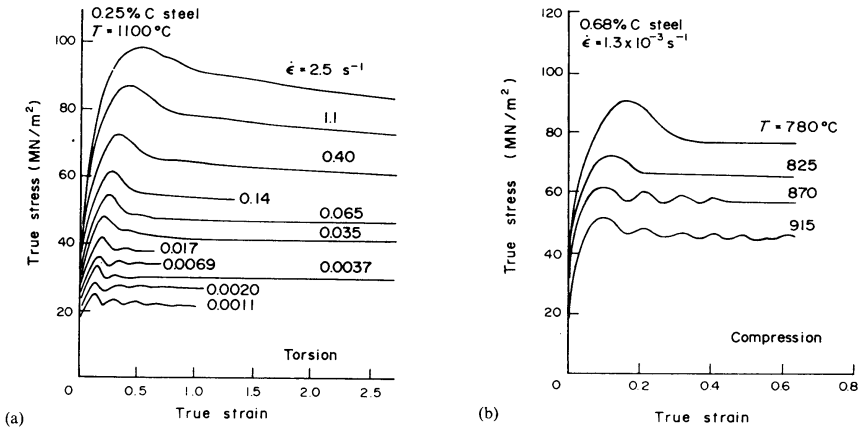

Figure 2-11 a) Influence of strain rate on the flow curves [29] b) Effect of temperature of gamma iron at $\dot{\varepsilon} = 10^{-3} s^{-1}$ [30]

So, according to the above experimental observation, there is an equivalence between increasing/decreasing temperature and decreasing/increasing strain rate. The Zener-Hollomon parameter was introduced for this purpose:

$$Z = \dot{\bar{\varepsilon}} \exp(Q/RT) \qquad \text{(Equation 2-17)}$$

where $\dot{\bar{\varepsilon}}$ is the equivalent strain, Q is the activation energy of deformation ($J.mol^{-1}$), R is the ideal gas constant ($J.mol^{-1}.K^{-1}$) and T is the temperature (K).

As for the influence of temperature and strain rate on DRX kinetics,

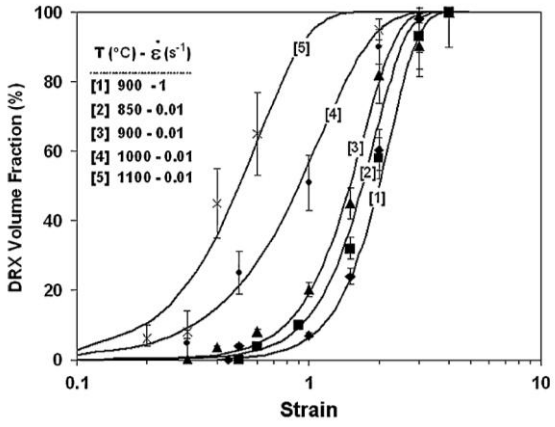

Figure 2-12 The effect of temperature and strain rate on the kinetics of 304 stainless steel, $D_0 = 35\mu m$ [39]

Similar observation was obtained by Ahlblom [58] on kinetics of DRX using an 18/8 austenitic stainless steel in the 1273-1473K temperature range, with two different strain rates of $\dot{\varepsilon} = 0.06$ and $\dot{\varepsilon} = 0.96$. According to our literature review, the experimental data on the kinetics of DRX, taking into account of the influence of both temperature and strain rate, is limited, especially for austenitic stainless steels.

It is also well known now that in condition of hot deformation, a decrease in the initial grain size will accelerate the onset of DRX, and increase DRX kinetics. The effect of initial grain size on the hot torsion behaviour of nickel has been examined by Sah *et al.* [31] in the range of 800-1000 ℃ over a wide range of strain rates. In Figure 2-13, faster kinetics of DRX is clearly observed when decreasing the initial grain size from 0.49mm to 0.14mm, the strain needed for

the onset of recrystallization also decreases with initial grain size. El Wahabi *et al.* [59] and Dehghan-Manshadi *et al*. [60] further confirmed this using 304 austenitic stainless steel. The recrystallized kinetics at two different strain rates were obtained from measurements made at two different depths within the same specimens. The strong influence of initial grain size on the kinetics of recrystallization is due to the change in the grain-boundary surface area, which is the principal nucleation site.

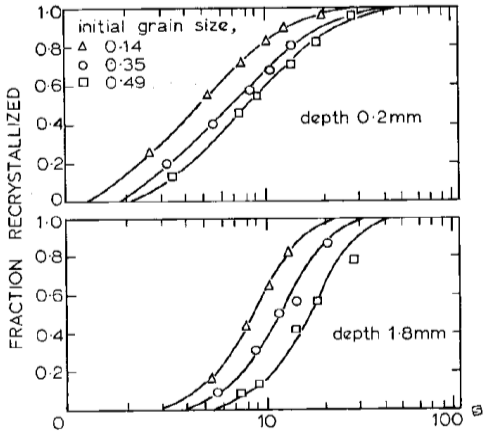

Figure 2-13 Relation between fraction recrystallized and angle of twist for different initial grain sizes in nickel at 1000 ℃ and 0.05 rev/min [31]

A transition from single- to multiple-peaks behavior is obtained on nickel when the initial grain size is decreased below a critical value, as observed by Sah *et al*. [31], and shown in Figure 2-14a. This phenomenon is reported using several other materials [35], including 304 stainless steel [59]. On the other hand, for a given temperature and strain rate, the effect of initial grain size on DRX final grain size and steady-state stress is less pronounced even negligible [31,61], as shown in Figure 2-14.

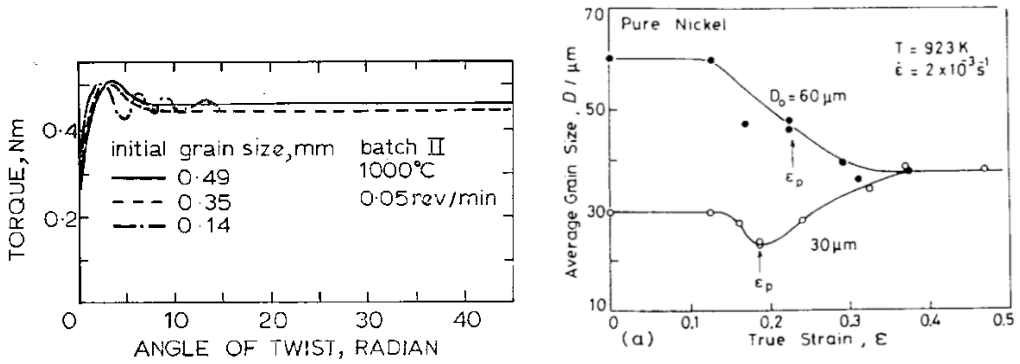

a) b)

Figure 2-14 a) Typical torque/twist curves for material with different starting grain size [31]

b) Effect of initial grain size D_0 on the average grain size [61]

The peak and critical strains were verified by Dehghan-Manshadi [60] to decrease with initial grain size and follow a power-law function with the Zener–Hollomon parameter. They also found that from a critical value ($Z \sim 10^{17}$), both the peak and critical strains of the finer-grain size (8 μm) showed almost no slope change with increasing Z; for the coarse-grain size (35 μm), there was no change in behavior over the entire Z range, i.e. the peak and critical strains increase linearly with Z, as shown in Figure 2-15a. Figure 2-15b suggests that the difference between the peak stress of fine and coarse grain materials is negligible at very high Z value.

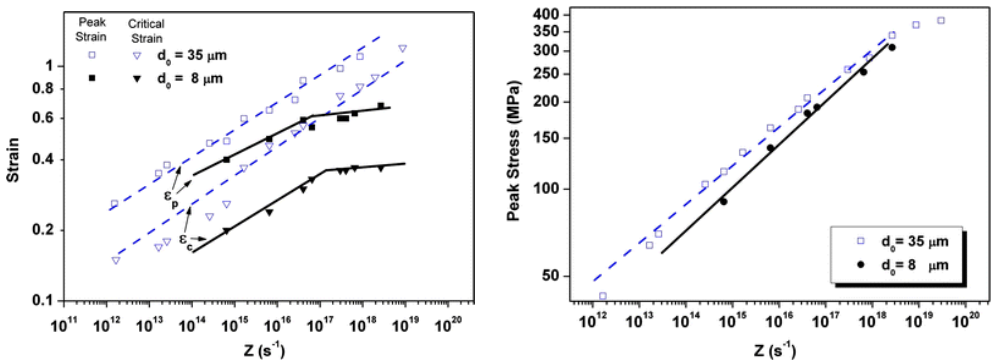

a) b)

Figure 2-15 a) Peak and critical strains as functions of Z for fine- and coarse-grain materials [60], b) Peak stress as a function of Z for fine- and coarse-grain materials[60].

Dehghan-Manshadi and Hodgson [60] confirmed an interesting transition from conventional (discontinuous) to continuous DRX (CDRX) with a decrease in the initial grain size, based on microstructural investigations on 304 stainless steel and on another austenitic stainless steel with an ultra fine initial grain size of 2.8 μm [62]. It was proposed that the ratio of recrystallized grain size, d_{drx}, to the initial grain size, d_0 can be considered as an important factor determining the DRX mechanism. When d_{drx}/d_0 is close to 1, no obvious change occurs in the initial microstructure during hot deformation, the operating DRX mechanism is through rearrangement of grain and subgrain boundaries, i.e. CDRX. If $d_{drx} << d_0$, on the other hand, DRX happens by break down of the initial grains to several smaller DRX grains by serration of initial grain boundaries and nucleation of new DRX grains on these boundaries (i.e. DDRX).

2.4.4. Microstructure changes associated with DRX

DRX generally starts at the pre-existing grain boundaries [1,57,22,25], as shown schematically in Figure 2-16a. New grains are subsequently nucleated at the boundaries of the growing grains seen in Figure 2-16b, and in this way a thickening band of recrystallized grains is formed as shown in Figure 2-16c. If there is a large difference between the initial grain size (D_0) and the recrystallized grain size (D_{rx}), then a 'necklace' structure of grains may be formed by the successive appearance of next layers (Figure 2-16b–c), and eventually the material will become fully recrystallized (Figure 2-16d). A micrograph of copper which has undergone partial dynamic recrystallization is shown in Figure 2-17.

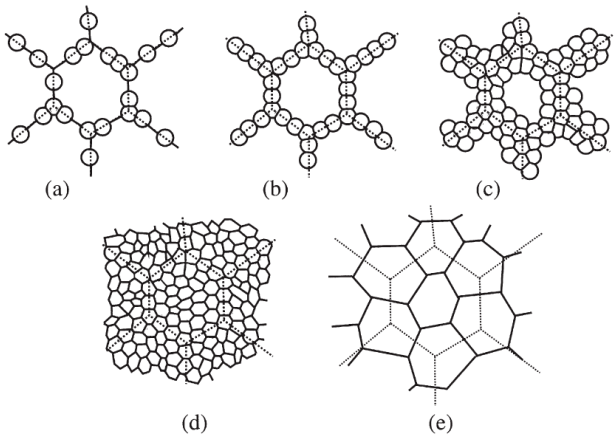

Figure 2-16 The development of microstructure during dynamic recrystallization. (a)–(d) Large initial grain size, (e) small initial grain size. The dotted lines show the prior grain boundaries [1].

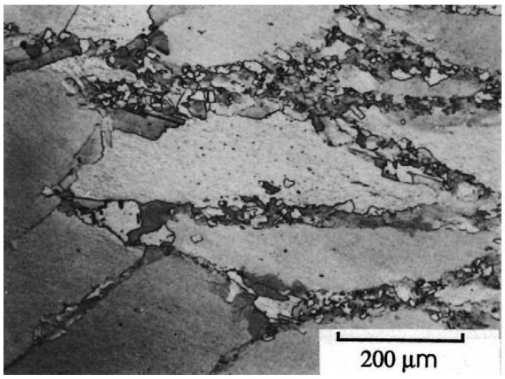

Figure 2-17 Dynamic recrystallization at prior grain boundaries in polycrystalline copper at 400 ℃, $\dot{\varepsilon} = 5.7 \times 10^{-2} s^{-1}$, $\varepsilon = 0.7$, (Ardakani and Humphreys 1992).

Unlike the case of static recrystallization, the mean size of the dynamically recrystallized grains does not change much as recrystallization proceeds as shown in Figure 2-18**.**

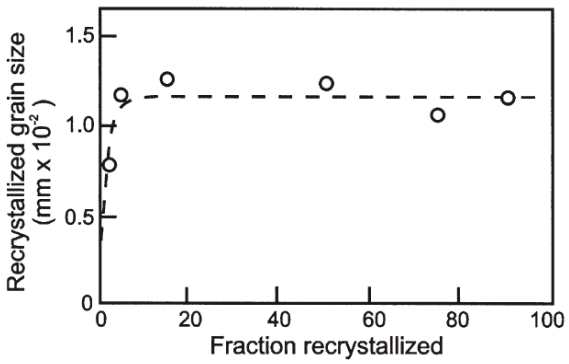

Figure 2-18 Relationship between dynamically recrystallized grain size and recrystallized fraction in nickel deformed at 880 ℃, $\dot{\varepsilon} = 5.7 \times 10^{-2} s^{-1}$ [31]**.**

During DRX, the original grains have irregular boundaries [63], indicating evidence of localized bulging and the formation of recrystallized grains near the grain boundaries. The recrystallized grains usually remain nearly equiaxed. The inhomogeneous dynamic structures can be classified into the three types of components, i) DRX nucleus (Figure 2-19a) with an

initial value of dislocation density ρ_0, ii) growing DRX grain (Figure 2-19b), and iii) critically work hardened DRX grain (Figure 2-19c).

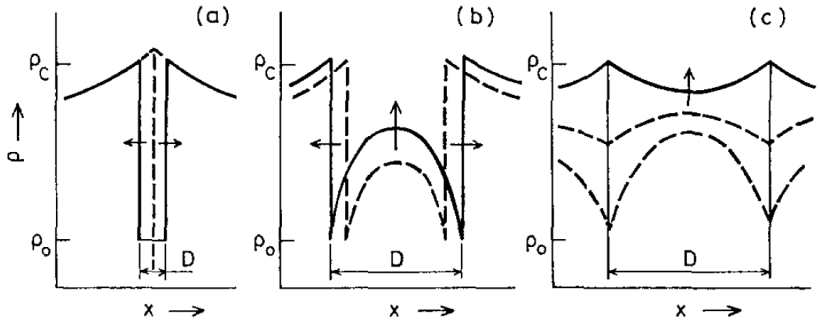

Figure 2-19 Three types of dislocation density distribution developed inside a crystallite of the DRX grain structure: (a) DRX grain nucleus, (b) growing DRX grain, and (c) DRX grain undergoing strain hardening. The present state is represented by the full lines, and one or more earlier states by broken lines [64 ,65].

Microstructural examination of the dynamically processed (T=1200 ℃, in the strain rate interval of $10^{-3}s^{-1}$ to$10^{2}s^{-1}$) type 304L austenitic stainless steels has been carried out by Sundararaman *et al.* [66] by TEM. Twins and twin bands that form at all strain rates examined were observed, even though it is generally known that only high deformation rates and low temperatures favor the occurrence of twins.

Luton and Sellars [32] concluded from metallographic and flow stress observations of nickel and three nickel-iron alloys that DRX occurs at strains greater than a critical value, and most importantly, the recrystallized grain size is determined entirely by the flow stress and follows a relationship with flow stress (σ) :

$$\sigma = \sigma_0 + kd_{rex}^{-m} \qquad \text{(Equation 2-18)}$$

where σ_0, k and m are constants. The same relation has been found by Sah *et al*. [31] for the DRX of nickel.

On the other hand, experimental observations generally show that the steady state grain size (D_R) during dynamic recrystallization is a strong function of the flow stress and is only weakly dependent on deformation temperature. Derby [67] proposed a relationship between the recrystallized grain size d_{rex} and σ, normalized by the shear stress G and subgrain size b respectively, which applies to a very wide range of materials:

$$1 < \frac{\sigma}{G}\left(\frac{d_{rex}}{b}\right)^{2/3} < 10 \qquad \text{(Equation 2-19)}$$

By a statistical analysis of the average recrystallized grain size of data obtained from experiments and published literature, including rolling, tension, torsion, extrusion and compression tests, Mataya *et al*. [68] found that the average recrystallized grain size of 304L depends on the strain, initial grain size, and the Zener-Hollomon parameter as follows:

$$d_{rex} = 83.9\varepsilon^{-0.537}d_0^{0.355}Z^{-0.0655} \qquad \text{(Equation 2-20)}$$

It was found that d_{rex} also depends on initial grain size and applied strain, which contradicts with the fact that the mean size of recrystallized grain is usually considered as independent of the initial grain size (see Figure 2-14b) and does not change during DRX as shown Figure 2-18. The disagreement might come from slightly different material chemical composition or testing

procedures when taking data from published literature.

2.4.5. Modeling of dynamic recrystallization

2.4.5.1. Constitutive models

Early attempts at modeling DRX focused on explaining the initial peak in flow stress and the transition from periodic to single peak behavior, which was already illustrated in detail in section 2.4.1. In recent years, a number of constitutive models have been proposed or modified to describe the strain-rate, stain and temperature-dependent flow behavior of metals and alloys. Lin and Chen [69] made a critical review on the experimental results and constitutive descriptions for metals and alloys in hot working, where the constitutive models were divided into the following three categories:

(1) Phenomenological constitutive models, which provide a definition of the flow stress based on empirical observations, are lacking physical background even though they fit experimental observations.

(2) Physically-based constitutive models, on the other hand, take into account physical aspects of the material behavior. They usually allow for an accurate definition of material behavior under wide ranges of loading conditions using physical assumptions but usually include a large number of material constants.

(3) Artificial neural networks (ANN) are a large class of parallel processing architectures, which can mimic complex and nonlinear processing units called neurons. The relationship can be 'learned' by a neural network through adequate training from the experimental data. Neural networks can provide a fundamentally different approach to materials modeling and material processing control techniques as compared to statistical or numerical methods.

Modeling of a processing stage may need several constitutive functions depending on the complexity of the flow curves. Moreover, for multistage processes, altered constitutive constants may be needed for different passes, due to inter-pass softening. This points out the need to incorporate microstructure concepts into the constitutive models.

2.4.5.2. The JMAK model

The analytical modelling of dynamic recrystallization very often uses modified versions of the Johnson-Mehl-Avrami-Kolmogorov [70] equation, which will be discussed in detail in section 2.5.2.3 when dealing with static recrystallization. The model was however only derived in static conditions, and was limited by two strong assumptions related to the random and homogeneous nucleation over the entire untransformed portion of the material, and to the isotropic and uniform growth rate. Furthermore, the calibration of the model requires a significant experimental effort, and the parameter values are difficult to interpret physically.

Using the JMAK model, the DRX of AISI 304 stainless steel was studied by Kim and Yoo [44] with torsion tests. The volume fractions of DRX (X) as a function of processing variables, such as strain rate ($\dot{\varepsilon}$), temperature (T), and strain (ε) were established. The calculation of grain size was based on X_V and the microstructure was investigated at a few points. It was found that the calculated results agreed with the microstructure of the alloy at any deformation conditions. Other attempts can be also found in the literature for DRX of steels, latest examples are summarized below in Table 2-1, including [39,71,72].

Table 2-1 JMAK models for DRX

Material	JMAK model	Reference
304L stainless steel	$X = 1 - \exp(-0.693(\frac{\varepsilon - \varepsilon_{cr}}{\varepsilon_{50}}))$ $\varepsilon_{cr} = 5.32 \times 10^{-4} e^{8700/T}$ $\varepsilon_{50} = 1.264 \times 10^{-5} d_0^{0.31} \varepsilon^{0.05} e^{6000/T}$ $d = 20560 \dot{\varepsilon}^{-0.3} e^{-0.25((Q/RT))}$	[72]
304 stainless steel	$X = 1 - \exp(-k(\varepsilon - \varepsilon_{cr})^{1.3})$ $\varepsilon_{cr} = 2.2 \times 10^{-3} Z^{0.15}$ $d = 5.2 \times 10^{3} Z^{-0.17)}$	[39]

JMAK models mostly work in constant temperature and strain rate conditions. When multi-pass recrystallization is of concern, multiple JMAK models are often combined to describe different regimes. The large number of fitting parameters, which usually have limited or no physical meaning, makes it very difficult to design such models in a robust manner.

2.4.5.3. The "old" theoretical models

The first formal theory of DRX was proposed in 1974 by Stuwe and Ortner [73]. The concept of impingement was taken into account in their model to make sure that new grains stop growing when they meet other grains traveling in the opposite direction. This model is capable of calculating the average dislocation density, and produces a theoretical stress-strain curve of a multi-peak nature. However, both dynamic recovery and DRX grain size evolution were neglected. A type of "onion" recrystallization was adopted, where repeated nucleation occurs in the center of a given grain, which contradicts with the general observation that nucleus is preferentially formed at pre-existing grain boundaries.

The model of Sandstrom and Lagneborg [74] is based on the evolution of the distribution of dislocation density within the material and effectively accounts for the transition from periodic to single peak behavior and the gradual disappearance of flow stress oscillation with strain. In their model, two dislocation density terms were put forward: the mean dislocation density within the subgrains, ρ, and the dislocation density in the subgrain boundaries, ρ_d. The former one determines the flow stress as given by (Equation 2-20), assuming that the flow stress contribution from the subgrains is quite small during hot working conditions.

$$\sigma = \alpha \mu b \sqrt{\overline{\rho}} \qquad \text{(Equation 2-21)}$$

where the average dislocation density is calculated through volume distribution of dislocations function $g(\rho, t)$, and given by:

$$\overline{\rho} = \int_{\rho_0}^{\rho_s} \rho \cdot g(\rho, t) d\rho \qquad \text{(Equation 2-22)}$$

Since ρ is much smaller than ρ_d, only the driving force from ρ_d is taken into account for grain boundary migration:

$$v = m \tau \rho_d \qquad \text{(Equation 2-23)}$$

Considering that an area which has just been passed by a grain boundary is almost free of dislocation, both of these two dislocation densities drop to zero there. These areas then suffer from both strain hardening and recovery (the recovery of dislocations in the subboundaries was neglected).

$$\frac{d\rho}{dt} = \frac{\dot{\varepsilon}}{bl} - 2M\tau\rho^2 \qquad \text{(Equation 2-24)}$$

$$\frac{d\rho_d}{dt} = \frac{\dot{\varepsilon}}{bl} \qquad \text{(Equation 2-25)}$$

Nucleation occurs when ρ_d reaches to the critical value of ρ_{cr}, which according to the Bailey and Hirsch analysis is [75]:

$$\rho_{cr} = \frac{4\gamma_b}{\tau d_{cr}} \qquad \text{(Equation 2-26)}$$

Stress-strain curves of vacuum-melted iron, zone-refined iron, as well as pure nickel were computed by Sandstrom and Lagneborg from their model by assuming appropriate values for the grain boundary and dislocation mobility terms, and by employing the postulated volume distribution of ρ and ρ_d. The model reproduces a number of features observed in experimental curves: the flow stress oscillations at low strain rates, the distinct peak stress at high strain rates, the strain rate dependence of the peak stress and of the steady state stress, the strain rate dependence of the recrystallized grain size.

The model of Sandstrom and Lagneborg, however, does not consider that DRX occurs preferentially at the grain boundaries. At the same time, the mobile fraction of the grain boundary area is assumed to be constant. Based on the general approach proposed by Sandstrom and Lagneborg, modifications have been made in order to improve the accuracy of the predicted results. Roucoules *et al*. [51] adopted a new recovery term proposed by Estrin and Mecking [12], which was assumed to be controlled by self diffusion instead of dislocation climb. The model is statistically based and tracks individual populations of the dislocation density during the work-hardening and softening phases. After tuning using available literature and test data, the model gave an accurate prediction of the stress-strain behavior.

2.4.5.4. The DRX model of Montheillet *et al*.

Even though there are vast existing investigations on the transient behavior in DRX, less attention has been paid to the steady-state regime to date. A grain scale semi-analytical approach for modeling DDRX was proposed by Montheillet *et al*. [76] using a few basic equations. Methods for evaluating the material parameters were also described and illustrated by the example of 304L stainless steel.

The driving force for dynamic migration of grain boundaries mainly comes from dislocation density difference between a grain and the surrounding matrix, hence:

$$\frac{dD_i}{dt} = 2m\tau(\bar{\rho} - \rho_i) \qquad \text{(Equation 2-27)}$$

There are several equations which can be used to account for strain hardening and dynamic recovery. A general differential equation was used:

$$\frac{d\rho}{d\varepsilon} = h\rho^{\zeta} - r\rho \qquad \text{(Equation 2-28)}$$

where ζ is a constant. This equation is able to represent Estrin & Mecking ($\zeta = 0$) model, as well as Kocks-Mecking ($\zeta = 1/2$) relationship, which can be found in Equation 2-2 and Equation 2-1 respectively.

A general form of the total number of new grains appearing per unit time was chosen to account for any physical type of nucleation:

$$\left(\frac{dN}{dt}\right)^{+} = k\bar{\rho}^{p}\sum D_i^2 \qquad \text{(Equation 2-29)}$$

where k is a temperature-dependent nucleation parameter and p a positive exponent. During the time increment dt, the increase of N^{+} is assumed to be proportional to the total surface of grain boundaries.

Using these above simple equations, the model was proved to be able to describe the fact that steady-state flow stress is independent of initial grain size. Figure 2-20 shows a series of curves computed numerically by their model, which demonstrates the qualitative behavior of the system for different initial average grain sizes. The flow stress, as well as the average grain size, converges to a steady-state value. The single peak and multiple peak behavior are captured by the numerical model. It is also important to notice that grain coarsening was captured for the cases where apparent multi-peak behavior of flow curves was observed.

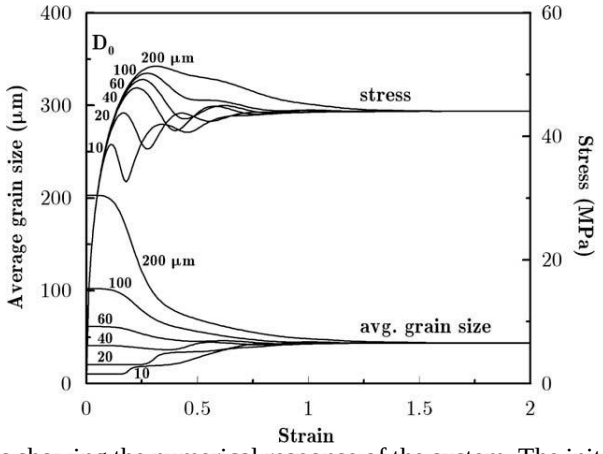

Figure 2-20 Bundle of curves showing the numerical response of the system. The initial grain size varies between 10 and 200 µm, and the curves from the multiple peak behavior to the single peak one. The stress and average grain size tend to a unique steady-state value. [76]

Quantitative agreement with experimental data on 304L steel is only reported on the stress-strain curves before the onset of recrystallization.

2.4.5.5. The model of Cram *et al.*

A physically based model for nucleation during DDRX has been developed by Cram *et al.* [77] and is coupled with polyphase plasticity and grain growth models to predict the macroscopic stress and grain size evolution during straining

The nucleation model is based on a recent description for static recrystallization and considers the dynamically evolving substructure size. Grain boundary bulging was considered as the only mechanism for nucleation of DRX grains, the effect of annealing twins at larger

strains was neglected. It is assumed that a nucleation event can occur during DRX when a subgrain located on a grain boundary reaches a critical radius, r_c. The critical subgrain size (Equation 2-30) corresponds to the condition when the stored energy of grain i is large enough to overcome the capillary force of a subgrain of radius r_i, lying on the grain boundary of grain i, as illustrated in Figure 2-21:

$$r_{c,i} = \frac{2\gamma_b}{\frac{1}{2}\mu b^2 \rho_i} \qquad \text{(Equation 2-30)}$$

The evolution of the average subgrain size ($\bar{r}_i$) of grain i is assumed to have two linearly additive competing terms: a term which increases the average subgrain size due to subgrain Growth ($(d\bar{r}_i/dt)^+$) influenced by capillary effects, and a term which decreases the average size due to the increasing stress applied on the dislocation structure ($(d\bar{r}_i/dt)^-$).

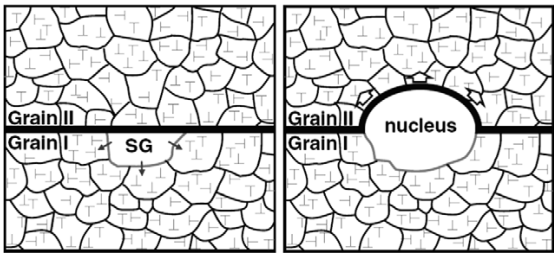

Figure 2-21 Schematic illustration of a subgrain growing (left) and once it reaches the critical size (right) bulging into the deformed matrix as a new strain-free grain [78].

From a preset subgrain size distribution as shown in Figure 2-22, a fraction of subgrains within each grain that have a size greater than the critical size will exist, which are large enough to nucleate. This fraction is shown as the shaded area in Figure 2-22.

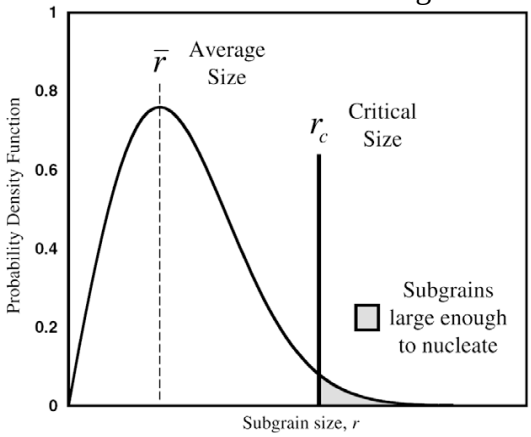

Figure 2-22 The subgrain size distribution within each grain of average radius $\bar{r}$. The shaded area represents the fraction of subgrains larger than the critical size r_c. [77]

The evolution of grains is driven by the stored energy difference between the individual grain (ρ_i) and the surrounding medium ($\bar{\rho}$), which is similar to that used by Sandstrom and Lagneborg [74], Motheillet *et al* [76].The model has been able to successfully predict most of the key features of DDRX:

1) The transition from single to multi-peak stress response in agreement with the experimental criteria, depending on deformation temperature, strain rate and initial grain size :

2) Steady-state grain sizes and stresses which are independent of the initial grain size and dependent only on the hot-working conditions.

3) A power-law relationship between the steady-state grain size and steady-state stress.

The model was however unable to predict the significant stress softening that is experimentally observed at high strain rates. Besides, the influences of temperature, strain rate and initial grain size on DRX kinetics were not analyzed.

2.4.5.6. The model of Fan *et al.*

Fan *et al*. [79] established a theoretical model which links the metallurgical principles of dynamic recrystallization, i.e. nucleation, recrystallized grain growth, impingement and dislocation density variation. Two new state variables: mobile grain boundary area and immobile grain boundary area are introduced, which were oversimplified by Sandstrom and Lagneborg [74] in their model.

Both mobile and immobile grain boundary area per unit volume evolve with nucleation, growth of recrystallized grains and impingement, which take the following form:

$$\frac{dS_m}{dt} = \left.\frac{dS_m}{dt}\right|_{nulceation} + \left.\frac{dS_m}{dt}\right|_{growth} + \left.\frac{dS_m}{dt}\right|_{imping} \quad \text{(Equation 2-31)}$$

$$\frac{dS_{im}}{dt} = \left.\frac{dS_{im}}{dt}\right|_{nulceation} + \left.\frac{dS_{im}}{dt}\right|_{growth} + \left.\frac{dS_{im}}{dt}\right|_{imping} \quad \text{(Equation 2-32)}$$

The reader is referred to [79] for more details of the calculation.

The velocity of grain boundary migration takes into account of both the stored energy term related to the dislocation content, and a capillarity term related to the grain boundary energy and curvature:

$$v = mf = m(\tau\rho - \frac{2\gamma_b}{r}) \quad \text{(Equation 2-33)}$$

where γ_b is the grain boundary energy, τ is the dislocation line energy.

When recrystallizing grain boundaries sweep through the material, the dislocation structures are annihilated, but concurrent work hardening and recovery gradually rebuild them. The KM model, see (Equation 2-1), was used to predict the variation of dislocation density by strain hardening and dynamic recovery, and flow stress σ is calculated according to (Equation 2-21).

The onset of nucleation occurs when the dislocation density of the deformed material reaches to a critical value, which takes the same form as (Equation 2-16), as proposed by Roberts and Ahlblom [57]. The volume nucleation rate $\dot{n}$ was defined as the number of new recrystallizing nuclei per unit grain boundary area per unit time, see (Equation 2-34), so that the influence of grain size on nucleation rate can be considered, and at the same time, the important role of the grain boundaries in providing nucleation sites for DRX was automatically considered.

$$\dot{n} = C\dot{\varepsilon}^m \exp(-\frac{Q_a}{RT})(\frac{r^*}{r_0})^2 \quad \text{(Equation 2-34)}$$

where r_0 is the radius of recrystallizing nuclei, r^* is a reference nucleus radius and equals to the value of r_0 at a given condition where the constant C is evaluated.

The predictions of flow stress are in good agreement with experimental observations. Predicted stress-strain curves show oscillation at high temperatures and low strain rate. A

single peak is observed when the temperature is low, and muti-peak can be found at low strain rates.

The recrystallization kinetics was also well captured by their model numerically, both high temperature and low strain rate promote recrystallization, as illustrated in Figure 2-23. When it comes to experimental verification, even though the data is limited, it tends to overestimate the percentage of DRX in the beginning and underestimate it at large strain.

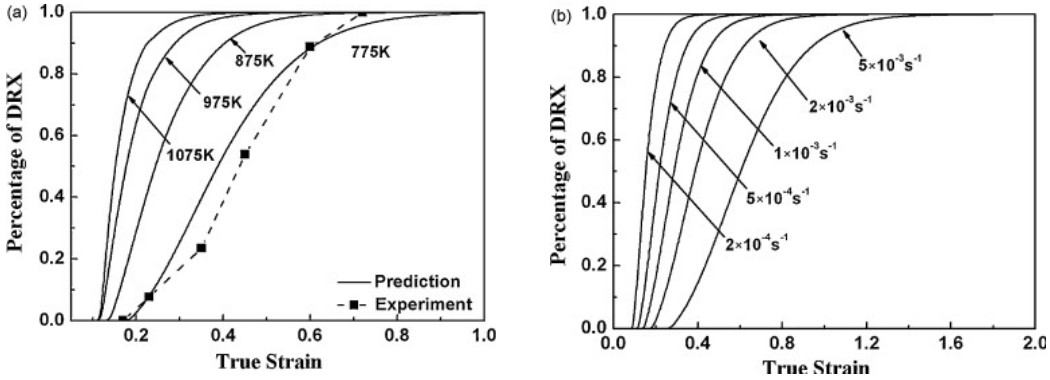

Figure 2-23 Influence of strain rate and temperature on the percentage of DRX: (a) influence of temperature at a fixed strain rate of 2×10^{-3} s^{-1} (b) influence of strain rate at a fixed temperature of 775 K. The experimental results were presented by Blaz *et al*. for copper [35]. [79]

The effect of initial grain size on the flow stress behavior was also simulated. Multi-peak flow stress was observed when the initial grain is fine, on the other hand, the flow curves of coarse-grain material are characterized by single-peak. The strain peak and stress peak are larger in initially coarse-grained material. The predicted results match well with experimental ones. The steady flow stress was found to be independent from the initial grain size, which was exhibited by the fact that the same steady state flow stress could be reached.

Both the influence of initial grain size on the kinetics of DRX and the fact that the steady state of DRX grain size is also insensitive to initial grain size, as demonstrated by the model of Jin and Cui [80], Montheillet [76], etc., were not addressed by Fan *et al.* [79] in their paper.

2.4.5.7. The models of DRX using other simulation methods

Recently, numerical simulation of DDRX has been undertaken by considering explicit representations of microstructures, meshed in different ways. Some of them fail to be sophistical enough to treat continuously the concurrent recrystallization and grain growth phenomena, especially when it comes to variable strain rate and temperature conditions. Examples include geometrical models [81], network models [82,83]. On the other hand, for numerical simulation models considering explicit representations of microstructures using: Monte Carlo [84,85], cellular automaton [86,87,88,89], phase field [90] and level-set methods [91,92,93,94], the evolution of the microstructure can be captured. The idea behind these approaches is that morphology and topology play a non-negligible role in the evolution of the microstructure, which is difficult to capture with other models. However the explicit representation of microstructures and the need to incorporate a statistical number of grains makes those methods computationally demanding, especially when dealing with 3D microstructures. These limitations also hold true for both SRX and PDRX. More details on the modelling and simulation methods of recrystallization are summarized in a review article by Rollett [95].

To some extent, many of the existing models are similar in the sense that some of the equations (of course not all) are similar. Even though there is a high computational resource

required in these models, the principles inside them are sometimes universal and could be used for semi-analytical models such as mean field models. Among them, the CA model proposed by Kugler and Turk [89], which is capable to predict multi-stage deformation and post-dynamic recrystallization as will be illustrated latter, allows recrystallization kinetics and microstructure evolution to be simulated.

Different from the model of Sandstrom and Lagneborg [74], the KM law was used to track dislocation evolution. Also, the driving force of grain boundary migration is typically composed of two terms: dislocation density difference and grain boundary energy term. Moreover, the boundary energy was considered as a function of the boundary misorientation. More details of this model will be discussed later for the modeling of PDRX. A single-peak flow curve is produced at high strain rates and/or low temperatures (high values of the Zener-Hollomon parameter Z) and multiple peaks at low strain rates and/or high temperatures (low values of Z), which is consistent with experimental observations of DRX under hot-working conditions.

The effect of initial grain size on the shape of the flow-stress curves was also well captured, as presented in Figure 2-24a, where simulations were run for four different initial grain sizes at a temperature of 800 K and a strain rate of 0.002 s^{-1}. It can also be seen that the peak flow stress is higher for larger D_0, and that the steady-state stress is insensitive to D_0, which is in agreement with experimental observations [4]. Figure 2-24b shows all the corresponding average grain size evolutions with strain, which all reach the same steady-state value of 18 μm, irrespective of D_0.

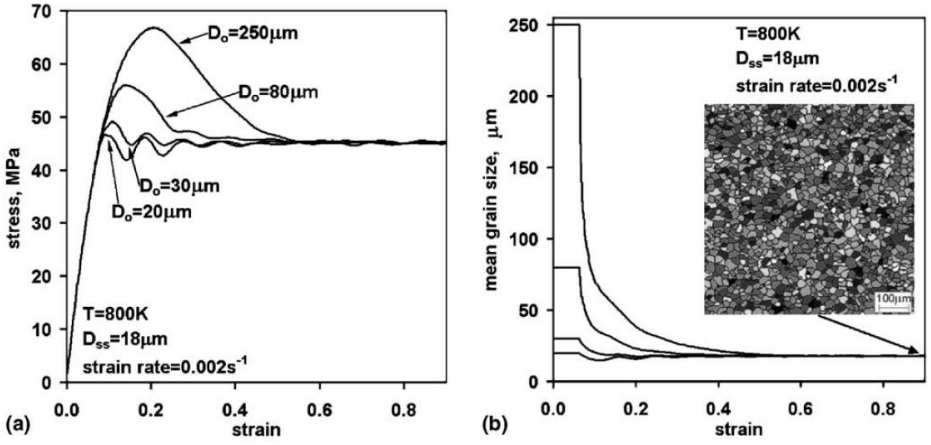

Figure 2-24 Simulated stress–strain curves (a) and dependence of mean grain size on applied strain (b) for different initial mean grain sizes at strain rate of 0.002 s^{-1} and temperature of 800 K. The inset (b) shows the steady-state microstructure [89].

Even though qualitative agreements can be obtained by the model of Kugler and Turk [89], experimental verification is unfortunately missing. And also, the fact that multi-peak behavior of flow stress curve usually corresponds to grain coarsening ($D_{ss} > D_0$) was not well captured by their model, as can be seen in Figure 2-24b.

2.5. Recrystallization after deformation

Even though difference exists between SRX and PDRX as will be illustrated below, modeling of these two processes is usually combined together.

2.5.1. Softening fraction

The softening fraction during annealing of dynamically recrystallized microstructures was often used due to the fact that it is difficult to distinguish SRX and PDRX [96]. Wilber *et al*. [97] are among the first ones who tried to evaluate the recrystallzation using the interrupted tensile test. The degree of static restoration during unloading, X , was defined by the following equation by Djaic and Jonas [98,99]:

$$X_{off} = \frac{\sigma_m - \sigma_y}{\sigma_m - \sigma_0} \qquad \text{(Equation 2-35)}$$

where σ_m is the flow stress immediately before unloading, and σ_0, σ_y are the yield stress for the first and the second deformation respectively. This is the so called offset method, because σ_0, σ_y are usually assumed to be corresponding to a certain amount of offset strain, from 0.2% to 2%. The measured fractional softening is actually due to the combination effect of recovery and recrystallization processes, and the individual attribution is difficult to distinguish.

At the same time, the lack of a standardized method to evaluate the yield stress leads to a wide variation of the softening fraction X . The offset yield stress using plastic strain ranging from 0.0005 to 0.01 was tested by Xu and Sakai [100] using the above equation, visible differences were found using different defined yield stresses. Other methods such as back extrapolation method (BE method) [101], mean flow stress method [102] or strain recovery method [103,104] were developed. The determination of the parameters used to calculate the softening fraction is detailed in [105].

The comparison of estimated softening fraction using these different methods, and the validation of these methods by quantitative metallographic observations of quenched samples were summarized by Rao *et al*. [104] and Fernandez *et al*. [106]. The offset-stress method, the back-extrapolation stress method and the strain-recovery method, have been utilized by Rao *et al*. [104] for the estimation of fractional softening in hot deformation. They found that the strain recovery method is the best in terms of predicting the softening mechanism realistically, and being able to establish the retained and recovered strains more easily. Three methods, namely the 2% offset, the 5% offset and the mean flow stress method, were proved to be practicable by Fernandez *et al*. [106] in terms of successfully excluding the effect of recovery and more suitably describing the static recrystallization kinetics of a Nb microalloyed steel.

2.5.2. Four mechanisms during recrystallization after deformation

2.5.2.1. Introduction

The deformed structure contains a large amount of stored energy in the form of dislocations, which makes the deformed microstructure thermo-mechanically unstable. After deformation or during deformation intervals, softening processes like static recovery (SRV), static recrystallization (SRX) or post-dynamic recrystallization (PDRX) are related to the level of accumulated strain. When dislocation densities have been reduced to the minimal value everywhere, no driving force exists anymore for these processes, normal grain growth proceeds to reduce the total surface energy.

2.5.2.2. Static recovery

Static recovery phenomenon competes with static recrystallization, as both are driven by the stored energy of the deformed state. Static recovery is defined (see section 2.2.2) as the decrease in density and change in distribution of the dislocations and other defects that takes place during annealing, where these changes do not involve the sweeping of the deformed material by migration of high angle boundaries [107]. Interrupted strain, annealing temperature, as well as the nature of the material all have an influence on static recovery. However, the stacking fault energy (SFE) of the material is the most important factor in affecting the extent of recovery, because it determines the mechanisms that control the rate of recovery: rate of dislocation climb and cross slip [1]. The driving force for dislocation climb or cross slip is the decrease of the stored energy. Metals of moderate or low SFE (austenitic stainless steel, copper, nickel etc.) polygonize less readily than those of high SFE (aluminum, ferrite, etc.), and thus cell structure is less obvious. After deformation, the mechanical and microstructural changes during recovery in austenitic stainless steel are subtle and occur on a small scale, it is generally ignored [1].

2.5.2.3. Static recrystallization

Static recrystallization may occur if a material is deformed to a strain lower than the critical strain for DRX at the corresponding temperature, but with sufficient stored energy to drive the recrystallization when it is subsequently annealed. A strain of about 10% is required to initiate classical SRX [108].

New SRX grains usually nucleate preferentially where the local deformation is the highest, i.e. on pre-existing grain boundaries, deformation bands and inclusions. The process of nucleation is thermally activated and a detectable incubation time is usually required [1]. Three different mechanisms of nucleation have been proposed for SRX: strain induced grain boundary migration (see section 2.3.1), subgrain growth or polygonization (see section 2.3.2), subgrain coalescence (see section 2.3.3).

Once a high angle boundary is formed, it is capable to move forward into deformed material. The migration velocity of such boundaries is quite sensitive to the presence of impurities, the structure of the grains into which they are migrating, and the orientation relationship between the growing grains and the deformed matrices as well. The moving grain boundary must drag the impurities along, or break away if the concentration of impurities is small enough or the driving force and temperature high enough [107].

Many experimental observations have shown that SRX kinetics can often be described approximately by the JMAK model which often appears in the form of:

$$X = 1 - \exp(-0.693(\frac{t}{t_{50}})^n) \qquad \text{(Equation 2-36)}$$

$$t_{50} = A\dot{\varepsilon}^m \varepsilon^p d_0^q \exp(\frac{Q}{RT}) \qquad \text{(Equation 2-37)}$$

where X : Recrystallizatioin fraction or softening fraction (%)

t : Time (second)

n : Avrami exponent

t_{50} : Time for 50% softening (second)

$\dot{\varepsilon}$: Strain rate (s^{-1})

d_0 : Initial grain size (μm)

Q: Apparent activation energy of SRX (J/mol)

A, m, p, q: Material dependent constants

According to Jonas *et al.* [109], the driving pressure and hence the recrystallization behaviour is strongly dependent on Z. It should be noted that the expression for t_{50} can be rewritten to include Z, which leads to:

$$t_{50} = A \cdot Z^{-m} d_0^q \exp(\frac{Q}{RT}) \qquad \text{(Equation 2-38)}$$

The accumulated strain, initial grain size, strain rate and temperature are proved to have a pronounced effect on the static recrystallization kinetics. Chemical composition of the material, on the other hand, also has significant influence on the kinetics of SRX. All of these affecting factors will be discussed in more detail in section 2.5.3.

In general, 304L has propensity for static recrystallization, which is attributed to its small SFE associated with a reduced degree of dynamic recovery.

2.5.2.4. Post dynamic recrystallization

Whenever the critical strain for DRX (ε_{cr}^{DRX}) is exceeded, recrystallization nuclei will be present in the material. If straining is stopped, but annealing continued, these nuclei will grow with no incubation period into the heterogeneous, partly dynamically recrystallized matrix. This phenomenon is known as metadynamic recrystallization or post dynamic recrystallization (PDRX) [99].

Comparing to the extensive literature available regarding the work on SRX, much less systematic studies have been conducted for the static restoration mechanisms operating after DRX at high strains. The researchers at McGill university are probably the first who investigated the post-dynamic softening of austenite, they proposed a mechanism involving three different restoration processes including recovery, PDRX and SRX based on further metallographic examination on polycrystalline copper [110,111,112]. According to them, the recrystallization nuclei formed during deformation, which grew during straining, continue to grow when the deformation is interrupted. No incubation time is needed, thus PDRX proceeds more quickly than classical SRX. However, full softening cannot be obtained through sole PDRX, subsequent classical SRX provides further softening until the completion of the softening. The softening curve representing this process is characterized by a plateau caused by the incubation time of SRX.

Sakai *et al*. [100,113] later performed further research work on the above subject using a nickel alloy and austenitic steel and provided a detailed description of the above restoration processes. A further softening mechanism, termed post dynamic recovery (PDRV), which takes place in the growing DRX grains that do not recrystallize neither by PDRX or SRX due to the fact that their density is too low for the onset of recrystallization.

The effects of the four softening mechanisms can be distinguished for the three different categories of grains in dynamic recrystallization structure described above, which is summarized below in Figure 2-25 considering three stages. In the first stage, these dynamically formed nuclei grow as a form of PDRX until they are impinged by other growing grains, at the same time, the moderate and fully work hardened grains are softened by PDRV or SRV. After a certain incubation time, classical SRX occurs in stage II in the fully work hardened regions where the dislocation density is still above the critical value for SRX, this continues until the statically formed nuclei impinge with each other, as well as with PDRV and PDRX grains. After the completion of recrystallization, a period of classical grain growth further contribute to the softening process in stage III.

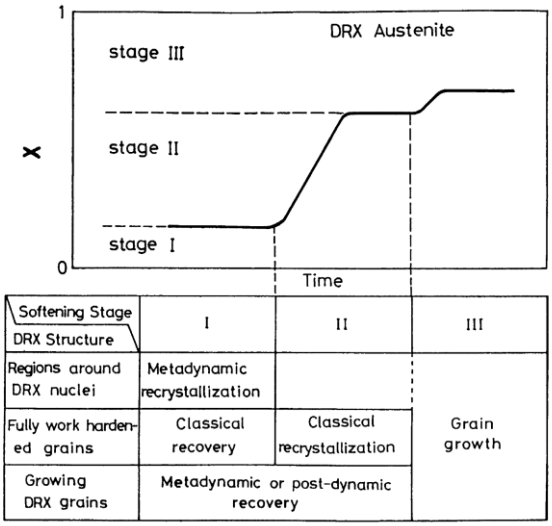

Softening Stage / DRX Structure	I	II	III
Regions around DRX nuclei	Metadynamic recrystallization		
Fully work hardened grains	Classical recovery	Classical recrystallization	Grain growth
Growing DRX grains	Metadynamic or post-dynamic recovery		

Figure 2-25 Schematic illustration showing the relation between each of the softening stages and restoration process operated mainly after DRX [100]

The different mechanisms acting after hot deformation have been further studied by Hodgson *et al*. [114,115,116]. Recently, Hodgson and his co-workers [117,118] investigated the mechanism of PDRX softening in austenite after complete DRX (Figure 2-26a). The initial softening observed at an early stage of post-deformation annealing is due to a rapid growth of the dynamically formed nuclei (MDRX or PDRX according to Jonas *et al*.[99,110,111,112] and Sakai *et al*.[100,113]) having a high migration driving force because of their relatively low dislocation density compared to the adjoining grains (Figure 2-26 a and b). This results in the formation of dislocation-free regions behind the moving boundaries (Figure 2-26b). Progressive disintegration of sub-boundaries within DRX grains through the operation of dislocation climb and dislocation annihilation ultimately leads to the formation of near dislocation-free grains and reduction in the grain boundary migration rate (Figure 2-26 c and d).

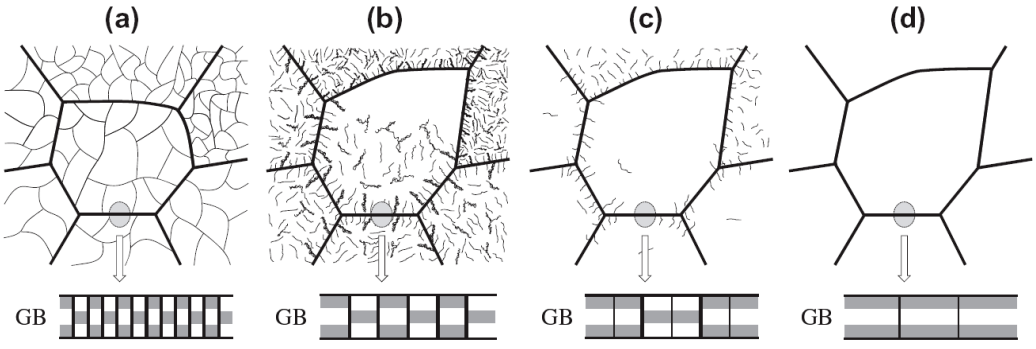

Figure 2-26 Schematic representation of the proposed post-dynamic softening mechanism: (a) the initial DRX state, (b) rapid grain boundary migration and disintegration of sub-boundaries, (c) removal of dislocations from the grain interiors, (d) formation of dislocation-free grains. The insets in (a–d) illustrate a progressive loss of visibility of extrinsic dislocations within the grain boundary (GB) structure [118].

Since the dislocation density decreases with annealing time, the driving force for the grain boundary migration also decreases. Most of the pre-existing DRX grains were found to change in size and become dislocation-free rather than being replaced by newly formed grains during post-deformation annealing [118].

The major difference between SRX and PDRX lies in their kinetic dependencies. PDRX is strongly dependent on strain rate, slightly dependent on temperature and composition, and almost independent of strain. SRX, on the other hand, is largely affected by temperature, strain and grain size and is a weak function of strain rate. It has been proposed by Roucoules *et al*. [115] that all the nuclei are present at the end of the peak strain, and further deformation does not lead to any more nuclei. This explains why softening is strain independent at strain beyond the peak. But, as will be discussed in section 2.5.3.1, dispute still exists over this topic.

2.5.2.5. Grain growth and twin formation

When recrystallization is complete, a dislocation free microstructure can be obtained, but the structure is not yet stable, grain growth (GG) then takes place to reduce the grain boundary energy. The growth of grains appears to be a relatively simple process compared to PDRX where three or four softening mechanisms are involved. However, many important questions remain unanswered despite a large amount of theoretical and experimental efforts [1].

Grain size directly determines the properties, especially the mechanical behavior, which makes it very important for industrial practice. Large grain size is favorable to improve the high temperature creep resistance of the materials, while on the other hand, a small grain size is required to optimize the strength, toughness and fatigue resistance for materials used in structural application at relatively lower temperatures. A good understanding of grain growth is therefore a pre-requisite for control of the microstructures and properties of metals during solid state processing.

The main factors affecting grain growth are: temperature, solutes and particles, as well as texture. The influence of temperature comes from its effect on the migration of high angle grain boundaries, high temperature promotes grain growth. The growth of grain is however inhibited through the pinning of grain boundaries by solutes and second-phase particles, which adds the uncertainties to the control of grain growth. A strongly textured material contains many low angle boundaries with low energy, and therefore also reduces the growth kinetics [1].

A key observation in grain growth is that an isolated small grain will shrink and eventually vanish in response to the tendency to minimize grain boundary area and thus obtain a more stable system. The kinetics of grain growth proposed by Burke *et al*. [119,120] is based on the assumption that the driving pressure (P) on a boundary arises only from the curvature of the boundary:

$$P = \gamma_b (\frac{1}{c_1} + \frac{1}{c_2}) \qquad \text{(Equation 2-39)}$$

where c_1 and c_2 are the two principal radii of curvature in mutually perpendicular directions of a local section of boundary. Observations on a planar section made by quenching the specimen at intervals during growth or by observing continuously with a hot stage microscope or a field emission gun microscope show that boundaries generally migrate towards their centers of curvature, as required by the above assumption about the driving force [121].

For simplicity it is assumed the radius of curvature (c) is proportional to the mean radius (r) of an individual grain (not necessarily spherical) and that γ_b is the same for all boundaries. Since the boundary velocity is proportional to the driving pressure P ,

$$P = \frac{\alpha \gamma_b}{r} \quad \text{(Equation 2-40)}$$

$$\frac{dr}{dt} = mP = m\frac{\alpha \gamma_b}{r} \quad \text{(Equation 2-41)}$$

$$r^2 - r_0^2 = 2\alpha m \gamma_b t \quad \text{(Equation 2-42)}$$

where r is the mean grain size at time t, r_0 is the initial mean grain size and m is the mobility of grain boundary. For ideal static grain growth the value of 2α is ~0.5 in three dimensions and ~1.12 in two dimensions [122,123].

Hillbert [124] conducted a more specific analysis, following (Equation 2-39), a factor g was introduced to take into account the shape of the grain,

$$P = \gamma_b(\frac{1}{c_1} + \frac{1}{c_2}) = \gamma_b \cdot g \cdot (\frac{1}{c_1} + \frac{1}{c_2})_{average} \quad \text{(Equation 2-43)}$$

where g is unity for a spherical grain and somewhat larger for ordinary grains. Considering that large grain will grow, small grains will shrink, and intermediate critical sizes will not move much, a simple relation was proposed,

$$g \cdot (\frac{1}{c_1} + \frac{1}{c_2})_{average} = \beta \cdot (\frac{1}{r_{cr}} - \frac{1}{r}) \quad \text{(Equation 2-44)}$$

where β is a dimensionless constant. And finally, the average growth of each grain is,

$$\frac{dr}{dt} = m \cdot \gamma_b \cdot \beta \cdot (\frac{1}{r_{cr}} - \frac{1}{r}) \quad \text{(Equation 2-45)}$$

where the constant is estimated as $\beta \cong 1$ for 3D system, while the critical size r_{cr} is equal to the mean grain radius ($\bar{r}$), both of which are obtained from topographic consideration. The grain growth equation becomes,

$$\frac{dr}{dt} = m \cdot \gamma_b \cdot (\frac{1}{\bar{r}} - \frac{1}{r}) \quad \text{(Equation 2-46)}$$

Hillbert's result is very similar to the work of Feltham [125] obtained earlier.

Experimentally, it is found that a more general form can be written as:

$$r^n - r_0^n = \eta \cdot t \quad \text{(Equation 2-47)}$$

If $r >> r_0$,

$$r = \eta \cdot t^{1/n} \quad \text{(Equation 2-48)}$$

where η is a constant, n is the grain growth exponent. Values of $1/n$ range from 0.056 to 0.60 according to [15,126], more details can be found in Figure 2-27 for different materials. The failure to follow the theoretical relation (Equation 2-47) can be attributed to the effects of impurities or inclusions and, when these are absent, good agreement is observed [125,127,128].

There are generally two types of explanations for the discrepancy between the theoretical and experimental value for n [1]:

(i) The boundary mobility (m) varies with the boundary velocity

The boundary velocity is not always in linear relation with boundary driving pressure as shown in (Equation 2-41). For the case with high solute concentration, for example, the curve of boundary velocity with respect to driving force is S-shaped instead of linear.

(ii) There is a limiting grain size

Grey and Higgins [129] took into account the solute clusters which are unable to diffuse with the boundary, and introduced a new term C which is similar to the Zener pinning term in two-phase materials:

$$v = m(P - C) \qquad \text{(Equation 2-49)}$$

where C is a constant for the material, which suggests that if the driving pressure P decreases to the value C, there will be no net pressure for grain growth and it will stop at a limiting value.

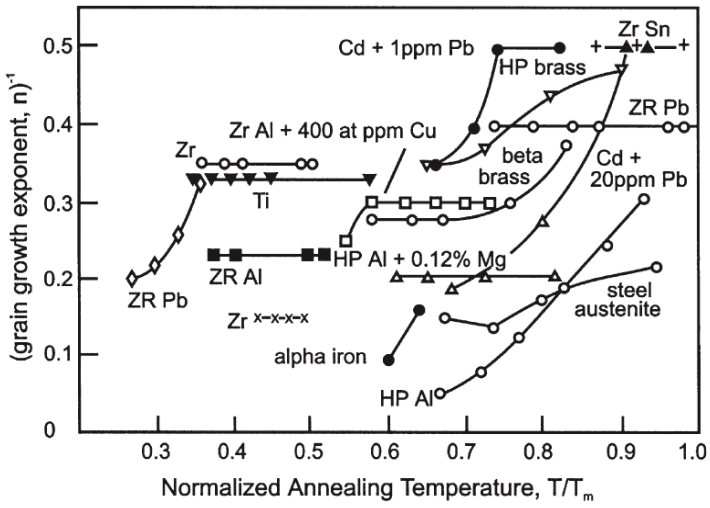

Figure 2-27 The temperature dependence of the grain growth exponent n for isothermal grain growth in a variety of materials [129].

Another important aspect of grain growth is the space-filling requirements of the microstructure, which is neglected in the above analyses. In a two-dimensional grain structure, the only stable arrangement which can fulfill both the space-filling and boundary tension equilibrium requirements is an array of regular hexagons as shown in Figure 2-28a. In order to obtain this condition most boundaries cannot be planar, and hence will migrate towards their centres of curvature (on average) by a process of atom transfer across the boundaries. Figure 2-28b shows how migration of the boundaries towards their centres of curvature gives a four-grain junction which immediately separates into two new three-grain junctions. The growing grains A and C each acquire a new surface as a result of this process and the shrinking grains B and D each lose a surface. By means of processes like this, grains occasionally increase or decrease the numbers of their bounding interfaces, and grains with only three interfaces are periodically eliminated completely.

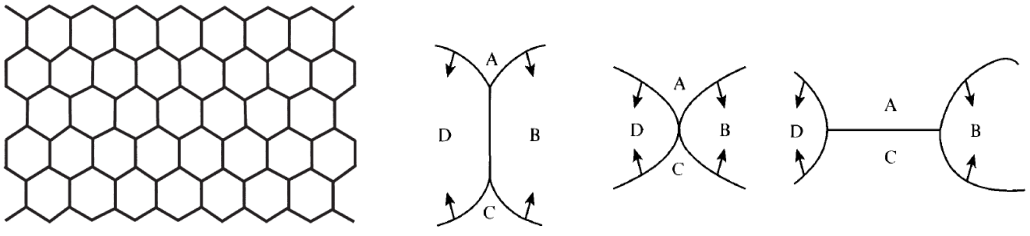

a) b)

Figure 2-28 a) A 2-dimensional array of equiaxed hexagonal grains is stable [1] b) The migration of the grain boundaries in (a) produces the unstable four-grain junction which immediately splits into two new three-grain junctions [121].

The large number of annealing twins, which appear in the recrystallized microstructure, is also a prominent feature of many low SFE F.C.C metals and alloys. They usually appear as paralled-side bands bounded by coherent {111} planes but occasionally the twins terminate within a grain on some other interface, as shown in Figure 2-29. During annealing, the {111} twin interfaces are very immobile, but the other interfaces often migrate. A F.C.C. twin is equivalent to a growth fault and may be considered to arise after a growth accident. If stacking

faults exist in the deformed matrix, there is obviously a favourable situation for twin formation when a growing grain reaches a fault. This is supported by a good correlation between the density of stacking faults as measured by X-rays and the frequency of annealing twins after recrystallization [121].

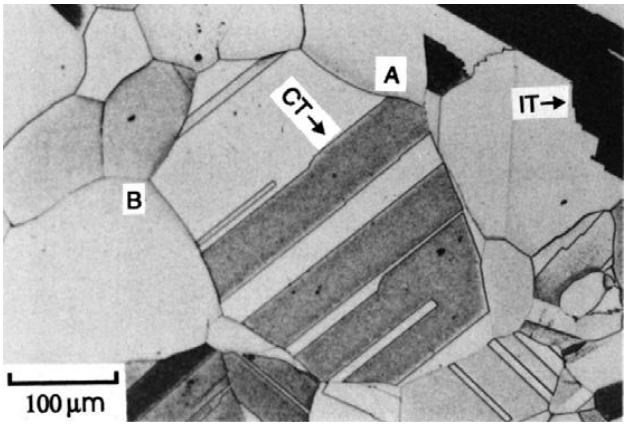

Figure 2-29 Annealing twins in annealed 70:30 brass. Some coherent (CT) and incoherent (IT) twin boundaries are marked, (courtesy of M. Ferry).

The standard theory of twin formation is proposed by Fullman and Fisher [130] and is illustrated schematically in Figure 2-30. Since grain growth is occurring such that the triple point between grains S, U and V is moving horizontally, during this process, it is assumed that a growth fault may occur at some point leading to the formation of a grain (T) which is twinned with respect to grain S and initially small. Despite the extra boundary area created, the total interfacial free energy will decrease if:

$$S^{ST}\gamma_b^{ST} + S^{TU}\gamma_b^{TU} + S^{TV}\gamma_b^{TV} < S^{TU}\gamma_b^{SU} + S^{TV}\gamma_b^{SV} \qquad \text{(Equation 2-50)}$$

where S^{ST} etc. are the surface areas and γ_b^{ST} etc. are the specific free energies of the various interfaces. When (Equation 2-50) is satisfied, the boundaries moving away from the triple junction will finally lead to a macroscopically twinned region T.

As the twin boundary energy will be very low when the twin interface is fully coherent, there is a reasonable probability of the inequality being valid. A sufficient difference in the right-hand side of this equation might come from two different ways. Firstly, when the SU, SV interfaces are high angle boundaries and the TV, TU interface are low angle boundaries, or an approximation to a twin boundary. The other possibility is that both boundaries are high angle but the TV, TU boundaries are special or coincident site boundaries of low energy.

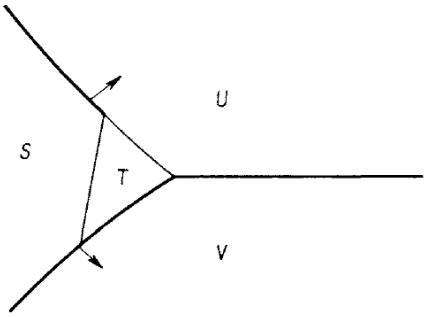

Figure 2-30 The formation of an annealing twin at a three-grain junction (after Pullman and Fisher [130]).

The Fullman-Fisher theory also applies to the situation shown in Figure 2-31 where a new grain contact is established between grains S and V. If a twin has an orientation close to that of

grain V then the TV interface will have low energy and the configuration with the twin will have a lower energy than the configuration without it. A possible sequence leading to the formation of a terminated twin is shown in Figure 2-31. The coherent twin interface becomes tangential to the main migrating grain boundary, after which another interface must form.

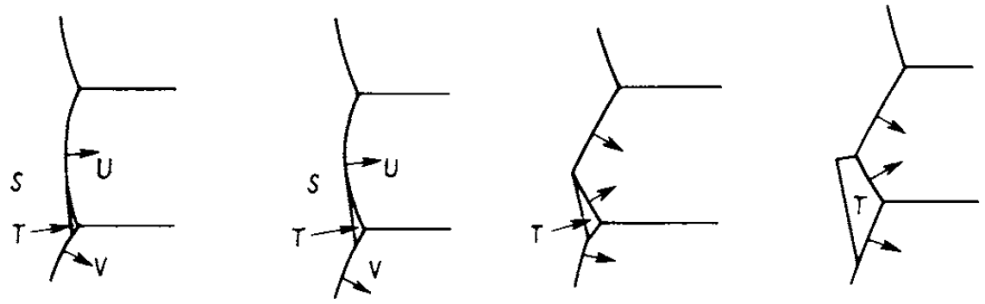

Figure 2-31 Formation of a twin with a coherent and a non-coherent interface during grain boundary migration (after Fullman and Fisher [130]).

The Fullman-Fisher theory is supported by direct observations of twins at moving grain corners [119,131]. A parallel-sided twin which crosses a grain may be explained by a second growth accident which restores the original orientation S. This would be energetically unfavourable if T is still in contact with U and V, but could still occur at a later stage of recrystallization when T is growing into quite different grains.

Special boundaries promote this mechanism because they combine a low energy with a high mobility. Annealing twins played an important role during the recrystallization process. When a grain appeared to stagnate in growth, it would often twin and rapid growth would resume [132]. The number of twin lamellae was found to be proportional to the number of triple point interactions by Hu and Smith [133] in alpha and alpha-beta brasses, which suggests that the type of sequence shown in Figure 2-31 is frequent. The actual atomistic mechanism of twin formation during grain growth is however out of the scope of this review, and can be found in the textbook of Humphreys and Hatherly [1].

2.5.3. Factors affecting the recrystallization behavior after hot deformation

2.5.3.1. Effect of stop strain

Djaic and Jonas [99] studied the static softening by interrupted compression tests on 0.68% C steels at 780 ℃. As illustrated in Figure 2-32, at the smallest accumulated strain (Figure 2-32b, curve a) in the work hardening region of the flow stress, static recovery is the sole mechanism which leads to about 30% of softening. Softening occurs by means of both static recovery and SRX after higher accumulated strain, and a single inflection plateau can be observed (Figure 2-32b, curve b). When deformation is stopped in a place on the flow curve between peak stress and steady state stress, DRX is followed by PDRX, static recovery, SRX, and the softening curve is characterized by two inflection plateaus (Figure 2-32, curve c). If the stop strain goes further, in the steady state region, static recovery and PDRX are the responsible mechanisms for softening, one plateau or single sigmoidal curve can be obtained (Figure 2-32, curve d).

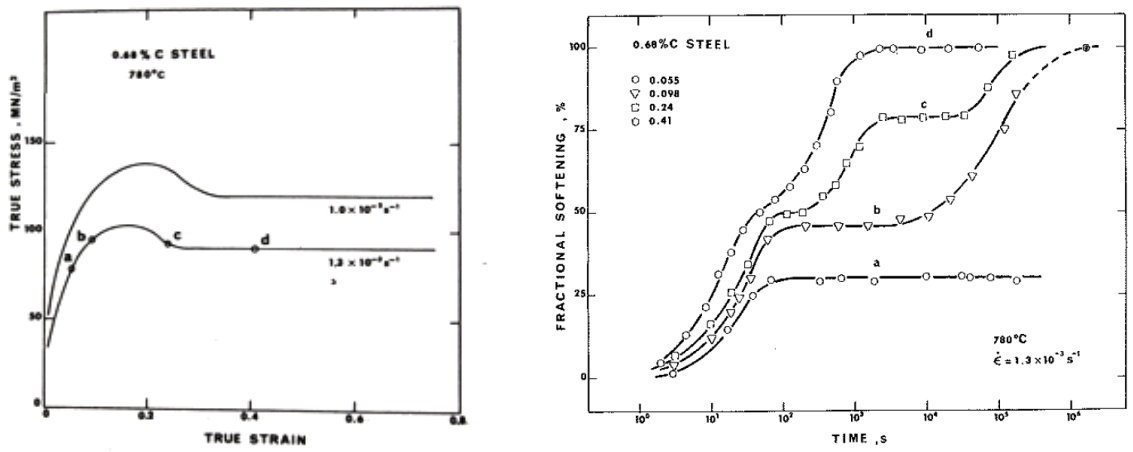

a) b)

Figure 2-32 a) Flow curves for AISI C1060 carbon steel compressed at 780◦C, the one deformed at $1.3\times10^{-3}s^{-1}$ was used to study softening in b), letters a,b,c,d in the represent the interruption strains, b) Effect of strain on the static softening of a 0.68% C steel [99]

Jonas and his co-workers continued their work on kinetics of softening after hot deformation of steel [108], and copper [111,112], and similar type of softening behavior was again acquired.

On the other hand, the fractional softening was measured by Dehghan-Manshadi *et al*. [134] as a function of un-loading time for different applied strains (all of them are beyond the critical strain for DRX) and for a given deformation condition (same temperature and strain rate). The material examined was 304 stainless steel, with an initial grain size of $d_0 = 35\mu m$. As shown in Figure 2-33a, the softening follows a typical sigmoidal behavior for all the applied strains, similar shapes were also obtained by Di Schino and Kenny for AISI 316 stainless steel [135]. Obviously, this contradicts with the observation by Djaic and Jonas [99], who claim that two softening plateaus can be seen for PDRX if the stop strain is between the peak stress and steady state stress. It is clear from Figure 2-33b that smaller prior strains produce bigger grain size at the same heating time or softening fraction, the same tendency has also been reported by other research works [114,135,136]. The decrease and then increase in the average grain size with increasing un-loading time is an indication of the formation of new small SRX and PDRX grains and the growth of these grains, respectively.

For classic SRX, an increase in the applied strain can increase the SRX kinetics by the increase of the amount of nucleation sites, and also lead to a shorter incubation time to initiate SRX [111,137].

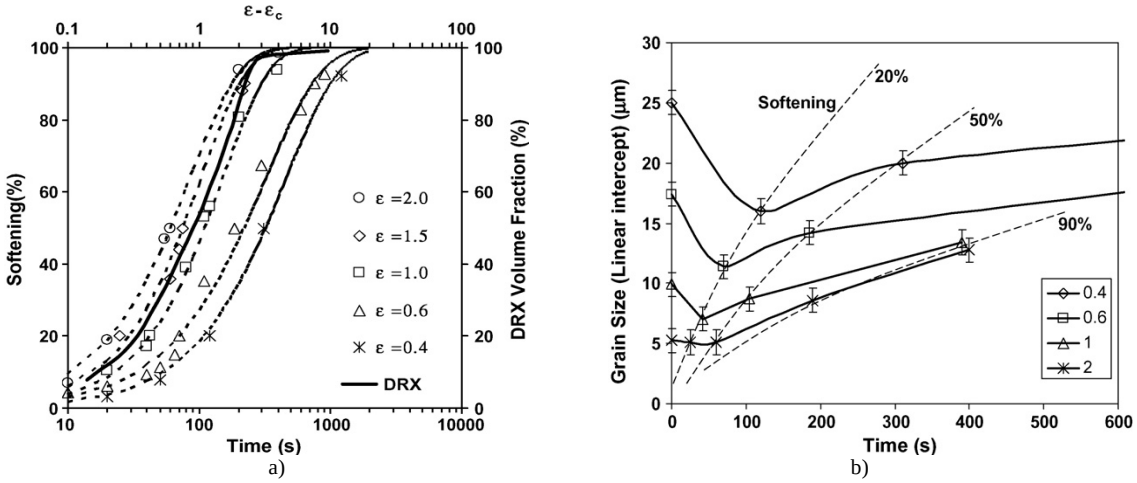

Figure 2-33 a) The average grain size (linear intercepts) as a function of un-loading time at different strains, for deformation at 900 ◦C and a strain rate of 0.01 s^{-1} b) The effect of applied strain on the softening fraction at 900◦C and a strain rate of 0.01 s^{-1} [134] .

Therefore, the discussion regarding the recrystallization kinetics after hot deformation still opens. More experimental data are needed in order to clarify the softening fraction behavior and further understand of the mechanisms behind this.

2.5.3.2. Effect of temperature and strain rate

Temperature is found to have a profound influence on SRX kinetics [4] through affecting the nucleation rate and the mobility of grain boundaries. Strain rate also promotes the kinetics of SRX, which is due to the reduced extent of dynamic recovery at higher strain rates. But usually the effect of strain rate on SRX kinetics is less significant than the effect of temperature [138].

The weak dependence of the softening rate of PDRX on temperature was found for C-Mn steel [114], HSLA steels [115] and carbon steels [139]. However, stronger relation between temperature and PDRX kinetics was found for 304 austenitic stainless steel [150] and hypereutectoid steel [140], as well as carbon steel [108]. This effect was ascribed to the increasing mobility of the grain boundaries during both SRX and, which outweighs the decreased driving force due to static recovery. Recently, the times for 50% softening (t_{50}) obtained by Dehghan-Manshadi *et al*. [134] using 304 austenitic stainless steel again showed that softening kinetics increased with temperature (Figure 2-34a), this effect can still be found when the strain is bigger than the transition strain (ε_T) where the softening becomes strain independent.

It is believed that strain rate has a pronounced influence on the PDRX kinetics for different materials [108,114,115,139,140]. This was also proved by Dehghan-Manshadi *et al*.[134] with 304 austenitic stainless steel, which is clearly illustrated in Figure 2-34b. At a given strain, the time for 50% recrystallization decreased with increasing strain rate.

The effect of temperature, strain rate on the rate of softening of PDRX were also analyzed by Cho *et al*. [141] on 304 austenitic stainless steel, who obtained similar conclusions as mentioned above.

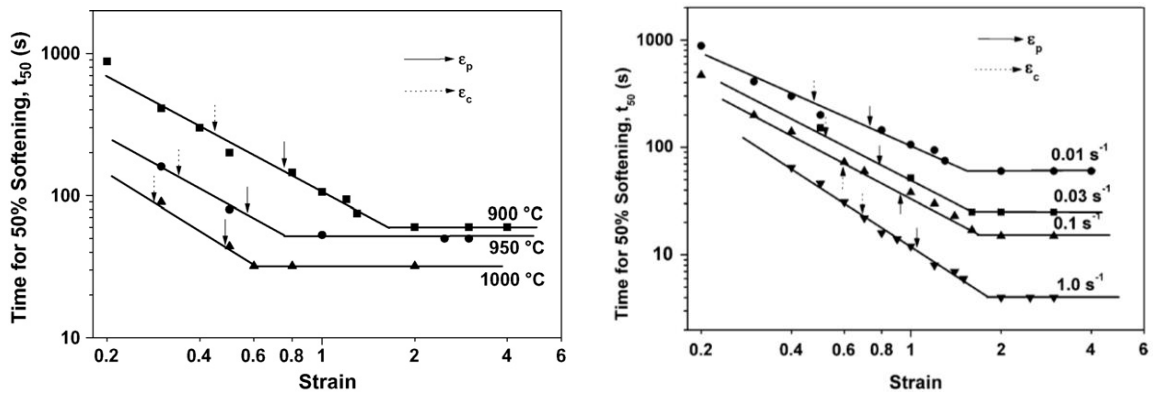

a) b)

Figure 2-34 a) The time for 50% softening after deformation at different temperatures and a constant strain rate of $0.01\ s^{-1}$ b) The time for 50% softening after deformation at different strain rates as a function of applied strain. Also superimposed are the DRX volume fraction for strain rates of 0.01 and 1.0 s^{-1}. [134].

Besides the kinetics of softening, the grain size after hot deformation is also affected by temperature and strain rate to different extents. It has been observed that the PDRX grain size decreases with decreasing temperature and increasing strain rate. Using three different steels, a general equation was obtained by Roucoules [136] which is similar for the one related to the time for 50% PDRX:

$$d_{pdrx} = A\dot{\varepsilon}^{-B} \exp(-\frac{Q_C}{RT}) \qquad \text{(Equation 2-51)}$$

where A, B, Q_C, are positive constants and can be found in [136].

The microstructural evolutions during PDRX of 42CrMo steel were investigated by Lin and Chen [142] using hot compression deformation tests, similar results were obtained. Dehghan-Manshadi *et al*. [134] examined 304 austenitic stainless steel, and it was found the recrrystallized grain size after PDRX (fully recrystallized state) is directly linked with Z, which is shown in Figure 2-35.

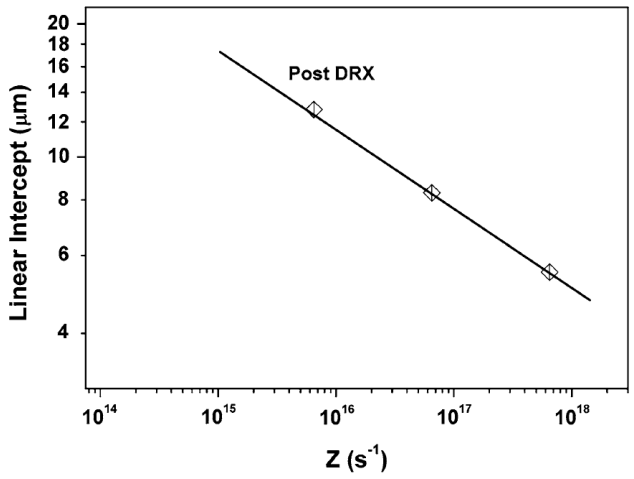

Figure 2-35 Dependency of postdynamic recrystallized grain size of 304 stainless steel to Z [134].

2.5.3.3. Effect of initial grain size

As new SRX grains usually nucleate on the pre-existing grain boundaries, initial grain size will naturally affect the kinetics of SRX by changing the number of nucleation sites. It has been

shown that initial grain size has a pronounced effect on the kinetics and microstructure of SRX [143,144]. Sellars [145] obtained equations (see (Equation 2-52)and (Equation 2-53)) for time to 50% recrystallization (t_{50}) and for recrystallized grain size (d_{rex}) based on the analysis of published data on C-Mn steels. The dependence of initial grain size is clear in the equations:

$$t_{50} = 2.5\times10^{-19} d_0^2 \varepsilon^{-4} Z^0 \exp(\frac{300000}{RT}) \quad \text{(Equation 2-52)}$$

$$d_{srx} = 0.5 d_0^{0.67} \varepsilon^{-1} Z^0 \quad \text{(Equation 2-53)}$$

For PDRX, which consists of the growth of DRX nuclei, the effect of initial grain size on its kinetics is expected to be lower, for example, the following equations were established by Sellars [145] based on experimental data:

$$t_{50} = 1.06\times10^{-5} Z^{-0.6} \exp(\frac{300000}{RT}) \quad \text{(Equation 2-54)}$$

$$d_{pdrx} = 1.8\times10^{3} Z^{-0.15} \quad \text{(Equation 2-55)}$$

However, Lin and Chen [142] found by hot compression of 42CrMo steel that the final grain sizes rapidly increases with increasing the initial austenitic grain sizes when the initial austenitic grain size is less than a critical value. If the initial grain size is higher than this value, no influence will persist on the final grain size. The considerable effect of initial grain size on both the strain dependent and strain independent regions was observed by Dehghan-Manshadi *et al.*[60] even though its influence on the strain-dependent region is stronger (see Figure 2-36).

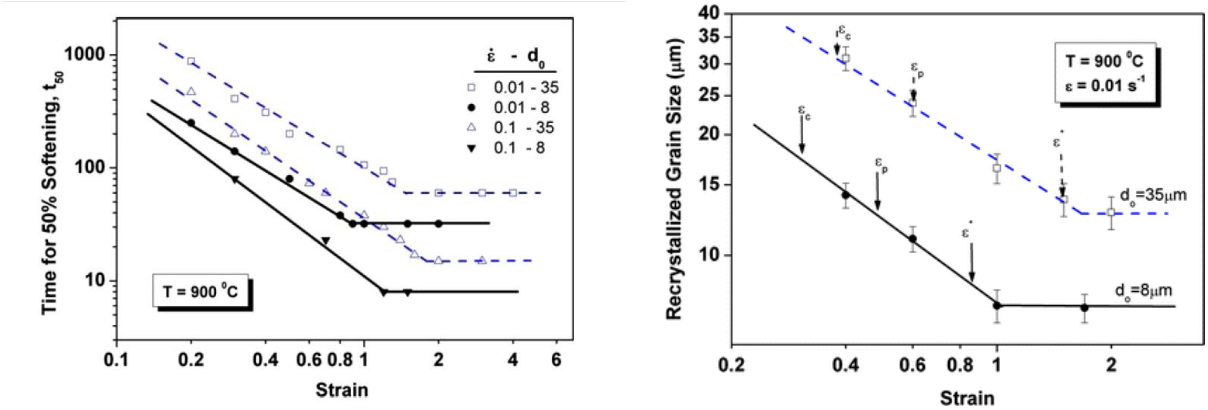

Figure 2-36 a) Time for 50% softening as a function of strain, 304 stainless steel, b) Post deformation recrystallized grain size as a function of strain for fine- and coarse-grain materials, 304 stainless steel. [60]

To summarize, it is generally accepted that initial grain size will affect both the kinetics and microstructure of SRX. On the other hand, it is still unclear whether or not it has an influence on PDRX. It seems the initial grain size dependence is strongly connected to the material itself.

2.5.4. Modelling of recrystallization after deformation

2.5.4.1. JMAK modeling

Substaintial research works has been performed to describe the microstructure evolution after hot deformation using the JMAK equation approach. The kinetics modeling of SRX by JMAK modeling is summarized below in Table 2-2, it is important to notice that the

dependence of softening fraction on the initial grain size was found for all materials reviewed.

Table 2-2 The SRX kinetics models for stainless steel were summarized below:

Material	t_{50} model	Reference
Nb steel	$t_{50}=1.9\times10^{-18}d_0^2\varepsilon^{-2.8}\dot{\varepsilon}^{-0.41}\exp(\frac{32400}{RT})$	[146]
304 stainless steel	$t_{50}=2.0\times10^{-10}\varepsilon^{-1.56}\dot{\varepsilon}^{-0.81}d_0(\frac{197000}{RT})$	[141]
	$t_{50}=3.72Z^{-0.38}d_0^2(\frac{425000}{RT})$	[144]
	$t_{50}=4.0\times10^{-5}Z^{-0.375}\varepsilon^{-4}d_0^2(\frac{365000}{RT})$	[147]
C-Mn steel	$t_{50}=2.1\times10^{-16}d_0^2\varepsilon^{-3.1}\dot{\varepsilon}^{-0.43}\exp(\frac{26400}{RT})$	[148]
Nb-V steel	$t_{50}=1.57\times10^{-14}d_0^2\varepsilon^{-2.9}\exp(\frac{21700}{RT})$	[149]

PDRX kinetics is also characterized by the typical sigmoidal shape, which suggests that it can also be represented by the JMAK model [115]. Some equations applied to steels are listed below in Table 2-3.

Table 2-3 PDRX kinetics models

Material	t_{50} model	Reference
304 stainless steel	$X=1-\exp(-0.693(\frac{t}{t_{50}})^{1.1})$	[134]
	Strain dependent $t_{50}=8.0\times10^{-9}\varepsilon^{-1.48}Z^{-0.42}(\frac{375000}{RT})$	
	Strain independent $t_{50}=2.7\times10^{-2}Z^{-0.61}(\frac{292000}{RT})$	
304 stainless steel	$X=1-\exp(-0.693(\frac{t}{t_{50}})^{1.06})$	[150]
	$t_{50}=1.33\times10^{-11}\dot{\varepsilon}^{-0.41}d_0\exp(\frac{230300}{RT})$	
C-Mn steel	$t_{50}=8.4\times10^{-9}\dot{\varepsilon}^{-0.84}\exp(\frac{186000}{RT})$	[146]
Nb austenite	$t_{50}=4.3\times10^{-8}\dot{\varepsilon}^{-0.84}\exp(\frac{160000}{RT})$	

The equation for 50% recrystallization in this case can be simplified since strain and initial grain size have almost no influence on the kinetics, which leads to the following form:

$$t_{50}=A\dot{\varepsilon}^{p}\exp(\frac{Q}{RT}) \qquad \text{(Equation 2-56)}$$

where t_{50}: Time for 50% softening (second), $\dot{\varepsilon}$: Strain rate (s^{-1})

Q: Apparent activation energy of PDRX (J/mol)

A, p: Material dependent constants

A more complex model using the JMAK approach has been developed by Uranga *et al*.[151] recently, where a transition strain ε_T, $\varepsilon_{cr} < \varepsilon_T < \varepsilon_{ss}$, separating the post-dynamic softening strain-dependent range from that which is strain-independent, was introduced. At strains below ε_{cr}, SRX is the only softening mechanism. At strains above ε_T, the kinetics of recrystallization is independent of strain but strongly dependent on strain rate. At strains between ε_{cr} and ε_T, both PDRX and classical SRX are involved in post-dynamic softening. JMAK equations were established for these three different regions.

The JMAK analysis is based on the assumptions that the recrystallized nuclei form randomly in the cold-worked microstructure and that the growth of these nuclei is isotropic. The ideal JMAK behavior is rarely exhibited by real materials. For many materials, the JMAK exponent obtained experimentally is smaller than that predicted by the JMAK analysis. Also, the JMAK exponent varies during recrystallization, and a significantly smaller exponent is obtained at the later stages of recrystallization. Such a deviation from ideal JMAK behavior is due to the presence of recovery, non-uniform distribution of stored energy of deformation, non-random distribution of recrystallized nuclei, and anisotropic growth of the recrystallized nuclei [152].

2.5.4.2. Physically based models

There are increasing demands from many major metal producing companies, particularly in the aluminum and steel industries, to develop models which are based on sound physical concepts in order to have predictive capabilities in complex (industrial) conditions[153]. Only coupled models or multi-pass models which may involve two or even more physically based models, deformation and annealing models for example, can be successfully used to simulate a real industrial process such as multi-pass hot rolling. A small number of these models were found in the literature, and two examples are listed below:

(i) The model of Roucoules et al.

Based on the Sandstrom and Lagneborg approach [74,154], a mathematical model has been developed by Roucoules *et al*. [51] which describes the hot deformation and recrystallization behavior of austenite using a single internal variable: dislocation density. The dislocation density is incorporated into equations describing the rate of recovery and recrystallization. The basic model equations used are listed below in Table 2-4

Table 2-4 Basic model equations

Process	Condition	Equation
Hardening	$\dot{\varepsilon} > 0$	$d\rho/d\varepsilon = 1/bl$ (1)
Recovery	Always	$d\rho/d\varepsilon = k_0 - k_2\rho$ (3)
Recrystallization	$\rho > \rho_{cr}$	$dX/dt = v\gamma/Dm\tau G_i\rho_i$ (4)
Grain refinement	$\rho > \rho_{cr}$	$dD/dt = -D dX/dt \ln N$ (5)
Grain growth	Always	$dD/dt = \sigma_s m_o/D \exp(-Q_m/RT)$ (6)

Even though no distinction is made between static and dynamic events, the model seems to be able to simulate multi-pass processes. After tuning the model parameters using available data the model gave an accurate prediction of the stress-strain behavior and the static recrystallization kinetics for C-Mn steels, which is shown in Figure 2-37.

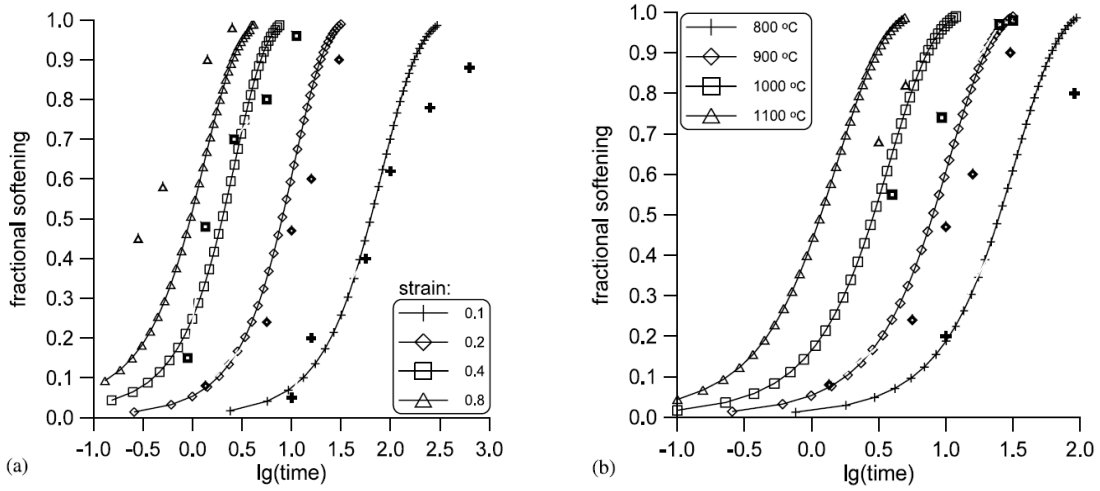

Figure 2-37 Comparison of the experimental and predicted softening curves, (a) effect of strain and (b) effect of temperature [51].

The model successfully predicted the sensitivity of the post deformation recrystallization behavior to affecting factors such as strain, strain rate and temperature. The model was able to demonstrate that PDRX kinetics is a weak or independent function of strain and temperature, but a strong function of strain rate, which is illustrated in Figure 2-38. This is in accordance with some of the experimental results. It is important to point out, however, that temperature and strain dependence of PDRX were sometimes observed to be significant for some materials, see sections 2.5.3.1 and 2.5.3.2

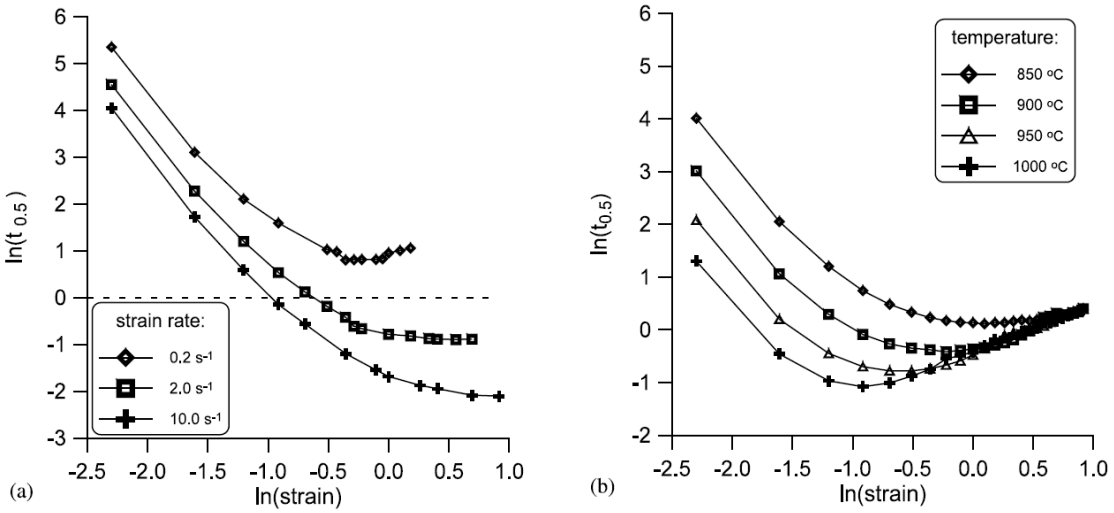

Figure 2-38 Evolution of the time for 50% recrystallization with strain at different (a) strain rates and (b) temperatures predicted by the model [51].

Due to the lack of detailed knowledge in the literature, the model contains a large number of simplifications of the envisaged physical processes. Moreover, the recrytallized grain size, which is of interest in most of the industrial applications, was not analyzed (it is introduced as seen in Table 2-4). Finally, the mechanisms that take place during dynamic and static recovery or during dynamic, static or metadynamic recrystallization are assumed to be the same.

(ii) The model of Kugler and Turk

Kugler and Turk [89] developed a Cellular Automaton model for the simulation of multi-stage deformation and post-dynamic recrystallization for the case when DRX is initiated

in the material during deformation. The details regarding the modeling of DRX are already presented in section 2.4.5.7.

When deformation is interrupted, dislocation density of each grain (each cell in their CA model) is calculated by setting k_1 in KM equation (Equation 2-1) to be zero, which gives an exponential decrease in dislocation density with time:

$$\rho_{i+1}(\Delta t) = \rho_i \exp(-k_2 \dot{\varepsilon} \Delta t) \qquad \text{(Equation 2-57)}$$

where $\dot{\varepsilon}$ is the strain rate during deformation before interruption. No other distinction was made between the dynamic and static processes.

The softening fraction during the isothermal annealing of metals as a function of time was calculated. The right tendency of the influence of temperature and strain rate on softening kinetics was captured. A stronger dependence on strain rate and a much weaker dependence on temperature are shown in Figure 2-39.

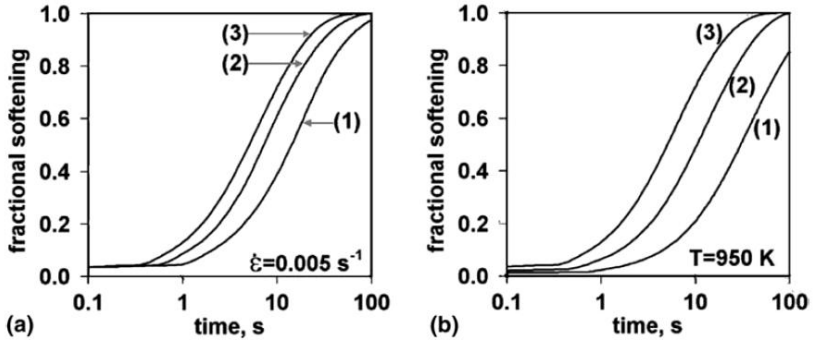

Figure 2-39 Fractional softening vs. interruption time for: (a) constant strain rate and temperatures of 750 K (curve 1), 850 K (curve 2), 950 K (curve 3); (b) for constant temperature and different strain rates of 0.0005 s^{-1} (curve 1), 0.002 s^{-1} (curve 2), 0.005 s^{-1} (curve 3).

The influence of deformation on the recrystallization kinetics is analyzed and shown in Figure 2-40. A strain-independent range was found at different temperature and strain rates. The fact that the rate of PDRX softening is a weak function of temperature (Figure 2-40a), and is significantly affected by the strain rate (Figure 2-40b) were again demonstrated.

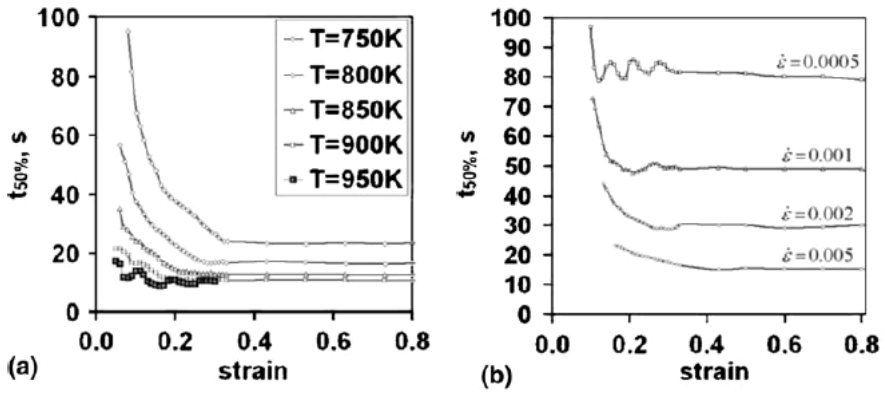

Figure 2-40 a) Evolution of the time for 50% recrystallization with strain at different temperatures ($\dot{\varepsilon} = 0.005 s^{-1}$), b) at different constant strain rates with recovery (T =750 K).

The model enables both quantitative and topographic simulations of microstructural evolution before and during PDRX and it allows the simulation of multi-stage deformation. However, the evolution of grain size was again not mentioned in this case. Experimental verifications on grain size aspect are needed.

2.6. Summary of existing investigation on recrystallization

2.6.1. Experimental investigation on recrystallization of austenitic stainless steel

Austenitic stainless steels have a low value of SFE, so their hot deformation is characterized by the typical DDRX behavior under a wide range of deformation conditions. Single peak type flow stress curves were observed when deformed at low temperature and high strain rate. Multiple peaks, on the other hand, can be obtained by deformation at very low strain rate, relatively high temperature and small initial grain size as well. Many studies have been carried out on the mechanical and microstructural aspects of DRX, much less were however found on the post deformation recrystallization, especially PDRX. For DRX, where literature shows experimental data, but it is hard to find all the information regarding recrystallized fraction, recrystallized grain size and flow stress curves together from the same source. The data produced in the early days of 1950s to 1980s are still widely used. To find these data which take into account influences such as deformation temperature, strain rate or initial grain size, is almost impossible for a particular material. Conserning recrystallization after hot deformation, most of the work has focused on the mechanical aspects such as softening, and the microstructural evolution is very often neglected. When it comes to the particular material of 304L stainless steel, experimental data are extremely limited. As the aim of the experimental investigation in this thesis work is to provide experimental data to both verify the developed model and identify the model parameters, sufficiently detailed experimental measurements of deformed microstructures are needed. Considering that many of the general conclusions regarding recrystallization are material sensitive, some of the aspects which need further investigation are summarized below:

1) A full set of experimental data on 304L stainless steel is required to further understand the mechanisms. For DRX, this includes the recrystallized fraction, recrystallized grain size, flow stress curves. The microstructure before deformation also needs to be characterized. For the recrystallization after hot deformation, the recrystallized grain size evolution, from immediately after the interruption of deformation until steady state, is needed. Investigation on conditions with different initial grain sizes, deformation or annealing temperature, different strain rates, as well as different interruption strains, are necessary to understand their quantitative effects on microstructural evolution during recrystallization process.

2) The relation between DRX microstructure and PDRX microstrural evolution needs to be analyzed, including the fast changing microstructure after deformation, the effect of strain rate and accumulated strain in DRX, and grain size evolution from DRX to PDRX/GG.

3) The nucleation behavior of PDRX should be further investigated. Discrepancies still exist on whether there is classic SRX during PDRX. For SRX, site saturated type of nucleation is often used for numerical modeling, but experimental verification is needed, especially for 304L stainless steel.

4) The effect of annealing twins, which adds difficulties to understand well the recrystallization process, needs to be addressed: grain size measurement should exclude twins, their effect on recrystallization nucleation and grain boundary migration rate should be clarified.

5) Multi-pass (deformation + heat treatments) data are needed to test models. A few in situ heating experiments would give the opportunity to study microstructure evolution in SRX and PDRX, starting from a known strain-hardened or DRX microstructure.

2.6.2. Existing models for recrystallization

Based on our literature review, there have been several methods of approach, each with its own particular advantages and disadvantages. To summarize, the current models are however limited by several factors:

- The size of the model, although this becomes less of a problem as computing power increases, but it still matters if the developed model needs to be implemented into commercial FE softwares. Very likely, it becomes impossible to handle the spatial complexities of recrystallization in real materials at this level.

- Whereas it is feasible to describe simple processes with some accuracy by analytical means, the mechanisms which depend not upon the average microstructure, but upon heterogeneities in the microstructure are inevitably difficult to describe.

- The lack of accurate input data, this includes the initial state of the material, material properties, the fitting parameters over a wide range of conditions in the model, deformation structures, boundary properties, etc.

- Inadequate understanding or over simplified modelling of the basic physical processes. For example, most 'recrystallization' models are similar to growth models, since no detailed or physically-based modelling of nucleation was introduced. And the driving force from the capillarity term, as well as static recovery, is very often neglected.

- It is noted that analytical and semi-analytical models of recrystallization in the literature tend to illustrate good trends but fail to show quantitative agreement with experimental data over a range of processing conditions, and considering (i) the stress-strain behavior (multi-stage deformation when investigating SRX OR PDRX), (ii) the recrystallized fraction, (iii) the recrystallized grain size, (iv) effects of initial grain size.

- For these models which are successful in predicting the microstructure evolution in some particular cases, a larger range of deformation conditions should be taken into account. Sensitivity analyses should be performed to show that estimated model parameters are physically reasonable.

- No existing physically based models are found which are capable to predict recrystallization under multi-pass conditions: SRX, DRX, PDRX and any combination of these three types of recrystallization and at the same time consider the effects from deformation temperature, strain rate and initial grain size.

2.6.3. Focus of the thesis

According to the above discussion, and as already underlined in the previous chapter, the literature lacks accurate recrystallization models which are able to predict microstructure evolution under multi-pass conditions. Although some efforts have been reported in this direction, most of them either lack experimental validation or can only provide a qualitative agreement for selected deformation conditions. The connections between SRX, DRX and PDRX are usually oversimplified. Furthermore, most of these models are not designed for variable conditions which prevail in industrial applications.

With these remarks in mind, the two-site incremental mean field recrystallization model developed in Chapter 4, introduces the required improvements. Physical processes are modelled individually, and the identified parameters allow for quantitative agreement with experimental data of mechanical and microstructural types, as shown in Chapters 5 and 6.

2.7. French summary

L'étude de la recristallisation qui a lieu pendant les étapes thermomécaniques de mise en forme des matériaux remonte à 150 ans. Considérant que de nombreux aspects liés à la recristallisation ne sont pas entièrement compris jusqu'à présent, et sachant que les résultats expérimentaux sont souvent pauvres et contradictoires, une révision minutieuse de la littérature a été réalisée.

Parmi les nombreux ouvrages existants, nous nous sommes concentrés sur les phénomènes prenant en compte l'écrouissage, la restauration, la migration des joints de grains, la germination et la croissance des grains des matériaux, directement liés à la recristallisation dynamique (DRX), la recristallisation statique (SRX) ou encore à la recristallisation post-dynamique (PDRX), dans un matériau avec une faible énergie de défaut d'empilement.

Un aperçu des modèles numériques de recristallisation existants est également présent dans ce chapitre, avec une attention toute particulière aux modèles physiques. Notre attention se portera aussi sur les modèles de recristallisation en conditions multi passes de mise en forme, ainsi que sur l'identification des paramètres du modèle.

Finalement, nous avons aussi collecté des données sur les différents types de recristallisation (DRX, SRX, PDRX) des aciers austénitiques inoxydables. Le mécanisme de chaque type de recristallisation est expliqué, ainsi que sa dépendance à la température de déformation, à la vitesse de déformation, au taux de déformation et à la taille initiale des grains.

3. Experimental methods

3.1. Introduction

Changes of mechanical behavior during hot working that are reflected by the flow curves are a direct consequence of microstructure changes: the generation of dislocations (strain hardening), the rearrangement and self-annihilation of dislocations, and their absorption by grain boundaries (dynamic recovery), the nucleation and growth of new grains (discontinuous dynamic recrystallization, DDRX). All of these phenomena are actually related to the material properties, so the properties of 304L austenitic stainless steel are presented first.

In order to study the mechanical behavior of 304L during hot deformation, torsion tests were carried out. The associated microstructure evolutions were either characterized by optical microscope (OM), and Scanning Electron Microscope (SEM) with the Electron Backscatter Diffraction (EBSD) technique. A few in situ heating experiments were also performed in order to have a close look at the mechanisms of recrystallization by following the gradual evolution of microstructure on the *same* observed surface. So, the details of experiments, which include both the principles and experimental set up of torsion tests, and in situ heating experiment are all included in this chapter. The microstructure characterization itself is described next. The procedures to prepare the sample for EBSD and OM observation are presented, together with the measurement of recrystallized fraction and recrystallized grain size.

3.2. 304L austenitic stainless steel

3.2.1. Chemical composition

The major feature of stainless steels is their resistance to corrosion by adding more than 10.5% of chrome. There are three different types of steels according to their crystal structure, which are austenitic steels, martensitic steels and ferritic steels. Austenitic stainless steels, which do not undergo discernible phase transformation during their hot working over a wide temperature range, are ideal model alloys to investigate recrystallization [96]. 304L austenitic stainless steels were used in the current study, the chemical composition of which is presented in Table 3-1 Composition (Weight percentage) of 304L austenitic stainless steel [155]. Except for chromium, the principal added element of austenitic steels is nickel which helps stabilizing austenite to a very low temperature.

Table 3-1 Composition (Weight percentage) of 304L austenitic stainless steel

Material	C	Mn	Si	P	S	Cr	Ni	N
304L	<0.03	<2.00	<0.75	<0.045	0.03	18.0 ~ 12.0	8.0 ~ 12.0	<0.10

Purity effects during hot working in austenitic stainless steels were analyzed in detail by Wahabi *et al*. [156, 157] and Gavard [158]. They study showed that the dynamically recrystallized grain size decreased at increasing carbon content due to the decrease in grain boundary migration caused by drag effect. In general, alloying elements reduce the diffusion coefficient, and consequently, the recovery rate, since atoms will interact with the dislocation core and reduce their climb rate.

3.2.2. Physical and mechanical properties

Austenitic stainless steels find frequent applications in a variety of fields like power generation plants, petrochemical and refinery, spacecrafts, due to their advanced properties. The investigations on physical and mechanical properties of 304L are very useful to calibrate a numerical model of microstructure evolution.

The fusion temperature T_f of 304L is 1400 ℃ [159], with face-centred cubic (F.C.C) crystal structure, the lattice parameter α is 3,586.10^{-10} m [160]. The Burger's vector can be obtained according to: $b = a/\sqrt{2} = 2{,}54.10^{-10} m$. A phenomenological correlation was found between strength and hardness values for 304L [68]. Other material parameters can be found in Table 3-2.

Table 3-2 Mechanical properties of 304L [161]

T (℃)	24	149	260	371	482	593	704	816
E (GPa)	196/200	189/188	183/180	175/171	159/163	153/155	141/146	124/138
μ (GPa)	79/77	73/72	70/68	66/64	55/61	59/58	55/55	50/52
ν	0,24/0,30	0,28/0,31	0,30/0,31	0,32/0,32	0,28/0,32	0,30/0,32	0,28/0,33	0,25/0,34

Following the method proposed by Frost and Ashby [162], Gavard [158] analyzed the shear modulus evolution with temperature shown in Table 3-2, a linear decrease with temperature was found between 24 and 816 ℃, as shown in Figure 3-1.

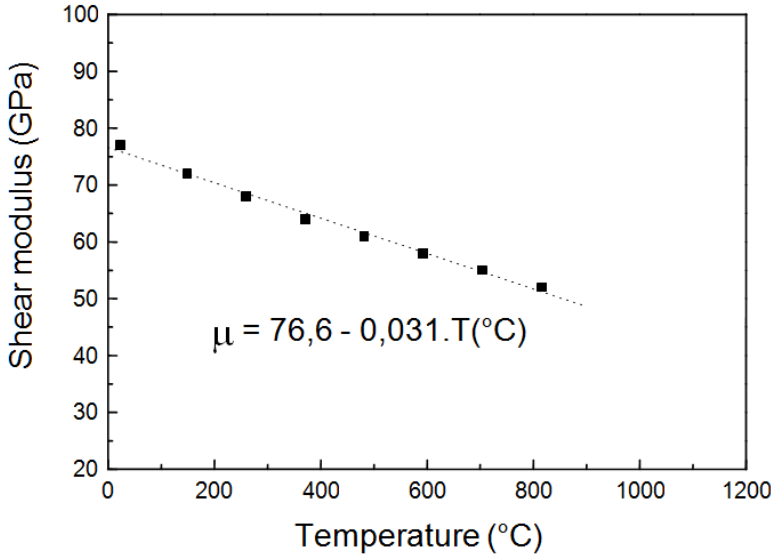

Figure 3-1 Shear modulus evolution of 304L with temperature [158]

Extrapolation values up to 1200 ℃, which are presented in Table 3-3.

Table 3-3 Shear modulus from room temperature until 1200 ℃

T (℃)	25	850	950	1000	1050	1100	1200
μ (GPa)	75,8	50,2	47,0	45,5	43,9	42,4	39,3

The Stacking-fault energy (SFE), noted as γ_{SFE} in units of joules per square meter, is another important parameter. Stacking faults associated with dislocations can be an extremely

significant feature of the structure of many materials, particularly those with F.C.C and H.C.P structures. When the SFE is high, the dissociation of a perfect dislocation into two partials is unlikely and dislocation can easily cross-slip and climb. In 304L austenitic stainless steel, which is typical of a low stacking fault energy (SFE) material (~20 mJm^{-2}) [1], the dislocations do not organize easily into subgrains and the nucleation site for recrystallization is then visualized in terms of a relatively dislocation-free region/cell in the vicinity of the grain boundary.

3.3. Hot torsion test

3.3.1. Introduction

In torsion testing, unlike tension and even compression, large strains can be applied before plastic instability occurs. The principle virtue of torsion test is that the samples do not undergo significant shape change as they are deformed as long as the gage section is restrained to a fixed length. Another favorable feature is that a constant true strain rate can be imposed on any given annular region of the sample by simply twisting one end relative to the other at a constant angular velocity. However, the interpretation of torsion test data is more complex than that used for axial-testing methods due to the fact that the strain and strain rate vary linearly with the specimen radius.

As mentioned in section 2, large strains are often needed for DRX investigation, especially when it comes to reaching a microstructure at steady state. The advantage of being able to deform up to a large strain also makes it easy to perform multi-pass deformation, which is of particular interest for the present work.

3.3.2. Torsion test sample

Torsion samples used in this work are cylindrical (Figure 3-2). The shear strain varies linearly from a value of zero at the centre of the bar to a maximum value at the surface

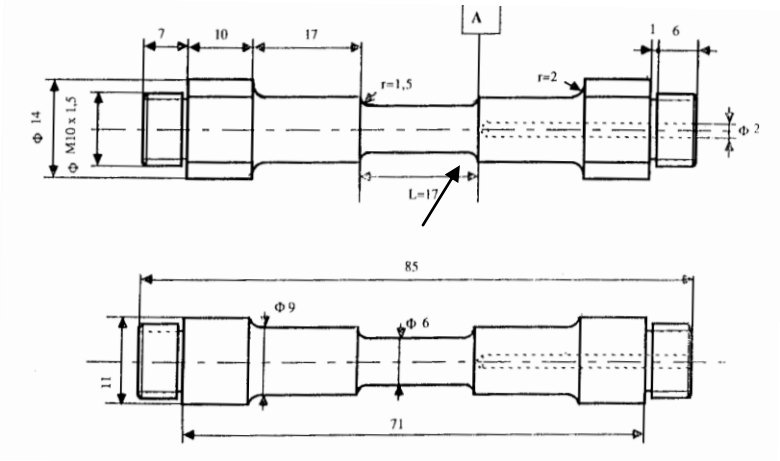

Figure 3-2 Geometry of the torsion test samples

Torsion samples were machined from the as-received bulk metals, according to the shape shown in Figure 3-2. The most important aspects of designing solid-bar specimen are gage

section diameter (d) and length (L), while shoulder and fillet should also be considered. The dimension of the sample is chosen in a way such that the following principles are satisfied. The torsion specimen gage section diameter should include at least 20 grain diameters (maximal of ~300 μm in the present work), since each grain has its specific crystallographic orientation and directional plastic deformation behavior. Deformation occurs in the fillets (as pointed out by the arrow) between the gage section and the shoulders will induce error for strain and strain rate calculation, this error decreases with an increase in L/d ratio if the fillet radius is the same. Since the torsion tests need to be performed at high temperature, the shoulder should be longer to ensure temperature uniformity, and the shoulder diameter should be at least 1.5 times the gage section diameter d to avoid plastic deformation. An interesting aspect of shoulder design for torsion testing is that there are no "end effects" in contrast to the considerations that apply to tension testing. This is often referred to as St.Venant's principle for tension, which signifies that stress concentrations arising from changes in cross section persist for a distance of about one diameter along the axis. More detailed description of specimen design can be found in the handbook [163]. A hole of 2 mm diameter is drilled along the centre line of each specimen from the shoulder to the start of the gauge length. This hole allows a thermocouple to be inserted into the specimen during testing to measure and regulate the torsion test temperature.

A fine axial straight line is marked using a metal scribing instrument on the gage section surface, to check whether flow localization occurs. After twisting to a certain deformation, this line should exhibit a regular helix at a fixed angle from the torsion axis. Places where a larger angle to the torsion axis is found comparing to the remainder of the line indicates flow localization has occurred there.

3.3.3. Conversion of torsion test data to stress-strain curves

The stress-strain curves are derived from the torque-time data recorded automatically by the torsion test system. Assuming that the deformation along the rotation axis is homogeneous, the equivalent strain is calculated following equation:

$$\bar{\varepsilon}(R) = \int_0^t \frac{2}{\sqrt{3}} \frac{\pi \dot{N} R}{L} dt = \frac{2}{\sqrt{3}} \frac{\pi N R}{L} \qquad \text{(Equation 3-1)}$$

Where:

N : number of laps

$\dot{N}$: rotation speed (Rad/s)

L : Gauge length (mm)

R : Gauge radius (mm)

The equivalent tensile stress, $\bar{\sigma}(R)$, can be obtained using the Fields and Backofen [164] analysis:

$$\bar{\sigma}(R) = \frac{\sqrt{3}T(R)}{2\pi R^3}\left(\tilde{n} + \tilde{m} + 3\right) \qquad \text{(Equation 3-2)}$$

where:

T : Torque (N.m)

$\tilde{m}$: The slope of the straight line $\ln T = f(\ln(\dot{N}))$, for a given number of laps N

$\tilde{n}$: The slope of the straight line $\ln T = f(\ln(N))$, for a given rotation speed $\dot{N}$

$\tilde{m}$ and $\tilde{n}$ correspond respectively to:

$$\tilde{m} = \left(\frac{\partial \ln T}{\partial \ln \dot{N}} \right)_N \qquad \text{(Equation 3-3)}$$

$$\tilde{n} = \left(\frac{\partial \ln T}{\partial \ln N} \right)_{\dot{N}} \qquad \text{(Equation 3-4)}$$

3.3.4. Hot torsion test

The hot torsion tests performed in the present work were all performed on a computer controlled torsion machine, shown in Figure 3-3. This machine is composed of three main parts: the deformation system, the heating system and the quenching system.

Figure 3-3 Hot torsion machine at CEMEF

The deformation system consists of a rotating end on the left side and a fixed end on the right side, with a grip on both sides where the torsion sample is installed by threading. The machine is driven by a dynamo electric motor which allows constant strain rates between 0.01 s^{-1} and 10 s^{-1} to be imposed. This system is able to perform multi-stage deformation with practical minimum inter-pass time of around 500ms. The applied torque with respect to time is transferred to a computer, after which it is converted to stress-strain data according to the principles described in the previous section.

The heating system (see Figure 3-4) , which is able to heat the sample up to 1200 ℃, use a lamp heating furnace. The furnace is closed during the heating and deformation process. A thermocouple, which gives the feedback of the temperature to a PID controller, is installed near the shoulder to control the heating speed and temperature (see Figure 3-2). The PID controller can be programmed such that multi-stage heating procedures can be performed automatically.

As seen in Figure 3-4, three quartz tubes are used. After the installation of the sample, the two smaller tubes are pushed horizontally close to each other, the larger tube was then moved to the middle part, and this configuration forms a container for water quench. During quenching, when the water flows on the gage length, the vapor is able to escape the container since it is not sealed up. Nitrogen gas may also flow during heating and deformation to protect the sample from oxidation. After the deformation and/or heating treatment, the furnace opens, and at the same time, water flows very quickly though four pipes to fill the quartz tubes. The sample is fully immersed into water in less than 2s.

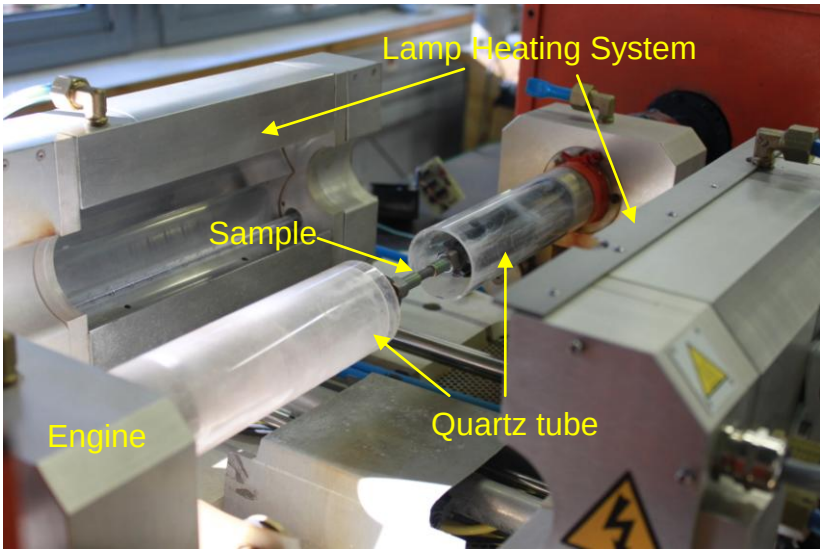

Figure 3-4 The open status of specimen chamber

All 304L samples were preheated at the test temperature for 3 min to get homogenous temperature. The deformation temperature ranged from 900 ℃ to 1150 ℃ and strain rates varied between 0.01s^{-1} and 1.0 s^{-1}. Deformation heating was thus neglected, this assumption is quite reasonable at low strain rates like 0.01 s^{-1}, up to 0.1 s^{-1} [165]. But at high strain rate of 1.0 s^{-1}, the deformation heating increases, and on the other hand, the heating system has no enough time to adjust the temperature, in that case the deformation heating has an influence on the stress softening.

In order to study the microstructure of the samples, quick quenching is necessary to preserve as much as possible of the hot deformation structure. The procedures of preparing the sample for microstructure observation are presented in the section 3.4.1.

3.4. Microstructure characterization

Metallographic observations were performed on tangential sections of the deformed torsion sample at a depth of ~100 μm for both in situ heating experiments and bulk measurement.

3.4.1. Sample preparation

The gage length part of the quenched torsion samples are cut by abrasive saw, and mounted in conductive or transparent resin depending on whether they are prepared for EBSD or optical microscope observation. Standard metallographic preparation was then conducted which consists of successive wet grinding from 600 grit paper until 4000 grit, a final procedure using colloidal silica (OPS) is used to obtain a well finished surface.

For EBSD analysis, the samples were moved to another polishing stage with vibratory polishing for 6 h after the above procedures. For the optical microscope, the polished samples were etched by chemical solution composed of 50ml hydrochloric acid (HCL) and 15 drops of H_2O_2 (~5ml).

Using the procedures mentioned above, the microstructure of the initial state of the received material was obtained as shown in Figure 3-5. The initial microstructure consisted of equiaxed grains with some annealing twin boundaries. These equiaxed grains were formed by full static recrystallization. The presence of twin boundaries in the microstructure is expected as 304L belongs to those of a low stacking fault energy material [120]. The grain size of initial state is

about 165 µm in diameter, excluding twins.

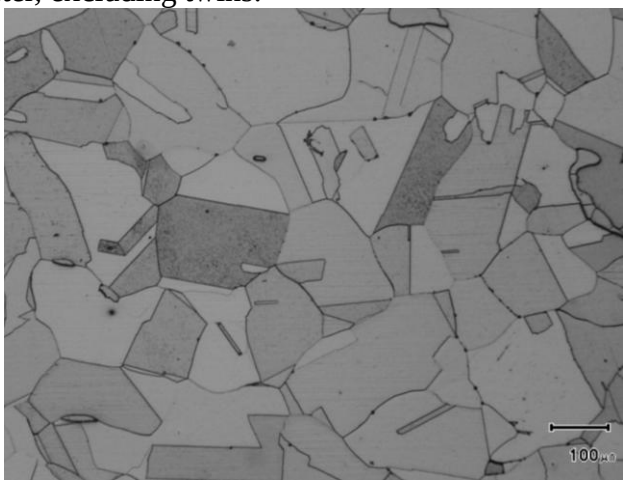

Figure 3-5 Initial state of the received material (Optical Microscope)

3.4.2. Characterization by SEM+EBSD and Optical microscope

Electron Backscattered Diffraction (EBSD) is based on the acquisition of diffraction patterns from bulk samples in the scanning electron microscope (SEM). Electron microscopy has the advantage that it is possible to obtain high resolution micrographs together with the crystallographic orientations of the region of interest by the use of electron diffraction.

The EBSD acquisition hardware generally comprises a sensitive CCD camera, and an image processing system for pattern averaging and background subtraction. Figure 3-6 is a schematic diagram showing the principal components of an EBSD system. The EBSD acquisition software (TSL OIM data collection 5) will control the data acquisition, solve the diffraction patterns and store the data. TSL OIM Analysis version 5.0 software is used to analyze, manipulate and display the data.

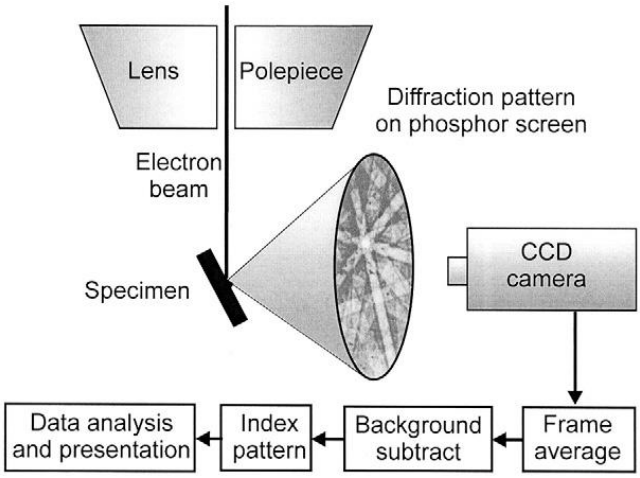

Figure 3-6 Schematic diagram of a typical EBSD installation in an SEM [1].

When combined with an SEM of sufficiently high resolution, the measurements performed by EBSD provide much information not available by optical microscope, like the clear boundary of very small grains. However, it is of great convenience to obtain some micrographs by optical microscope in the conditions where there are only big grains and the crystallographic orientation is not mandatory, such as when measuring grain size during the grain growth regime. In the current work, optical micrographs were analyzed using Visilog 6 image analysis

software. Although this software can automatically measure the recrystallized grain size and recrystallized fraction, it was chosen to measure these quantities manually.

3.4.3. The qualification of recrystallization

In this section, the frequently used quantification methods of some important features of microstructures are briefly presented. Since experimental data from other sources with different measurement methods are used in the current work, the differences of these methods are underlined here. More details can be obtained in these references [166,167,168].

3.4.3.1. Grain size

Measurement of grain volumes, which gives the best description of the size of three-dimensional grains, required in the past either separation of polycrystals into individual grains [169], serial sectioning [170]. All these methods were found to be relatively time consuming and, as a result, materials science practice until now has been dominated by mean intercept measurements in 2D. There are two different types of approaches:

i) Mean linear intercept

For a single-phase material of uniform grain size, the grain size may be related to L, the mean linear intercept distance across a grain as measured on a plane section. $\bar{L}$ is determined by measuring the average number of boundary intercepts (N_L) with a line of unit length so that

$$\bar{L} = 1/N_L \qquad \text{(Equation 3-5)}$$

If it is assumed that the grain shapes approximate to spheres of diameter $\bar{D}$ (or radius $\bar{r}$), then according to stereological relations [166], $\bar{L}$ will be less than the true grain size because of sectioning effects and is given by:

$$\bar{L} = \frac{4}{3}\bar{r} = \frac{2}{3}\bar{D} \qquad \text{(Equation 3-6)}$$

And finally, the spherical diameter $\bar{D}$ is obtained according to:

$$\bar{D} = 1.5\bar{L} \qquad \text{(Equation 3-7)}$$

If the grains are not equiaxed then they can be characterized by mean linear intercepts in the different directions. However, these cannot readily be converted to a mean diameter [1]. By assuming a tetrakaidecahedral shape for every grain, the following relation was found [58,171,172,173]:

$$\bar{D} = 1.68\bar{L} \qquad \text{(Equation 3-8)}$$

ii) Equivalent circle diameter

Similarly, the mean intercept area $\bar{S}$ can be obtained by first counting the number of grains (N) and measure the total area of the analyzed surface (S_{tot}):

$$N_A = N / S_{tot} \qquad \text{(Equation 3-9)}$$

$$\bar{S} = 1/N_A \qquad \text{(Equation 3-10)}$$

If spherical grains of diameter $\bar{D}$ intersect a random plane, the mean area of intersection is [167,174]:

$$\bar{S} = \frac{2}{3}\pi\bar{r}^2 = \frac{1}{6}\pi\bar{D}^2 \qquad \text{(Equation 3-11)}$$

and hence the diameter of spherical grains (3D) is:

$$\bar{D} = \sqrt{\frac{6\bar{S}}{\pi}} \quad \text{(Equation 3-12)}$$

However, the mean diameter, which is named as the Equivalent Circle Diameter (ECD) and can be obtained directly from EBSD analysis software, is very often used in the literature and is calculated according to:

$$\bar{S} = \pi(\frac{ECD}{2})^2 \quad \text{(Equation 3-13)}$$

$$ECD = (2/3)^{1/2}\bar{D} = 0.816\bar{D} \quad \text{(Equation 3-14)}$$

and in this case, the real diameter of spherical grains (3D) is:

$$\bar{D} = 1.224ECD \quad \text{(Equation 3-15)}$$

If the grains are not equiaxed, an ECD is less valid and alternative parameters such as the mean grain area $\bar{S}$ or the mean grain dimensions in orthogonal directions can be used.

It is important to notice that the converting factors from 2D mean intercept measurements to 3D real grain size obtained above are based on the assumption that all grains are perfect spheres. In the real case, and the converting factors will vary depending on the shape of the grains [175].

In the current work, the latter method, i.e. ECD, is used to measure the 2D grain size, the true mean volumetric grain size, $\bar{D}$, is then obtained by multiplying the mean ECD by 1.224. The initial state of 304L was scanned by EBSD, as presented in Figure 3-7. In the present study, high angle grain boundaries were defined as boundaries with misorientations greater than 15 ° (in red), low angle grain boundaries were selected as boundaries with misorientations between 2 °and 15 °, those boundaries with a rotation of 60 °± 5 °about <111> were assumed to be twin boundaries (in white). After deleting the noise points and areas (pointed by the pink and black arrows respectively), the ECD was found to be 165 µm excluding twin boundaries for ~300 grains.

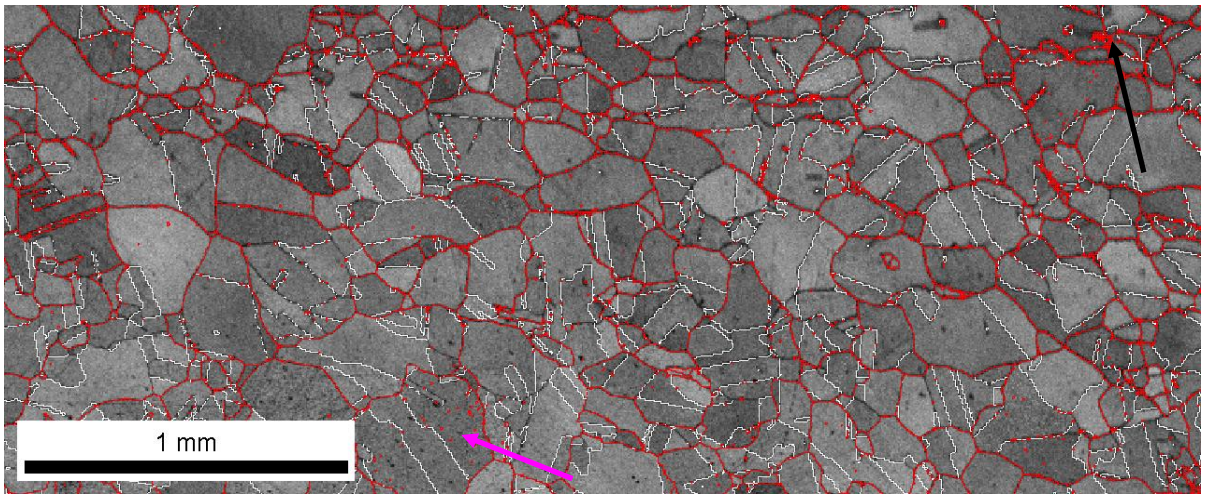

Figure 3-7 Part of analyzed area of the initial state (EBSD map)

At the same time, about 30 micrographs taken from optical microscope were combined together as shown in Figure 3-8, and the twin boundaries were identified by the eye according to their morphology. The measured ECD was 171 µm for ~ 600 grains, which is quite close to that obtained by EBSD analysis, suggesting that optical microscope characterization is accurate enough to measure the average grain size even in the presence of twins. The very small errors might due to the difficulty in etching the boundaries in 304L when preparing the sample for optical microscope observation.

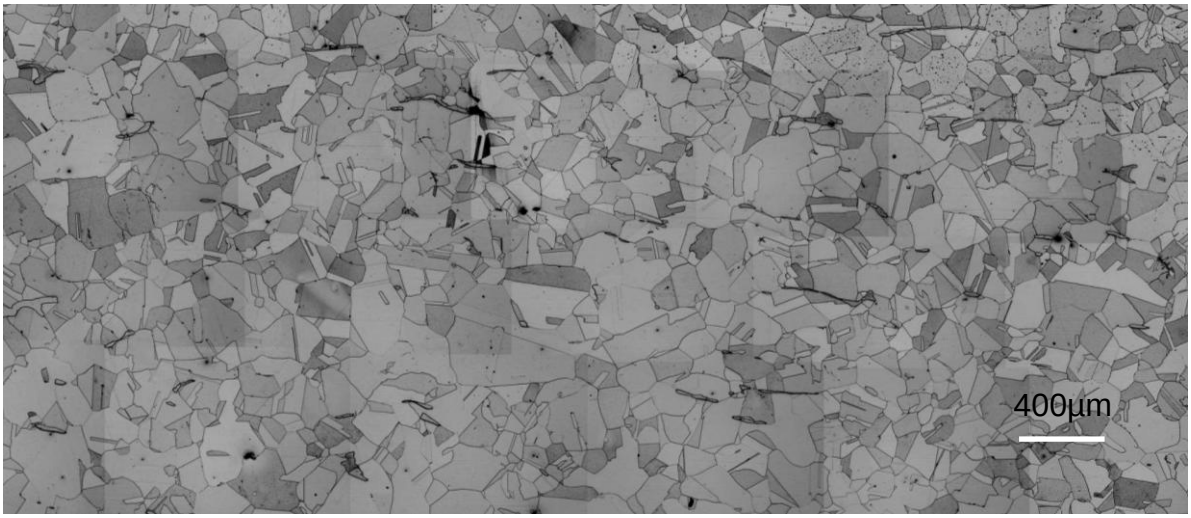

Figure 3-8 Part of the analyzed area of the initial state (Optical microscope)

In the present study, the grain size is measured using the optical microscope through the equivalent circle diameter (ECD) method for both SRX and PDRX where the grain sizes are usually big enough for optical microscope analysis, while the dynamically recrystallized grains are all measured by EBSD since they are too small and it is difficult to identify the grain boundaries by optical microscope.

3.4.3.2. Recrystallized fraction

Measurement of the recrystallized fraction is an essential part of the determination of recrystallization kinetics. Although some indication of this parameter may be obtained from indirect measurements of e.g. hardness or resistivity, accurate measurements can only be obtained by studying the microstructure [1].

The French geologist Delesse [176] was the first one to point out the equivalence of volume fraction ($\bar{V}_V$) and area fraction ($\bar{S}_S$):

$$\bar{V}_V = \bar{S}_S \qquad \text{(Equation 3-16)}$$

which states that the average area fraction $\bar{S}_S$ determined on sections through a volume, represents an estimate of the volume fraction $\bar{V}_V$ of the grains under investigation. In this work, the volume fraction of recrystallized grains is calculated according to the above equation.

The recrystallized fraction may be obtained directly from analysis of EBSD maps on the basis of pre-defined size, grain orientation spread (GOS), criteria, etc., depending on the type of microstructure. The GOS is calculated by the TSL software by averaging first the orientation for each grain. The spread is then obtained by averaging the deviation between the orientation of each point in the grain and the average orientation for the grain. For example, during DRX, the recrystallized grains are small and usually with an equiaxed shape. By contrast, the original deformed grains are usually elongated in the deformation direction. While for SRX, the recrystallized grains usually have a low GOS value.

Standard methods of quantitative metallography using area, or point counting methods may be employed. Point counting is believed to be the most efficient method, it is done by counting (i) the number of points falling in recrystallized grains, (ii) the number of points falling in unrecrystallized grains, (iii) the number of points where it is uncertain in which type of grains they fall. The volume fraction is thus determined from the counts made in the base direction. However, for a sample which is <10% or >90% recrystallized, the number of points required is

unrealistically large for such a manual technique. In the current study, area counting is used to measure recrystallized volume fractions. With the EBSD technique, the recrystallized regions may be identified on the basis of pre-defined size, GOS value, pattern quality criteria. For the optical microscope, it is mainly according to the shape and size of the grains, NR grains are usually big and elongated, while RX grains are very often small in size and more equiaxed.

3.5. Quasi in situ heating experiments

3.5.1. Introduction on quasi in situ heating experiments

Recrystallization is one of the most important microstructural events in the hot working of steels, but it is a much debated process. One reason is that we cannot understand recrystallization in depth before we understand the nature of the deformed state which is complex. Second, the heterogeneous nature of recrystallization prevents our progress in understanding it [1]. The most frequently used experimental techniques for studying recrystallization phenomena are "static" descriptions of the recrystallization by considering a series of samples. The recrystallization kinetics can thus only be studied by combining several static descriptions of different samples, resulting in average kinetic descriptions, which is the basis for the present day understanding [177]. The role of stored energy in SRX of deformed materials is complex but difficult to obtain from these experiments even though it is well established that stored energy acts as a driving force for both nucleation and growth. More accurate investigations of the intragranular heterogeneity of the stored energy and its link with recrystallization call for new characterization techniques.

Recent developments in EBSD are enabling recovery, recrystallization and grain growth to be investigated *in situ* using instruments with specimen stages that can reach elevated temperatures. Modern commercial systems have speeded at least over three orders of magnitude to the first fully automated EBSD system in early 1990s where four seconds were required to index each EBSD pattern [178]. Also, the improvements have made OIM systems more capable of capturing the evolving microstructures during in situ experiments. Extensive insight can generally be gained by simultaneously collecting OIM scan data repeatedly during in situ experiment. For most of the studies, only a small surface (~ 250*250 μm) was analyzed to decrease the scanning time (a few minutes) for each step. In order to study the formation of nuclei and their subsequent growth at elevated temperature, especially when dealing with big initial grain sizes (which is the case for the present study), it is required to examine a sufficient area to generate statistically viable data. In this case, however, the microstructure may evolve significantly during one scan time which thus makes repeated in situ observations impractical.

A compromised method was set up with the capacity to heat specimens up to a temperature of 1200 ℃. By using a combination of a heating stage with the automated EBSD technique, the sample was annealed at desired temperature for a short time and was then cooled to room temperature without removing the samples from the vacuum chamber. Instead of simultaneous scanning, a relatively big area was subsequently analyzed by EBSD at room temperature. By repeating these procedures, quasi in situ observation of microstructural changes at elevated temperature is possible, on a sufficient area. It provides a possibility to examine the nucleation sites, grain boundary migration and most importantly their relation with crystalline orientations. The technique remains, of course, limited by its two dimensional nature.

In the present work, the static/post dynamic recrystallization of 304L austenite stainless steel was investigated with these quasi in situ experiments. The stored energy was characterized by GOS, and its effects on recrystallization and grain growth were investigated.

The next section (section 3.5.2) deals with a detailed description of the experimental set up for in situ heating experiments. Section 3.5.3 is devoted to the experimental procedures used for the preparation, the hot working and the annealing of the different samples.

3.5.2. Experimental set up

Hot deformed specimens were quickly water quenched within 2s of the end of the torsion test to preserve as much of the deformed microstructure as possible. The well polished samples were then sectioned using a diamond saw to approximately 2.5mm*3mm*0.3mm. Thin samples help minimizing heat input into the samples, thereby increasing the heating and cooling speed.

This thin sample is welded on a tantalum sheet which has a fusion temperature higher than 3000 ℃ and high conductivity. Two thermocouples are positioned on the sample surface, with one on each side, as illustrated in Figure 3-9a. All welding points are obtained using capacitive discharge welding. One of the thermocouples is used in a feedback loop to set the input current to a specified temperature with a desired heating speed. The other thermocouple is used to record the temperature evolution. The sample is heated by the tantalum sheet through the Joule effect (i.e. electric current flows through the sheet). Calibration runs showed that the temperature difference between the sample top surface and tantalum slice was negligible, since the sample thickness is small. The time to reach 1000 ℃ is about 10s.

The heating stage is assembled and mounted onto the standard microscope stage as shown in Figure 3-9b, the entire stage being tilted 70 °towards the EBSD phosphor screen. In the middle of the sample, an analysis area of around 1.0 mm^2 remains clean and is examined using the orientation imaging microscopy (OIM), with a step size between measurement points of 2.0μm, at a rate of 60 patterns per second. The approximate time per scan is 20 minutes.

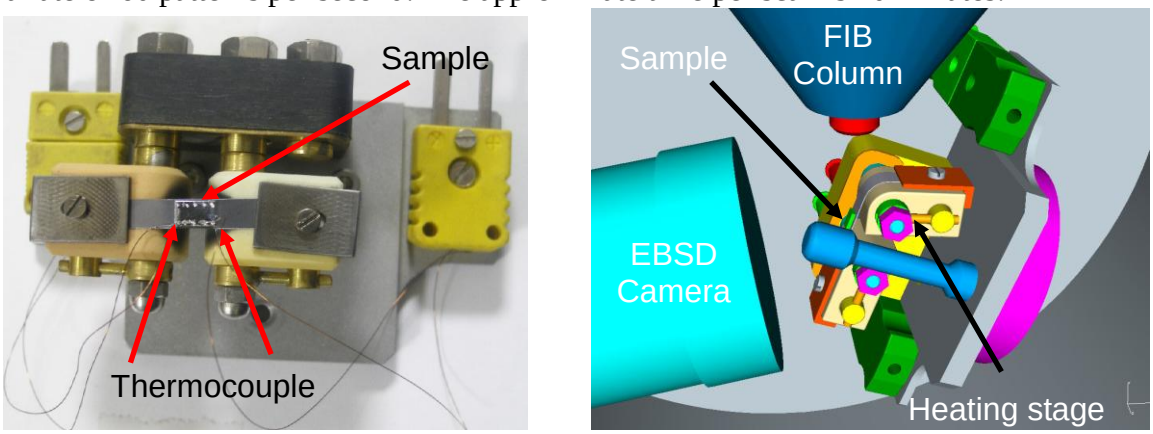

a) b)

Figure 3-9 a) Heating stage, b) The configuration of heating stage inside the SEM chamber [179]

3.5.3. In situ heating experiments

To produce the driving force for static/post dynamic recrystallization, small deformation by isothermal hot torsion test were applied at 1000 ℃ using a strain rate of 0.01/s, up to an equivalent strain of 0.3 for SRX, and 1.5 for investigating PDRX.

A scan of the deformed state was collected prior to heating. Then, the sample was annealed at 1000 ℃ for a desired time before cooling to room temperature. The EBSD patterns and automated scans were obtained using an EDAX/TSL DigiView camera and OIM version 5.0 software. The data was collected at an acceleration voltage of 20 keV, with an approximate

incident beam current of 2 nA. Around 10 scans had been collected when recrystallization was complete. After each annealing procedure, the sample was repositioned before scanning. An analyzed area shared by all heating steps measurement was cropped from the entire analyzed surface to follow the microstructure evolution at the same position. The procedures of thermal treatment sequences are schematically illustrated in Figure 3-10.

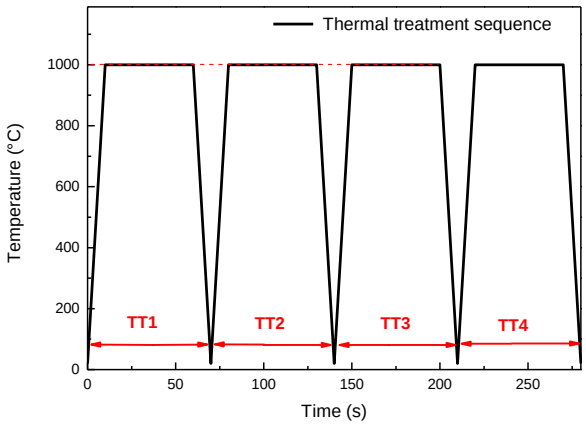

Figure 3-10 Schematic representation of the thermal treatment sequences

The details of the obtained results and the interpretation will be illustrated in section 6.4 when dealing with SRX and PDRX.

3.6. French summary

Les changements de comportement mécanique qui ont lieu pendant la déformation à chaud, et qui sont observés à partir de l'évolution de la courbe contrainte-déformation, sont une conséquence directe de l'évolution microstructurale : la génération des dislocations (écrouissage), le réarrangement et l'auto-annihilation des dislocations, leur absorption par les joints de grains (restauration), la germination et croissance de nouveaux grains (recristallisation dynamique discontinue – DDRX). Tous ces phénomènes sont intimement liés aux propriétés du matériau. Pour cette raison, les propriétés de l'acier 304L sont initialement présentées.

Afin d'étudier le comportement mécanique de l'acier 304L pendant la déformation à chaud, des tests de torsion ont été réalisés. L'évolution de la microstructure associée à ces tests a été caractérisée à l'aide de microscopie optique (OM), microscopie électronique à balayage (SEM) ainsi que de diffraction d'électrons rétrodiffusés (EBSD). Des traitements thermiques *in situ* ont aussi été réalisés afin d'analyser plus finement les mécanismes de recristallisation en suivant l'évolution de la microstructure d'une même surface du matériau. Les détails des expériences décrites ci-dessus sont présentés dans ce chapitre. La caractérisation microstructurale est présentée ensuite. Les techniques de préparation d'échantillons pour les analyses OM et EBSD, ainsi que le calcul de la fraction recristallisé et la taille des grains recristallisés sont aussi présentés.

4. Description of numerical model

4.1. Introduction

One major microstructure evolution to consider in low to medium stacking fault energies alloys, where recovery processes are slow, is the so called "discontinuous" dynamic recrystallization (DDRX) process [1]. It is characterized by clear nucleation and growth stages, with a preferential location of nuclei at the old grain boundaries. Whenever the critical strain for DRX (ε_{cr}^{DRX}) is exceeded at relatively high temperature, recrystallization nuclei will be present in the material. If deformation is interrupted, but annealing continued, these nuclei will grow with no incubation period into the heterogeneous, partly dynamically recrystallized matrix. This phenomenon is known as metadynamic recrystallization or post dynamic recrystallization (PDRX) [99]. On the other hand, if a material is deformed to a strain lower than ε_{cr}^{DRX} at the corresponding temperature, but with sufficient stored energy to drive the recrystallization, static recrystallization (SRX) may occur when it is subsequently annealed. When recrystallization is complete, an almost dislocation free microstructure is obtained, grain growth (GG) keeps taking place to reduce the grain boundary. During DDRX and/or recrystallization after hot deformation, the evolution of the microstructure is due to various phenomena. Strain hardening and recovery tend to modify the dislocation density, while grain boundary migration leads to grain size changes and dislocation density evolution, and new grains are created by nucleation. Final stages of grain growth, on the other hand, continue until a limiting value is reached, where the driving force does no longer allow to overcome pinning/dragging forces.

The proposed model allows following the evolution of the microstructure through different recrystallization regimes, under multi-pass conditions. In this chapter, a semi-analytical model of DDRX is developed in which the full distributions of grain sizes and dislocation densities are considered as state variables. The data structure is given by a set of representative grains, defined by their dislocation density and size. Traditional equations are used to account for strain-hardening, recovery, grain boundary migration, and predict flow stress. The originality of the model lies in: (a) the interaction of each representative grain with two homogeneous equivalent media (usually only one is considered [76]), with high and low dislocation density, respectively; (b) the relative weight of the two media is functionally related to their volume fractions; (c) nucleation and disappearance of grains make the data structure variable in time, until a steady-state is reached. Elements (a) and (b) represent a new way of introducing topology in a DDRX model and, together with an appropriate nucleation law, lead to an automatic and accurate account of initial grain size effects.

The numerical model is programmed in C++, and can be combined with a non-dominated sorting genetic algorithm (NSGA II) [180] in order to optimize the parameter values. The model parameters vary with temperature and strain rate, but do not depend on grain size. The comparison with experimental results is provided in chapter 5. Many of the elementary components of the DDRX model are of direct use for the recrystallization model after deformation, as the physical mechanisms are similar in many aspects to those controlling SRX, PDRX and GG [181]. Therefore, based on the DDRX model, some special aspects corresponding to recrystallization in static conditions are considered, which finally leads to the SRX/PDRX/GG model. This opens the possibility of modelling multi-pass operations compatible with industrial applications. Experimental investigation and comparison with numerical results on recrystallization after deformation in static conditions are provided in chapter 6.

4.2. Material representation

The material microstructure is represented by a set of representative grains which are defined by two state variables: the grain diameter D, and the grain average dislocation density ρ. Each representative grain is composed of a number N_g of identical spherical grains, which in turn defines the volume fractions. As these N_g grains come from different points of the microstructure, the actual neighborhood of each grain is unknown. A representation of this neighborhood can be constructed based on the notion of Homogeneous Equivalent Medium (HEM), as illustrated in Figure 4-1. The unknown neighbors of a given grain in a recrystallizing microstructure (Figure 4-1a) are replaced by two HEMs with low and high average dislocation densities, respectively (Figure 4-1b). These HEMs are designated as Recrystallized (RX) and Non Recrystallized (NR) media, for simplicity.

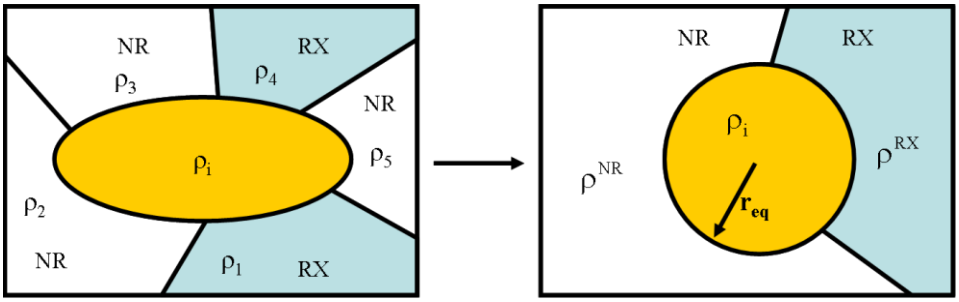

Figure 4-1 Schematic representations of a recrystallizing microstructure, real case (left) and as considered in the DDRX model (right)

As the microstructure evolves, the volume fractions X and $1-X$ associated to the RX and NR media change, which has the consequence of modifying the neighbourhood of each representative grain, and therefore its subsequent evolution. The grain shape is retained as spherical at all times, which is not considered as a strong assumption in the context of DDRX [1].

The initial set of representative grains typically associates log-normal and Gaussian distributions of grain sizes and dislocation densities (Figure 4-2), but any kind of distribution could be chosen. Because the model works in 3D, the measured 2D distributions of grain sizes must be converted to 3D distributions using standard stereology analysis [167], more details of this can be found in section 3.4.3.1.

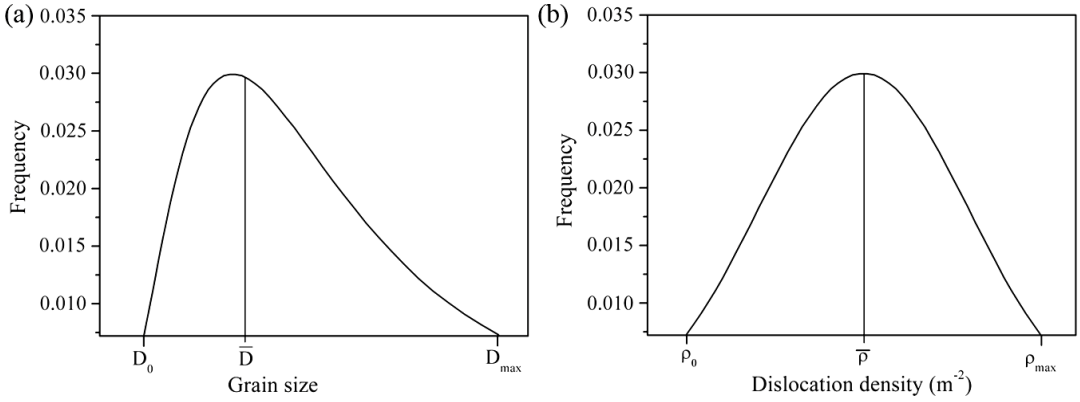

Figure 4-2 Initial distributions of grain sizes (log-normal distribution) and dislocation densities (Gaussian distribution).

4.3. Discontinuous dynamic recrystallization model

4.3.1. Strain hardening, recovery and flow stress

Kocks and Mecking [10,11] describe the evolution of dislocation density ρ by two concurrent effects of storage and recovery. Storage is associated with immobilization of dislocations at impenetrable obstacles, and dynamic recovery is assumed to be linear in ρ. When the dislocations mean free path is assumed to be constant [12], the evolution of dislocation density ρ as a function of the equivalent plastic strain ε is given by

$$\frac{d\rho}{d\varepsilon} = K_1 - K_2\rho \qquad \text{(Equation 4-1)}$$

where K_1 and K_2 represent respectively the strain hardening and the recovery terms. A similar equation is found in [13].

The flow stress σ_i associated to a given grain category *i* is determined from the dislocation density of that category, using the Taylor equation [182]

$$\sigma_i = \sigma_0 + M\alpha\mu b\sqrt{\rho_i} \qquad \text{(Equation 4-2)}$$

with μ the shear modulus, b the Burgers vector, M the Taylor factor, σ_0 a "dislocation free" yield stress and α a constant.

The material flow stress $\bar{\sigma}$ is then obtained from (Equation 4-2) by considering a volume average:

$$\bar{\sigma} = \langle \sigma_i \rangle \qquad \text{(Equation 4-3)}$$

4.3.2. Grain boundary migration

The driving force ΔE for grain boundary migration is described as the sum of a stored energy term related to the dislocation content [1], and a capillarity term related to the grain boundary energy and curvature in (Equation 2-46):

$$\Delta E = \tau\Delta\rho + \gamma_b\Delta(1/r) \qquad \text{(Equation 4-4)}$$

where $\tau \approx \mu b^2/2$ is the average energy per unit dislocation length, γ_b the energy per unit area of the grain boundary, $r = D/2$ the grain radius of grain. $\Delta\rho$ considers differences in dislocation density on either side of the grain boundary. In the context of the present model, one side of the boundary refers to the HEM (RX or NR) state variables, hence $\Delta\rho = \rho_{HEM} - \rho_i$ and $\Delta(1/r) = (1/r)_{HEM} - (1/r)_i$. Both ρ_{HEM} and $(1/r)_{HEM}$ are computed from volume average over all representative grains belonging to the considered HEM.

The grain boundary velocity is described by a kinetic relation:

$$v = m\Delta E \qquad \text{(Equation 4-5)}$$

where *m* is the grain boundary mobility. Physically, $v > 0$ indicates that the grain grows, and $v < 0$ indicates that the grain shrinks. The grain boundary mobility *m* is temperature dependent and is usually found to obey an Arrhenius type of the following form [1],

$$m = m_0 \exp(-\frac{Q_b}{RT}) \qquad \text{(Equation 4-6)}$$

where m_0 is a constant, Q_b is the boundary migration activation energy and which is close to the activation energy for grain boundary diffusion. A set value of these two parameters is listed for different materials in [1].

4.3.3. Nucleation

It is assumed that new grains appear in areas where the dislocation density is greater than a critical value ρ_{cr}. Since the nucleation rate is difficult to evaluate experimentally [1], it is presumed that a certain percentage per unit time of the potential nucleating sites actually nucleates. If nucleation happens in the bulk, the number of potential nucleating sites N_p will be proportional to the total volume of grains with a dislocation density higher than ρ_{cr}^{DRX}. If nucleation happens mainly at grain boundaries, the total surface of the same grains will be considered instead of the volume. In the general situation, the number of potential nucleation sites N_p is therefore written as

$$N_p \propto \sum_{\rho_i > \rho_{cr}} r_i^q \qquad \text{(Equation 4-7)}$$

where q = 2 in case of necklace-type nucleation, and q = 3 in case of bulk nucleation. In the present work, the value q = 2 is chosen. (Equation 4-7) is then applied to each representative grain, considering that the amount of activated nucleation sites (i.e. the number of new nuclei) per unit time increases for increasing dislocation densities:

$$\dot{N}_{i,nucl} = K_g S_{cr} \frac{N_i r_i^q \left(\rho_i - \rho_{cr}\right)^{b_g}}{\sum_{\rho_k > \rho_{cr}} N_k r_k^q \left(\rho_k - \rho_{cr}\right)^{b_g}} \qquad \text{(Equation 4-8)}$$

where b_g is a constant which should be close to 3 according to [76], $K_g = K_g(T, \dot{\varepsilon})$ a probability constant depending on the processing conditions, S_{cr} the total surface area of grains with $\rho > \rho_{cr}$, and N_k the number of grains composing the kth representative grain. All nuclei are assumed to start with the same initial radius r_u^{DRX}. The nucleated volume V_{nucl} during a time step Δt is therefore given by

$$V_{nucl} = \frac{4}{3}\pi (r_u^{DRX})^3 \dot{N}_{nucl} \Delta t \qquad \text{(Equation 4-9)}$$

where $\dot{N}_{nucl} = \sum \dot{N}_{i,nucl}$ and Δt is the time step. At each time step, if $V_{nucl} > 0$, a new grain category is created with size r_u^{DRX} and dislocation density ρ_0.

Both the activating probability K_g and the critical dislocation density ρ_{cr}^{DRX} are assumed to depend on temperature and strain rate. Replacing some of the parameters in (Equation 2-16) estimated value of ρ_{cr}^{DRX} can be expressed as a function of other parameters of the model:

$$\rho_{cr}^{DRX} = \left(\frac{20 \cdot K_1 \cdot \gamma_b \cdot \dot{\varepsilon}}{3 \cdot K_3 \cdot \tau}\right)^{1/3} \qquad \text{(Equation 4-10)}$$

where $K_3 = m\tau$, γ_b and τ are the grain boundary energy and dislocation line energy, respectively. It is observed from (Equation 4-10) that ρ_{cr}^{DRX} is indirectly influenced by temperature and strain rate through the parameters K_3 and K_1. Temperature variation of ρ_{cr}^{DRX} is mainly dictated by K_3 through the exponential temperature dependence of m in (Equation 4-6). The influence of strain rate is incorporated by the variations of K_1, which is equal to $1/bl$ in (Equation 2-10). In general, (Equation 4-10) tells that the critical dislocation density increases with decreasing temperature and increasing strain rate which is physically justified.

The critical dislocation density obtained by (Equation 4-10) neglects dynamic recovery, see section 2.4.2. It may not be a good approximation to calculate ρ_{cr}^{DRX} in some cases. Appendix

A shows how ρ_{cr}^{DRX} can be analytically expressed with (Equation 4-11), taking into account dynamic recovery,

$$\rho_{cr}^{DRX} = \left[\frac{-2\gamma_b \dot{\varepsilon} \frac{K_2}{K_3 \tau}}{\ln\left(1 - \frac{K_2}{K_1}\rho_{cr}^{DRX}\right)} \right]^{1/2} \qquad \text{(Equation 4-11)}$$

The initial guess value of ρ_{cr}^{DRX} is obtained directly from (Equation 4-10), and iterative calculation by (Equation 4-11) leads to the converged value of ρ_{cr}^{DRX} which is then used in the model.

A nucleus becomes viable when its radius reaches a critical value r_u^{DRX}. This corresponds to the condition when the stored energy of the material is large enough to overcome the capillary force of the nucleus, so we have,

$$\rho_{cr}^{DRX} \cdot \tau = \frac{2\gamma_b}{r_u^{DRX}} \qquad \text{(Equation 4-12)}$$

To overcome the problem that a nucleus may shrink soon after its creation, a scaling constant ω is introduced, and this gives,

$$r_u^{DRX} = \omega \cdot \frac{2 \cdot \gamma_b}{\rho_{cr}^{DRX} \cdot \tau} \qquad \text{(Equation 4-13)}$$

where $\omega > 1$. This will ensure that a created nucleus has the needed driving force (see (Equation 4-4)) for growth.

In the context of a Mean field model, the dislocation density is uniform throughout each grain, and the increased amount of dislocations along grain boundaries is not accounted in the model. Because of this, it can be envisaged that the calculated critical nucleus size is a little bigger than the critical size we observed from experimental observation.

4.3.4. Interaction with the surrounding HEMs

It is considered that every grain is surrounded by two different HEMs. Therefore, one part of the boundary for which $|\Delta E|$ is high will move faster than the other part. This leads to the existence of "mobile surface fractions" [51,56,79]. Two of them are defined in Figure 4-3, and considered homogeneous throughout the material, at a given time. The first one corresponds to the mobile fraction γ^{RX} of a RX representative grain (i.e. which started from a nucleus), while the second one refers to the mobile fraction γ^{NR} of a NR representative grain (i.e. which was part of the initial description of the material).

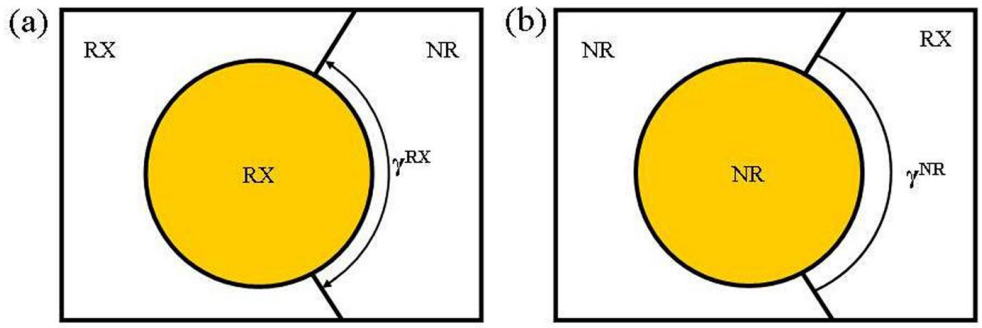

Figure 4-3 Schematic representations of mobile surface fractions (a) of a recrystallized representative grain (γ^{RX}), and (b) of a non-recrystallized representative grain (γ^{NR}).

For simplicity, subscripts *i* and *j* will be used from now to designate RX and NR grains, respectively. Different driving forces are then distinguished using the notation $\Delta E_k^{HEM} = E_{HEM} - E_k$, with HEM = NR or RX, $k = i$ or j.

4.3.4.1. Migration of RX-NR interfaces

A fundamental problem encountered in the formal kinetics of recrystallization is the interference that occurs between growing regions. Individual grains cannot grow freely indefinitely, because sooner or later they impinge on each other.

Using (Equation 4-5), the variation of recrystallized volume during a time step Δt , and considering only the movement of mobile fractions of the grain boundaries, is given by

$$\Delta V_{RX/NR} = \sum_{RX} \gamma^{RX} \Delta V_{i,RX/NR} = -\Delta V_{NR/RX} = -\sum_{NR} \gamma^{NR} \Delta V_{j,NR/RX} \quad \text{(Equation 4-14)}$$

with $\Delta V_{i,RX/NR} = 4\pi r_i^2 m \Delta E_i^{NR} \Delta t$ and $\Delta V_{j,NR/RX} = 4\pi r_j^2 m \Delta E_j^{RX} \Delta t$, leading to

$$\gamma^{NR} = -\gamma^{RX} \frac{\sum_{RX} r_i^2 \Delta E_i^{NR}}{\sum_{NR} r_j^2 \Delta E_j^{RX}} \quad \text{(Equation 4-15)}$$

or in the other way

$$\gamma^{RX} = -\gamma^{NR} \frac{\sum_{NR} r_j^2 \Delta E_j^{RX}}{\sum_{RX} r_i^2 \Delta E_i^{NR}} \quad \text{(Equation 4-16)}$$

Assuming homogeneous nucleation in the material, one can write

$$\Delta V_{RX/NR} = (1 - X) \Delta V_{ext} \quad \text{(Equation 4-17)}$$

where X is the recrystallized volume fraction (RX HEM volume fraction), and V_{ext} the "extended" recrystallized volume, i.e. with no consideration of grain interactions. Comparing (Equation 4-14) and (Equation 4-17) leads to

$$\gamma^{RX} = 1 - X \quad \text{(Equation 4-18)}$$

Similarly, considering this time the non recrystallized volume change, one finds

$$\gamma^{NR} = X \quad \text{(Equation 4-19)}$$

Expressions (Equation 4-18) and (Equation 4-19) must be changed if nucleation is heterogeneous in the material. In DDRX the preferred location of nuclei is at the old grain boundaries, i.e. necklace-type nucleation usually prevails (Figure 4-4). This results in faster impingement of recrystallizing grains, compared to the homogeneous case. Therefore, γ^{RX}

will decrease faster than $1-X$ does, and a new expression replacing (Equation 4-18) is proposed:

$$\gamma^{RX} = 1 - X^{n} \qquad \text{(Equation 4-20)}$$

with $n < 1$. Similarly, one can also choose a new expression of (Equation 4-19) as

$$\gamma^{NR} = X^{p} \qquad \text{(Equation 4-21)}$$

with $p < 1$, since γ^{NR} must increase faster than X does.

As the relations in (Equation 4-20) and (Equation 4-21) must satisfy volume conservation expressed by (Equation 4-15) and (Equation 4-16), the proposed strategy consists either in evaluating γ^{RX} from (Equation 4-20) and computing γ^{NR} from (Equation 4-15), or evaluating γ^{NR} from (Equation 4-21) and computing γ^{RX} from (Equation 4-16). Figure 4-5a shows a typical calculated evolution of γ^{RX} using (Equation 4-20) for γ^{RX} with $n = 2/3$. The non linear evolution of γ^{NR} makes it reach a value of 1 while X is still limited, which corresponds well to the illustration of Figure 4-4. When γ^{NR} reaches 1, it is set at that value, and γ^{RX} is then computed using relation (Equation 4-16). This switching procedure leads to a change of the slope of the γ^{RX} curve as can be noticed in Figure 4-5a.

The above strategy reflects well the physics of DDRX as long as the following conditions are met:

$$\frac{d\gamma^{NR}}{dX} > 0 \qquad \text{(Equation 4-22)}$$

$$\frac{d\gamma^{RX}}{dX} < 0 \qquad \text{(Equation 4-23)}$$

By differentiating (Equation 4-15), one can check that the condition in (Equation 4-22) might not always be satisfied before γ^{NR} reaches 1, due to the strong decrease rate of γ^{RX} as expressed by (Equation 4-20). γ^{NR} then reaches a peak value below 1, which is not physically acceptable. This behavior was not found to happen when applying the model to 304L stainless steel (see section 5.6), but can mathematically present itself for other materials. Therefore a second approach has been tested for such cases, as discussed below.

Based on Figure 4-4, a reasonable approximation consists in setting $\gamma^{RX} = 1$ when X is small, instead of using (Equation 4-20). In this case, the condition in (Equation 4-22) is automatically met before γ^{NR} reaches 1. Figure 4-5b shows the typical difference between this approach and the previous one (Figure 4-5a). The predicted evolution of X is shown to be very similar.

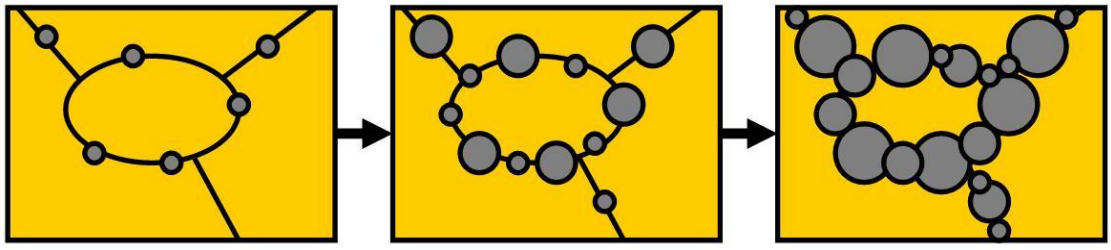

Figure 4-4 Schematic representation of necklace-type nucleation mechanism

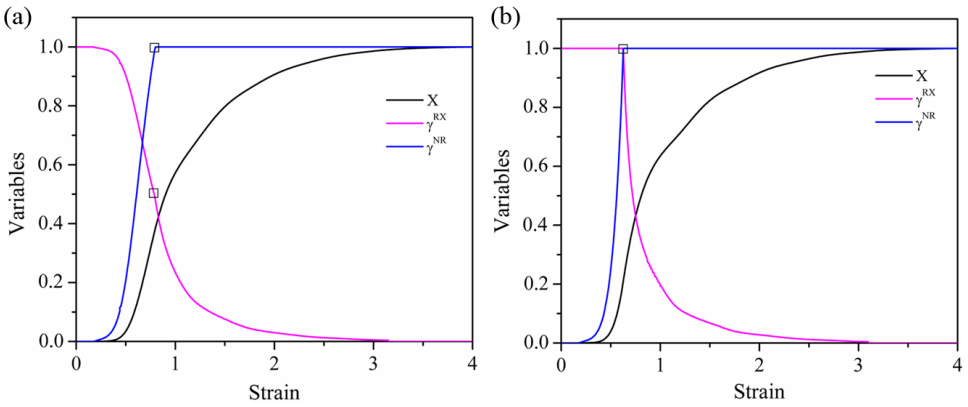

Figure 4-5 Evolution of γ^{RX} and γ^{NR} surface factions, and of the recrystallized fraction X as a function of strain. (a) initially setting $\gamma^{RX} = 1 - X^n$, (b) initially setting $\gamma^{RX} = 1$.

4.3.4.2. Migration of RX-RX and NR-NR interfaces

Although RX-RX and NR-NR interfaces are characterized by smaller magnitudes of driving forces, the interfaces are allowed to move. Indeed, the grain boundary motion itself results in a reduction of dislocation densities (see section 3) and therefore influences both the stress-strain behavior and the recrystallization kinetics.

Based on (Equation 4-5), one can describe the motion of these interfaces by distinguishing growing grains for which $\Delta E_k^{HEM} > 0$, and shrinking grains for which $\Delta E_k^{HEM} < 0$. Growing grains can be described through

$$\Delta V_{i,RX/RX} = 4\pi r_i^2 m \Delta E_i^{RX} \Delta t \;\; ; \;\; \Delta V_{RX/RX} = \sum_{\Delta E_i^{RX}>0} N_i \Delta V_{i,RX/RX} \quad \text{(Equation 4-24)}$$

$$\Delta V_{j,NR/NR} = 4\pi r_j^2 m \Delta E_j^{NR} \Delta t \;\; ; \;\; \Delta V_{NR/NR} = \sum_{\Delta E_j^{NR}>0} N_j \Delta V_{j,NR/NR} \quad \text{(Equation 4-25)}$$

The volume changes of shrinking grains, on the other hand, are computed from

$$\Delta V_{i,RX/RX} = -\Delta V_{RX/RX} \frac{r_i^2 \Delta E_i^{RX}}{\sum_{\Delta E_k^{RX}<0} N_k r_k^2 \Delta E_k^{RX}} \quad \text{(Equation 4-26)}$$

$$\Delta V_{j,NR/NR} = -\Delta V_{NR/NR} \frac{r_j^2 \Delta E_j^{NR}}{\sum_{\Delta E_k^{NR}<0} N_k r_k^2 \Delta E_k^{NR}} \quad \text{(Equation 4-27)}$$

4.3.4.3. Overall volume change

Using relations in (Equation 4-14) and (Equation 4-24) to (Equation 4-26), the volume change of RX and NR grains attributed to grain boundary migration alone can be expressed by:

$$\Delta V_i = \gamma^{RX} \Delta V_{i,RX/NR} + (1-\gamma^{RX}) \Delta V_{i,RX/RX} \quad \text{(Equation 4-28)}$$

$$\Delta V_j = \gamma^{NR} \Delta V_{j,NR/RX} + (1-\gamma^{NR}) \Delta V_{j,NR/NR} \quad \text{(Equation 4-29)}$$

Volume conservation is automatically satisfied when using these relationships, which means that $\sum_i \Delta V_i + \sum_j \Delta V_j = 0$. If nucleation conditions are met, volume conservation continues to apply, by transferring volumes defined by (Equation 4-8) to a new representative grain of total volume given by (Equation 4-9).

A zone that was just swept by a boundary is almost dislocation free. The total amount of

dislocations of the grain is not affected by this increase in volume, but the average dislocation density in the considered grain decreases according to

$$\Delta(\rho V) = 0; \qquad \frac{\Delta\rho}{\rho} = -\frac{\Delta V}{V} \qquad \text{(Equation 4-30)}$$

4.3.5. Computational aspects of mathematical modeling

The model results are obtained through solving the governing equations by Euler's implicit method as an initial value problem for the dislocation densities and grain sizes of all representative grains. Some technical aspects of the computation are commented below.

4.3.5.1. Time step management

The value of the time step is limited by two conditions: (i) based on the magnitude of changes of the dislocation densities, and (ii) based on volume changes of shrinking grains. The first condition, which must be met for all representative grains *i*, is written as:

$$\frac{\Delta\rho_i}{\rho_i} < \delta \qquad \text{(Equation 4-31)}$$

where ρ_i is the dislocation density at the beginning of the time step. When implicitly integrating (Equation 4-1), condition in (Equation 4-31) leads to the limiting time step

$$\Delta t = \underset{i}{Min}\left(\frac{\delta\,\rho_i}{\dot{\varepsilon}\left(K_1 - K_2\rho_i(1+\delta)\right)}\right) \qquad \text{(Equation 4-32)}$$

This condition ensures a good accuracy of the integration procedure, particularly at low dislocation densities where evolution is very fast.

The second condition relates to representative grains which tend to shrink at the expense of others which are expanding. When using the time step defined by (Equation 4-32), the algorithm (see next section) will compute volume changes according to (Equation 4-28) and (Equation 4-29), and including nucleation. If some of the grains shrink to a negative volume, the chosen time step is reduced in order to remove exactly the volume of the first representative grain to disappear. If the magnitude of the time step variation is limited, volume change can be approximated as linear with the time step, and the time step correction is straightforward.

4.3.5.2. Numerical implementation of the model

The algorithm starts with the initialization of variables. All representative grains are assigned a dislocation density, size and number of grains in order to match desired distributions (Figure 4-2). During a time step:

- If $X = 0$, there is no RX grains, dislocation densities and grain sizes evolve according to (Equation 4-1), (Equation 4-25) and (Equation 4-27).
- If $X > 0$, the surface fractions γ^{RX} and γ^{NR} are computed using the procedure accounting for necklace structures (see section 4.3.4.1). Size and dislocation densities are then updated for all representative grains following (Equation 4-28), (Equation 4-29) and (Equation 4-30).
- The default time step is adapted with the two conditions described in section 4.3.5.1, and previous calculations are updated according to the new time step.
- Nucleation of a new representative grain is evaluated based on the criteria defined in section 4.3.3. If these criteria are met, the corresponding volumes are transferred, and the recrystallized volume fraction *X* is updated.

- The material flow stress is evaluated using (Equation 4-2) and (Equation 4-3). The recrystallized and total average grain sizes are also computed.

4.4. Static/Post dynamic recrystallization model

4.4.1. Introduction

The investigation on recrystallization after hot deformation mainly focuses on the different mechanisms occurring after the interruption of deformation, much less attention has been paid so far to the modeling of this mechanisms. The model developed by Roucoules *et al*. [51] assumed no mechanistic difference between dynamic, static and metadynamic recrystallization, with the same recrystallization equation governing the three regimes. Of course, the storage of dislocations ceases once deformation is interrupted. Kugler and Turk [89] used the same treatment in their model. Even though the above models can predict the microstructure evolution quantitatively to a certain extent, some key aspects are however still missing as illustrated in section 2.5.4.2, which is very likely due to the fact that their models are oversimplified. For example, regarding the nucleation process, a small strain of about only 10% is required to initiate classical SRX for copper in the temperature range 450–540 ℃, which is about half of that of DRX [108]. The different mechanisms (Static recovery, SRX, PDRX), as described in section 2.5.2.4, acting differently after hot deformation were not addressed in these models.

In the current work, a numerical model dedicated to predict the microstructural evolution after hot deformation is developed. The framework of this model is the same as that of the DRX model, however, some modifications have been carefully implemented according to the different nature of PDRX and SRX as compare to DRX. Static recovery, which does not exist in DRX model, is included here. The smaller critical dislocation density required for triggering nucleation is also implemented. Another important modification is the definition of the RX and NR grains after deformation according to their dislocation densities since some of the dynamically RX grains have high dislocation densities, these grains should be considered as NR grains in the subsequent step. This special treatment helps to better describe different mechanisms acting after the interruption of deformation and the evolution of the two mobile surface fraction terms (γ^{RX} and γ^{NR}) as well. Finally, a limiting value similar to the Zener pinning term which accounts for a limiting grain size in two-phase materials is included in the grain boundary migration equation.

4.4.2. Static recovery

As illustrated earlier in section 2.5.2.4, Sakai *et al*. [100,113] introduced two types of recovery operating after strain interruption. The recovery in growing DRX grains whose dislocation density is inferior to the critical dislocation density for SRX is referred to as post dynamic recovery (PDRV), microstructural changes due to this recovery are generally limited [1]. The other type of recovery concerns non-recrystallized old grains or fully hardened DRX grains and is referred to as static recovery (SRV).

For the statically recrystallized grains, whose dislocation density reached a minimum value (typical value of $\rho_0 \sim 10^{11}$ m^{-2}) [1], clearly no static recovery is involved. In the current case,

since 304L austenitic stainless steel is of low SFE and thus little recovery occurs, it is assumed that recovery alone will not lead to the minimal dislocation density ρ_0, instead, the steady state dislocation density of recovery would be ρ_{ss}^{SRV}. The value of ρ_{ss}^{SRV} may vary according to the nature of the analyzed material, but it is above ρ_0 according to the definition of recovery.

In the current thesis, the static/post dynamic recovery is considered as the same, for simplification purpose, recovery model by setting K_1 in (Equation 2-2) to zero is implemented. In the current thesis, static recovery is modeled, for simplification purpose, with (Equation 4-33) evolving only one parameter K_s. This parameter depends only on the annealing temperature,

$$\frac{d\rho}{dt} = -K_s \rho \qquad \text{(Equation 4-33)}$$

The model proposed by Estrin [14] in (Equation 2-5) is however not considered, due to the fact that too many unknown parameters are involved.

4.4.3. Nucleation

Static recrystallization may occur when a hot deformed material is subsequently annealed. Below some critical strain for static recrystallization, limited softening takes place by static recovery as shown in Figure 2-32b, which involves only fine-scale changes in the deformed structure. Even though the critical condition at which DRX starts has been widely investigated both theoretically and experimentally, much less efforts have been paid on the critical strain for SRX. Besides, the effect of deformation conditions IS usually not considered.

Since statically recrystallized grains do not suffer concurrent deformation, $\rho(x) = 0$ could be set in (Equation 2-8), and we can easily get the critical dislocation density for initiation of SRX from (Equation 4-12),

$$\rho_{cr}^{SRX} = \frac{2\gamma_b}{r_{cr}\tau} \qquad \text{(Equation 4-34)}$$

It is straightforward from Figure 2-9 that if $\rho(x) = 0$, the critical dislocation density of SRX will decrease as compared to the DRX one. A quantitative comparison will be discussed in the next sections. It is important to notice that the same equation was obtained when analyzing bulging mechanism nucleation as illustrated in section 2.3.1. This approach of evaluating critical dislocation density, however, needs the input of critical nucleus size which might vary according to the deformation or annealing temperature.

The critical strain for SRX (ε_{cr}^{SRX}) has been analyzed experimentally in various conditions instead of establishing theoretical critical conditions. Xu *et al.*[100] found $0.10 < \varepsilon_{cr}^{SRX} < 0.26$ at temperature of 860 ℃ and with strain rate of $2\times10^{-3}s^{-1}$ for an austenitic steel with initial grain size of 16 μm. Sakai *et al.* [113] observed in nickel (initial grain size of 97 μm), at condition of 777 ℃ and $2\times10^{-3}s^{-1}$, that ε_{cr}^{SRX} was in the rage of 0.08~0.14. Other similar cases can be found, examples include [108,183].

Petkovic *et al.* [111] examined the critical dislocation density for SRX at three different combinations of temperature and strain rate on copper: 450 ℃ and $1.8\times10^{-3}s^{-1}$; 500 ℃ and $1.8\times10^{-2}s^{-1}$; 540 ℃ and $1.8\times10^{-2}s^{-1}$. They found that $0.05 < \varepsilon_{cr}^{SRX} < 0.15$ for these three conditions. SRX occurred after an accumulated strain of 0.05 at 540 ℃ and $1.8\times10^{-2}s^{-1}$, while no SRX was observed, for the larger strain of 0.10 applied at 450 ℃ and $1.8\times10^{-3}s^{-1}$. So, it

seems ε_{cr}^{SRX} is also dependent on the deformation conditions, which is similar to the case of DRX.

Based on the above considerations, in the current work, ε_{cr}^{SRX} is related to the critical dislocation density for DRX to take into account the effect of deformation conditions,

$$\rho_{cr}^{SRX} = \xi \cdot \rho_{cr}^{DRX} \quad \text{(Equation 4-35)}$$

where ξ is a constant, $0 < \xi < 1$. Following the same strategy as for DRX (section 4.3.3), the critical nucleus size for classic static recrystallization is given by

$$r_u^{SRX} = \omega \cdot \frac{2 \cdot \gamma_b}{\rho_{cr}^{SRX} \cdot \tau} \quad \text{(Equation 4-36)}$$

The same nucleation law (see (Equation 4-8)) as in DRX is used, since the argument that the amount of activated nucleation sites (i.e. the number of new nuclei) per unit time increases for increasing dislocation densities still holds true in static case. An incubation time t_0 is introduced for SRX, no nucleation will be triggered unless the annealing time exceeds a value higher than t_0.

4.4.4. Definition of RX and NR grain

If the applied strain is beyond ε_{cr}^{DRX} before interruption, dynamically recrystallized grains exist in the microstructure. As shown in Figure 2-19, the inhomogeneous dynamic structures can be classified into the three categories, i) DRX nuclei with an initial value of dislocation density ρ_0, ii) growing DRX grain with $\rho > \rho_0$, and iii) critically work hardened DRX grain ($\rho > \rho_{cr}^{DRX}$). These grains will act differently during the subsequent annealing process. Obviously, the critically work hardened DRX grains lost the typical characteristics of recrystallized grains: low dislocation densities, growing toward NR grains.

In our work, a new term named critical dislocation density for re-defining RX and NR grains after deformation (ρ_{cr}^{Dis}) was introduced as shown in Figure 4-6. The value of ρ_{cr}^{Dis} corresponds to the minimal dislocation density that can be achieved through recovery alone (steady state dislocation density for recovery). It is reasonable that the recrystallized grains should have a dislocation density lower than that of a fully recovered one. The grains with a dislocation density higher than ρ_{cr}^{Dis} are considered as NR grains.

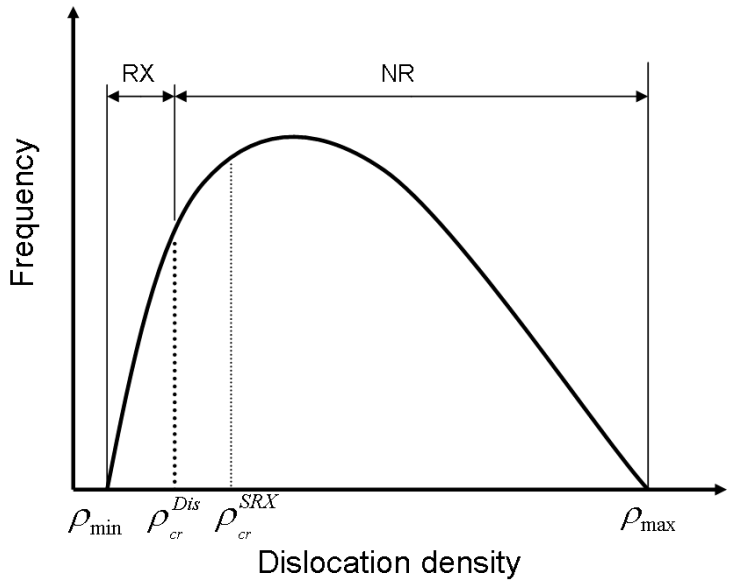

Figure 4-6 Schematic representation of the critical dislocation density for redefining RX and NR grains

For the case where the applied strain ε is such that $\varepsilon_{cr}^{SRX} < \varepsilon < \varepsilon_{cr}^{DRX}$, classic SRX will operate during further annealing. So, after the interruption of deformation, there is no need to re-define RX and NR grains since all the grains have similar level of dislocation density. The initial recrystallized fraction in this case is zero, statically formed nuclei and subsequent growth will control the increase of recrystallized fraction. For materials which has very fast static recovery, theoretically, the dislocation density of some slightly deformed grains may fall to a value close to ρ_{cr}^{Dis} before they are consumed by the growing RX grains. However, this is unlikely to happen for the low SFE 304L, where static recovery is not very active.

If the interruption strain is below ε_{cr}^{SRX}, static recovery is the only mechanism acting during the annealing process, 30-50% of the flow stress increase due to work hardening can be removed by recovery alone [100, 108,111]. No recrystallization is involved in this case, all the grains will see their dislocation density reduced asymptotically to a value close to ρ_{cr}^{Dis} by static recovery, provided that the annealing time is sufficiently long. The recrystallized volume fraction is then always zero.

In the current model, ρ_{cr}^{Dis} is simply related to ρ_{cr}^{SRX} by a constant:

$$\rho_{cr}^{Dis} = \beta \cdot \rho_{cr}^{SRX} \qquad \text{(Equation 4-37)}$$

where $0 < \beta < 1$, ρ_{cr}^{Dis} should be of course higher than $\rho_{\min}$ which is ρ_0 in the current case.

The advantage of re-defining RX and NR grains is that the recrystallized volume fraction can be obtained at any time from the model and compared to experimental results. The definitions of RX and NR are uniquely based on the dislocation densities and there is no need to identify work hardened old grains and critically work hardened recrystallized grains. The traditional way to study PDRX is through tracking the softening fraction, however the measured fractional softening is actually due to the combination effect of recovery and recrystallization processes, the individual attribution being difficult to distinguish. The softening or hardening effects introduced by grain boundary migration and grain size change is also an issue and further deepens the problem. On the other hand, the lack of a standardized method to evaluate the yield stress, which is the input value for calculating softening fraction, leads to a wide variation of the measured value. The softening fraction was found to differ from

the recrystallzed volume fraction [111]. More details regarding these issues on the softening fraction can be found in section 2.5.1.

Another important benefit of re-defining RX and NR grains lies in the fast growth rate of the recently created DRX nuclei. After the interruption of deformation beyond ε_{cr}^{DRX}, some of the RX grains are re-defined as NR grains, as a result, the recrystallized volume fraction X decreases. The mobile surface fraction of these grains then increases accordingly, see (Equation 4-20).

4.4.5. Grain growth and Zenner pinning effect

Grain growth is defined as the uniform coarsening of a material with minimal dislocation content at a high temperature [121]. As long as the stored energy due to the dislocation densities still exists, the grain boundaries keep migrating according to (Equation 4-4) and (Equation 4-5).

However, when a fully recrystallized structure is reached ($X = 100\%$) after primary recrystallization, the driving force is solely due to the inter-granular boundary energy remaining in the specimen.

A dispersion of stable second-phase particles will reduce the rate of grain growth because the driving pressure for growth is opposed by a boundary pinning term (E_z). For grain growth, the driving force in (Equation 4-4) becomes

$$\Delta E = \gamma_b \left(\frac{1}{r_{HEM}} - \frac{1}{r}\right) \pm E_z \qquad \text{(Equation 4-38)}$$

The effects of pinning pressure E_z on the kinetics of grain growth were analyzed by Hillert [124], who used the hypothetical back stress proposed by Zener, the pinning pressure E_z due to the presence of particles was given by

$$E_z = \frac{3F_V\gamma_b}{4r_p} \qquad \text{(Equation 4-39)}$$

which leads to the final grain growth equation,

$$\frac{dr}{dt} = m\Delta E = m\left(\gamma_b\left(\frac{1}{r_{HEM}} - \frac{1}{r}\right) \pm \frac{3F_V\gamma_b}{4r_P}\right) \qquad \text{(Equation 4-40)}$$

where F_V is the volume fraction of randomly distributed spherical particles of radius r_p. The sign of the pinning pressure term must be chosen in each case carefully such that the pinning effect is acting against the movement of the grain boundary. The negative sign holds when $1/r < 1/r_{HEM} - E_z$ and the positive sign applies when $1/r > 1/r_{HEM} - E_z$. Between these two limits, the pinning pressure would exceed the driving force which is physically not true, and therefore $dr/dt = 0$ (boundary is pinned). The pinning pressure E_z is combined together with grain boundary mobility m as $K_p = mE_z$ to be consistent with other K parameters.

4.4.6. Computational aspects of mathematical modeling

4.4.6.1. Continuity from dynamic to static conditions

The model is controlled by the total time, which involves both deformation and annealing time. Starting from the simple hot deformation process, where the deformation temperature

and strain rate are both constant, it is relatively easy to define the total time. In variable conditions corresponding to hot forming conditions, the information of temperature (T_i), strain (ε_i) and strain rate ($\dot{\varepsilon}_i$) or holding time (t_i^{ht}) is available at each time step. Summing up all the time steps in each thermo-mechanical process, the total time t^{tot} would be,

$$t^{tot} = \sum \frac{\varepsilon_i}{\dot{\varepsilon}_i} + \sum t_i^{ht} \qquad \text{(Equation 4-41)}$$

The calculation will stop when t^{tot} has been reached, the information of each representative grain is tracked through the state variables: dislocation density ρ_i, grain size r_i, and number of grain N_i. Whenever the deformation is interrupted, $\dot{\varepsilon} = 0$ and this information allows to switch from DRX to SRX/PDRX model. The redefining of RX and NR grains after deformation will be conducted only if $X^{DRX} > 0$.

In this work, the simple case of multi-pass condition recrystallization is tested: a DRX process plus the recrystallization process after DRX, namely SRX/PDRX and GG. The extension to more complicated applications will be considered in the future, it is reasonable to say that it will be easy to achieve since all the key ingredients have already been incorporated in the current model.

4.4.6.2. Time step management

When deformation is interrupted, the two conditions limiting the value of the time step in the case of DRX also apply: (i) based on the magnitude of changes of the dislocation densities, similar as DRX, see (Equation 4-31), (ii) based on volume changes of shrinking grains. Different from DRX, the time step during SRX/PDRX should be appropriate such that the decrease of dislocation density for all representative grains *i*, does not exceed a limit. This is implemented to ensure the accuracy of the calculation, particularly after the interruption of deformation when dislocation densities decrease fast by both recovery and grain boundary migration. The adapting of time step to avoid that a grain shrinks to a negative volume is exactly the same as in the case of DRX as previously described in section 4.3.5.1.

By implementing these two limiting values, the initial time step could be given as any arbitrary value, since the real time step will automatically adapt. The initial time step is defined as 2s in the current work, which is already sufficiently small for calculations up to 6000s.

4.4.6.3. Numerical implementation of the SRX/PDRX/GG model

- After the deformation step, the strain rate is $\dot{\varepsilon} = 0$, and model parameters in (Equation 4-33), (Equation 4-35) to (Equation 4-37), as well as (Equation 4-40) are all defined according to the current temperature.
- If $X = 0$, there is no RX grains, dislocation densities and grain sizes evolve according to (Equation 4-33), (Equation 4-25) and (Equation 4-27).
- If $X > 0$, the RX and NR grains are re-defined according to the distribution of dislocation densities. The surface fractions γ^{RX} and γ^{NR} are computed based on the new X using the procedure accounting for necklace structures (see section 4.3.4.1). Grain boundary migrates according to (Equation 4-40), where the pinning term is taken into account (absent in the DRX case). Size and dislocation densities are then updated for all representative grains following (Equation 4-28), (Equation 4-29) and (Equation 4-30).
- The default time step is adapted with the two conditions described in section 4.4.6.2, and previous calculations are updated according to the new time step.

- Nucleation of a new representative grain is evaluated based on the criteria defined in section 4.4.3. If these criteria are met, the corresponding volumes are transferred, and the recrystallized volume fraction X is updated according to (Equation 4-8).
- The material flow stress is evaluated using (Equation 4-2) and (Equation 4-3), which can be then used to calculate softening fraction (see section 2.5.1). The recrystallized and total average grain sizes are also computed.
- The calculation stops when the total time t^{tot} is reached.

4.5. Conclusions

In this chapter, a two-site mean field recrystallization model has been developed and is based on the interaction between a set of representative grains and two HEMs having different properties. Representative grains are fully defined by their dislocation density, grain size, and volume fraction. HEM properties are derived as volume averages of the individual representative grains and influence themselves the evolution of the representative grains state variables. The respective influences of the two HEMs are linked to the values of mobile surface fractions which evolve with the microstructure, with explicit account of volume conservation.

Comparing to the existing models in literature, this proposed model has the following outstanding features:

i) It provides data on recrystallization kinetics, stress-strain curves and recrystallized grain size together;

ii) It is able to simulate recrystallization under multi-pass conditions, including DRX, SRX, PDRX and GG;

iii) It takes into account the initial distribution of grain size and topology effects are partially introduced (necklace structure);

iv) It is not computationally demanding, since no explicit representation of microstructures is introduced, so it can readily be coupled to a FEM formulation describing standard forming processes.

4.6. French summary

Dans ce chapitre, un modèle à champ moyen à deux-sites des phénomènes de recristallisation a été développé. Celui-ci est basé sur l'intégration d'un ensemble représentatif des grains avec deux milieux homogènes équivalents (HEMs) ayant des propriétés différentes. Les grains sont définis par leur densité de dislocations, taille et fraction volumique. Par ailleurs, les propriétés des HEMs dérivent du volume moyen des grains représentatifs et influencent l'évolution des variables d'état de l'ensemble des grains. L'influence de chaque HEM est liée aux valeurs des fractions de surface mobile qu'ils induisent, évoluant avec la microstructure, en prenant en compte la conservation du volume.

En comparant ce modèle aux autres déjà existants dans la littérature, il peut être observé que celui-ci présente plusieurs avancées majeures :

i) Il fournit des données sur la cinétique de recristallisation, courbes contrainte-déformation et taille de l'ensemble des grains recristallisés ;

ii) Il est capable de simuler la recristallisation en conditions multi passes, incluant ainsi la DRX, la SRX, la PDRX et aussi la GG ;

iii) Il prend en compte la distribution initiale de tailles de grain et des effets topologiques sont partiellement introduits (structure en collier) ;

iv) Il n'est pas couteux en temps de calcul puisqu'aucune représentation des microstructures n'est explicitement réalisée, et peut par conséquent être facilement couplé à une formulation éléments finis qui décrit les procédés standards de mise en forme.

5. Discontinuous dynamic recrystallization

5.1. Introduction

When plastic deformation is carried out at high enough temperature, new grains may originate at the old grain boundaries once a critical strain ε_{cr} has been reached. As the material continues to deform, the dislocation density of the new grains increases, thus reducing the driving force for further growth, and the recrystallizing grains eventually cease to grow. Another factor which may limit the growth of the new grains is through impingement where the growing grain meets with other recrystallized grains. This type of dynamic recrystallization, which has clear nucleation and growth stages, can be classified as discontinuous dynamic recrystallization (DDRX) [1].

In this chapter, the effects of accumulated strain, strain rate, temperature as well as initial grain size on DDRX are all examined by experiments. A full set of experimental data was obtained including flow stress, recrystallized volume fraction and recrystallized grain size for each deformation condition. Based on these experimental results, together with an inverse analysis, the parameters of the model proposed in section 4.3 are identified. Comparisons have been made between the experimental and numerical results and it is found that excellent agreement has been obtained.

The successful prediction of DDRX provides the basis for further investigation of subsequent SRX/PDRX, which will be presented in the next sections.

5.2. Experiment

All the 304L samples were preheated at the test temperature for 3 min to get a homogenous temperature. A constant strain rate is then applied until the pre-set deformation is reached, the deformed sample is subsequently quenched by water to preserve as much as possible the microstructure for examination by optical or electron microscope, the procedure is shown schematically in Figure 5-1.

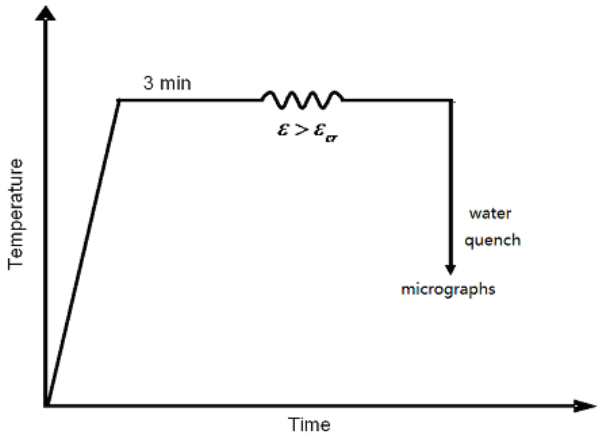

Figure 5-1 Schematic diagram of DRX experiment using the torsion test

The torsion tests of a wide range of conditions were conducted as listed below in Table 5-1, the deformation temperature and strain rate were chosen such that comparisons with literature data are possible. At each deformation temperature from T=900℃, to T=1150℃, three different strain rates 0.01, 0.1 and 1.0s^{-1} were applied with an initial grain size of 165μm. The effect of initial grain size is studied by using other smaller value of 45μm in a few conditions. It

is important to mention that some of the sample ruptured before the steady state was obtained, at lower temperatures and higher strain rates, which will be discussed later in this chapter.

Table 5-1 The conditions analyzed for DDRX described in this chapter

	0.01 (s^{-1})	**0.1 (s^{-1})**	**1.0 (s^{-1})**
900 ℃	Δ ×	Δ ×	×
1000 ℃	Δ ×	Δ ×	×
1100 ℃	×	×	×
1150 ℃	×	×	×

Initial grain size d_0 ×: 165 μm Δ :45 μm

During the preparation of this thesis work, the system for acquiring micrographs was changed once, that is why the scale bars are not uniform.

5.3. Influence of deformation temperature

The planned tests at 900, 1000, 1100 and 1150 ℃ were conducted with the constant strain rate of 0.01s^{-1}, the smoothed stress-strain curves and the microstructure images are presented below in Figure 5-2 to Figure 5-7.

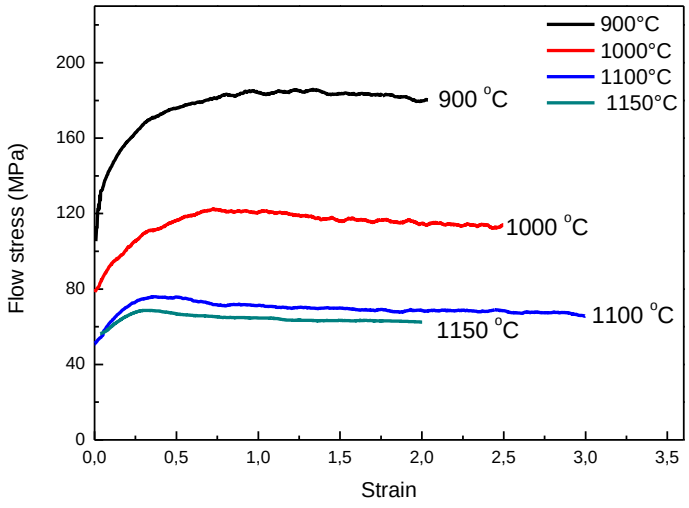

Figure 5-2 Flow curves of 304L deformed at different deformation temperatures ($d_0 = 165\mu m$, $\dot{\varepsilon} = 0.01/s$)

At low deformation temperature (900℃), the flow stress increased gradually, no apparent peak stress was found before fracture strain. As shown in Figure 5-3a where the accumulated strain is 0.5, the initial grains started to elongate, the elongation continued and became more severe in Figure 5-3b at a deformation of 1.0. In Figure 5-3c, where the strain is 1.5, a few small grains can be found among some of the grain boundaries, especially at triple junctions, which demonstrates that recrystallization has taken place. More small grains can be found with further deformation at $\varepsilon = 2.0$ (Figure 5-3d). Although it is hard to see the individual

recrystallized grains clearly using optical microscopy, it is safe to say the size of the small grains is about 5μm or lower. One thing which needs to be noted is that the recrystallized fraction is pretty small even at the fracture strain. As austenitic stainless steels have higher critical strain for DRX and deformation resistance than those of normal carbon steels [184] and the initial grain size is relatively large, it is not surprising that a fully recrystallized structure is not obtained yet at this temperature after a deformation of 2.0.

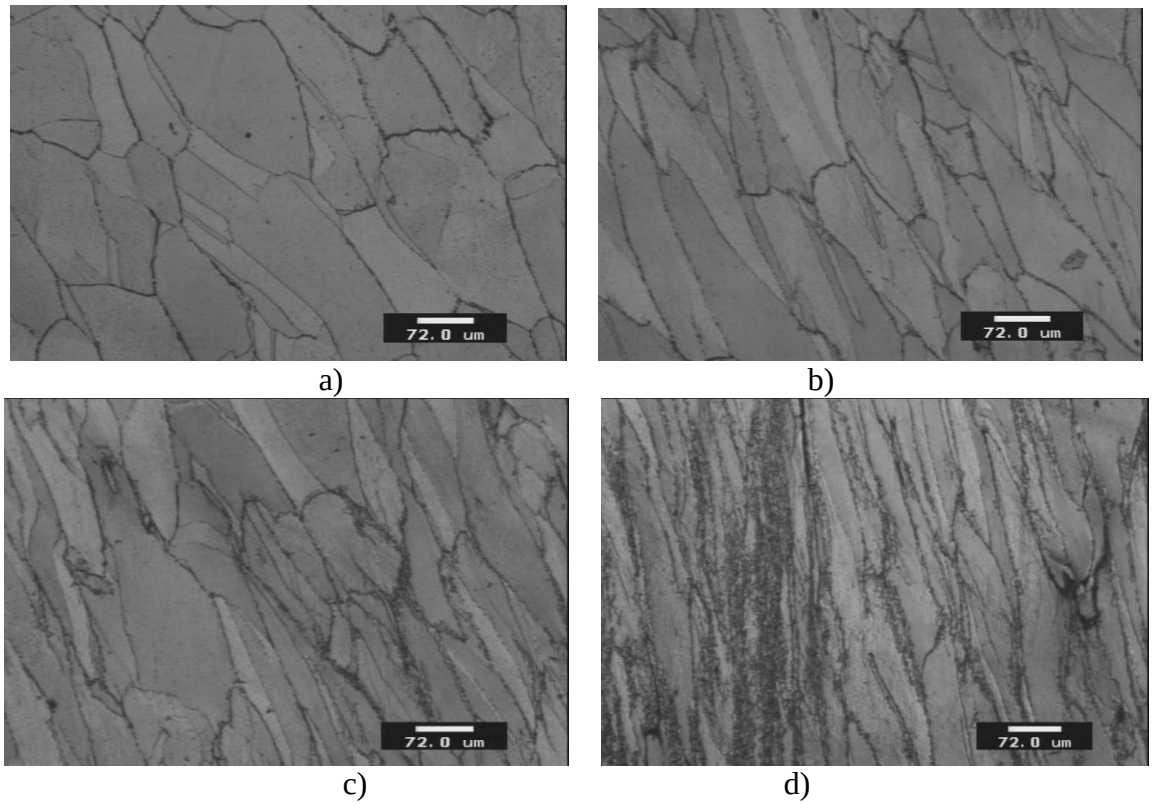

a) b)

c) d)

Figure 5-3 Microstructure of samples deformed at 900℃, $\dot{\varepsilon} = 0.01s^{-1}$ (Optical Microscope)

a) $\varepsilon = 0.5$ b) $\varepsilon = 1.0$ c) $\varepsilon = 1.5$ d) $\varepsilon = 2.0$

At a moderate temperature (1000℃), some changes of flow stress curves are found compared to the previous one (900℃). The flow stress shows more softening compared to the temperature of 900℃ which demonstrates again the importance of temperature in investigating the microstructure evolution of 304L. A mechanical steady-state stress is reached after a strain of ~1.5, but the associated microstructure is not fully recrystallized as shown in Figure 5-4d. At 1000℃, the sample was fractured at a strain slightly after $\varepsilon = 2.5$.

As for microstructure evolution, the flat grain boundaries become irregular after a small deformation of 0.3 (Figure 5-4a), and start to serrate at a strain of $\varepsilon = 0.5$ (Figure 5-4b). Some small grains can be found among the original grain boundaries while other initial grain boundaries remain un-decorated at $\varepsilon = 1.0$, as shown in (Figure 5-4c). Conclusion can be made that the recrystallization starts at a strain ~0.5-1.0 at 1000℃, with a strain rate of $\dot{\varepsilon} = 0.01s^{-1}$, it is faster than the evolution at 900℃ where the critical strain is around $\varepsilon = 1.5$. With further deformation, illustrated in Figure 5-4d and Figure 5-4e, the DRX grains volume fraction increase gradually and a large fraction of the initial microstructure is replaced by the newly formed small DRX grains. In Figure 5-4f, corresponding to a quasi steady state in the flow curve, see Figure 5-2, some initial coarse grains still exist and the recrystallized fraction less than 70%. This could possibly be due to flow localization in the torsion test sample since the

evolution between $\varepsilon = 2.0$ and $\varepsilon = 2.5$ is small, in terms of the recrystallized volume fraction (X_V). It is also important to notice that the recrystallized grain size keeps a value ~10 μm.

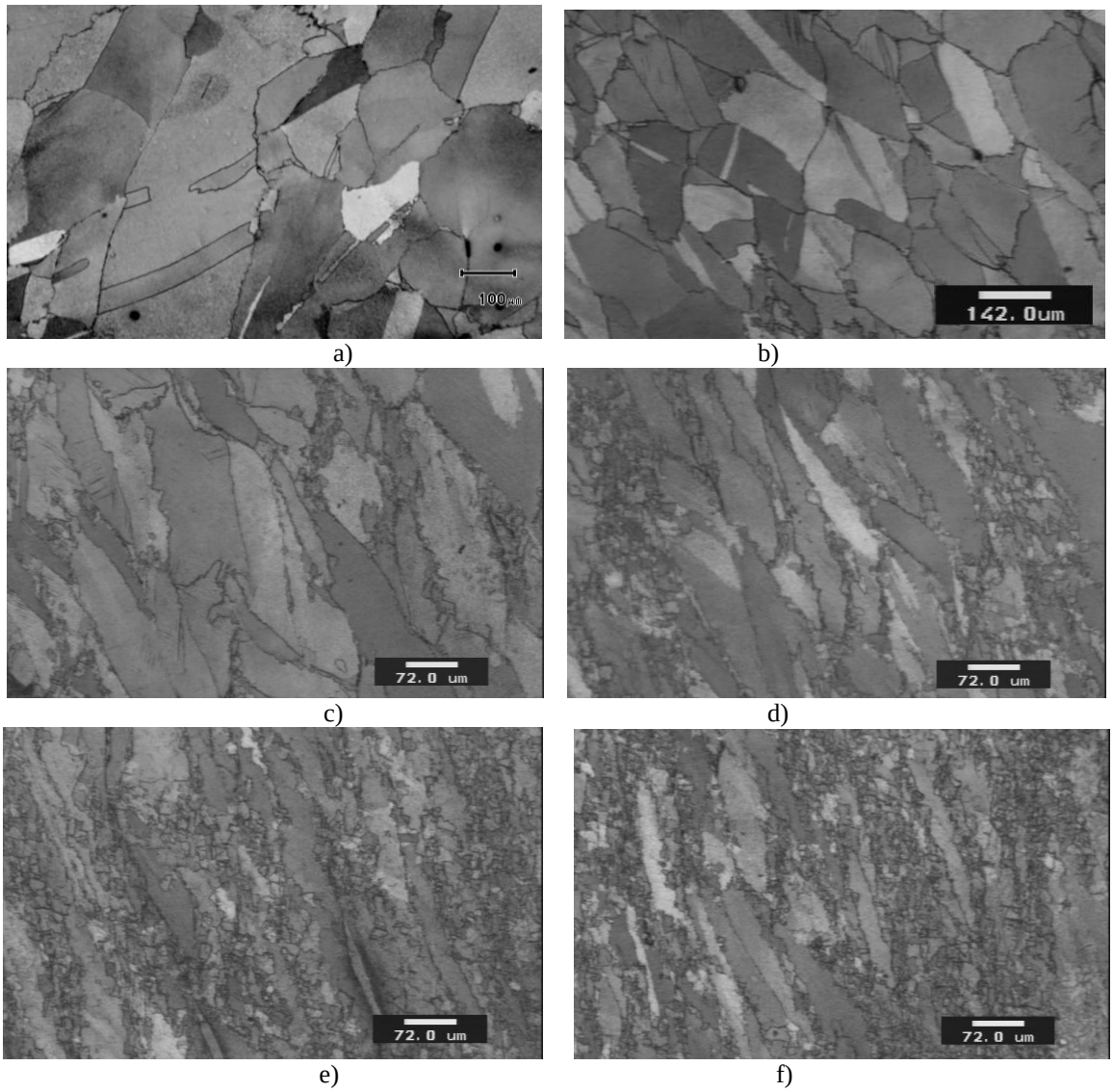

a) b) c) d) e) f)

Figure 5-4 Microstructure of samples deformed at 1000℃, $\dot{\varepsilon} = 0.01\text{s}^{-1}$ (Optical Microscope)

a) $\varepsilon = 0.3$ b) $\varepsilon = 0.5$ c) $\varepsilon = 1.0$ d) $\varepsilon = 1.5$ e) $\varepsilon = 2.0$ f) $\varepsilon = 2.5$

The stress-strain curves of samples deformed at higher temperature (1100℃) and with a constant strain rate of $\dot{\varepsilon} = 0.01\text{s}^{-1}$ exhibit typical DRX flow curves characteristics, with a distinct peak followed by a long steady state (see Figure 5-2). The steady state continued until the sample was fractured. The flow stress decreases with the increase of deformation temperature from 900 to 1100℃. The peak strain, corresponding to the peak stress is smaller than 0.5. As shown in Figure 5-5a, where the strain is 0.5, the initial grains started to serrate, and a few small grains, with a size comparable to the bulging length of the serrations (pointed by black arrows), can be found among some of the grain boundaries. It is important to notice that the newly recrystallized grains are much larger than the previous ones at lower temperature. The number of new grains increased dramatically with further deformation in Figure 5-5b to Figure 5-5e, but elongated grains (indicated by the white arrows) could still be found which means full recrystallization was not reached. The microstructure after

deformation of 2.0, where a steady state can be observed on the flow stress, is examined by EBSD and presented in Figure 5-6. A recent study by Alvi *et al* [185] showed that in a hot rolled commercial purity aluminum alloy, the dynamically recrystallized grains have a GOS value of ~1-3 °. The GOS value for recently created nuclei should be below 1 ° (in blue in Figure 5-6b), which will be further explained when dealing with nucleation for SRX in the next chapter. These "recent" grains only represent a small amount of the microstructure. It is important to notice that the DRX grains formed a little earlier (in green in Figure 5-6b) usually grow by forming a twin on the moving front. However, twins are rarely observed on the severely deformed DRX grains (in yellow Figure 5-6b), which indicates that the twins have lost their crystallographic relation with their parent grains by the concurrent deformation. The microstructure after a deformation of 2.0 is still composed of a mixture of recently created nuclei, deformed DRX grains, and old NR grains (in orange and red Figure 5-6b) characterized by their elongated shape. In Figure 5-5f, almost completely recrystallized microstructure is finally obtained, but small grains can be found near the larger ones, indicating that the microstructure is not homogenous.

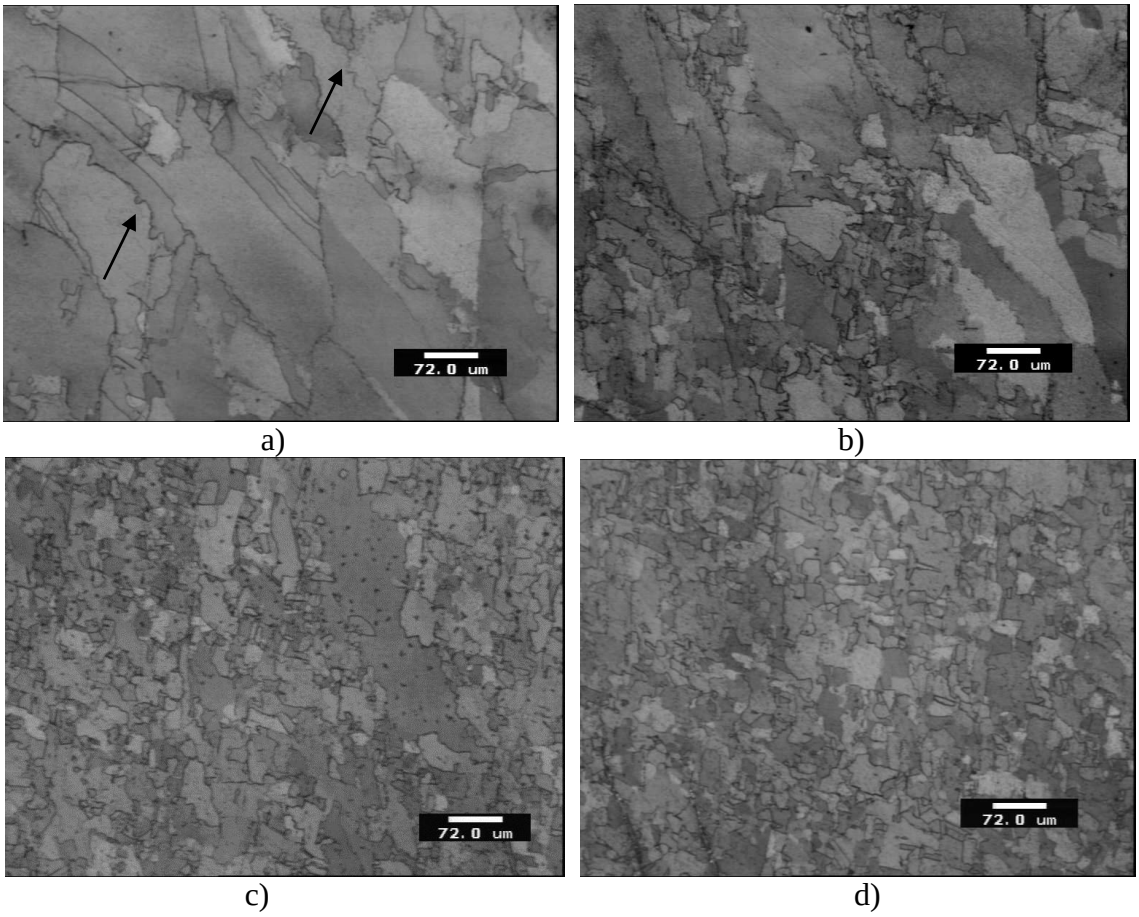

a) b)

c) d)

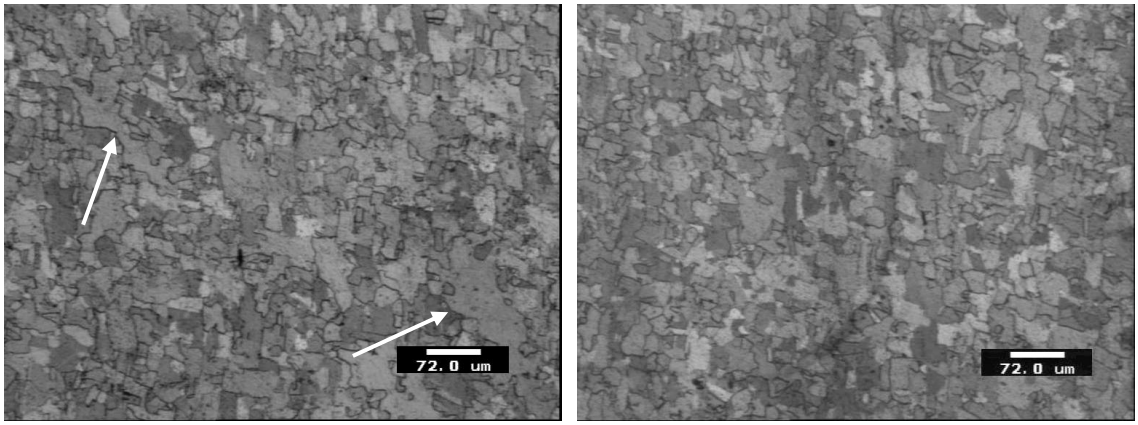

e) f)

Figure 5-5 Microstructure of samples deformed at 1100℃, $\dot{\varepsilon}$=0.01s^{-1} (Optical Microscope)

a) $\varepsilon = 0.5$ b) $\varepsilon = 1.0$ c) $\varepsilon = 1.5$ d) $\varepsilon = 2.0$ e) $\varepsilon = 2.5$ f) $\varepsilon = 3.0$

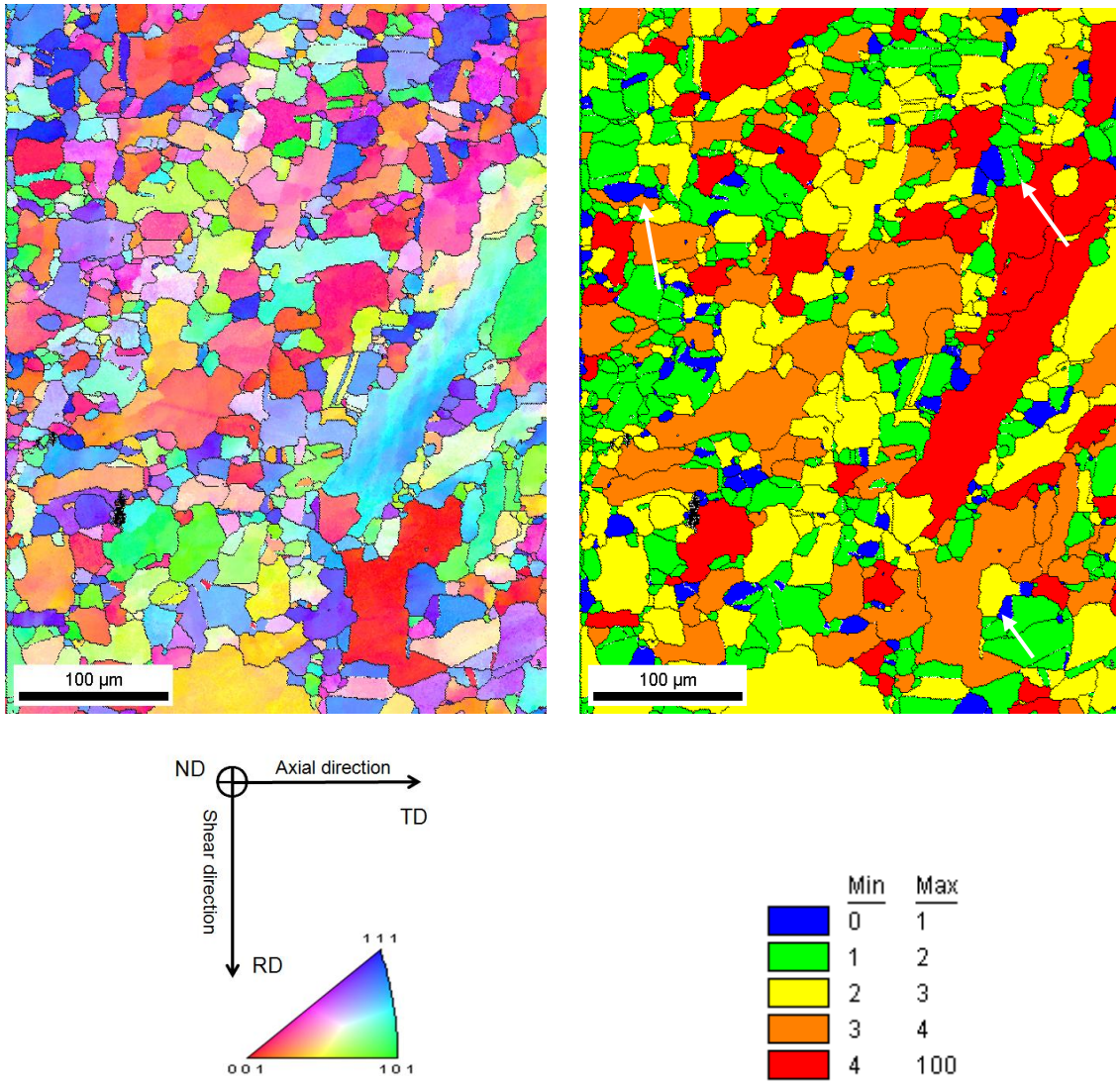

a) b)

Figure 5-6 EBSD map of the microstructure of samples deformed to a strain of 2.0 at 1100 ℃ and strain rate of $0.01s^{-1}$ with initial grain size 165 µm a) IPF map, b) GOS map

By further increasing the deformation to 1150 ℃, a similar type of flow stress was obtained as compared to 1100 ℃, but the peak stress in less pronounced. Comparing to lower temperatures, the peak strain is smaller (~0.3) and the steady state also occurs earlier. A significant fraction of recrystallized grains can already be seen along the original grain boundaries at a strain of 0.5 (Figure 5-7a), and this increases at $\varepsilon = 1.0$ as seen in Figure 5-7b. The distribution of grain size at the large strain of 2.0 is again very heterogeneous, as shown in Figure 5-7c, with a mixture of both large and small grains.

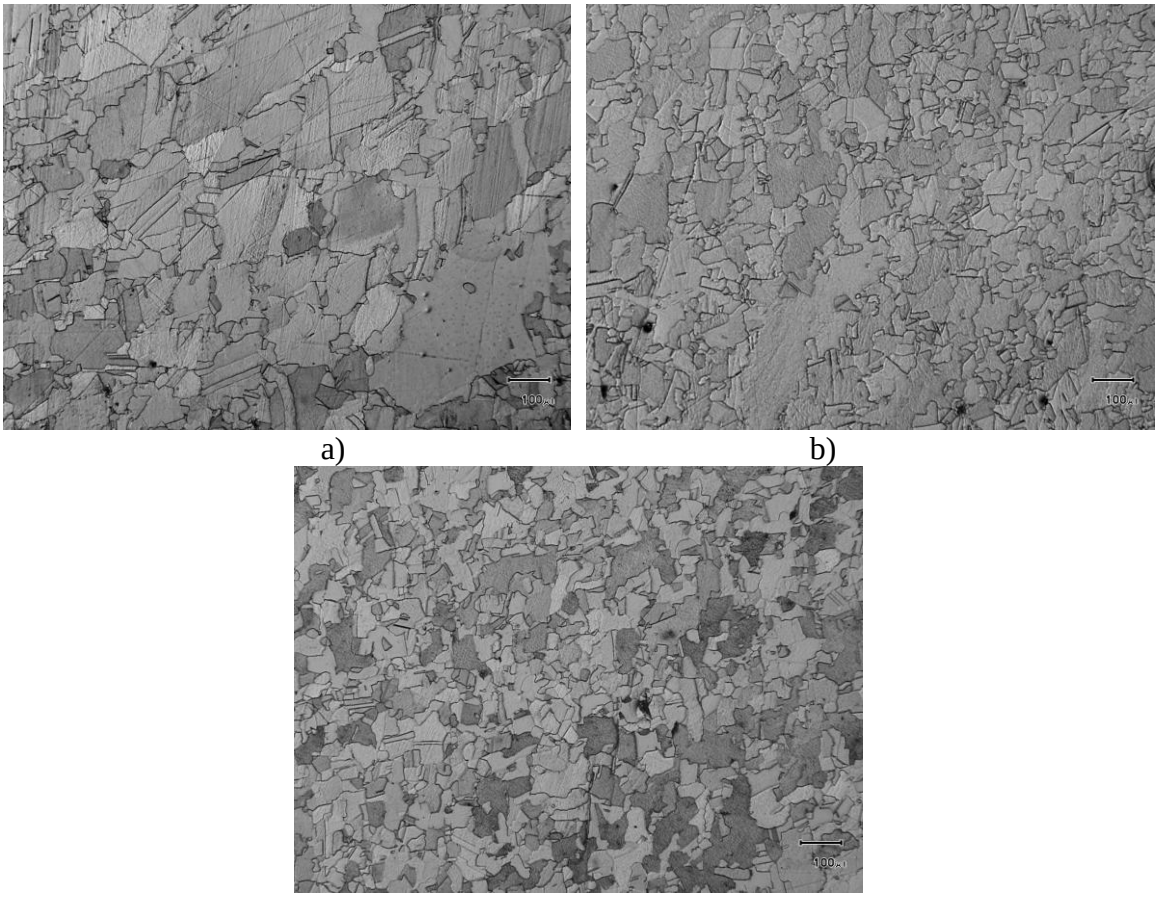

Figure 5-7 Microstructure of samples deformed at 1150℃, $\dot{\varepsilon}=0.01s^{-1}$ (Optical Microscope)

a) $\varepsilon = 0.5$ b) $\varepsilon = 1.0$ c) $\varepsilon = 2.0$

The progress of recrystallization with strain during hot deformation is represented by a plot of the volume fraction of material recrystallized (X_V) as a function of strain, as shown in Figure 5-8. Typical sigmoidal forms of the plots are observed, a relatively small deformation is usually needed before recrystallization is detected. It is apparent that increasing temperature significantly accelerates the DRX kinetics.

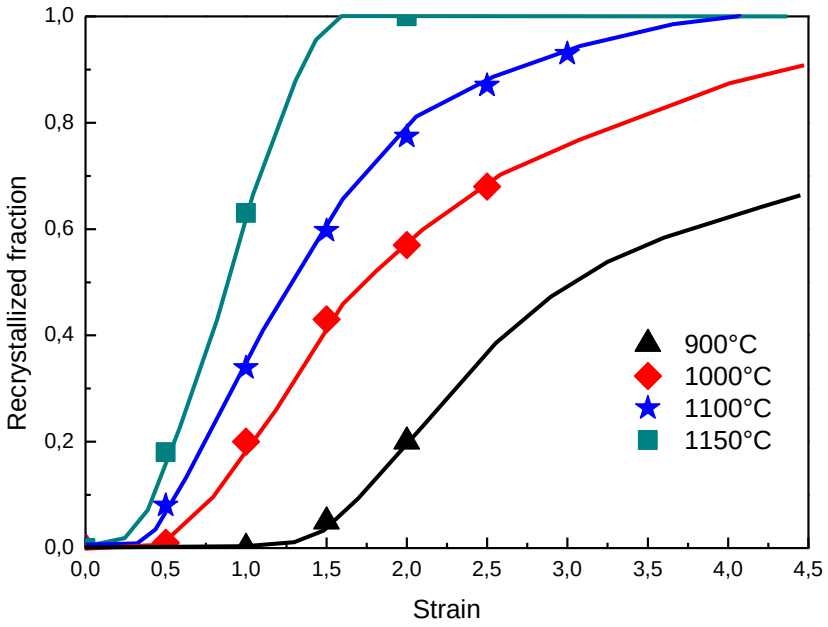

Figure 5-8 Effect of temperature on the kinetics of DDRX ($d_0 = 165\mu m$, $\dot{\varepsilon} = 0.01/s$)

5.4. Influence of strain rate

Effect of deformation temperature and strain rate on flow stress are similar. The strain rate sensitivity of flow stress is considerable over the used strain rate range. As illustrated in Figure 5-9, increasing the strain rate from $\dot{\varepsilon}$=0.01s^{-1} to $\dot{\varepsilon} = 1.0s^{-1}$leads to an increase of flow stress of about 70MPa, i.e. it doubled the flow stress. Only the results obtained at deformation temperature of T=1100℃ were presented here, because relatively higher deformation could be reached before fracture of the samples.

Microstructure images taken with optical microscopy are also presented below to help explaining the influence of strain rate on microstructure evolution, see Figure 5-10 and Figure 5-11.

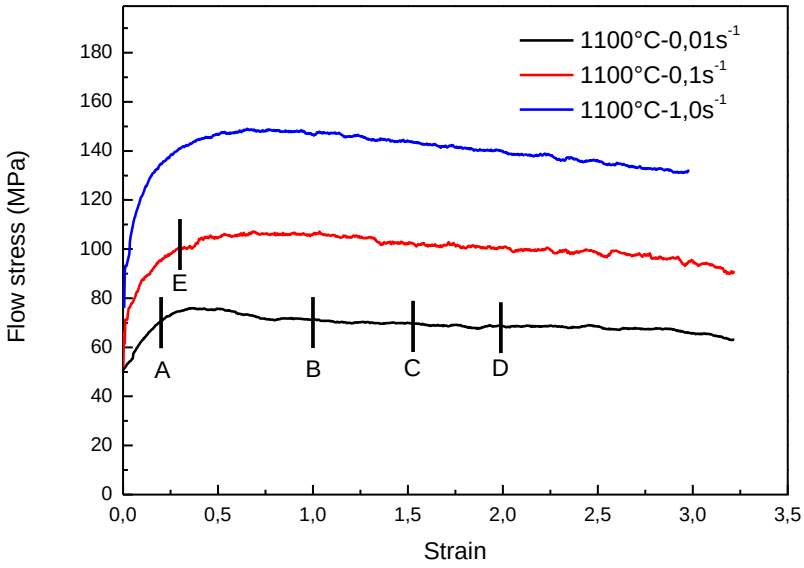

Figure 5-9 Flow curves of 304L deformed at different strain rate at T=1100℃ (The short lines on the flow stress curves correspond to the stop strain for the analysis of SRX/PDRX)

At lower strain rate ($\dot{\varepsilon}$=0.01s^{-1}), the typical flow stress with DRX was obtained , this was explained previously when dealing with the effect of temperature. As the strain rate increase to $\dot{\varepsilon}=0.1s^{-1}$ and $\dot{\varepsilon}=1.0s^{-1}$, the flow curves showed a broader peak followed by continuous softening. This is likely due to the fact that there are more deformation heating generated than with lower strain rate $\dot{\varepsilon}$=0.01s^{-1}, as documented in the literature [68].

Comparison between the microstructure images obtained at lower strain rate of $\dot{\varepsilon}$=0.01s^{-1} with that of samples deformed at $\dot{\varepsilon}=0.1s^{-1}$ and $\dot{\varepsilon}=1.0s^{-1}$ indicates that the recrystallized grain size for the former case (Figure 5-5) is larger than the latter ones (Figure 5-10 and Figure 5-11).

Increasing the strain rate to $\dot{\varepsilon}=0.1s^{-1}$ does not cause a major change in the deformed microstructure compared to the lower strain rate of $\dot{\varepsilon}$=0.01s^{-1}, except that slower kinetics of recrystallization is observed, and the recrystallized grain size is smaller (see Figure 5-10).

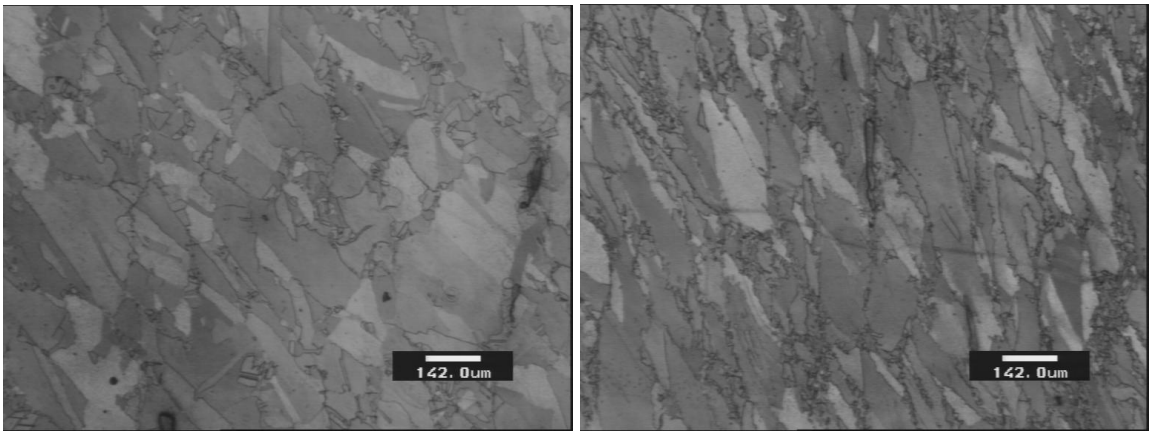

a) $\dot{\varepsilon}=0.1s^{-1}, \varepsilon=0.5$ b) $\dot{\varepsilon}=0.1s^{-1}, \varepsilon=1.0$

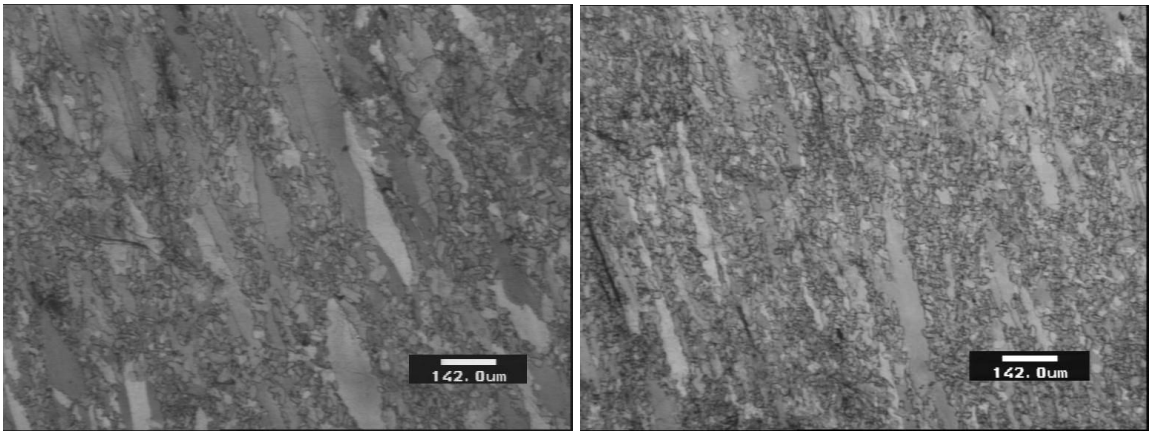

c) $\dot{\varepsilon} = 0.1s^{-1}, \varepsilon = 1.5$ d) $\dot{\varepsilon} = 0.1s^{-1}, \varepsilon = 2.0$

Figure 5-10 Microstructure of samples deformed at 1100℃, $\dot{\varepsilon} = 0.1s^{-1}$ (Optical Microscope)

a) $\varepsilon = 0.5$ b) $\varepsilon = 1.0$ c) $\varepsilon = 1.5$ d) $\varepsilon = 2.0$

It is surprising to find a faster recrystallization kinetics at the strain rate of $\dot{\varepsilon} = 1.0s^{-1}$, with ~70% of recrystallized volume fraction after a deformation strain of 1.0. At the same strain, the recrystallized fraction is ~33% and ~18% with strain rate of $\dot{\varepsilon}$=$0.01s^{-1}$ and $\dot{\varepsilon} = 0.1s^{-1}$ respectively. The results are suspicious and not used in the following sections. The reason might come from two different aspects, both of which promote the recrystallization kinetics. First, the neglected heating system does not have enough time to react to the deformation heating produced during torsion (reflected by the decrease of the flow stress shown in Figure 5-9), since it takes only 1s to reach a strain of 1.0. This increase of temperature from 1100 ℃ certainly accelerates the recrystallization kinetics, as already illustrated in Figure 5-8. The other reason is derived from the quench delay of ~2s as illustrated in section 3.3.4, this short delay is negligible at lower temperatures and with small strain rate, but it becomes important at high temperature and with large strain rate. It is well documented that PDRX after deformation at high strain rate can go to completion within a few seconds after cessation of deformation [68].

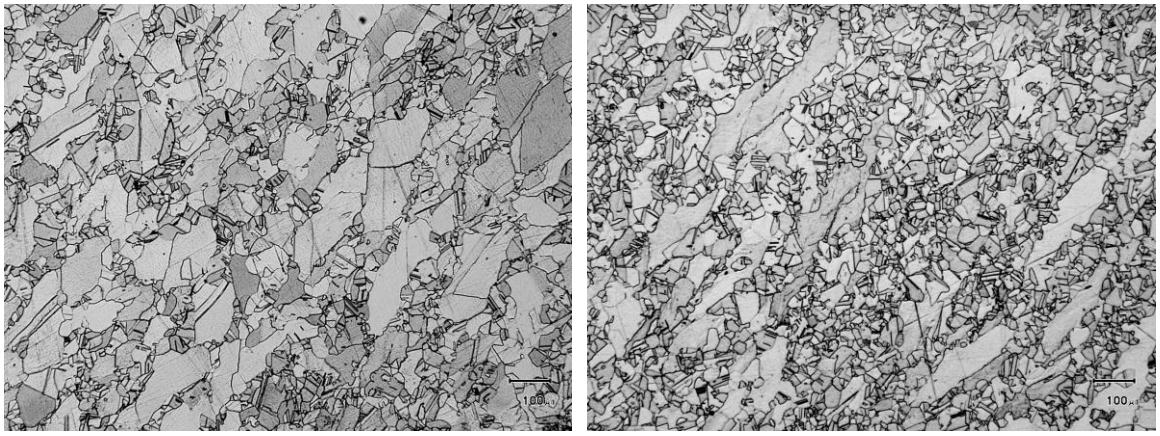

a) $\dot{\varepsilon} = 1.0s^{-1}, \varepsilon = 0.5$ b) $\dot{\varepsilon} = 1.0s^{-1}, \varepsilon = 1.0$

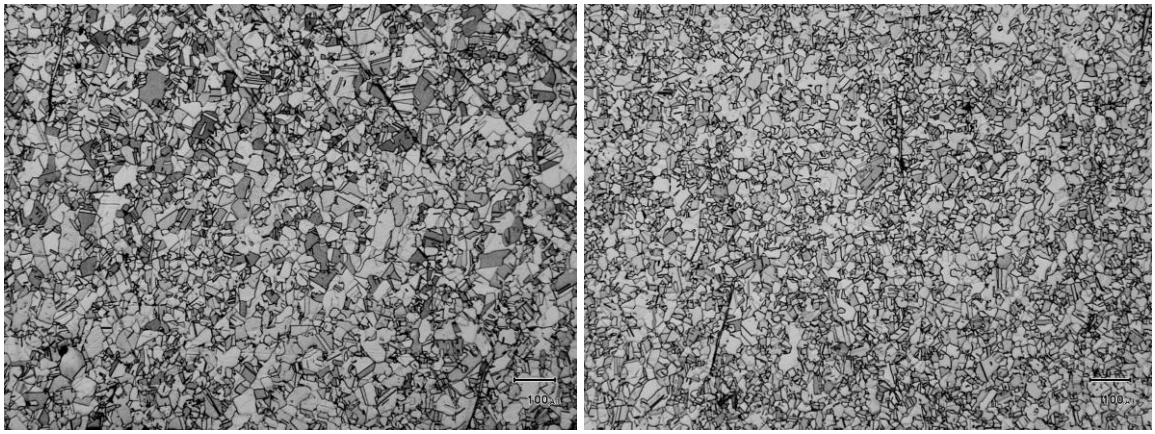

c) $\dot{\varepsilon}=1.0s^{-1}, \varepsilon=1.5$ d) $\dot{\varepsilon}=1.0s^{-1}, \varepsilon=2.0$

Figure 5-11 Microstructure of samples deformed at 1100℃, $\dot{\varepsilon}=1.0s^{-1}$ (Optical Microscope)

a) $\varepsilon=0.5$ b) $\varepsilon=1.0$ c) $\varepsilon=1.5$ d) $\varepsilon=2.0$

The microstructure after a deformation of 1.0 at 1150℃ and $\dot{\varepsilon}=1.0s^{-1}$ was examined by EBSD, and is presented in Figure 5-12. The stored energy of the grains is estimated using the microstructural parameter, GOS (illustrated in section 3.4.2). A considerable amount of grains (66%) with a GOS value below 1°is observed in Figure 5-12b, which is the typical value for newly formed grains. It is not likely that all of these grains are dynamically formed, since some of them have a big grain size of ~30μm. The large fraction of twins (the boundaries of which are plot as white lines), a typical phenomenon of F.C.C materials during annealing, further confirms that these grains with GOS value below 1°are produced during the quench delay by PDRX. The fast kinetics of PDRX at high temperature and with large strain rate will be addressed in the next sections.

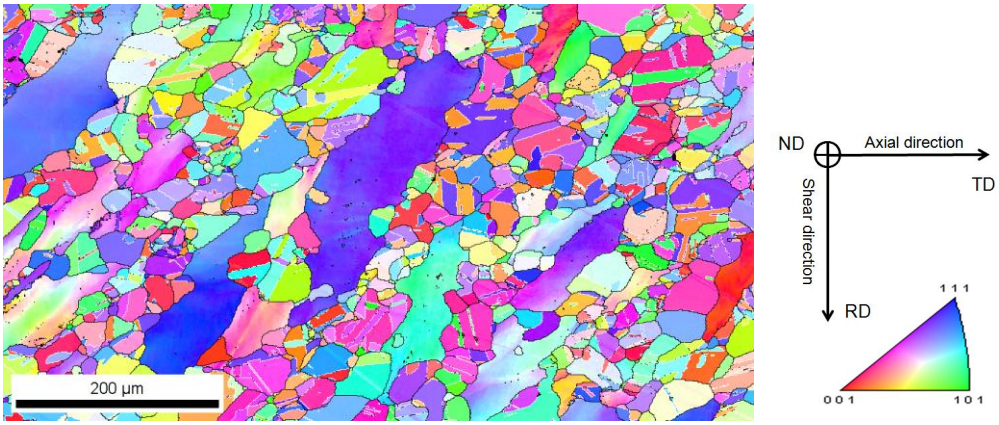

a)

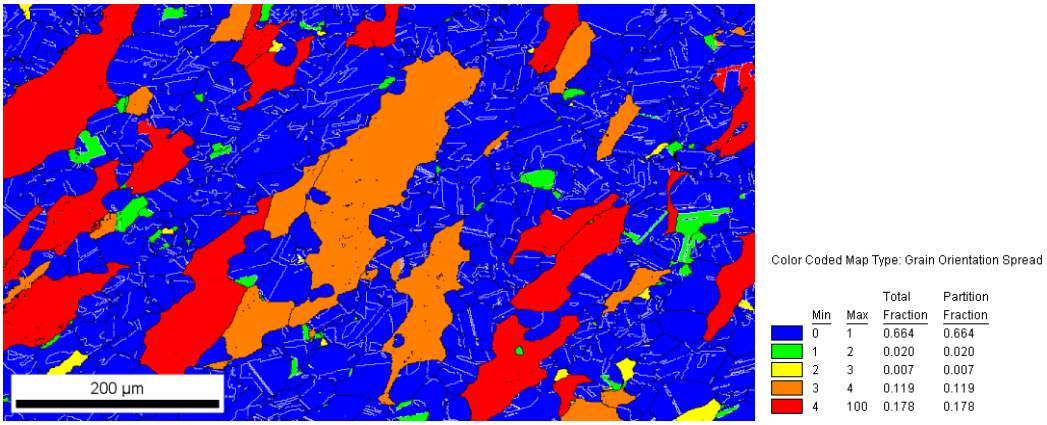

b)

Figure 5-12 Microstructure of samples deformed at 1100℃, $\dot{\varepsilon} = 1.0s^{-1}$ (EBSD map)

a) Inverse Pole Figure map, b) Grain Orientation Spread map

Figure 5-13 compares the kinetics of DRX for two different strain rates as a function of strain. The points correspond to the different strains considered in Figure 5-5 and Figure 5-11. Faster recrystallization kinetics is found at smaller strain rate, which corresponds to the experimental results work published by Dehghan-Manshadi *et al*. [39] (see Figure 2-12), as well as numerical data provided by Fan *et al*. [79] and Ding *et al*. [186].

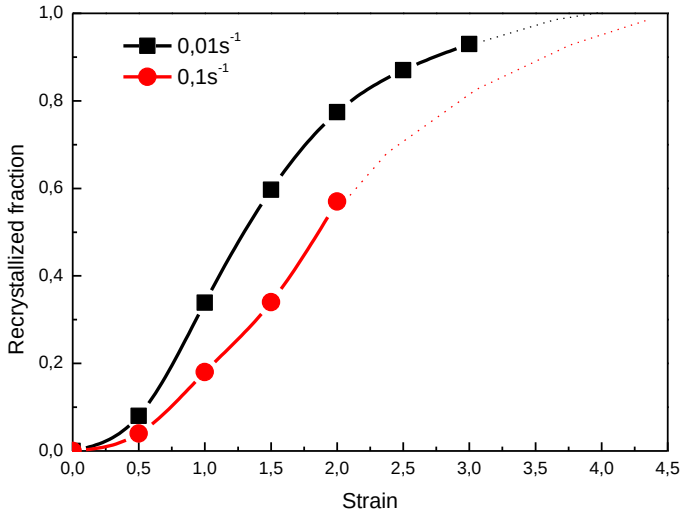

Figure 5-13 Effect of strain rate on the kinetics of DDRX ($d_0 = 165\mu m$, $T = 1100°C$)

5.5. Influence of initial grain size

The microstructures observed on the samples quenched at different strains and deformed at 1000 ℃ and $\dot{\varepsilon} = 0.01s^{-1}$ are shown in Figure 5-14. These tests were performed on samples with grain size of 45 µm. At the very early stage of DRX (Figure 5-14a), small new grains are found mostly along the original grain boundaries. These new grains continue to appear with increasing strain (Figure 5-14b), intragranular nucleation is not very often observed. Most of the non-recrystallized structure is replaced by new grains at $\varepsilon = 1.5$ in Figure 5-14c, only a

limited number of old grains (pointed by the black arrows) are still visible. At the strain of 2.0, a fully recrystallized microstructure is obtained with an average grain size of ~11 μm, which is quite close to that obtained earlier with the larger initial grain size of 165 μm.

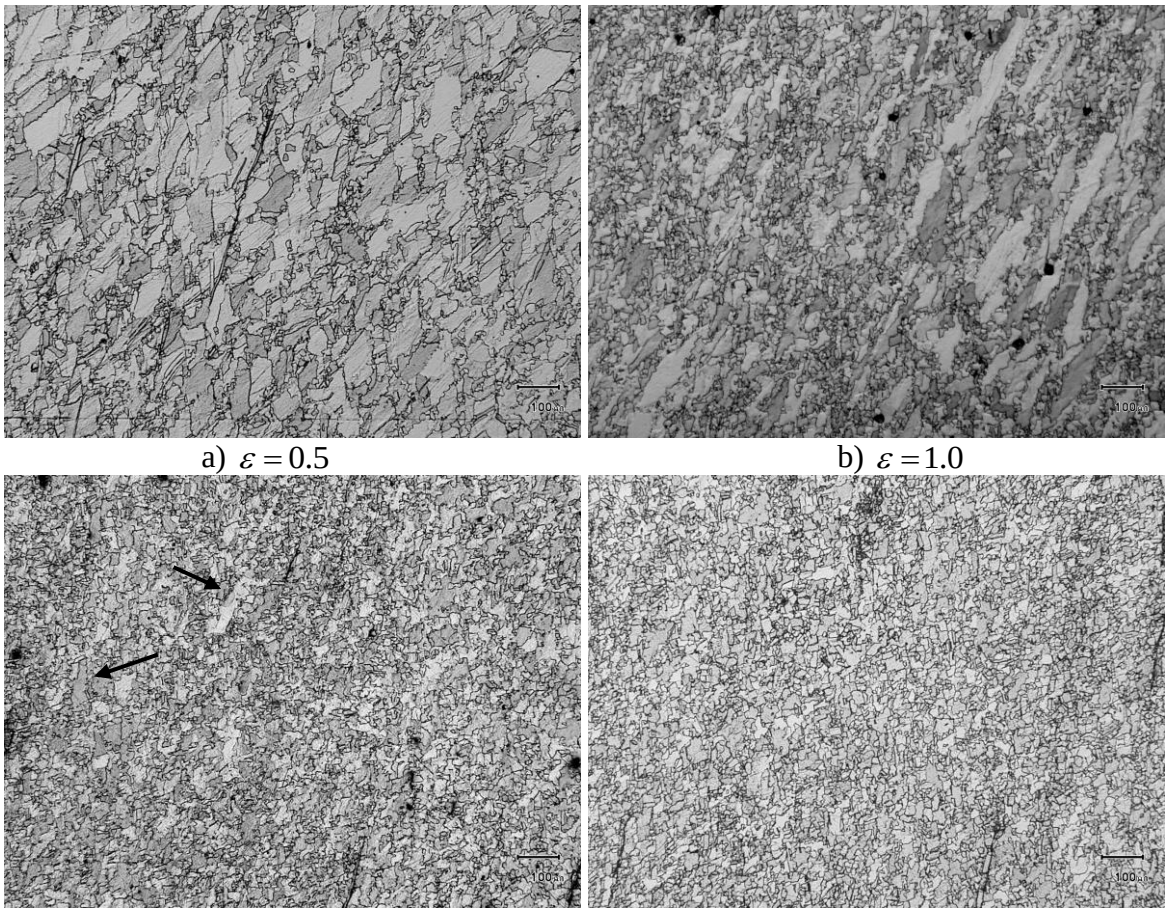

a) $\varepsilon = 0.5$ b) $\varepsilon = 1.0$

c) $\varepsilon = 1.5$ d) $\varepsilon = 2.0$

Figure 5-14 Microstructure of samples deformed at 1000℃, $d_0 = 45\mu m, \dot{\varepsilon} = 0.01s^{-1}$ (Optical Microscope)

As shown in Figure 5-15, the typical single peak type of DRX is observed for the two initial grain sizes, both of them are deformed at 1000 ℃ and $\dot{\varepsilon} = 0.01s^{-1}$. With the smaller initial grain size (45 μm), both the flow stress and the recrystallized fraction are in the same range as the experimental results of Dehghan-Manshadi *et al*. [39] who used an initial grain size of 35 μm for 304 stainless steel. When increasing the initial grain size to 165 μm, the peak strain increases from ~0.4 to ~0.8. At the same time, the recrystallization kinetics slows down, leaving an incomplete recrystallized structure after a deformation of 2.5, which also explains why the two flow stress curves do not converge at large strain, as expected from the classic work of Sah *et al*. [31] illustrated earlier in Figure 2-14a.

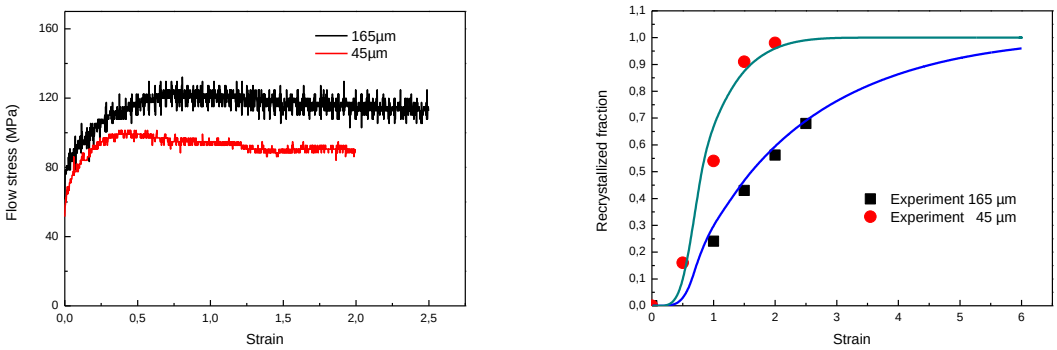

a) b)

Figure 5-15 The effect of initial grain size on a) Flow stress, b) Recrystallized volume fraction (deformed at 1000 ℃ with strain rate of $\dot{\varepsilon} = 0.01s^{-1}$)

In order to validate the DDRX model presented in chapter 4 for a wider range of conditions, other experiments have been conducted, especially in conditions where it is difficult to generate a significant amount of recrystallized volume fraction. As the typical evolution of DRX is already studied using the initial grain size of 165 µm, the objective here is to provide data to further validate the proposed DDRX model which is supposed to automatically account for initial grain size effect. Applied strains were chosen such that significantly different recrystallized fraction was obtained. Micrographs after quenching are presented below, at 1000 ℃ and $\dot{\varepsilon} = 0.1s^{-1}$ (Figure 5-16), at 900 ℃ and $\dot{\varepsilon} = 0.01s^{-1}$ (Figure 5-17), and at 900 ℃ and $\dot{\varepsilon} = 0.1s^{-1}$ (Figure 5-19).

Figure 5-16 shows the microstructure at strains of 1.0 and 2.0, T=1000 ℃ and $\dot{\varepsilon} = 0.1s^{-1}$. Again, at the deformation of 1.0 (Figure 5-16a), the recrystallized fraction is smaller than that obtained at a smaller strain rate (Figure 5-14b). After a strain of 2.0 (Figure 5-16b), the recrystallization is nearly completed.

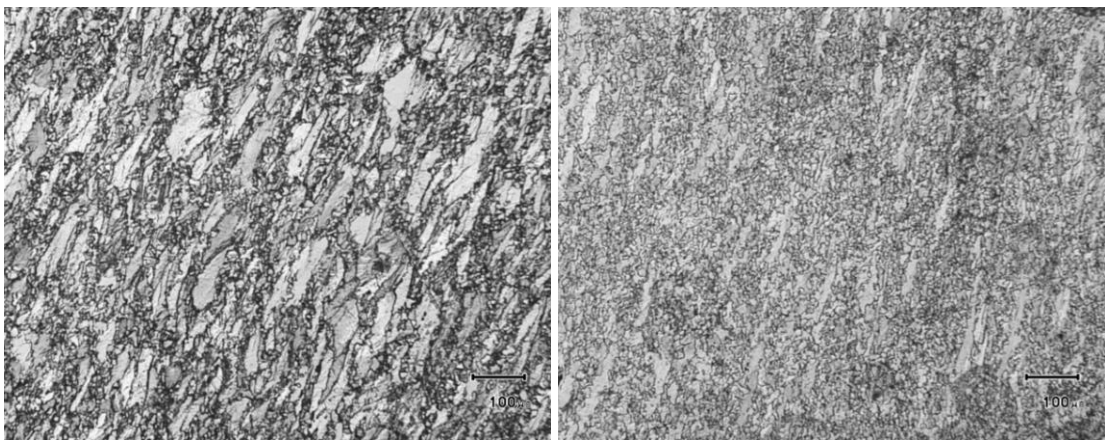

a) $\varepsilon = 1.0$ b) $\varepsilon = 2.0$

Figure 5-16 Microstructure of samples deformed at 1000℃, $d_0 = 45$ 微米, $\dot{\varepsilon} = 0.1s^{-1}$ (Optical Microscope)

Comparing to DRX using a larger initial grain size of 165 µm (Figure 5-3), a higher amount of dynamically formed small grains are present along the old grain boundaries at 900 ℃ with the strain rate of $\dot{\varepsilon} = 0.01s^{-1}$ (Figure 5-17a). AT $\dot{\varepsilon} = 0.1s^{-1}$ (Figure 5-19a), the microstructure also exhibits a typical necklace nucleation. When the deformation is increased to 2.0, more recrystallized fraction can be found with the smaller strain rate, along with a bigger

recrystallized grain size, as seen in (Figure 5-17b) and (Figure 5-19b). It is also clear that DRX at this temperature is still dominated by bulging of existing grain boundaries (see Figure 5-18 and Figure 5-20), newly formed RX grains (in bleu) are found mostly along the pre-existing grain boundaries.

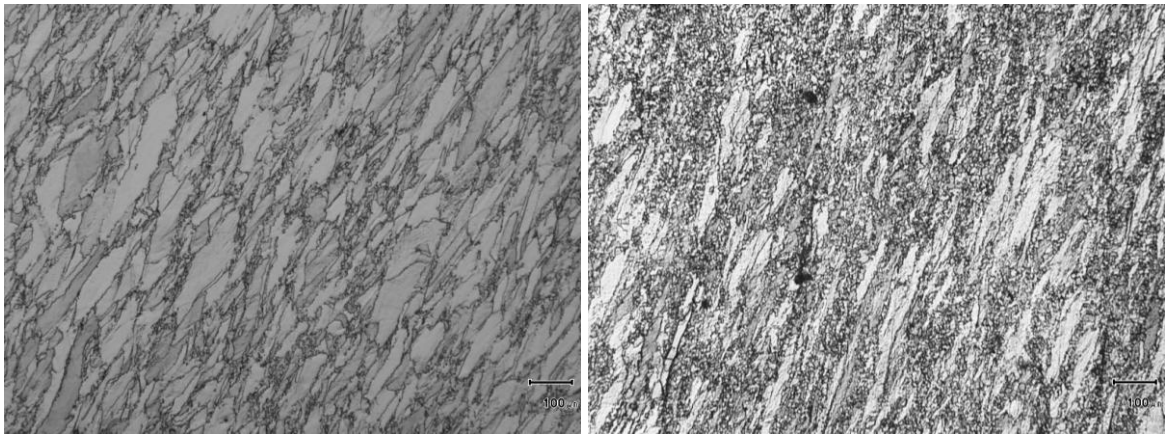

a) $\varepsilon = 1.0$ b) $\varepsilon = 2.0$

Figure 5-17 Microstructure of samples deformed at 900℃, $d_0 = 45\mu m$, $\dot{\varepsilon} = 0.01s^{-1}$ (Optical Microscope)

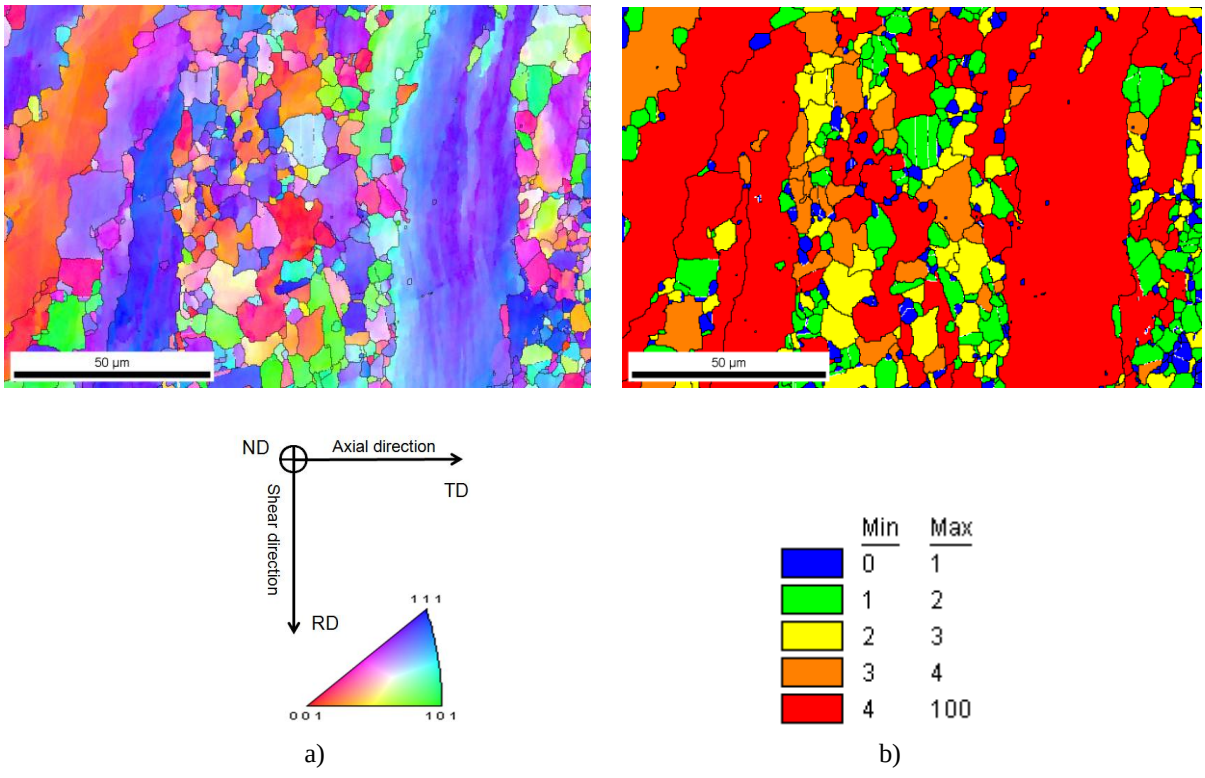

a) b)

Figure 5-18 EBSD map of the microstructure of samples deformed to a strain of 2.0 at 900 ℃ and strain rate of $0.01s^{-1}$ with initial grain size 45 µm a) IPF map, b) GOS map

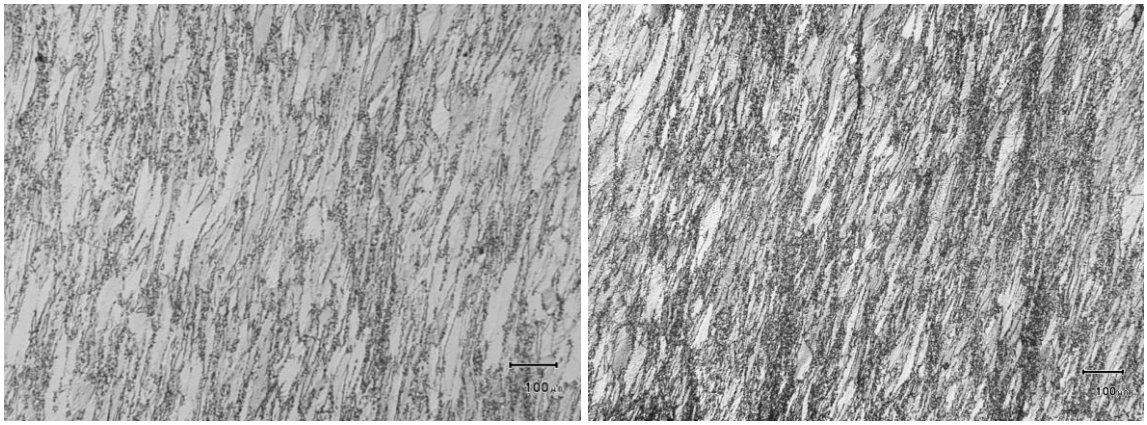

a) $\varepsilon = 1.5$ b) $\varepsilon = 2.0$

Figure 5-19 Microstructure of samples deformed at 900℃, $d_0 = 45\mu m$, $\dot{\varepsilon} = 0.1s^{-1}$ (Optical Microscope)

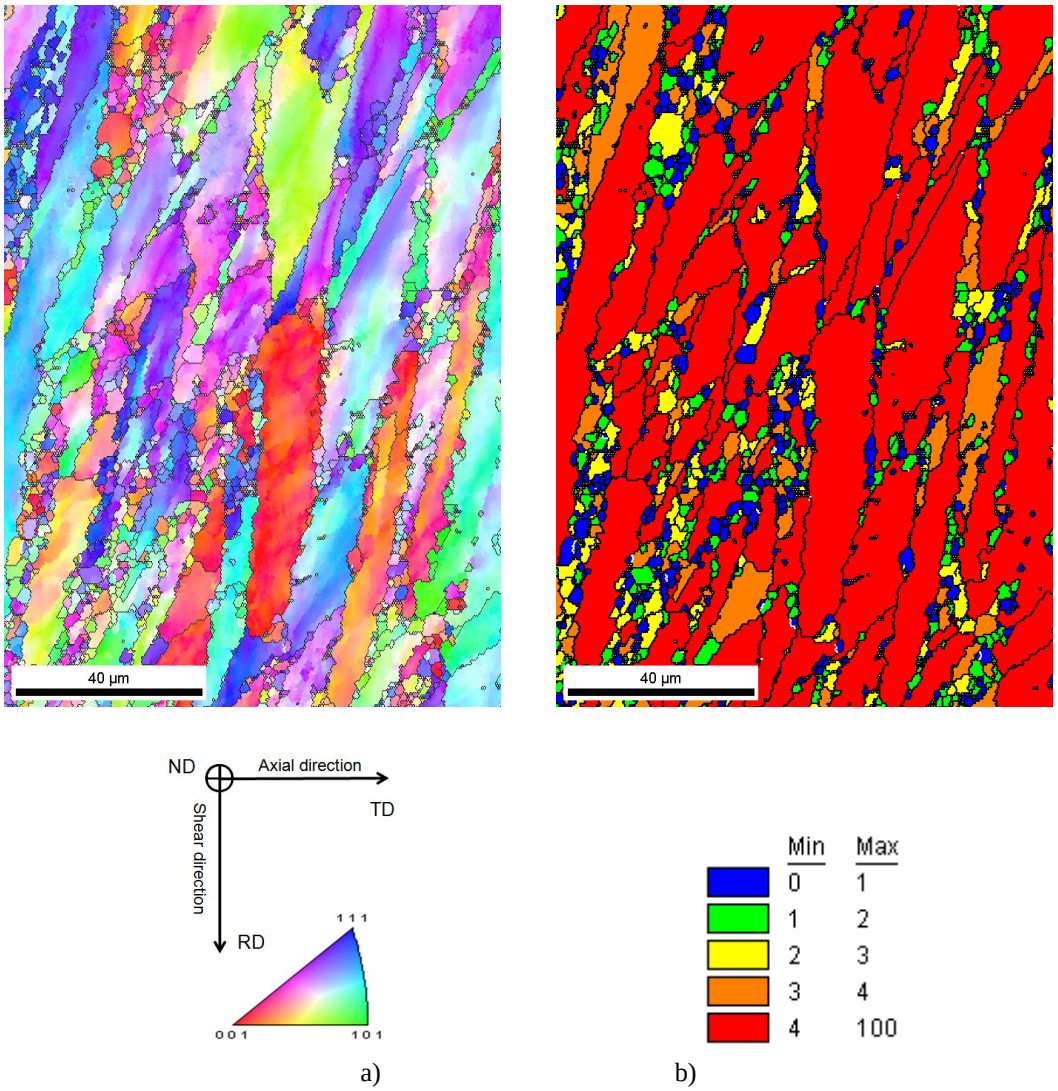

a) b)

Figure 5-20 EBSD map of the microstructure of samples deformed to a strain of 1.5 at 900 ℃ and strain rate of $0.1s^{-1}$ with initial grain size 45 μm a) IPF map, b) GOS map

DRX evolution under different conditions are presented and analyzed above, and additional details of the experimental results will be addressed later when comparing with numerical results.

5.6. Application of the DDRX model to 304L steel

5.6.1. Identification of fitting parameters

5.6.1.1. From experimental results and literature data

The two unknown parameters in (Equation 4-1) represent work-hardening (K_1) and recovery (K_2) respectively. These two parameters of the model can be estimated from the stress-strain curve prior to ε_{cr} , as schematically illustrated in Figure 5-21. The principle was presented earlier in section 2.4.2, more details of the identification procedures can be found in a recent paper published by Jonas *et al*. [187].

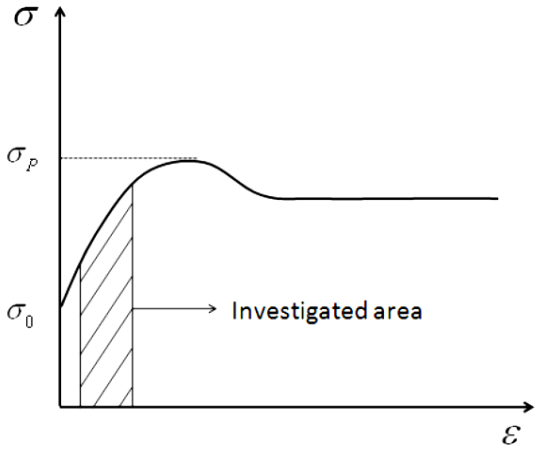

Figure 5-21 Stress-strain curve area to identify K_1 and K_2 parameters

In (Equation 4-2), σ_0 becomes negligible at high temperature [76], which is in accordance with the claim made by Smallman and Ngan that it should be close to zero for F.C.C metals like Ag and Cu [188] as shown in Figure 5-22. So, in the current work, this value is directly taken from the flow stress curve at lower temperatures while it is set to be zero at higher temperatures. It is important to notice that in (Equation 4-2), the average Taylor factor $M = \sigma / \tau = \gamma^p / \varepsilon^p$, which relates the shear stress τ and total shear strain γ^p on the dislocation slip planes to the macroscopic stress σ and plastic strain ε^p , is used to account for the polycrystallinity of the material. The average Taylor factor M will evolve as a result of texture evolution, however, in the current work, the variation of M is slow compared to that of the dislocation density and it is set to a typical value of 3.0 in accordance with literature data for isotropic cubic materials [189,190].

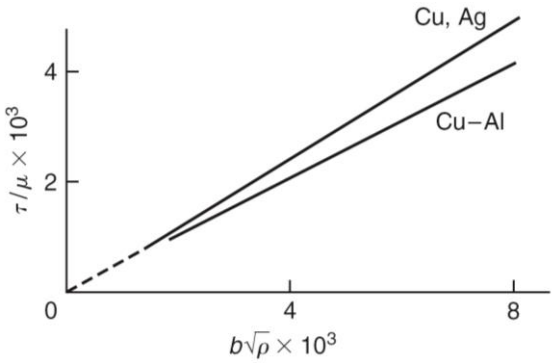

Figure 5-22 Dependence of flow stress on (dislocation density)$^{1/2}$ for Cu, Ag and Cu–Al [188].

Another constant α in (Equation 4-2), according to Basinski *et al*. [191], was found to be in the range of $\alpha = 0.35 \pm 0.15$. The α coefficient values calculated theoretically and obtained experimentally were compared by Kozlov and Koneva [192], they found that this coefficient is weakly dependent on the alloy type and is mostly defined by the type of the formed substructure. The more the order of dislocation arrangement in the dislocation ensemble the better mutual compensation of elastic fields of separate dislocations and the lower the α coefficient. Since the α coefficient only has influence on the flow stress curve in the model, so we choose in this work, α =0.15, in accordance with the work by Backer [193].

As mentioned earlier in section 3.2.2, Burger's vector can be obtained according to: $b = a/\sqrt{2} = 2{,}54.10^{-10} m$. The elastic shear modulus μ was found to linearly decrease with temperature as show in Table 3-3. Since the variation at high temperature is very small, the shear modulus was set to be constant value.

In (Equation 4-4) and (Equation 4-5), three unknown parameters are involved which are the mobility of grain boundary (m), the dislocation energy per unit length (τ) and the grain boundary energy (γ_b). $\tau \cong 0.5\mu b^2$ and both μ and b are known. The grain boundary energy γ_b is considered as constant in the current study, the typical value of $\gamma_b = 0.6 Jm^{-2}$ is used. The grain boundary mobility m is temperature dependent and is usually found to follow an Arrhenius type relationship as shown in (Equation 4-6). The slope of a plot of $\ln(m)$ against $1/T$ directly yields a value of Q_b, but this requires that the driving pressure of grain boundary migration is constant. So, the evaluation of this value was conducted in the grain growth regime during SRX/PDRX where the dislocation density term is negligible exists under each annealing temperature. Very often, the mobility of grain boundary (m) and dislocation energy per unit length (τ) are combined together, so we use in this work $K_3 = m\tau$ in order to compare with literature data such as [76].

It is also worth underlining that nucleation happens inhomogeneously throughout the material: nuclei appear mostly at grain boundaries. This necklace type nucleation will affect the value of mobile fractions γ^{RX} and γ^{NR} in (Equation 4-20) and (Equation 4-21). As nuclei appear on the grain boundaries, they will impinge much more rapidly on each other than for randomly distributed nucleation, limiting their growth. Therefore, γ^{RX} will decrease faster than (1−X) does, the index n in (Equation 4-20) is chosen as 2/3, which is the ratio between surface and volume exponent. By taking into account the fact that there are some preferential nucleation sites instead of simply assuming randomly distributed nucleation, our model has actually considered some topological information which could lead to a more accurate results.

The last fitting parameter in the DRX model lies in (Equation 4-8), and it is the nucleation parameter K_g which is a probability constant depending on the processing conditions. The

nucleation rate is believed to depend on both strain rate and temperature [1]. However, that is all what we know about this parameter, since it is too difficult to get the quantitative value by experiments. But we have an upper limit for this parameter, which is, the value such that all potential nucleation sites (the boundaries of grains with a dislocation density higher than ρ_{cr}^{DRX}) nucleate at each time step.

According to the procedures mentioned above, we can get rough values for K_1, K_2 and K_3, and a few manual optimizations were launched to get a reasonable starting value for K_g. These four parameters were subsequently used as starting points for the inverse analysis, which will be described in the next section.

5.6.1.2. Inverse analysis

The DDRX model involves four main "*K*" uncertain parameters which are assumed to vary with strain rate and temperature:

$$\{\mathbf{K}\} = \{K_1(\dot{\varepsilon}) \quad K_2(\dot{\varepsilon},T) \quad K_3(\dot{\varepsilon},T) \quad K_g(\dot{\varepsilon},T)\}^t \qquad \text{(Equation 5-1)}$$

This means that the parameters can be identified on a point-by-point basis in the temperature/strain rate space. Once a grid of points has been identified, numerical values at other points could be determined by interpolation. These parameters are assumed to be *independent from grain size*.

The well established real number based non-dominated sorting genetic algorithm (NSGA II) [180] was modified at CEMEF by Swarup Bag, and is used in the present work as a multi-objective optimization tool for the identification of the *K* variables. Three objective functions depict the discrepancy between model predictions and experimental data, and are based on three measurable quantities: the recrystallized volume fraction *X*, the average recrystallized grain size $\overline{D}_{RX} = 2r_{RX}$, and the flow stress $\overline{\sigma}$. The objective function, *O(K)*, is defined as the sum of the squared errors between the computed and the corresponding measured values of *X*, r_{RX} and $\overline{\sigma}$ as follows:

$$O_i(K) = \sum_{m=1}^{M_i}\left[\frac{(f_i^c)_m - (f_i^{obs})_m}{(f_i^{obs})_m}\right]^2 = \sum_{m=1}^{M_i}[(f_i^*)_m - 1]^2 \qquad \text{(Equation 5-2)}$$

$$\{f_1 \quad f_2 \quad f_3\}^t \equiv \{X \quad r_{RX} \quad \overline{\sigma}\}^t \qquad \text{(Equation 5-3)}$$

where 'c' refers to computed value from the model, 'obs' refers to experimentally measured values and '*' refers to the non-dimensional form of the variables that indicate the extent of over or under-prediction of these variables. $M_i (i = 1,3)$ corresponds to the number of known measured values of recrystallized fraction (M_1), flow stress (M_2) and average recrystallized radius (M_3) for which the processing conditions are also known.

The integrated model returns multiple solutions in the form of a Pareto optimal set after a given number of generations. The choice of the best solution is dictated by the numerical value of the objective functions in (Equation 5-2). The first preference is given to the choice of minimum value of $O_1(K)$, then $O_2(K)$, and finally $O_3(K)$.

5.6.2. Calibration of the DRX model

The parameters ρ_0 defining a fully recrystallized state (see Figure 4-2) is chosen with a value of 10^{11} m^{-2}. The time step was limited with a δ value of 0.2 in (Equation 4-31). Initial

distributions of grain sizes and dislocation densities (Figure 4-2) were approximated with 50 representative grains, and considering $D_{max} / D_0 = 2$, and $\rho_{max} / \rho_0 = 10$. The scaling factor w in (Equation 4-13), which is artificially used to make sure the newly created nuclei will subsequently grow and not shrink, is set to be 1.5. A set of acceptable parameters values are found for 304L stainless steel, the trend of *K* parameter values identified from comparison with experimental data (as detailed in the next sections) is presented in Figure 5-23. Parameters are expressed in a dimensionless form, dividing by the reference values obtained at 0.01 s^{-1} and 1100 ℃.

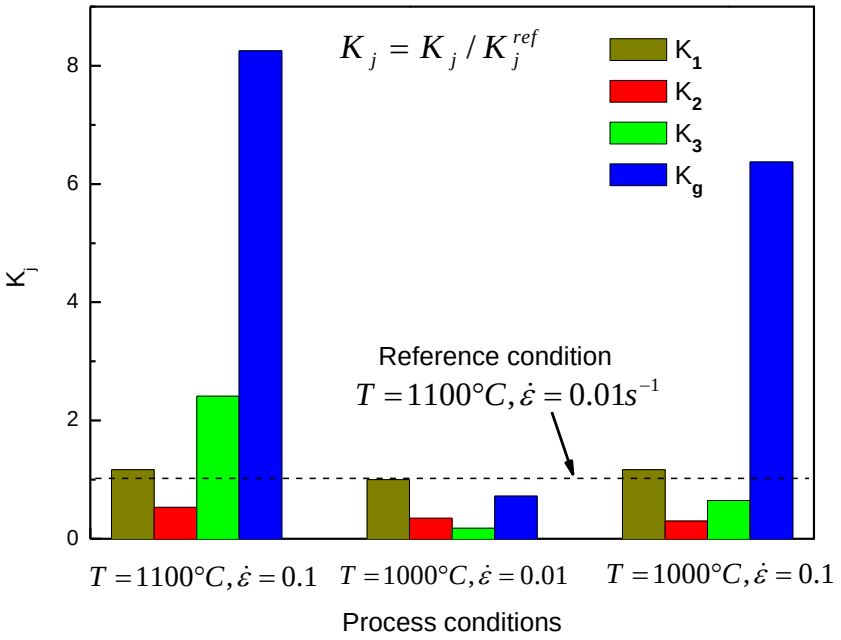

Figure 5-23 Relative evolution of *K* parameters as a function of temperature and strain rate, with respect to the reference values (represented by the broken line) obtained at 0.01 s^{-1} and 1100 ℃.

When the temperature decreases to 1000 ℃ (four columns in the middle), while keeping the same strain rate of 0.01s^{-1}, dynamic recovery (K_2), grain boundary mobility (K_3) and nucleation probability (K_g) decrease, which is physically consistent. The work hardening term K_1 is considered constant over this temperature range.

Keeping the same temperature of 1100 ℃, an increase of strain rate to 0.1 s^{-1}(four columns on the left) leads to an increase of hardening rate and grain boundary mobility (K_1, K_3), a decrease of dynamic recovery (K_2), and a faster nucleation rate (K_g). The same tendency of variation for the four parameters is found when increasing the strain rate from 0.01s^{-1} to 0.1s^{-1} at 1000 ℃ (four columns on the right). These trends are again physically consistent and in agreement with literature data [76], where the sensitivity of grain boundary mobility to strain rate was also found.

5.6.3. Qualitative grain size effect

One of the outstanding features of the proposed DDRX model is that the fitting parameters of the model are grain size independent. Figure 5-24 shows a series of curves computed numerically without changing any of the model parameters, the model feeds back correctly the

behaviour of the system for different initial average grain sizes. The flow stress increases with initial grain size, a common steady sate is finally obtained, the transition from multi-peak to single peak seems to be captured by the model, even though the peaks do not apparent very clearly in Figure 5-24a. At the same time, the recrystallization kinetics slows down as the initial grain size increases (Figure 5-24b), with the largest initial grain size of 300µm, the fully recrystallized state is still not obtained at $\varepsilon = 6.0$. The average grain size converges to a common steady-state value in all cases, with grain coarsening for the smallest initial grain size (increases from 5µm to ~12µm) and grain refinement for the other sizes.

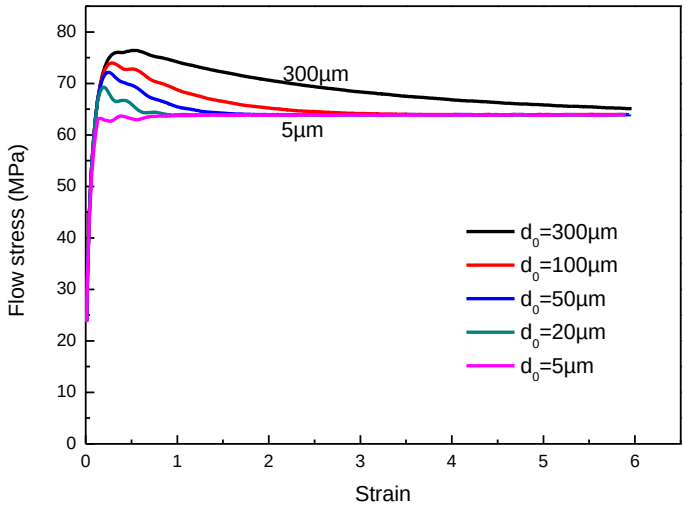

a)

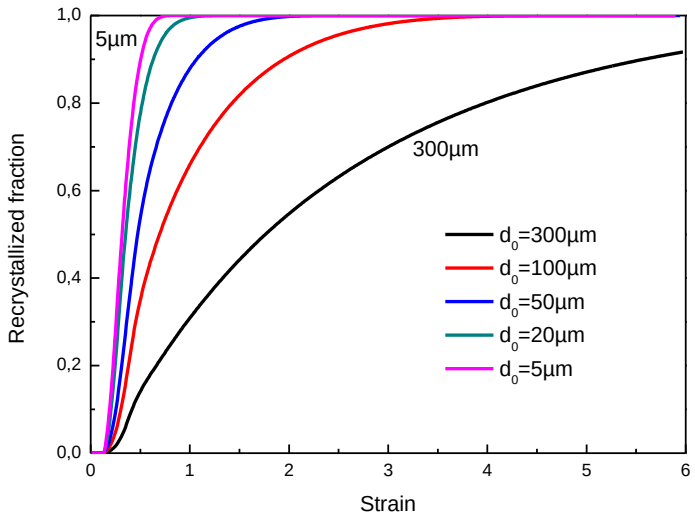

b)

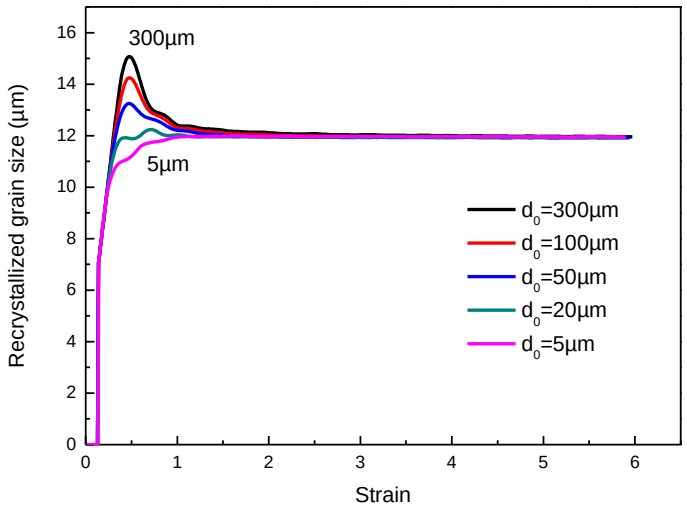

c)

Figure 5-24 Sensitivity analysis of initial grain size effect, varying from 5 to 300 μm, without changing any model parameters: a) The flow stress curves, b) The kinetics of recrystallization, c) The recrystallized average grain size. (T=1100 ℃, $\dot{\varepsilon} = 0.01s^{-1}$)

5.6.4. Quantitative temperature effect

In Figure 5-25, a constant strain rate of 0.01 s^{-1} is chosen to validate the model at different temperatures (1000 and 1100 ℃), starting with an initial grain size of 165 μm. The experimental and numerical results match extremely well, including the peak stress and steady state stress, shown in Figure 5-25a. Both of the flow stress curves exhibit single peak type character, the peak strain, ~0.5 at 1100 ℃ and ~1.0 at 1000 ℃ correspond to the beginning of the DDRX process, as shown in Figure 5-4c and Figure 5-5a respectively.

Similarly, the effect of temperature on recrystallization kinetics is also well predicted, with faster kinetics at higher temperature (Figure 5-25b). The critical strain (corresponding to the critical dislocation density in (Equation 4-10)) is found to be smaller at higher temperature. It also takes a shorter time to reach the fully recrystallized state.

In terms of recrystallized grain size, the simulation results not only correctly produce a larger steady state grain size at higher temperature, but also fit well with the experimental data. Better agreement is observed at 1100 ℃, where a steady state is reached. A peak value can be found for the two recrystallized grain size curves, both of them occur at around the peak strain where recrystallization just starts, the old grain boundaries are not yet fully replaced by the nuclei. Grains nucleated earlier grow to a value higher than the steady state size, since they are not impinged by other grains. The factor *w* introduced in (Equation 4-13), which can successfully avoid the nuclei shrinking promotes larger initial sizes, but with no major consequence for the grain size evolution. The initial grain size also plays an important role, according to the sensitivity analysis presented in the previous section (Figure 5-24), the peak disappearing progressively when decreasing the initial grain size.

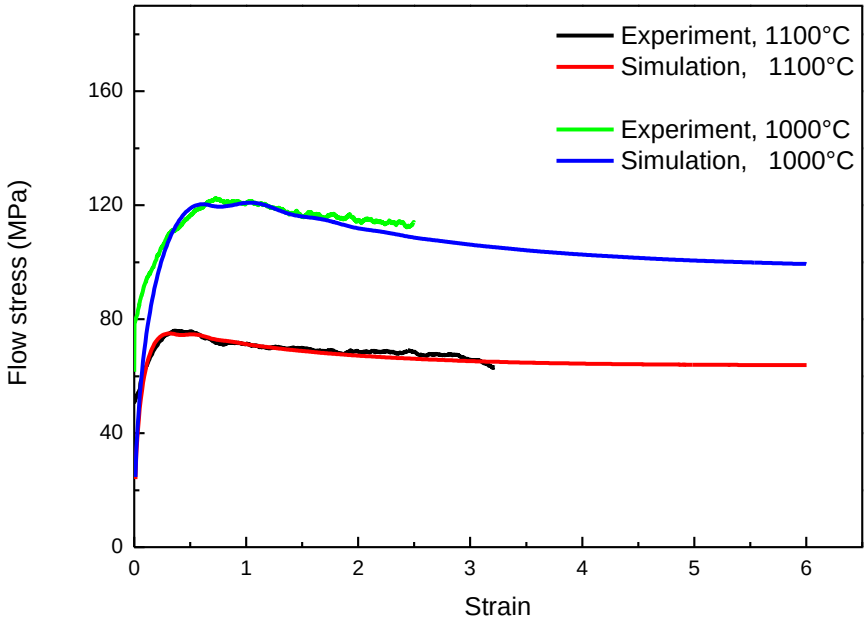
Experiment, 1100°C
Simulation, 1100°C
Experiment, 1000°C
Simulation, 1000°C
Flow stress (MPa)
Strain
0
40
80
120
160
0
1
2
3
4
5
6

a)

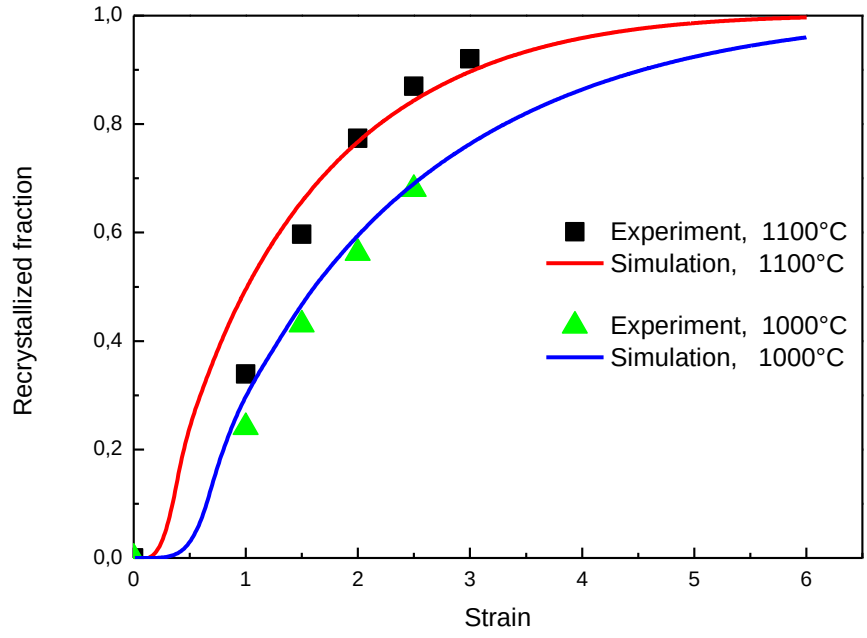
Experiment, 1100°C
Simulation, 1100°C
Experiment, 1000°C
Simulation, 1000°C
Recrystallized fraction
Strain
0,0
0,2
0,4
0,6
0,8
1,0
0
1
2
3
4
5
6

b)

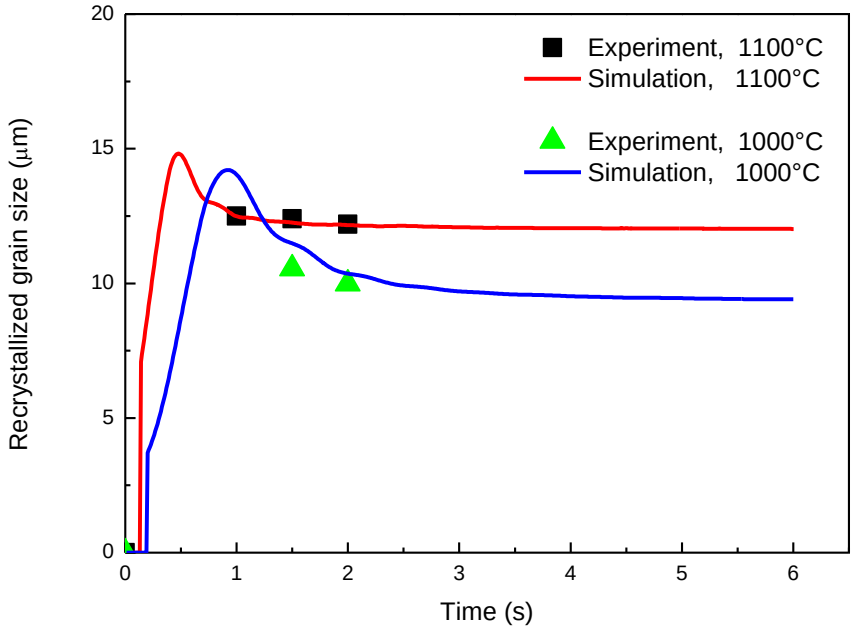

c)

Figure 5-25 Comparison between experimentally measured and numerically obtained a) Flow stress curves, b) Recrystallized fraction, and c) Recrystallized grain size of 304L steel. Conditions are $\dot{\varepsilon} = 0.01\text{s}^{-1}$ and initial grain size 165μm. Results are shown for two different temperatures (1000 ℃ and 1100 ℃).

5.6.5. Quantitative strain rate effects

Figure 5-26 compares the simulated and experimental effects of strain rate on the flow stress, recrystallized fraction and mean size of recrystallized grains, at the temperature of 1100 ℃

The flow stress at 1000 ℃ and 0.1s^{-1} is slightly overestimated, possibly due to self heating in the experiment, which is not taken into account in the model, while the flow stress at 0.01s^{-1} is perfectly matched with experimental flow stress, as presented in Figure 5-26a.

Figure 5-26b shows the influences of strain rate on the kinetics of DRX. In Figure 5-25b, the critical strain is larger with larger strain rate, which corresponds well to (Equation 4-10) where the critical dislocation density is proportional to $\dot{\varepsilon}^{1/3}$. The rapid increase of recrystallized fraction after the onset of DRX is more apparent at a lower strain rate, which is directly associated with the fact that there is more time associated to a given level of applied strain.

The strain rate effect on the average recrystallized grain size is illustrated in Figure 5-26c. The fact that the mean size of recrystallized grains decreases with strain rate is also well captured. It takes longer time to reach to a steady-state grain size by increasing strain rate, and also, this steady state comes before a fully recrystallized structure is obtained.

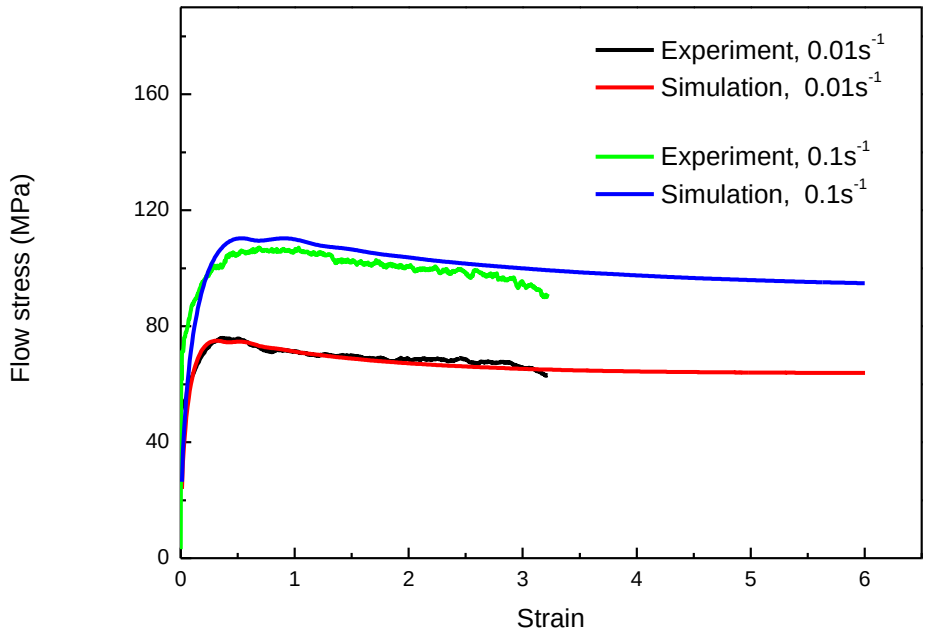
Flow stress (MPa)
Strain
Experiment, 0.01s-1
Simulation, 0.01s-1
Experiment, 0.1s-1
Simulation, 0.1s-1
0
40
80
120
160
0
1
2
3
4
5
6

a)

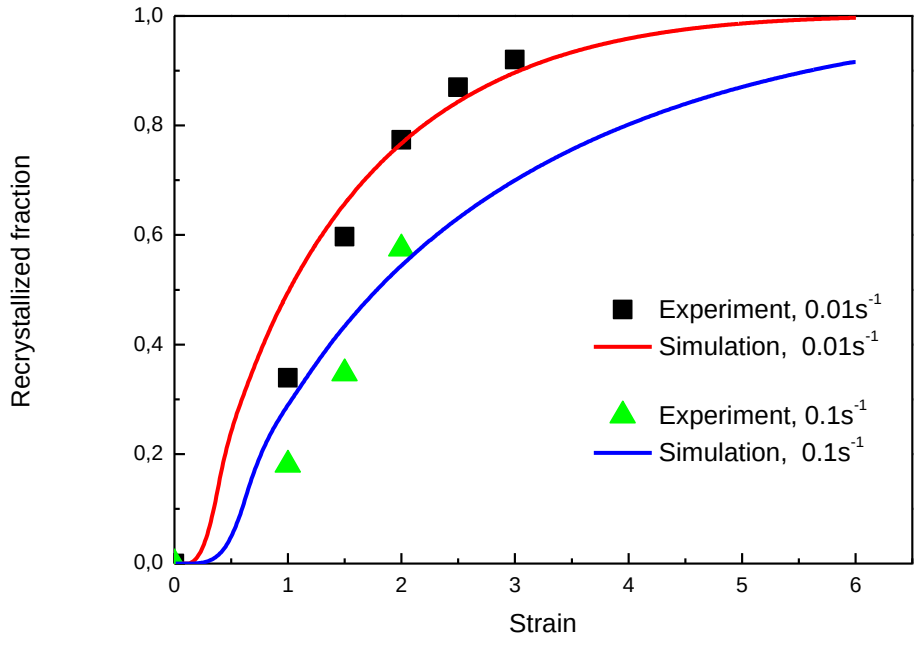
Recrystallized fraction
Strain
Experiment, 0.01s-1
Simulation, 0.01s-1
Experiment, 0.1s-1
Simulation, 0.1s-1
0,0
0,2
0,4
0,6
0,8
1,0
0
1
2
3
4
5
6

b)

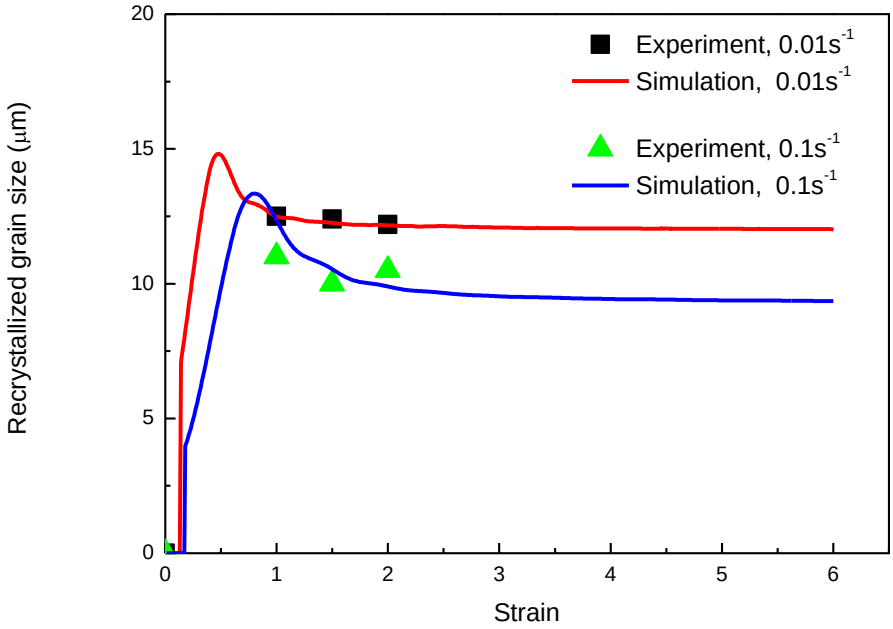

c)

Figure 5-26 Comparison between experimentally measured and numerically obtained a) Flow stress, b) Recrystallized fraction and c) Recrystallized grain size in 304L steel. Conditions are T = 1100 ℃ and initial grain size =165μm. Results are shown for two different strain rates ($0.01s^{-1}$ and $0.1s^{-1}$).

5.6.6. Quantitative initial grain size effect

The successful prediction of DDRX under different deformation conditions in the above two sections demonstrate that steady state values evolve in the expected way as a function of the Zener-Hollomon (*Z*) parameter, i.e. smaller grain sizes and increased flow stress for increased values of *Z*. Initial grain size, on the other hand, does not change the steady state grain size and flow stress, even though it affects the kinetics of recrystallization and changes the shape of the flow curves [1,31]. A sensitivity analysis has been presented earlier in Figure 5-24, the model predicts quantitatively the flow stress, recrystallized fraction and recrystallized grain size. The verification by experimental data is given below at 1000 ℃ with two strain rates, namely $\dot{\varepsilon} = 0.01s^{-1}$ and $\dot{\varepsilon} = 0.1s^{-1}$, with initial grain sizes of 165 μm and 45 μm.

Starting with $\dot{\varepsilon} = 0.01s^{-1}$, the flow stress is slightly overestimated by the model with the smaller initial grain size as shown in Figure 5-27a, this probably comes from the over simplification that all the model parameters are independent of the initial grain size. In fact, the critical strain for the onset of DDRX is actually dependent on the initial grain size, it has been shown that in a hot deformation process an increase in initial austenite grain size will delay the onset of dynamic recrystallization [194, 195,60]. Our experiments further confirm this effect. No nuclei are observed when it is deformed to 0.5 at 1000 ℃ with the strain rate of $0.01s^{-1}$ (Figure 5-4b), with the initial grain size of 165 μm. When the initial grain size is decreased to a smaller size of 45 μm, ~10% of recrystallized volume fraction is already present when

deformed under the same conditions, as shown in Figure 5-14a. A better match between the numerical and experimental results of flow stress is possible if the size dependence of critical strain (critical dislocation density in the present work) is incorporated into the model.

Figure 5-27b and Figure 5-27c show the evolution of recrystallized fraction and grain size for the two initial grain sizes (165 and 45 μm). The well known phenomenon, that a fine-grain structure can promote faster rate of recrystallization due to the increase of the amount of available nucleation sites as the grain boundary area per unit volume is increased [31], is obtained from the model and corresponds well to experimental data. Typical evolutions of the recrystallized grain size include a peak followed by a steady state value, the peak value decreasing with initial grain size. In terms of flow stress and grain size, the steady state is reached as soon as the material is fully recrystallized (even though experimentally the steady state has not been reached due to fracture of samples), and the required deformation to reach such a steady state is strongly dependent on the initial grain size. Both quantities stabilize to *the same value*, independent from the initial microstructure, which is a well-known feature of DDRX.

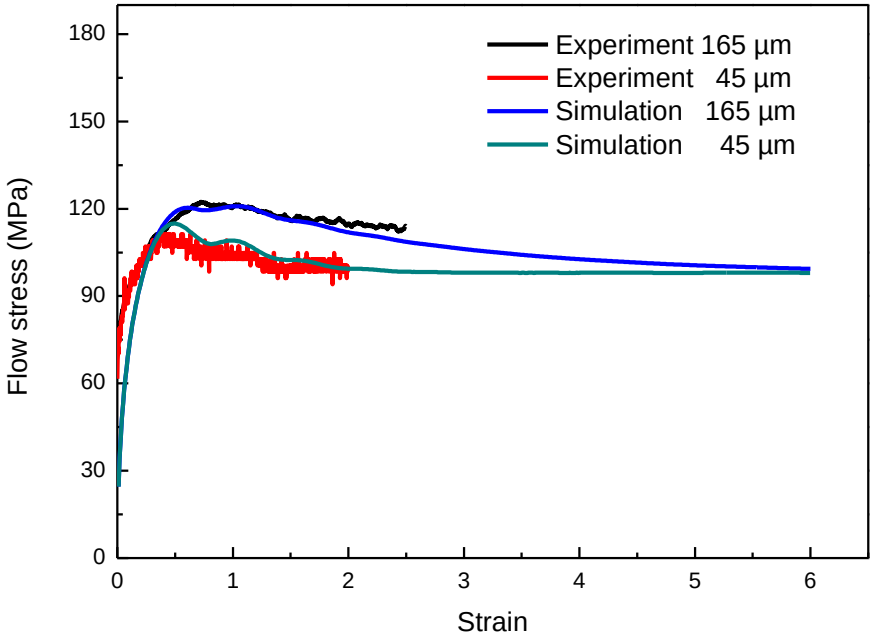

a)

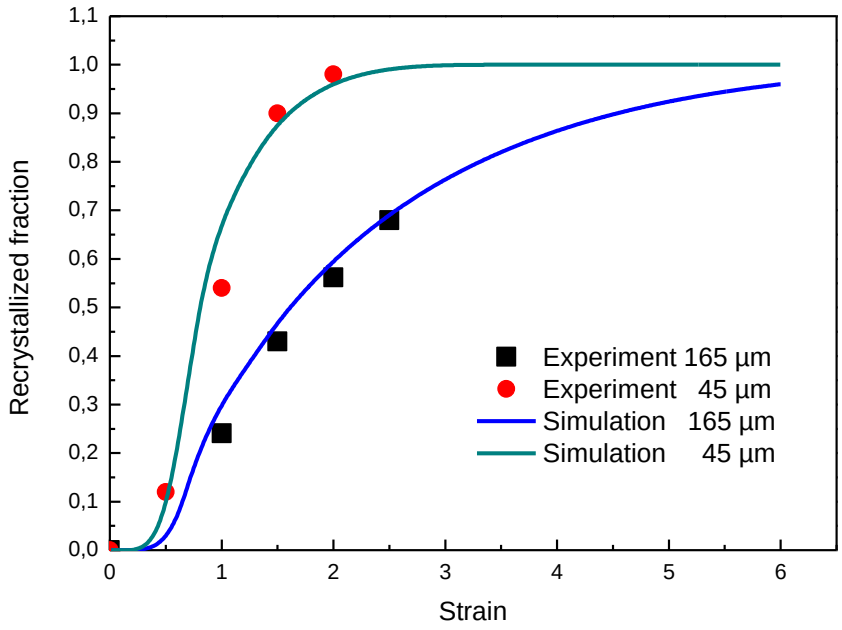

b)

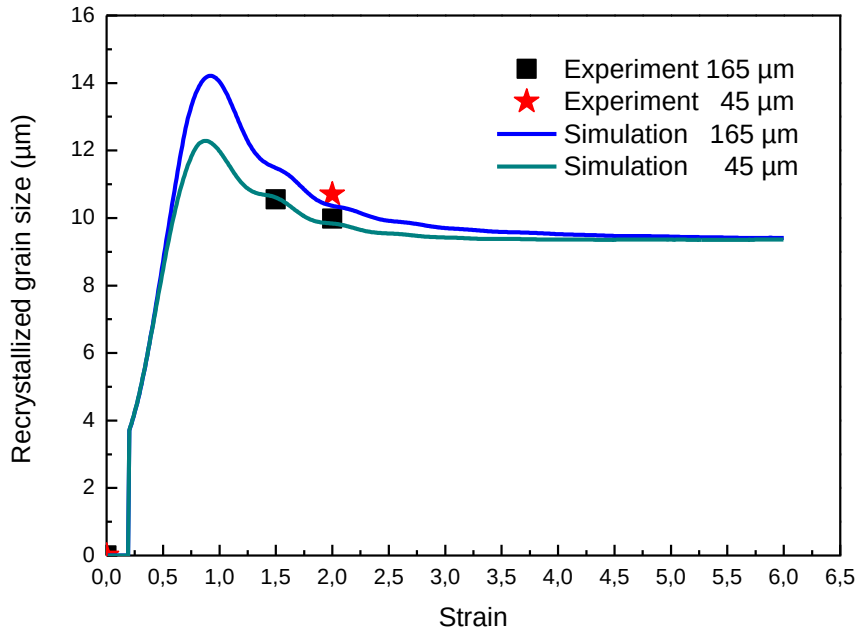

c)

Figure 5-27 Effect of initial grain size (45 µm and 165 µm) on the recrystallization behaviour at T = 1000°C, $\dot{\varepsilon} = 0.01 s^{-1}$. a) Flow stress, b) recrystallized fraction, and (c Average recrystallized grain size.

The performance of the DDRX model with different initial grain size is further evaluated by increasing the strain rate to $\dot{\varepsilon} = 0.1s^{-1}$. Again, it is found that the simulated results agree reasonably well with the experimental curves in terms of flow stress, recrystallized fraction and recrystallized grain size, as shown in Figure 5-28. The fact that the model overestimates the flow stress at smaller grain size (Figure 5-28a) is again observed here, even though the discrepancy is relatively small. The flow stress corresponding to the initial grain size of 165 µm does not converge to the steady-state value even after a very large deformation of 6, which is not surprising since a fully recrystallized structure is not yet reached (see Figure 5-28b). Some discrepancies are also observed on the recrystallized grain size and experimental measurements, the error is however only ~1 µm (Figure 5-28c), which is negligible when considering subsequent PDRX phenomena where the grains dramatically increase in a few seconds (see section 6.2.3).

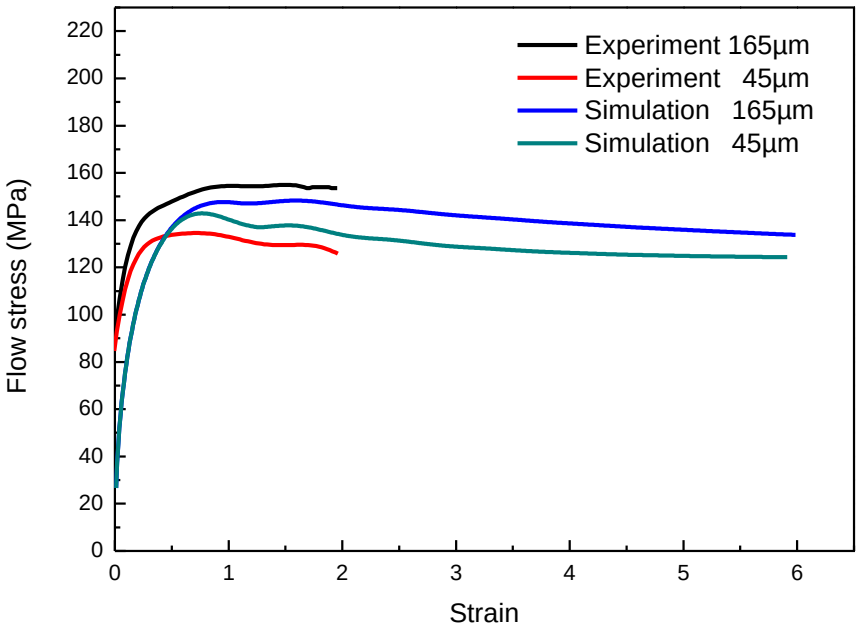

a)

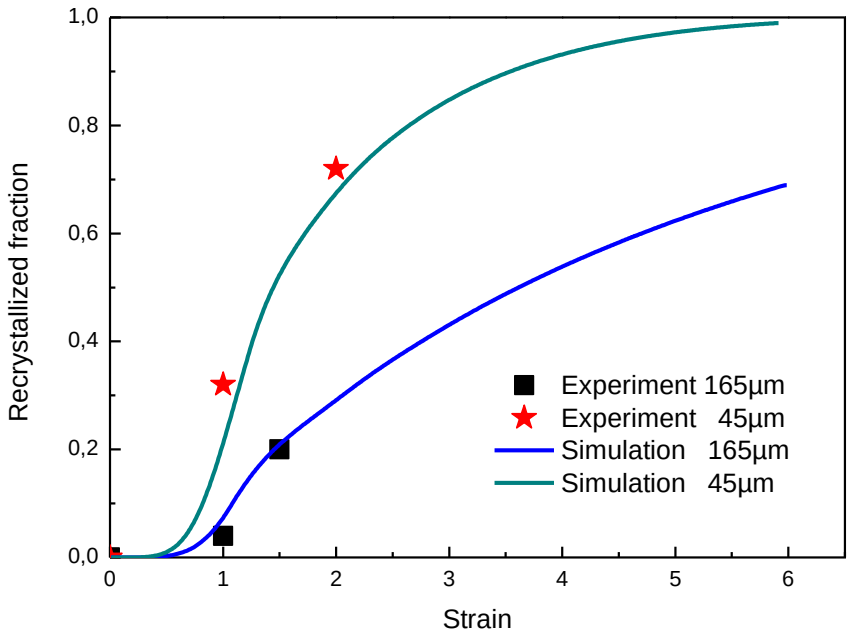

b)

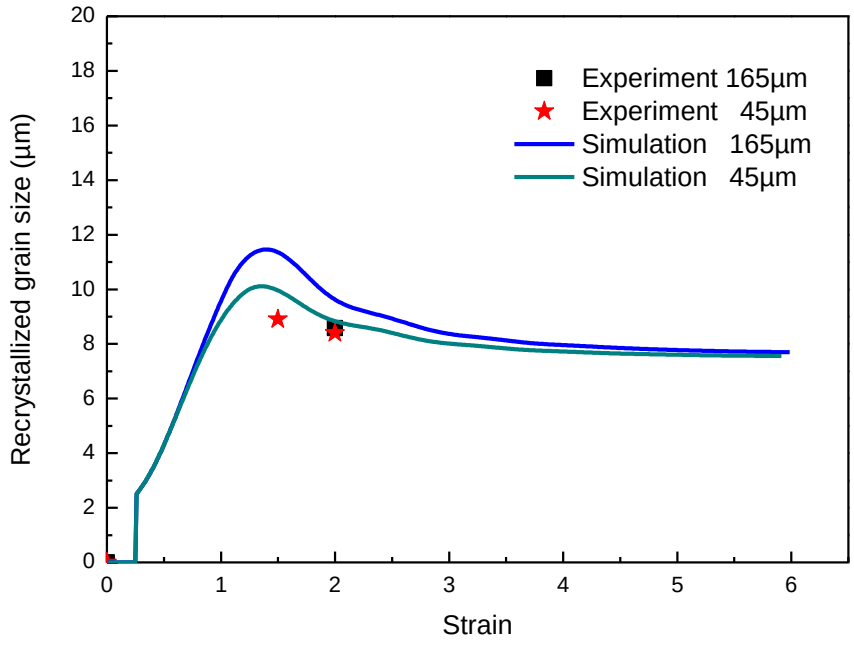

c)

Figure 5-28 Effect of initial grain size (45 µm and 165 µm) on the recrystallization behaviour at T = 1000 ℃, $\dot{\varepsilon} = 0.1s^{-1}$. a) Flow stress, b) recrystallized fraction, and c) Average recrystallized grain size.

The above validation, together with the sensitivity analysis shown in Figure 5-24, demonstrates that a set of identified *K* parameters based on data with one initial grain size predicts accurately the behaviour with the other initial grain size. Indeed, the necklace nucleation mechanism is included in the model through the nucleation law and the use of

mobile surface fractions, and this leads to the grain size dependence of the recrystallization behaviour. No additional parameter must be introduced to accurately account for this grain size dependence. The good match between experimental and numerical results seems to reasonably support the simplification that model parameters are independent of the initial grain size. Actually, grain boundaries affect work hardening by acting as barriers to slip from one grain to the next. In addition, the continuity criterion of polycrystals enforces complex slip in the neighborhood of the boundaries, which spreads across the grains with increasing deformation. This introduces a dependence of work-hardening rate on grain size which extends to several percent elongations. After this stage, however, the work-hardening rate can be reasonably considered as independent of grain size [188].

5.7. Conclusions

In this chapter, the two-site mean field DDRX model has been successfully applied to 304L austenitic stainless steel, comparisons between experiment and model calculations show very good agreement over a range of deformation conditions with different temperature, strain rates and initial grain sizes.

In the first part, the effect of deformation temperature, strain rate, strain and initial grain size on DDRX are analyzed experimentally. The methods to calibrate the model are described, and the main four parameters are tuned to match with experimental data using a genetic algorithm. It is found that these four parameters evolve with physical meaning, and can be reasonably independent of initial grain size. The reaction of the model to different initial grain sizes is verified, the natural progress towards a steady-state in stress and in grain size with strain is observed.

It is observed both numerically and experimentally that recrystallization kinetics is faster at conditions with low Zener-Hollomon (Z) value, and steady state values evolve in the expected way, i.e. smaller recrystallized grain sizes and increased flow stress for increased values of Z. It has been shown that an increase in initial grain size will slower the recrystallization kinetics while a unique steady state in grain size and flow stress is obtained, regardless of the initial microstructure, and only as a function of the thermomechanical conditions (represented by Z parameter). The initial grain size slightly affects the shape of the flow curves, a decrease in the peak stress and steady state leading to lower stress values with a decrease in the initial grain size.

The good match between experimental results and predicted ones in terms of flow stress, recrystallized fraction and grain size will make the extension of the present model to the post-dynamic or static recrystallization behavior easier, and open the possibility of simulating multi-pass operations compatible with industrial applications.

5.8. French summary

Dans ce chapitre, le modèle à champ moyen 2-sites a été appliqué avec succès à l'acier austénitique 304L. Les résultats numériques présentés sont en accord avec les résultats expérimentaux pour une large gamme de conditions de déformations, avec des valeurs de température, de vitesse de déformation et de taille initiale de grain différentes.

Dans la première partie, l'influence de la température de déformation, de la vitesse de déformation, de la déformation totale et de la taille de grain initiale sur la DDRX ont été

analysées expérimentalement. Les méthodes de calibration du modèle sont décrites. En utilisant un algorithme générique, les quatre principaux paramètres sont réglés afin de bien représenter la courbe expérimentale. Il a pu être observé que ces quatre paramètres évoluent de manière physiquement cohérente et qu'ils sont indépendants de la taille initiale du grain. La réponse du modèle à différentes tailles intiales de grain est vérifiée, et l'évolution naturelle vers un état stable en contrainte et en taille de grain est observée.

Il est observé aussi bien numériquement qu'expérimentalement que la cinétique de recristallisation est plus rapide avec une valeur de Zener-Hollomon (Z) faible, et les valeurs de l'état stationnaire évoluent de façon attendue, i.e des tailles de grains recristallisés plus petites et une augmentation du champ de contrainte pour des valeurs de Z supérieures. Il est aussi montré qu'une augmentation de la taille initiale du grain va ralentir la cinétique de recristallisation, avec toutefois un état stationnaire caractérisé par une taille de grain et une contrainte d'écoulement qui ne dépendent pas de la microstructure initiale, mais uniquement des conditions thermomécaniques. La taille initiale du grain n'affecte que légèrement la forme des courbes de contraintes-déformations. Une diminution de la taille initiale du grain diminuera le pic de contrainte ainsi que les valeurs de contraintes menant à l'état stationnaire.

La bonne cohérence des résultats expérimentaux avec ceux issus des simulations pour les valeurs de contraintes, fraction de recristallisation et taille de grain, rend l'application de ce modèle aux comportements post-dynamique et à la recristallisation statique plus aisée, et offre des possibilités de simulations d'opérations mutli-passes compatible avec des applications industrielles.

6. Recrystallization after deformation

6.1. Introduction

The advantage of DRX is that dynamically recrystallized grain size does not depend on the initial grain size, instead, it is controlled solely by the Zener-Hollomon parameter Z which makes the control of the microstructure relatively easy. However, very few practical utilization of DRX as the final step to control the microstructure of steels can be found, because the dynamically recrystallized structure is in nature not stable, the recrystallized grains will grow in size immediately after termination of hot deformation (unless it is quenched), driven by the grain boundary surface energy and by the stored strain energy.

SRX/PDRX is likely to take place after hot working, such as hot rolling or hot forging because there is inevitably a post-deformation period of time where the workpiece remains at high temperature. In fact, in industrial practices, the frequently used rapid cooling to prevent recrystallization after deformation is often restricted by workpiece dimensions or process configuration [4]. As mentioned in Chapter 2, the recrystallization following deformation is usually termed SRX or PDRX depending on the applied strain. When this strain is below ε_{cr}^{DRX}, classical SRX takes place through nucleation and growth of grain after a certain incubation time. On the other hand, almost simultaneous PDRX occurs if the applied strain is beyond ε_{cr}^{DRX}.

Extensive investigations have been made on DRX, and comparatively few experimental studies have been done on the post deformation behavior. The recrystallization after deformation is usually studied in terms of softening fraction by using double twist tests under different conditions of strains, temperatures, strain rates and holding times, while grain size evolution was not examined, with the exception of limited examples, including those conducted by [63,117]. In the previous chapters, the effects of stop strain, strain rate and temperature on DRX have been examined by experiments, excellent matches between results produced by the numerical model and these from experiments are obtained for different conditions.

In this chapter, the post deformation recrystallization behaviour of 304L has been investigated. The effect of deformation parameters, including temperature, strain rate and strain, as well as annealing time on both recrystallized fraction and average grain size have been studied. The mechanisms of SRX/PDRX were also investigated by quasi in situ heating experiments to get a better understanding of these two processes. The application of the proposed numerical model to 304L for different conditions is illustrated in detail from the interruption of the deformation until the grain growth regime, the comparison between experimental and numerical results has been conducted and analyzed. Overall, the proposed numerical model successfully predicts (with some assumptions) the microstructure evolution after hot deformation.

6.2. Post dynamic recrystallization

6.2.1. Experiment

As the deformation conditions prior to the unloading time are characterized by large deformation, high temperature, and sometimes with high strain rate, a fully recrystallized

structure is obtained subsequently within a short time, and instantaneous quenching is needed in order to follow the fast evolution of the microstructure, which is beyond the capacity of the CEMEF torsion test machine (see section 3.3.4). Beladi *et al*. [117,118] found ~20% softening within a short inter-pass time of 0.1s at 1000 ℃ using an austenitic model alloy after a deformation of 6. Fujita *et al*.[63] observed by TEM that the microstructural features of DRX such as irregular shape of grain boundaries, relatively high dislocation density, disappear in a very short holding time of less than 1s at 1100 ℃ using 316L steel. This rapid evolution of microstructure makes the quantitative measurement of the progress of the recrystallized fraction extremely difficult to carry out by metallographic examination of the quenched microstructure. The concept of fractional softening discussed in 2.5.1 is thus adopted in some cases for the investigation of PDRX in complement to the characterization of micrographs, the double twist test is then used for the quantitative measurement of the softening fraction.

Hot torsion tests were carried out according to the schematic diagram illustrated in Figure 6-1. The samples were held for 3 min after reaching to the desired temperature T_0, the initial grain size is ~165 μm. The samples were deformed at the same temperature T_0 (from 1000 ℃ to 1150 ℃) to different strains, higher than the critical strain for DRX at strain rates of 0.01 to 1.0 s^{-1}. Two different kinds of experiments were then conducted. The samples were either kept on the torsion test machine at the same temperature for a certain holding time before quenching, or were double twisted using the same processing condition immediately after the pre-set unloading time, to measure the softening fraction, followed by water quench.

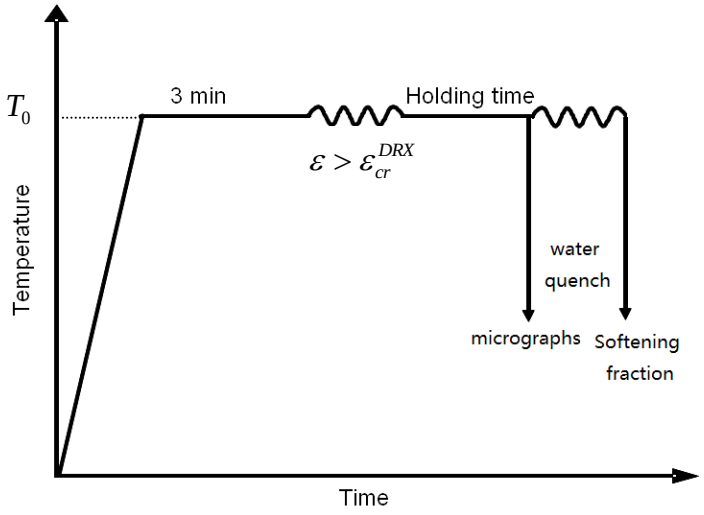

Figure 6-1 Schematic diagram of PDRX experiment

The unloading times were chosen such that gradual microstructural evolution could be followed, long unloading times were also used to reach asymptotic behaviors. The conditions used to analyze the effect of deformation temperature, strain rate and applied strain are listed below in Table 6-1, unloading times (15s,30s,60s,120s,600s,1800s,600s) are chosen such that gradual evolution during PDRX could be followed for each condition. PDRX is extremely fast when both the deformation temperature and strain rates are high, which then accordingly needs a simultaneous water quench device in order to preserve as much as possible the microstructure after deformation. In the current study, the typical quench delay is ~2s due to the limitation of the experimental devices as explained in section 3.3.4. An extreme example is shown in Figure 6-2, where the sample was deformed at both high temperature and large strain rate (at 1150 ℃ and 1.0s^{-1}). In that case the flow stress drops to the same level as the initial state in 5s' annealing time, and a considerable softening is already seen in 1s. In response to this, a smaller strain rate of 0.01s^{-1} was chosen to analyze the influence of temperature, while a lower

temperature of 1000 ℃ was used when investigating the effect of strain rate, in order to have a relatively slower kinetics of PDRX and therefore make the experimental data as accurate as possible. However, when it comes to the applied strain, a higher temperature of 1100 ℃ was adopted, below which steady state cannot be obtained (see section 5.3).

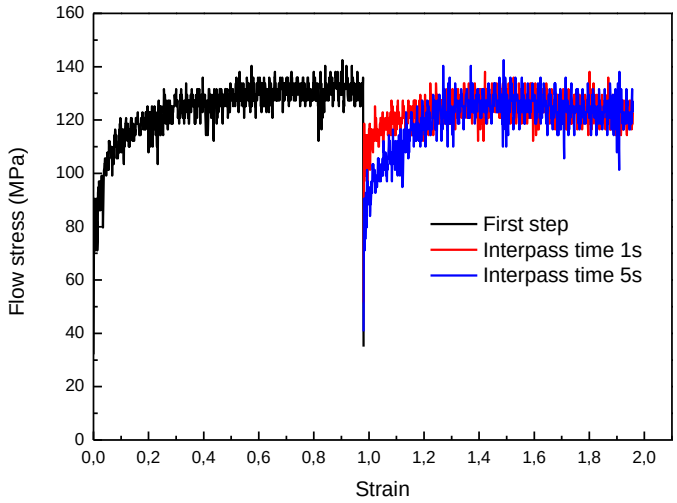

Figure 6-2 Double twist test at 1150 ℃ and 1.0s^{-1} showing that PDRX occurs rapidly after unloading

Table 6-1 The conditions analyzed for PDRX described in this chapter

Affecting factors	Conditions
Deformation temperature	$T=1000°C$， $\dot{\varepsilon}=0.01s^{-1}, \varepsilon=1.5$ $T=1100°C$， $\dot{\varepsilon}=0.01s^{-1}, \varepsilon=1.5$ $T=1150°C$， $\dot{\varepsilon}=0.01s^{-1}, \varepsilon=1.5$
Strain rate	$T=1000°C$， $\dot{\varepsilon}=0.01s^{-1}, \varepsilon=1.5$ $T=1000°C$， $\dot{\varepsilon}=0.1s^{-1}, \varepsilon=1.5$ $T=1000°C$， $\dot{\varepsilon}=1.0s^{-1}, \varepsilon=1.5$
Applied strain	$T=1100°C$， $\dot{\varepsilon}=0.01s^{-1}, \varepsilon=0.2$ $T=1100°C$， $\dot{\varepsilon}=0.01s^{-1}, \varepsilon=1.0$ $T=1100°C$， $\dot{\varepsilon}=0.01s^{-1}, \varepsilon=1.5$ $T=1100°C$， $\dot{\varepsilon}=0.01s^{-1}, \varepsilon=2.0$

P.S: A small strain of 0.2 leading to SRX is chosen for comparison.

Microstructure from different conditions were then characterized use standard methods by optical microscope. EBSD investigations were also conducted as complementary information in conditions where the grains are very small and optical microscopy is too limited to identify clearly the grain boundaries.

Similarly to the case of SRX, a few quasi in situ heating experiments were also conducted to follow the gradual microstructural evolution and understand the mechanisms during PDRX on a chosen area. The details and principles of the in situ heating experiments can be found in

section 3.5, the samples used here are previously deformed at $T = 1000°C, \dot{\varepsilon} = 0.01s^{-1}, \varepsilon = 1.5$ and $T = 1000°C, \dot{\varepsilon} = 0.1s^{-1}, \varepsilon = 1.5$.

6.2.2. Influence of temperature

To simplify the problem, the annealing temperature is always chosen to be constant and is the same as the deformation temperature. The temperature range is set to be from 1000 ℃ to 1150 ℃. When modeling PDRX in variable temperature conditions, the model just needs to consider the constant temperature and use the corresponding parameters at each time increment.

Three different conditions were investigated in detail, all of which with an initial deformation of 1.5 at strain rate of 0.01/s, the deformation temperatures being 1000 ℃, 1100 ℃, 1150 ℃ respectively. Micrographs are presented here to gain a better insight on the evolution of recrystallized fraction and grain size after hot deformation. For this purpose, different unloading times, from a few seconds to a few hours, were selected for each condition.

At 1000 ℃, an initial small fraction of DRX grains were formed along the boundaries of elongated grain, see Figure 6-3a, and a short unloading time of 30s led to an increased number of small grains through PDRX (Figure 6-3b). These small grains are probably formed by classical nucleation and growth phenomenon. The average recrystallized grain size after DRX and 30s' unloading time were both examined by EBSD. The grain size of 15.4 μm is found to be close to that of the quenched state which is 15.7 μm. The microstructure after a heating time of 30s is examined by EBSD, and it is presented in Figure 6-4. Considering that during unloading time, these dynamically recrystallized grains will certainly grow, the fail of increasing average recrystallized grain size is a clear indication that additional nuclei were formed during PDRX. At the early stage of recrystallization process, it is apparent that the twins taking the form of parallel sided lamellae (see Figure 2-29 or the one pointed out by the arrow in Figure 6-3f) are not often observed, instead, a straight line is usually found between the RX grains and associated twins (pointed out by arrows in Figure 6-4a). The twin is formed in that case by a growth accident, which is more likely to occur when the boundary velocity is high [196,197], i.e. when the driving force is high. This happens when RX grains are surrounded by the NR grains. The twinning process itself may have an effect on the mobility of the moving front. The small grains then keep growing towards the deformed elongated grains, the fraction of NR grains is decreasing (Figure 6-3c, Figure 6-3d). Fully recrystallized structure is obtained after an unloading time of 120s (Figure 6-3e). Grains keep growing with longer heating time (Figure 6-3f, Figure 6-3g, Figure 6-3h).

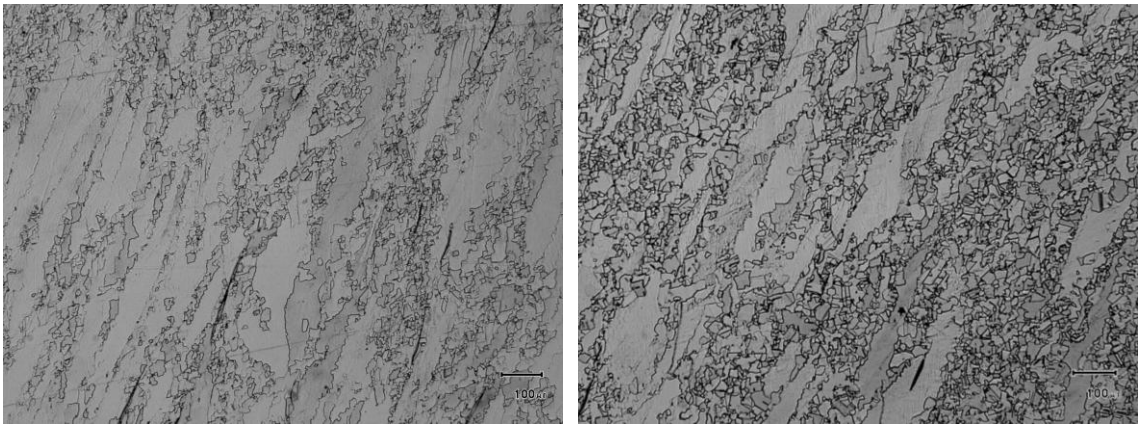

a) Quench after deformation b) 30s

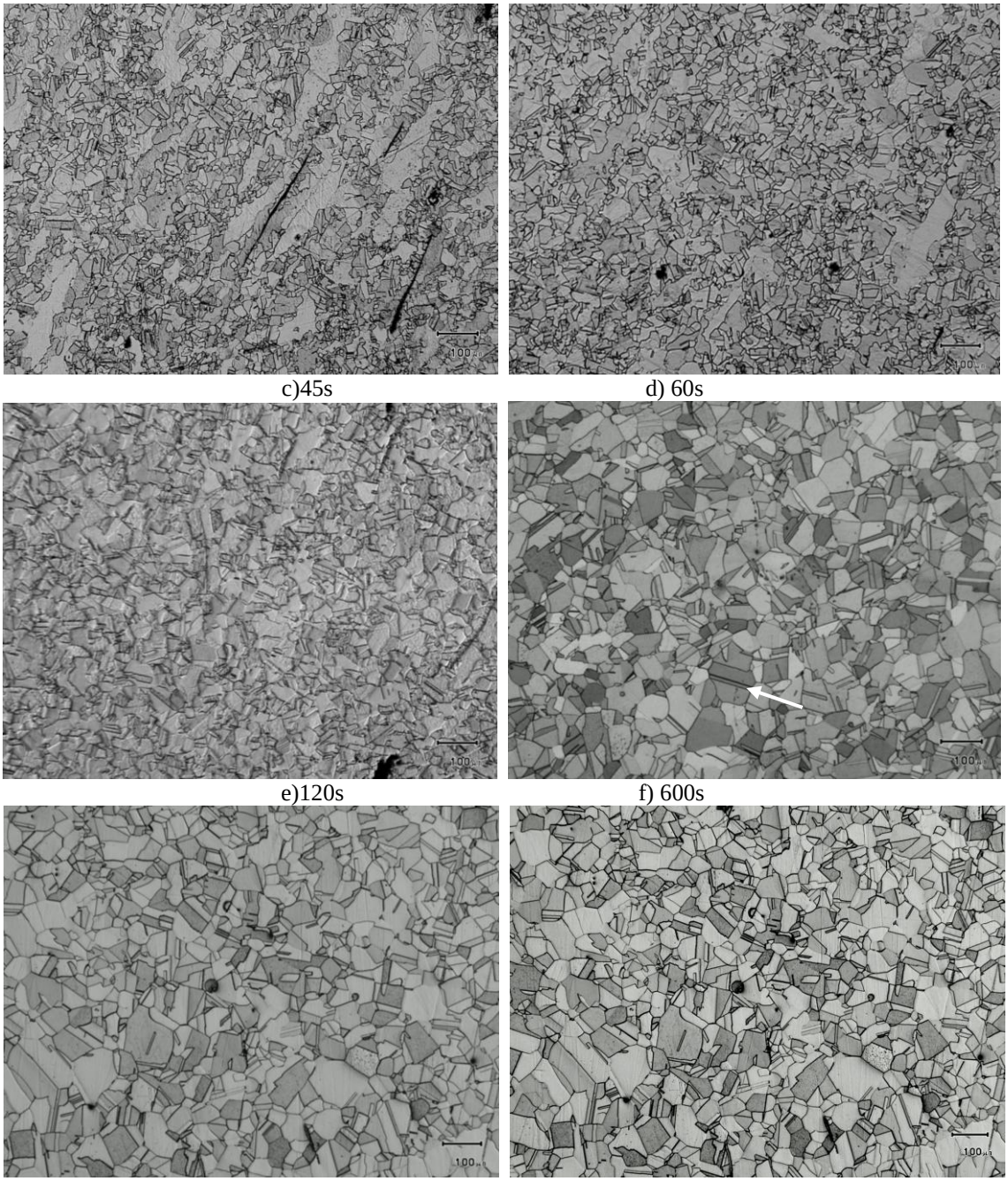

c)45s d) 60s

e)120s f) 600s

g) 1800s h) 6000s

Figure 6-3 Optical microscope micrographs of samples deformed to a strain of 1.5 at 1000 ℃ and a strain rate of $0.01s^{-1}$, followed by holding at this temperature for a) 0s, b) 30s, c) 45s, d) 60s, e) 120s, f) 600s, g) 1800s, h) 6000s

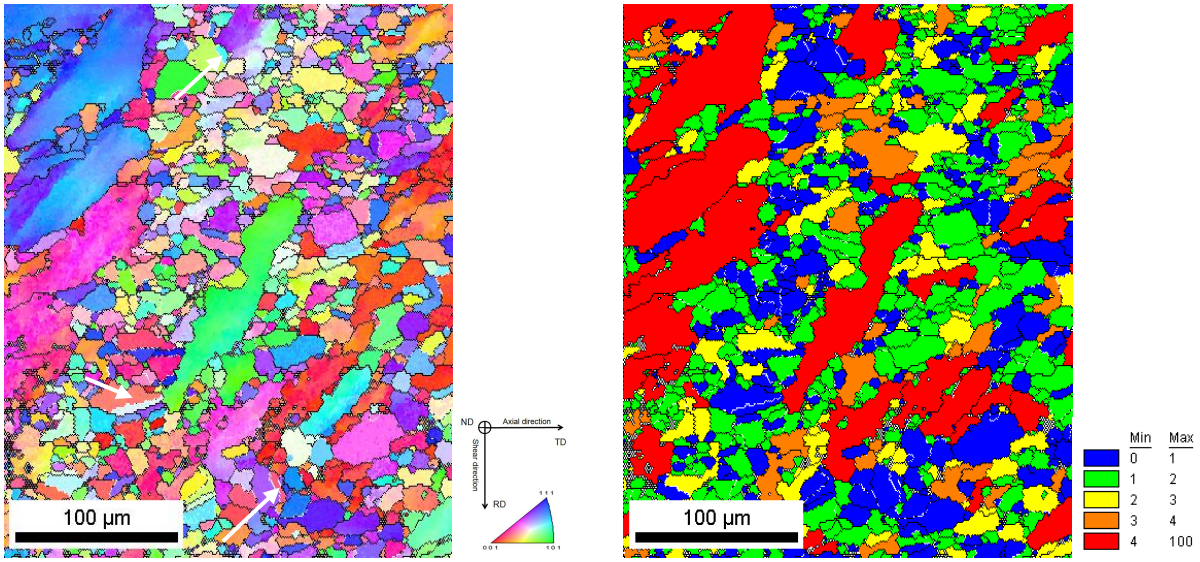

a) b)

Figure 6-4 EBSD map of the microstructure after 30s holding time of samples deformed to a strain of 1.5 at 1000 ℃ and a strain rate of $0.01s^{-1}$, white lines represent twin boundary, the arrows point to the twin boundaries taking the form of a line instead of lamellae a) IPF map, b) GOS map

At higher temperature of 1100 ℃, the dynamically recrystallized fraction after deformation is already about 60% and the recrystallized grain size is ~12 µm, see Figure 6-5a. The microstructure after a short heating time (15s) consists of work hardened initial grains, a large number of small grains and some big grains which have grown from dynamically recrystallized grains, as shown in Figure 6-5b. Both the non-recrystallized grains and PDRX grains are characterized by their big sizes and irregular grain boundaries, which makes it hard to distinguish them, even though the latter ones usually exhibit annealing twins as indicated by black arrows.

The microstructure was analyzed by EBSD, with which the non recrystallized grains were easily identified by looking at the grain orientation spread (GOS). As shown in Figure 6-6, we have recrystallized grains with GOS values less than 1.0 in Figure 6-6b and grain sizes around 100 µm. Non-recrystallized grains which are indicated by black arrows in Figure 6-6b, with GOS value above 3.0, still exist. Turning back to Figure 6-5c and Figure 6-5d, it is clear that the average grain size keeps increasing, fully recrystallized structure is obtained before 60s' heating time. A nearly equiaxed microstructure was found after 120s, as shown in Figure 6-5e. The recrystallized grains keep growing with time (Figure 6-5f), driven by grain boundary energy, until 1800s (Figure 6-5g) where the grain size reach to steady state (see section 6.5.3.2). Longer heating times up to 6000s (Figure 6-5h) does not provide any additional growth, the steady state grain size keeps at ~110 µm.

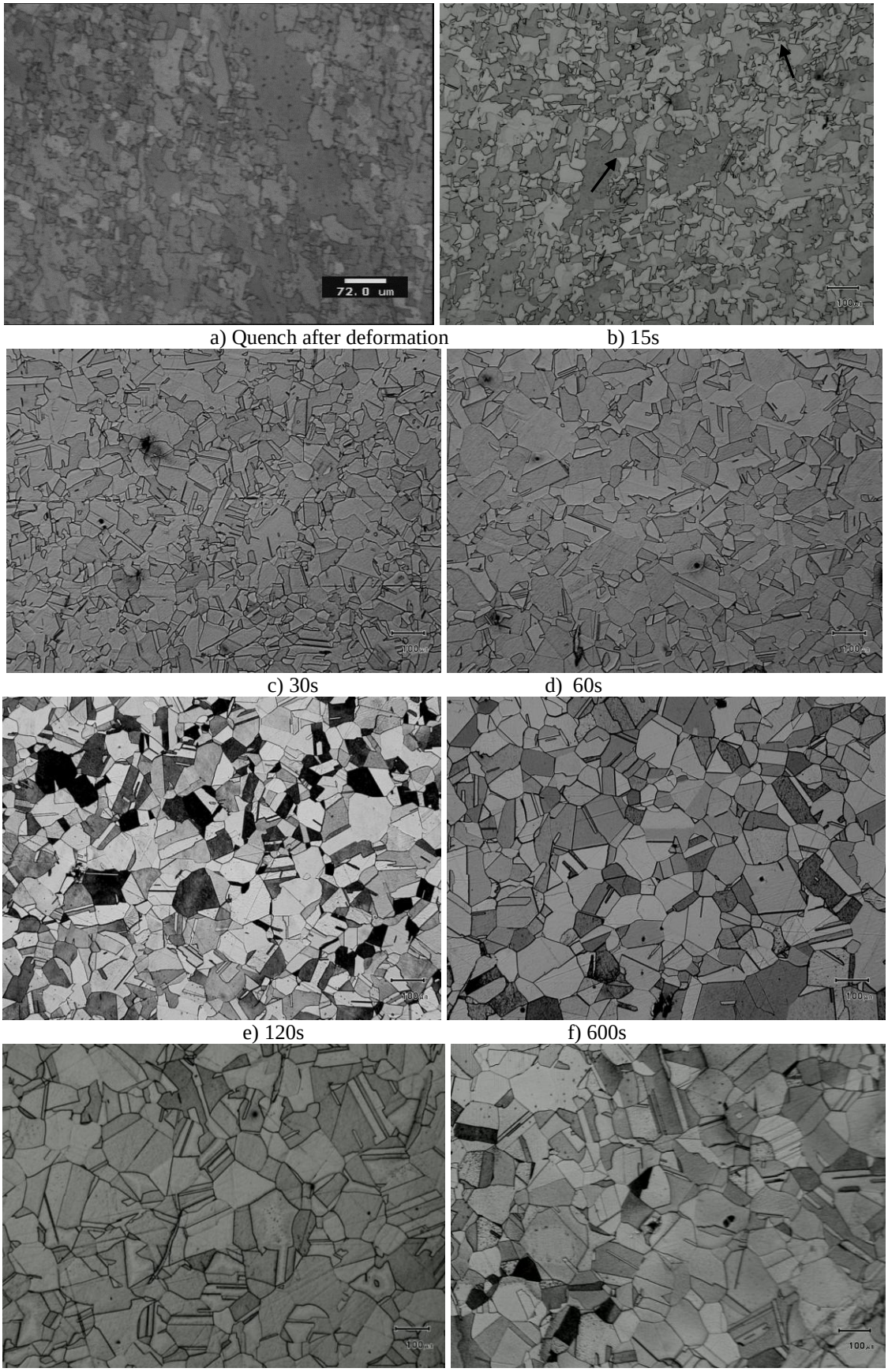

a) Quench after deformation b) 15s

c) 30s d) 60s

e) 120s f) 600s

g) 1800s h) 6000s

Figure 6-5 Optical microscope micrographs of samples deformed to a strain of 1.5 at 1100 ℃ and a strain rate of $0.01s^{-1}$, followed by holding at this temperature for a) 0s, b) 15s, c) 30s, d) 60s, e) 120s, f) 600s, g) 1800s, h) 6000s

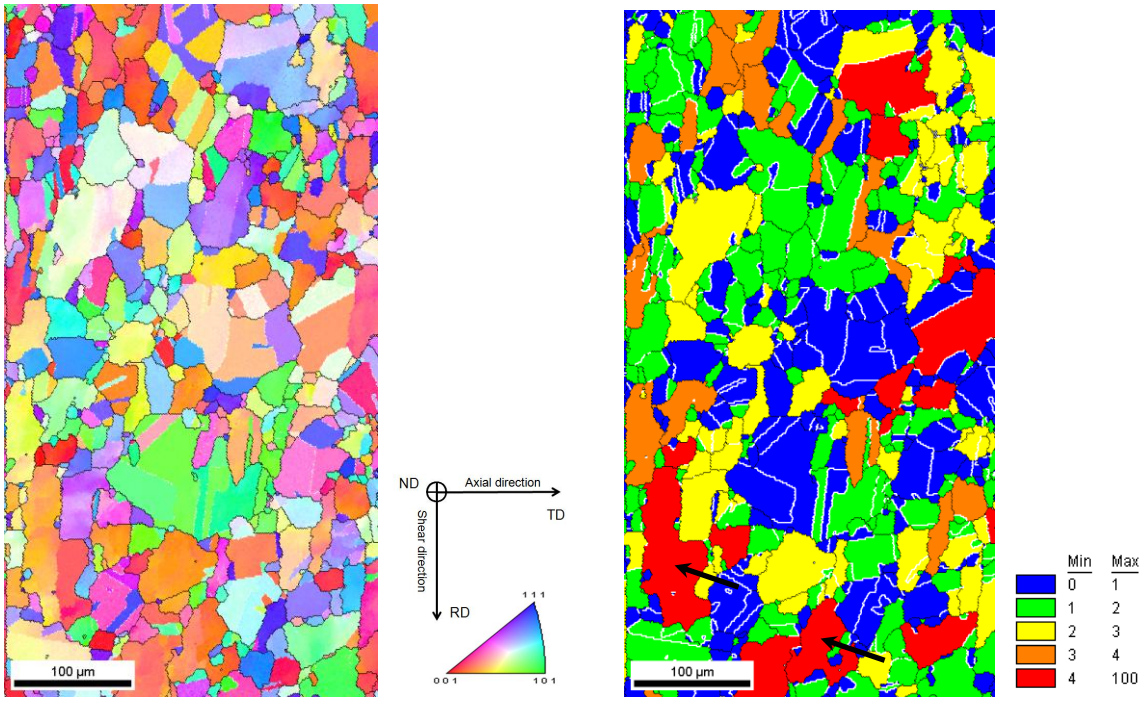

a) IPF map b) GOS map

Figure 6-6 EBSD map of the microstructure after 15s holding time of samples deformed to a strain of 1.5 at 1100 ℃ and a strain rate of $0.01s^{-1}$, white lines represent twin boundary, the arrows point to the NR grains a) IPF map, b) GOS map

By increasing the deformation and heating temperature to 1150 ℃, similar microstructural evolution (shown in Figure 6-7) was found compared to 1100 ℃. As expected, the recrystallized kinetics accelerated, coarser recrystallized grain size was also obtained. A fully recrystallized structure was found at around 30s' heating time (Figure 6-7a).

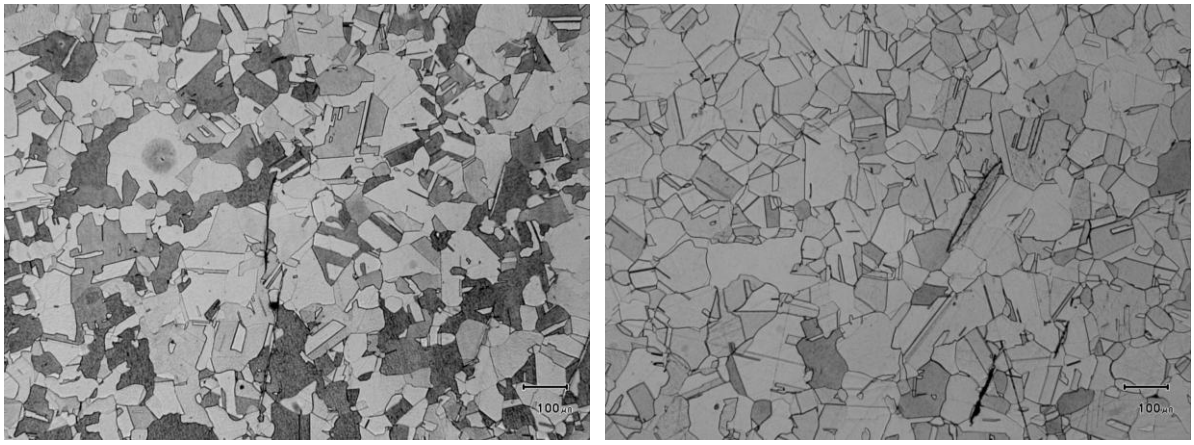

a) 15s b) 30s

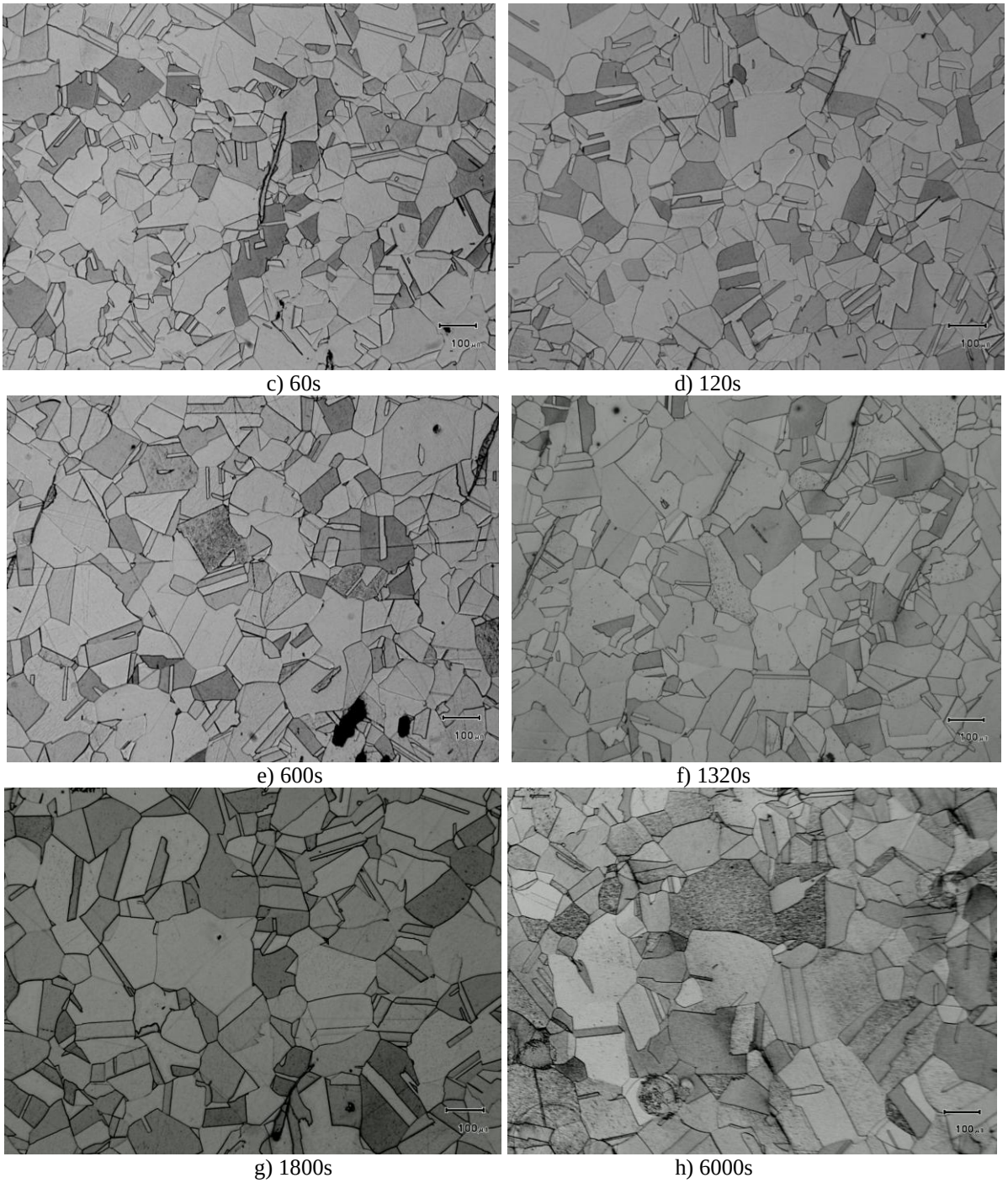

c) 60s d) 120s

e) 600s f) 1320s

g) 1800s h) 6000s

Figure 6-7 Optical microscope micrographs of samples deformed to a strain of 1.5 at 1150 ℃ and a strain rate of $0.01s^{-1}$, followed by holding at this temperature for a)15s, b) 30s,c) 60s, d)120s, e)600s, f)1320s, g)1800s, h)6000s

6.2.3. Influence of strain rate

It is well documented that strain rate has a pronounced influence on the subsequent PDRX kinetics for different materials, at a given strain, the time for 50% recrystallization decreases with increasing strain rate [134]. In the present work, the microstructure evolution after deformation to a strain of 1.5 at 1000 ℃ with different strain rates is studied, starting from the interruption of the deformation (0s holding time) to the grain growth regime (6000s holding time).

When the strain rate increases to $0.1s^{-1}$, a relatively smaller fraction of new DRX are found on the boundaries of the pre-existing elongated grain boundaries (Figure 6-8a) compared with that of lower strain rate of $0.01s^{-1}$ (Figure 6-3a). Clearly, an increased number of small grains are again observed after a short holding time of 15s (Figure 6-8b), but the microstructure still consists of a number of elongated work hardened initial grains. Since the recrystallized grains are relatively small, the microstructure is examined by EBSD, as shown in Figure 6-9. It is found the grains with a GOS value between 2 °and 3 ٩(in green and yellow respectively), which are typical values for DRX grains, only count for a small fraction, suggesting that they are either consumed by the statically formed growing nuclei or they continue to grow and hence decrease their GOS value. It is reasonable to infer that this small quantity of existing DRX grains will finally disappear with further heating time. Another interesting thing is that the RX grains which are consuming NR grains (pointed by the black arrow) usually have twinned on the growing front. As pointed out earlier, this may change the mobility of RX grains by changing their crystallographic. In general, it seems that twinning favors grain boundary migration, since the twinned grains are usually bigger than those without. However, one could draw an inverse conclusion, i.e. only these grains which grow fast (high driving force) are likely to twin. After 15s' heating time, the average recrystallized grain size increases to ~16.6μm, the recrystallized fraction is ~65%. At longer heating time of 30s (Figure 6-8b), ~85% of the microstructure is replaced by the recrystallized grains, where only ~65% recrystallization is observed when the deformation is conducted at $0.01\ s^{-1}$ (Figure 6-3b), the average grain size is found to be ~19.8μm. The amount of twins keeps increasing, and a twin is usually found in the front of the growing grains when they are growing toward the old grains (pointed out by the black arrows). Since a smaller volume fraction of DRX existed after deformation at higher strain rate, and a larger amount of recrystallization was measured after the same period of holding time, demonstrates that strain rate does accelerate PDRX kinetics. The recrystallization process completes at about 60s (Figure 6-8c), followed by the grain growth process with increased holding time (Figure 6-8d to Figure 6-8h).

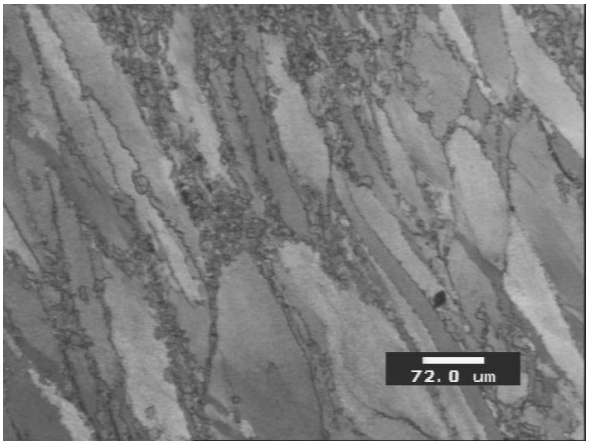

a) Quench after deformation

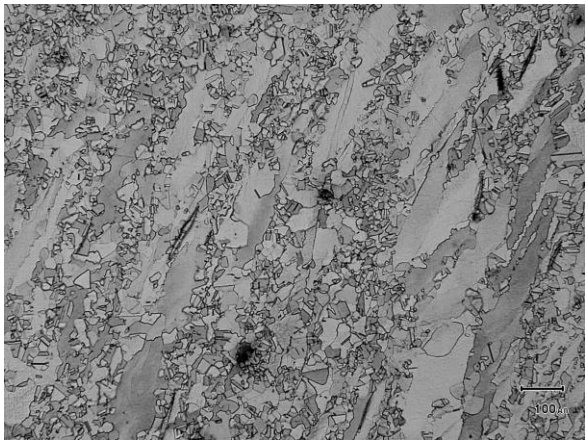
b)15s

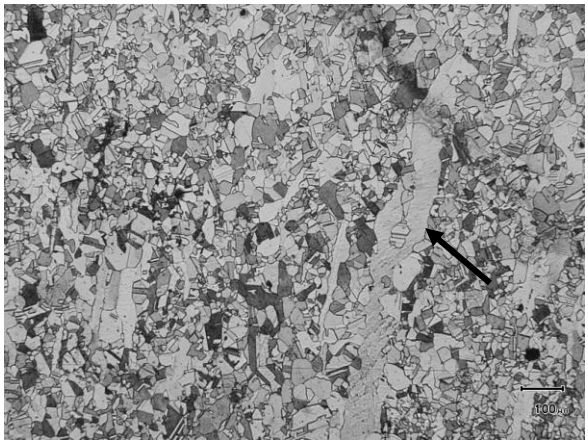

c) 30s

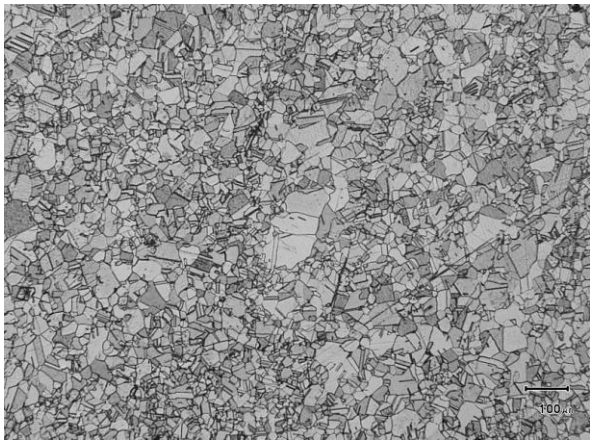

d)60s

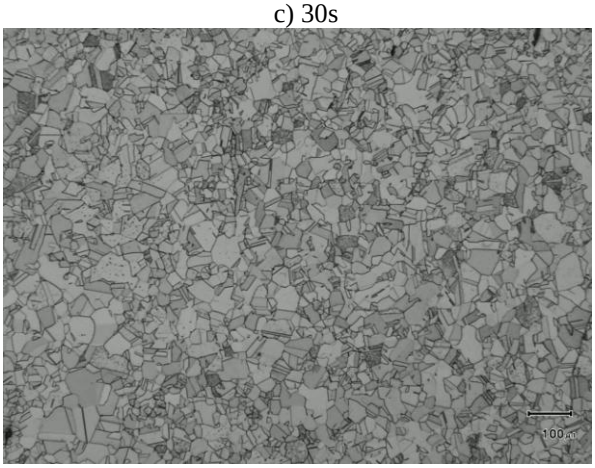

e) 120s

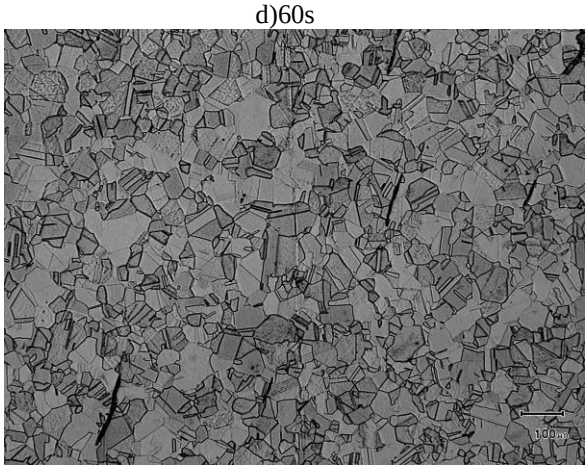

f) 600s

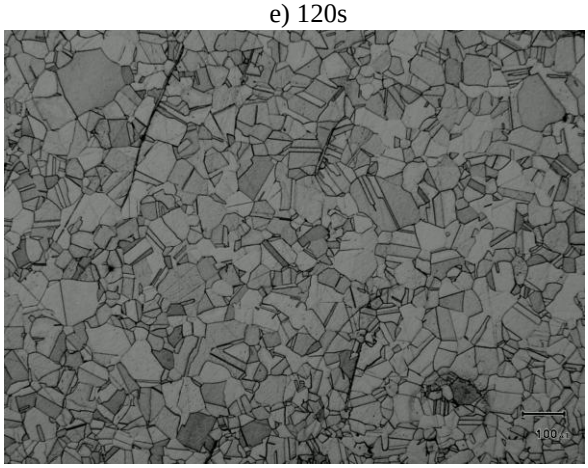

g) 1800s

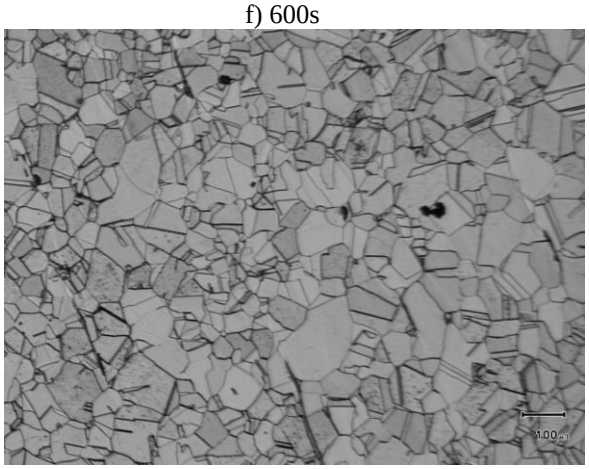

h) 6000s

Figure 6-8 Optical micrographs of samples deformed to a strain of 1.5 at 1000 ℃ and a strain rate of $0.1s^{-1}$, followed by holding at this temperature for a) 0s, b) 15s, c) 30s, d) 60s, e) 120s, f) 600s, g) 1800s, h) 6000s

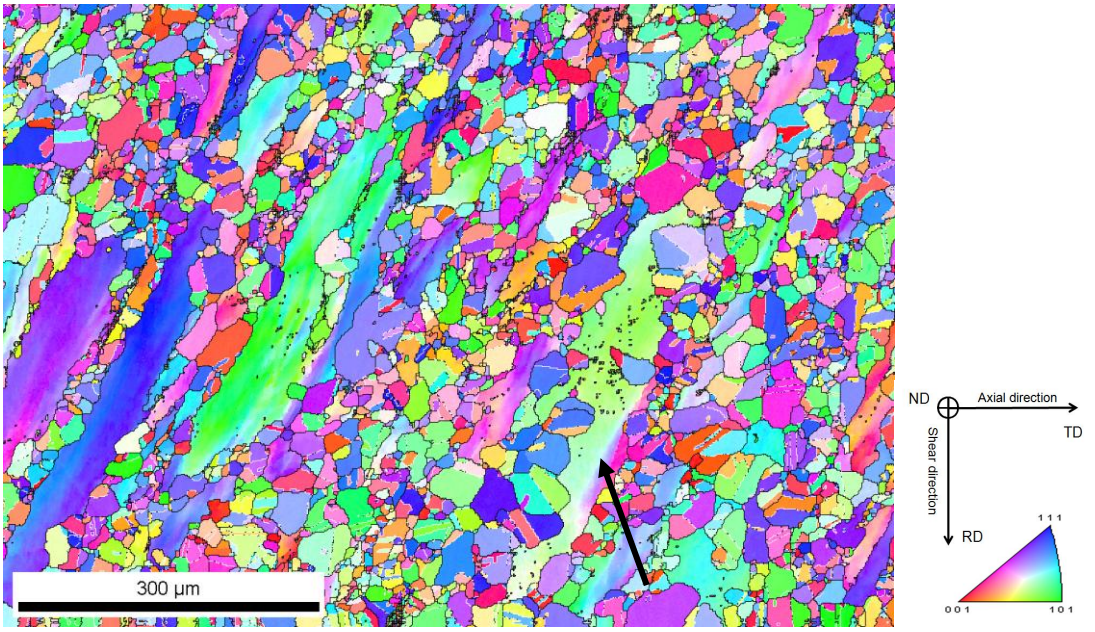

a)

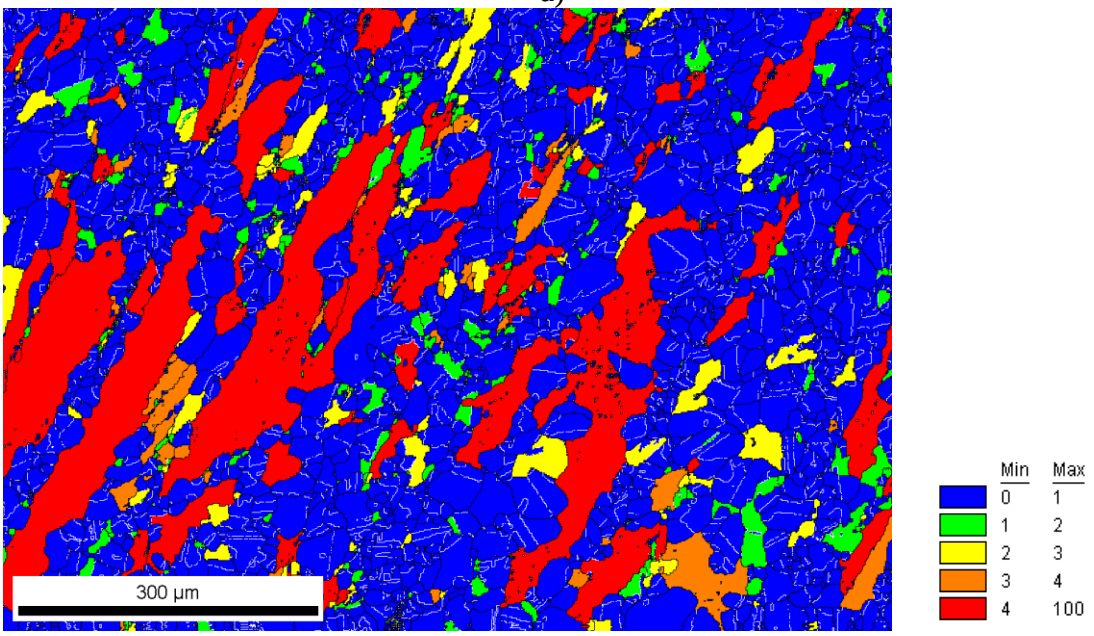

b)

Figure 6-9 EBSD map of the microstructure after 15s holding time of samples deformed to a strain of 1.5 at 1000 ℃ and a strain rate of $0.1s^{-1}$, white lines represent twin boundary, a) IPF map, b) GOS map

At even higher strain rate ($\dot{\varepsilon}=1.0s^{-1}$), the accelerated PDRX kinetics becomes more apparent. Only a small quantity of elongated old grains still exist after 15s (Figure 6-10b), the presence of a very large number of small grains let think that nucleation has taken place. A comparison between Figure 6-8b and Figure 6-10b, which correspond to micrographs of samples deformed at strain rate of $0.1s^{-1}$ and $1.0s^{-1}$ respectively, shows that apparently, more nuclei are statically formed when the applied strain rate increases. A Full recrystallized structure is obtained after a holding time of only 30s (Figure 6-10c), followed by significant grain growth (Figure 6-10d and Figure 6-10e), leading to a similar asymptotic microstructure as for lower strain rates (see Figure 6-3 and Figure 6-8) at long heating times.

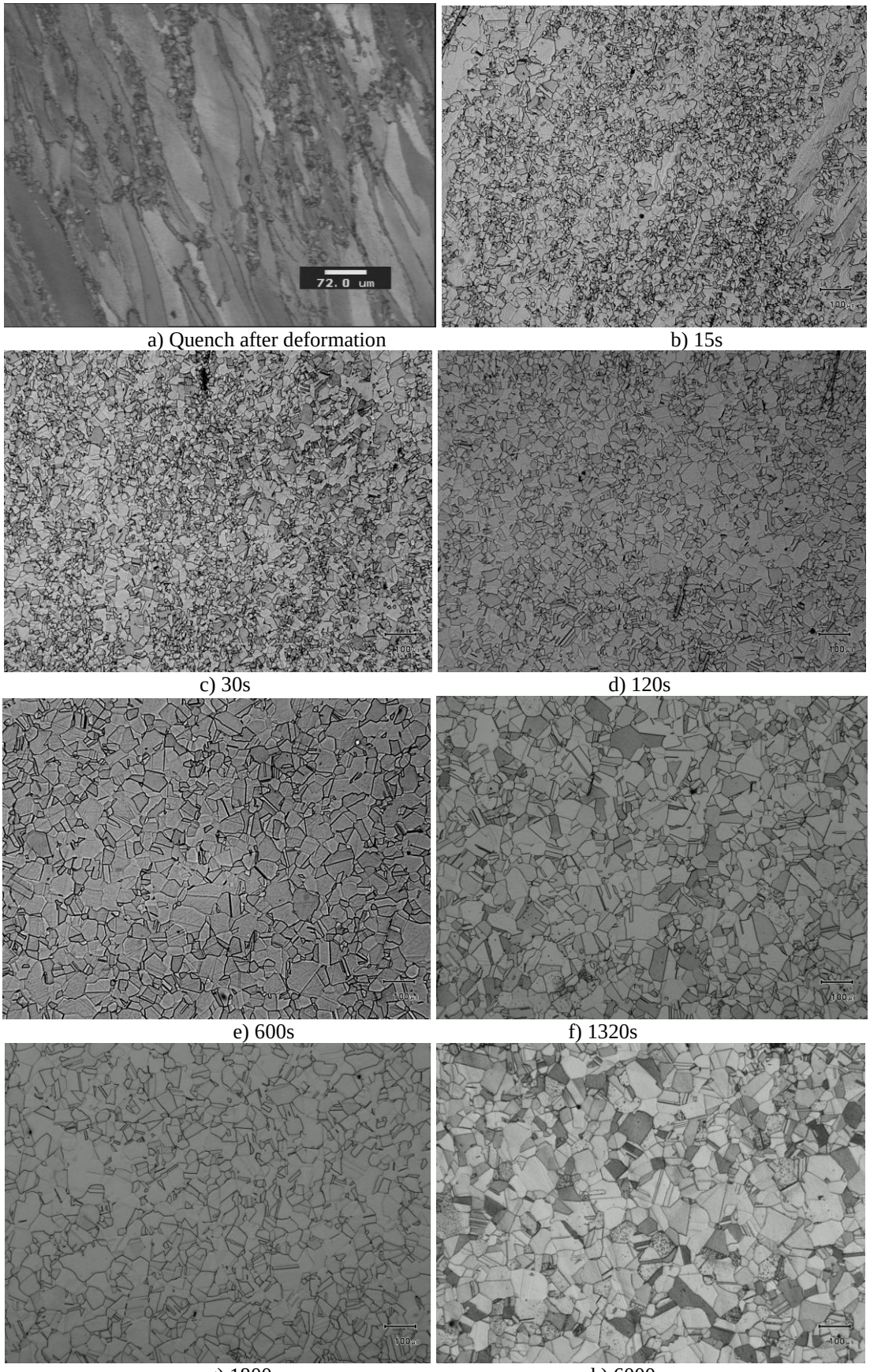

a) Quench after deformation b) 15s

c) 30s d) 120s

e) 600s f) 1320s

g) 1800s h) 6000s

Figure 6-10 Optical micrographs of samples deformed to a strain of 1.5 at 1000 ℃ and a strain rate of $1.0s^{-1}$, followed by holding at this temperature for a) 0s, b) 15s, c) 30s, d) 60s, e) 120s, f) 600s, g) 1800s, h) 6000s

6.2.4. Influence of applied strain

The applied strain is a key factor controlling the post deformation microstructural evolution, it directly determines which kind of (SRV, SRX, PDRX) softening mechanism occurs. It is observed that at a very small strain, in the work hardening region of the flow stress, SRV is the sole mechanism (Figure 2-32b, curve a). Since SRV only slightly changes the microstructure, it is not considered in the present study. In this section, the microstructural investigation is conducted to gain a better insight of the recrystallization phenomena after hot deformation, the corresponding applied strains of 0.2, 1.0, 1.5, 2.0 are designated as A, B, C, D respectively on the flow stress curve in Figure 5-9.

For a strain lower than the critical strain of DRX (Figure 6-11a), almost no small grains were formed on the pre-existing grain boundaries after a short holding time of 30s, suggesting that an incubation time is needed to initiate SRX. However, most of these boundaries are apparently serrated, nucleation by bulging is likely to occur with longer heating time. In Figure 6-11b, where the holding time is 60s, a significant amount of recrystallized grains are observed. Comparing to both DRX and PDRX, they are large in size but small in total number. As the stored energy in this slightly deformed sample is not high, it is not surprising that the formation of nuclei is less frequent. It is interesting to notice that a large fraction of annealing twins is found among these small grains. These created small grains continue to grow when increasing the holding time to 120s (Figure 6-11c), only a small part of the NR grains are left, which look concave (examples are pointed out by black arrows). A fully recrystallized structure is obtained after a holding time of 600s, most of the grains are twinned, which is illustrated in Figure 6-11d. Grains keep growing when the annealing time increases, as shown in Figure 6-11e. The grain size after a heating time of 6000s is ~ 170 μm, see Figure 6-11f.

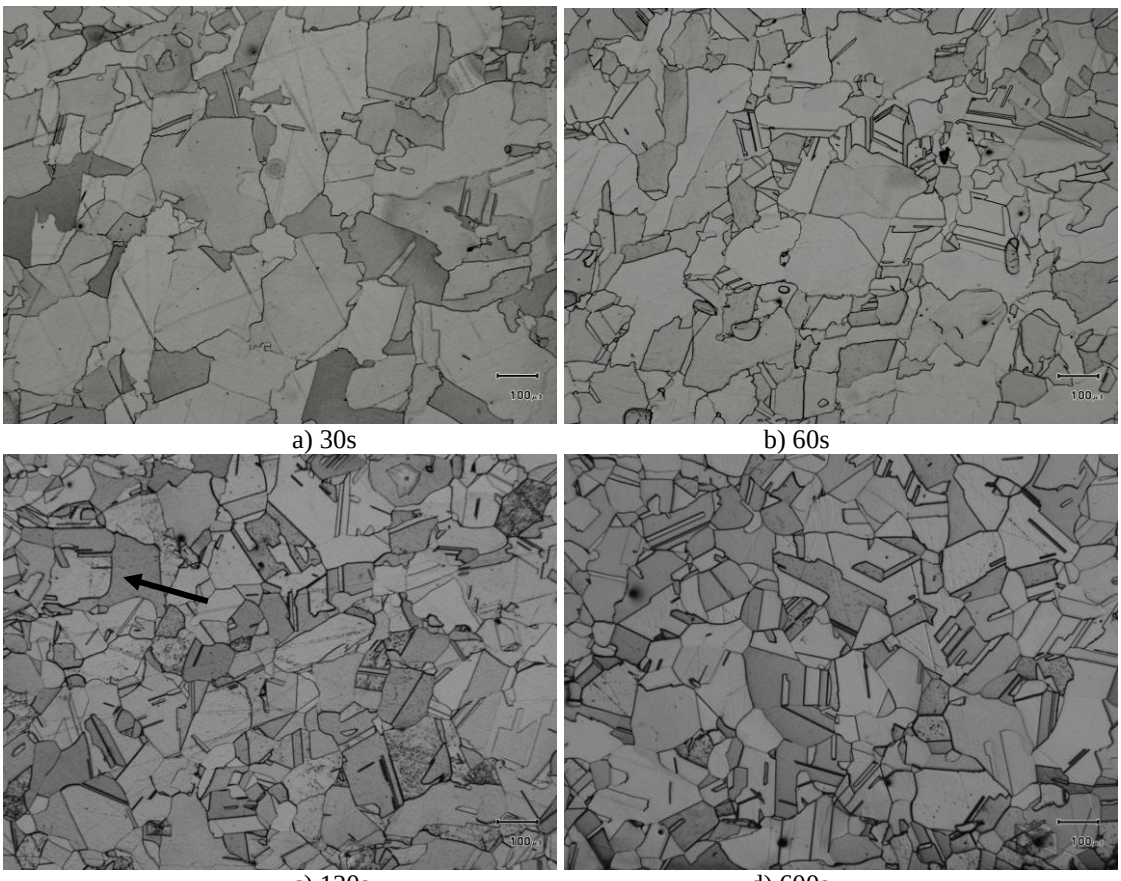

a) 30s b) 60s

c) 120s d) 600s

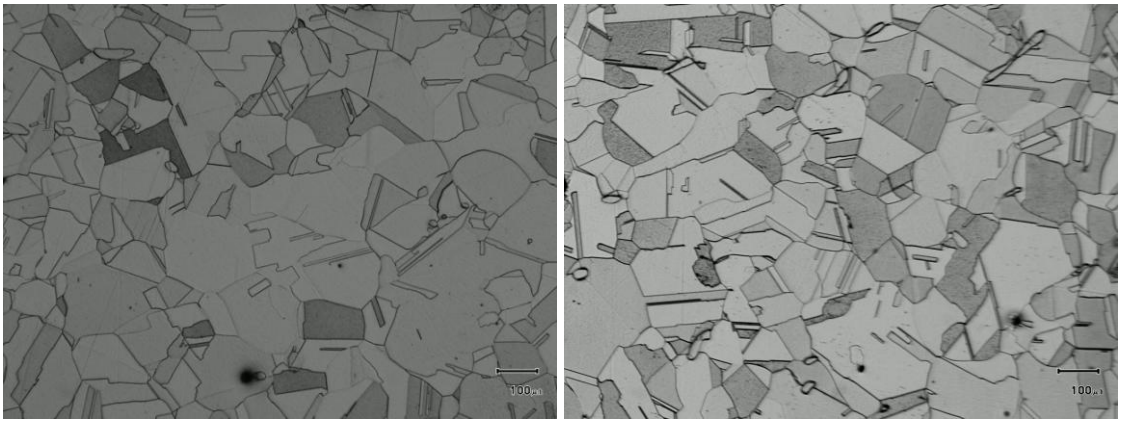

e) 1320s f) 6000s

Figure 6-11 Optical micrographs of samples deformed to a strain of 0.2 at 1100 ℃ and a strain rate of $0.01s^{-1}$, followed by holding at this temperature for a) 30s, b) 60s, c) 120s, d) 600s, e) 1320s, f) 6000s

After deformation to a strain beyond the peak strain (point B in Figure 5-9), where a relatively high fraction of DRX grains were formed during deformation (Figure 6-12a), the pre-existing old grains are almost fully replaced by RX grains after a short annealing time of 30s (Figure 6-12b). Some of the small grains, which formed during DRX or at the early stages of annealing, have grown larger than the other ones. The microstructure of the sample annealed for 30s is examined by EBSD, as shown in Figure 6-13. A large part of the microstructure is replaced by new grains, most of them contain at least one annealing twin. The average recrystallized grain size increases dramatically from ~12 μm to ~40 μm. Grains with at least one twin are systematically bigger than those without twins, suggesting again that either the creation of an annealing twin has accelerated the grain boundary migration or that those grain boundaries which moved the fastest were more likely to create twins. The large number of created special boundaries (see Figure 2-30) by the formation of twins might have played an important role, since it is known that (see Figure 6-14) special boundaries present higher mobilities and are less affected by atoms in solid solution. But, further investigation on this issue is clearly needed. The existing DRX grains, except these just created before the interruption of deformation, usually have a GOS value higher than 1°. An equiaxed microstructure is obtained after 120s (Figure 6-12c), after which smaller grains keep decreasing while larger grains continue to grow, a typical phenomenon of grain growth, see Figure 6-12d and Figure 6-11e) .

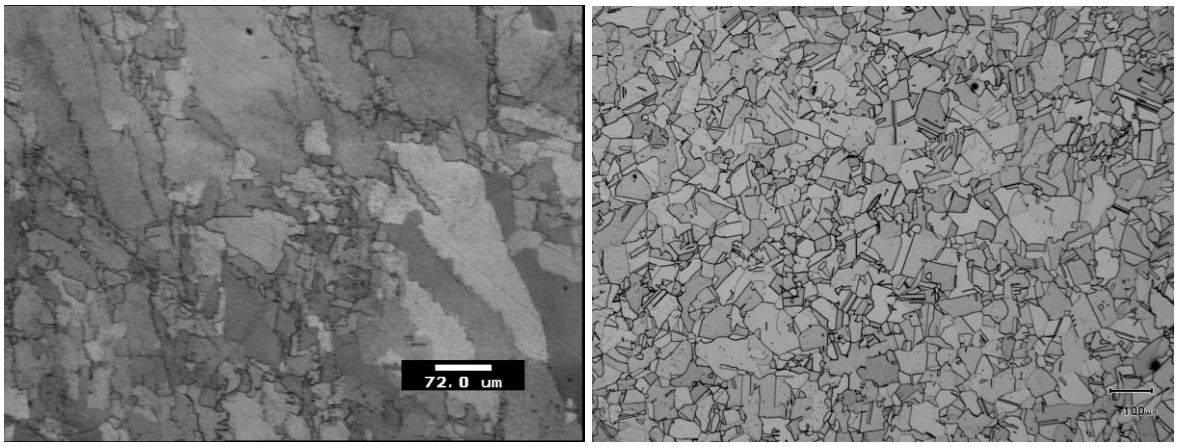

a) Quench after deformation b) 30s

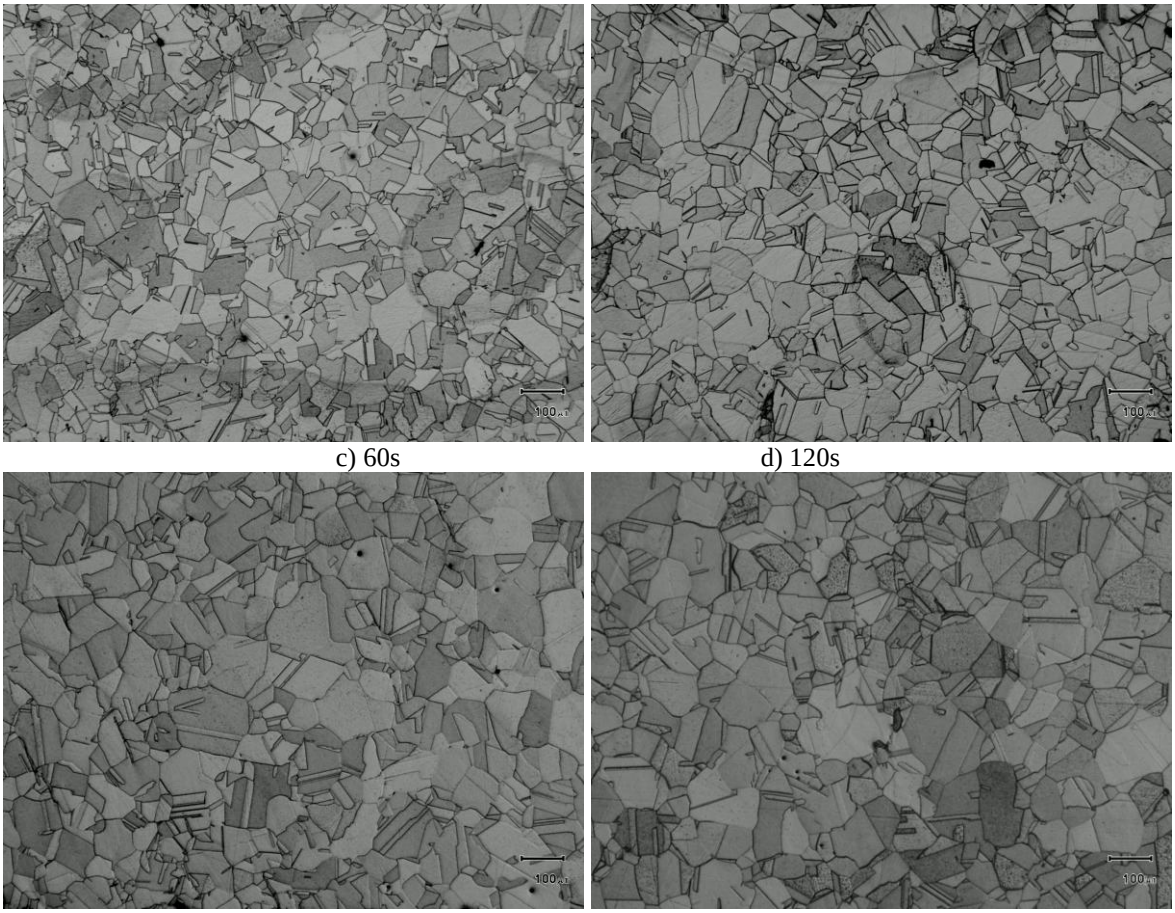

c) 60s d) 120s

e) 600s f) 1320s

Figure 6-12 Optical micrographs of samples deformed to a strain of 1.0 at 1100 ℃ and a strain rate of $0.01s^{-1}$, followed by holding at this temperature for a)0s, b) 30s, b) 60s, c) 120s, d) 300s, e)600s, f) 1320

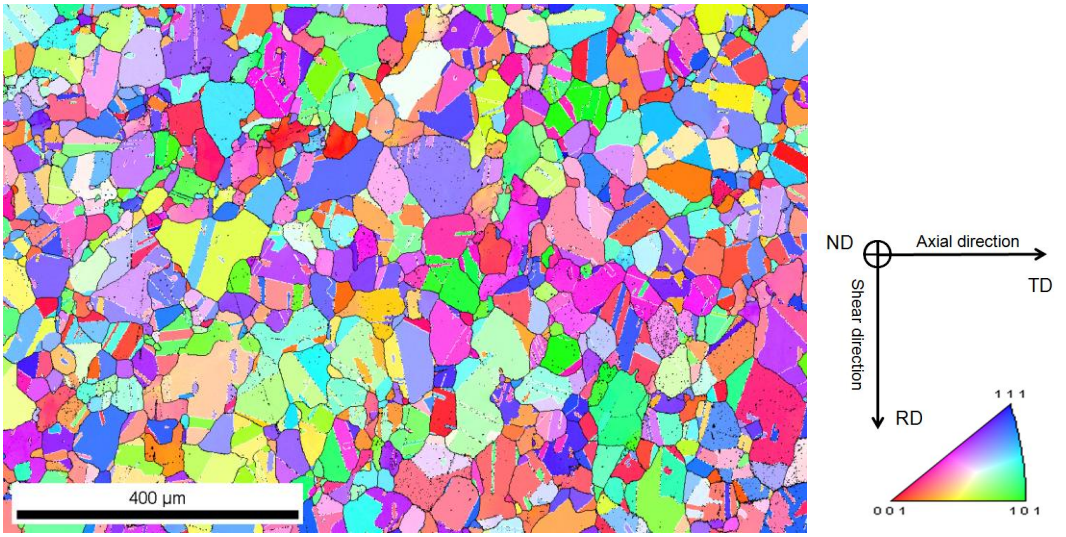

a)

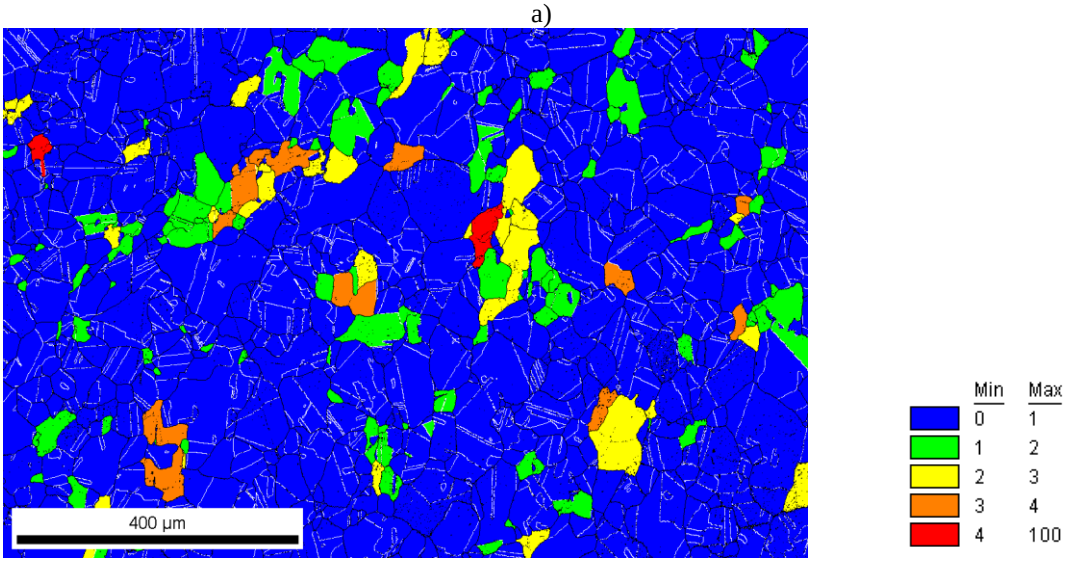

b)

Figure 6-13 EBSD map of the microstructure after 30s holding time of samples deformed to a strain of 1.0 at 1100 ℃ and a strain rate of 0.01s^{-1}, white lines represent twin boundary a) IPF map, b) GOS map

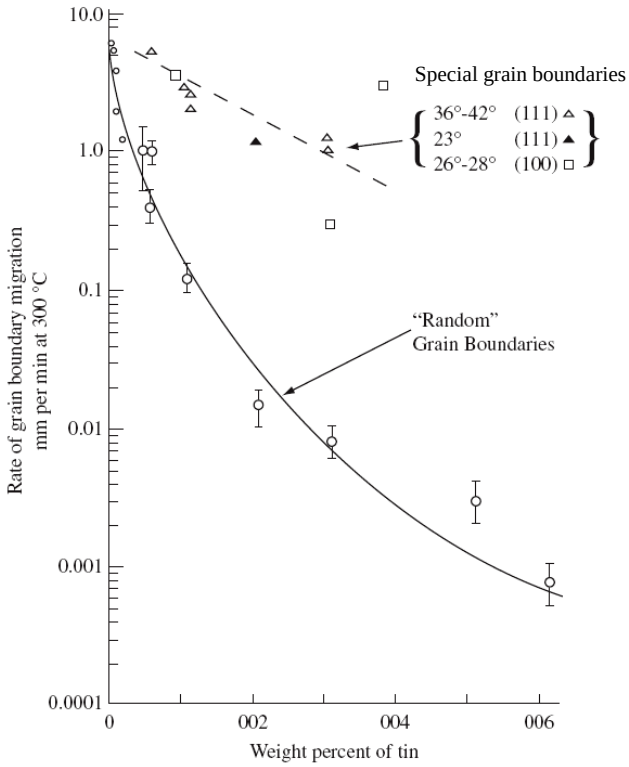

Figure 6-14 Changes on migration rate of grain boundaries of lead (F.C.C) at 300 ℃ as a function of tin content, for random grain boundaries and special grain boundaries [198,199].

By increasing the strain to 2.0, which corresponds to point D (steady state region) in the flow stress curve in Figure 5-9, most of the initial microstructure is replaced by new small DRX grains (Figure 6-15a). A similar PDRX process is found in Figure 6-15 as compared to strains of 1.0 and 1.5, shown in Figure 6-12 and Figure 6-5 respectively. The number of small grains in the microstructure after 30s' heating time (Figure 6-15b) is slightly increased and has replaced nearly all of the left original old grains. An apparent difference with the microstructure after deformation is the large number of twins. These grains continue to grow by further increasing the holding time (Figure 6-15c, Figure 6-15d), a nearly steady state is reached after a holding time of 600s (Figure 6-15e), since the average grain size does not increase after longer heating times (Figure 6-15f).

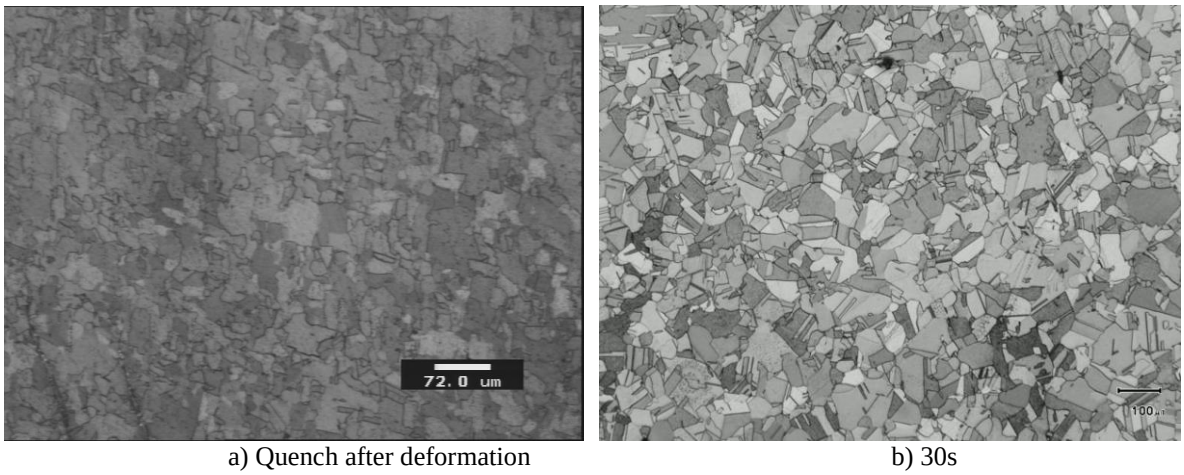

a) Quench after deformation b) 30s

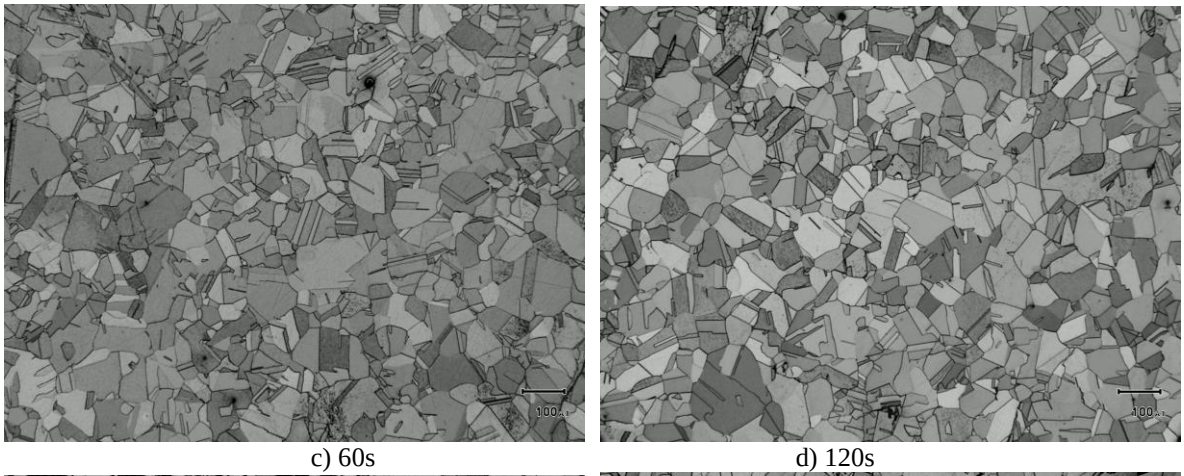

c) 60s d) 120s

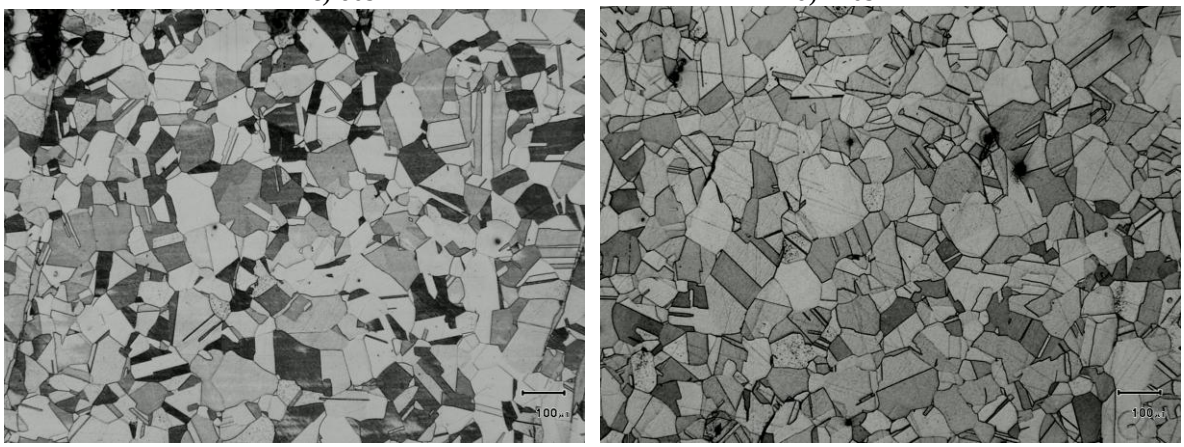

e) 600s f) 1320s

Figure 6-15 Optical micrographs of samples deformed to a strain of 2.0 at 1100 ℃ and a strain rate of $0.01s^{-1}$, followed by holding at this temperature for a) 0s, b) 30s, c) 60s, d) 120s, e) 600s, f) 1320s

It is obvious from the above analysis, that if the strain is smaller than the critical strain for DRX, SRX will take place during the subsequent annealing time, which has a quite different behavior as compared to PDRX. An incubation time is needed to initiate nucleation, the created nuclei are small in number and their growth toward the old grains is associated with twinning. The nucleation process seems to stop after a certain annealing time. Most importantly, the final recrystallized grain size is much larger than that obtained through PDRX. More details of SRX will be discussed in later sections.

When the strain increased to a value beyond ε_{cr}^{DRX} , even when the steady-state microstructure has not been reached yet, PDRX is less dependent on the value of applied strain. PDRX takes place very quickly, with no or limited incubation time, the fully recrystallized microstructure (at $t_{100\%}$) exhibits a much coarser grain size than that of DRX, but it is clearly smaller than that of SRX. Twinning is also active during the PDRX process, more details on this will be addressed in the next section.

The effect of deformation temperature, strain rate and applied strain on the evolution of the grain size, and the recrystallized fraction, will be further discussed in section 6.5.3.

6.3. Static recrystallization

6.3.1. Experiment

As mentioned in section 6.2.4, SRX seems to have a quite different behavior from PDRX. In order to quantify the SRX kinetics as well as grain size evolutions, experiments at different conditions have been performed, the schematic diagram of the process is shown in Figure 6-16. The samples were first preheated to the desired temperature followed by 3 min dwell time to get an homogeneous temperature throughout the gauge length of the sample, they were then deformed to a small strain ($\varepsilon < \varepsilon_{cr}^{DRX}$) with given strain rates. After the deformation, the samples were maintained at the same temperature on the torsion test machine for a certain time. For each deformation condition, around 5 different holding times ranging from 0 to 600s were chosen in order to get enough data points to follow the microstructure evolution.

As the deformation before the unloading time is rather small, the evolution of SRX is expected to be relatively slow. Quantitative measurement of the progress of the recrystallized fraction is feasible by metallographic examination of the quenched microstructure. Even though this procedure is tedious and time consuming, the non-recrystallized grains and recrystallized grains are easy to identify thanks to the big difference in size. An incomplete softening is often observed even at prolonged post-deformation annealing times [110,111,113] especially at conditions after a small deformation. The concept of fractional softening is thus not used in this section.

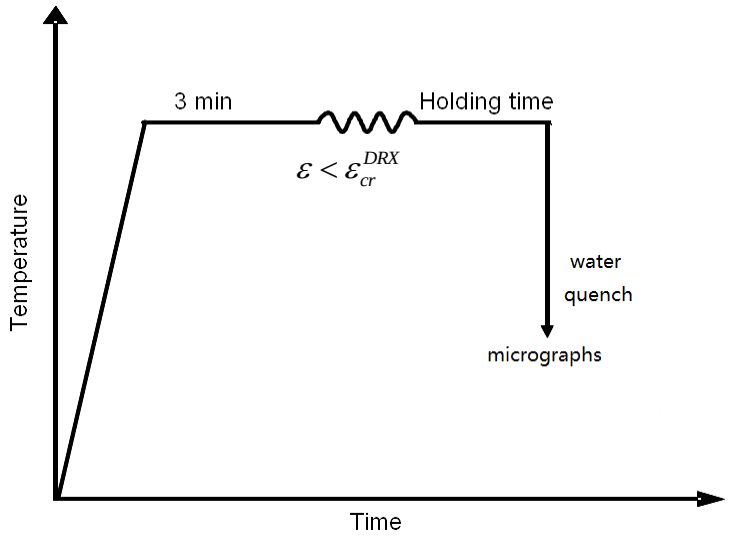

Figure 6-16 Schematic diagram of SRX experiment

A few tests (see Table 6-2) were conducted to validate the SRX model, these include conditions conducted at two deformation temperatures (1000 ℃ and 1100 ℃), two strain rates (0.01s-1 and 0.1 s-1), as well as two different applied strains (0.3 and 0.5). The conditions are chosen according to the experimental observation conducted in section 5, such that no DRX grains are present after the interruption of the deformation. The temperature after deformation was kept the same.

Table 6-2 The conditions analyzed for SRX described in this chapter

Affecting factors	Conditions
Deformation temperature	$T=1000°C$ ， $\dot{\varepsilon}=0.1s^{-1},\varepsilon=0.3$ $T=1100°C$ ， $\dot{\varepsilon}=0.1s^{-1},\varepsilon=0.3$
Strain rate	$T=1000°C$ ， $\dot{\varepsilon}=0.01s^{-1},\varepsilon=0.3$ $T=1000°C$ ， $\dot{\varepsilon}=0.1s^{-1},\varepsilon=0.3$
Applied strain	$T=1000°C$ ， $\dot{\varepsilon}=0.01s^{-1},\varepsilon=0.3$ $T=1000°C,\quad \dot{\varepsilon}=0.01s^{-1},\varepsilon=0.5$

6.3.2. Effect of temperature and strain rate

When the deformation is interrupted at $\varepsilon=0.3$ and 1000 ℃ with a strain rate of $0.01s^{-1}$, DRX has not started yet, serration is observed on some of the grain boundaries, while other ones are kept smooth (Figure 6-17a). With a short heating time of 20s, most of the pre-existing grain boundaries are serrated, but nucleation is still absent (Figure 6-17b). This process continues with a longer heating time of 60s (Figure 6-17c), indicating a large incubation time in these conditions. Small grains are finally found in Figure 6-17d, mostly at grain boundaries or near the triple junctions. When increasing the heating time to 300s, a large part of the microstructure is replaced by the small grains (Figure 6-17e), also notice that most of them have twinned. A fully recrystallized structure is achieved at 600s (Figure 6-17f), grain growth has already taken place.

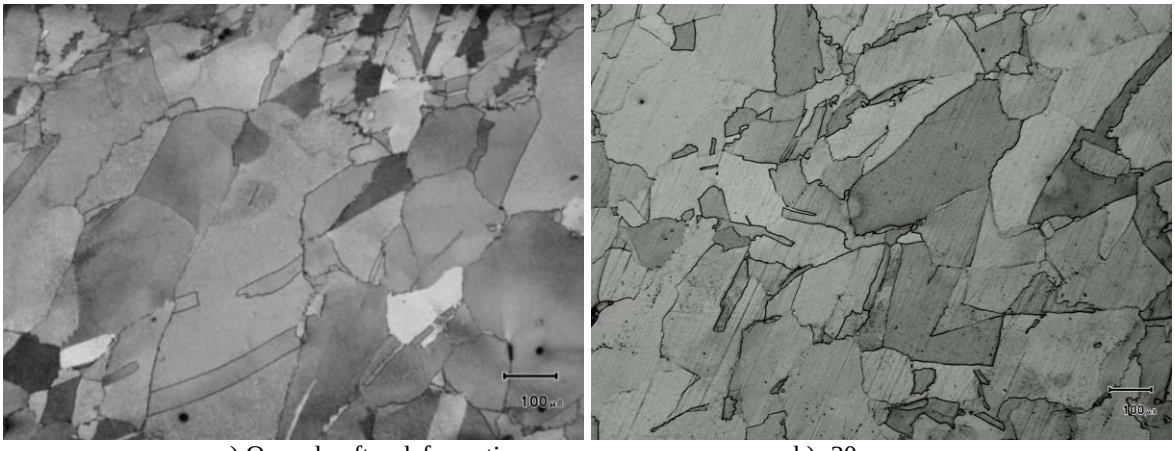

a) Quench after deformation b) 20s

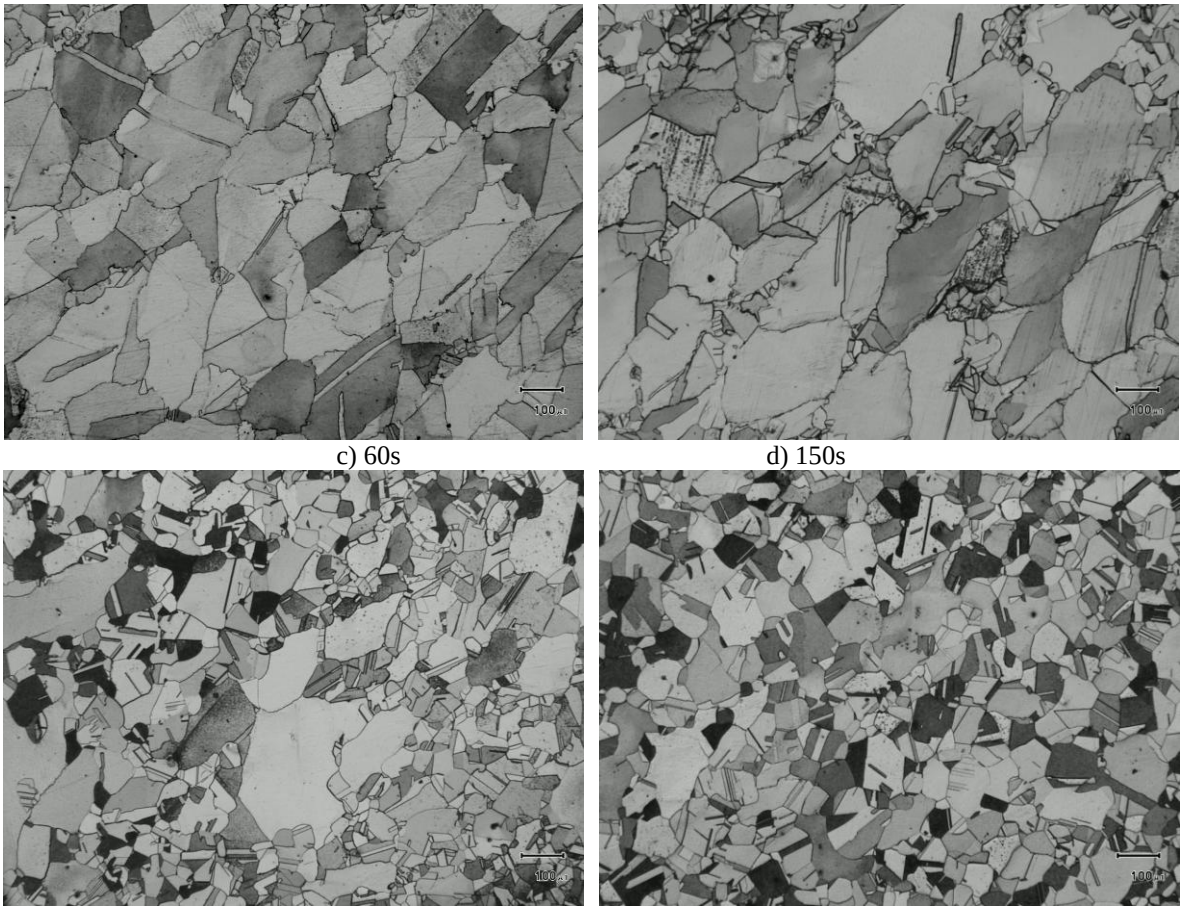

c) 60s d) 150s

e) 300s f) 600s

Figure 6-17 Optical micrographs of samples deformed to a strain of 0.3 at 1000 ℃ and a strain rate of $0.01s^{-1}$, followed by holding at the same temperature for a) 0s, b) 35s, c) 60s, d) 150s, e) 300s, f) 600s

As the strain rate increases ($\dot{\varepsilon} = 0.1s^{-1}$), the time available for dynamic recovery decreases, favoring SRX after deformation. Clearly, nucleation of small grains occurs (Figure 6-18a) after a shorter annealing time of 20s (see Figure 6-19). The small grains keep appearing on the grain boundaries during further annealing time (from Figure 6-18b to Figure 6-18d), again, most of them contain twins. The intragranular nucleation is not often observed. It seems the nucleation process is quite slow, since the number of small grains is not very much increased. The reduction of nucleation is probably due to continuous decreasing of dislocation density caused by recovery when increasing annealing time. The recrystallization finishes at about 300s (Figure 6-18e), and the recrystallized grains continue to grow with longer heating time (Figure 6-18f).

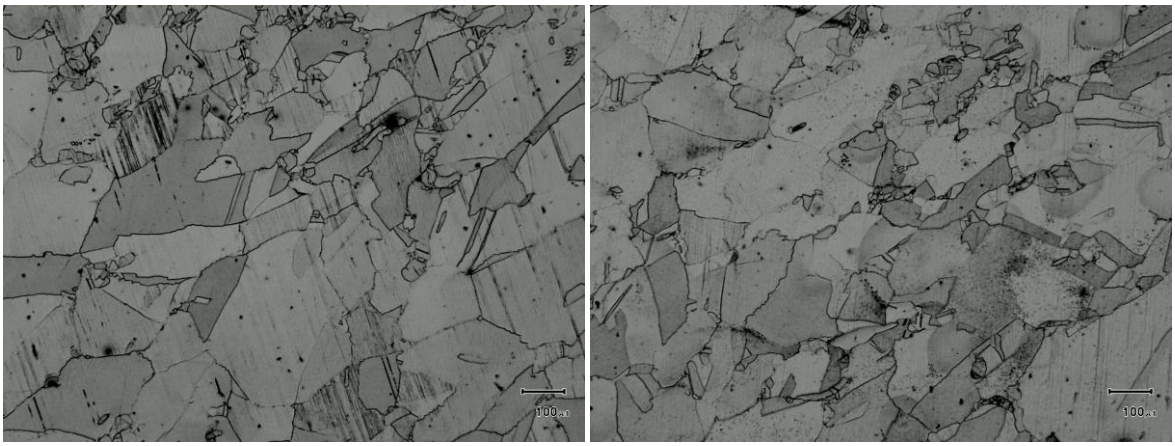

a) 20s b) 35s

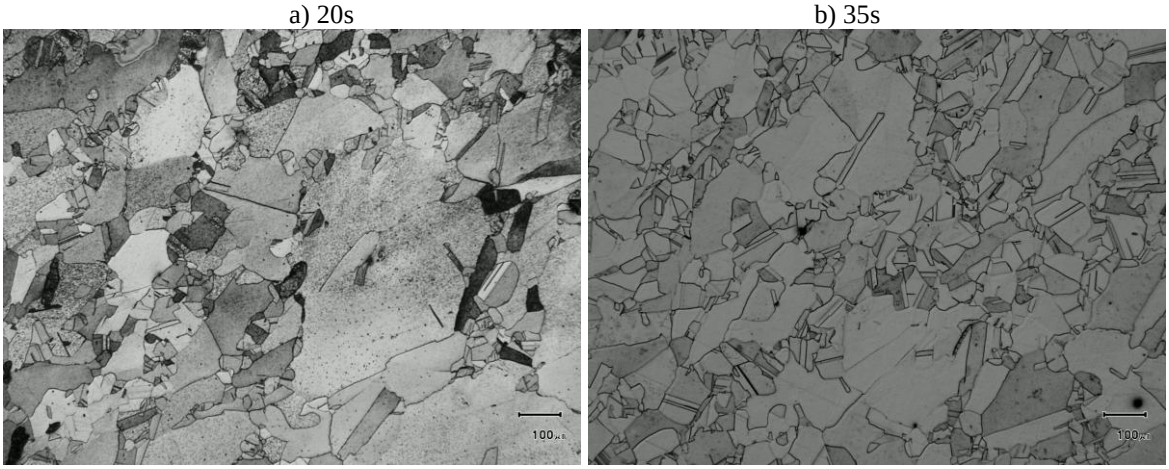

c) 60s d) 150s

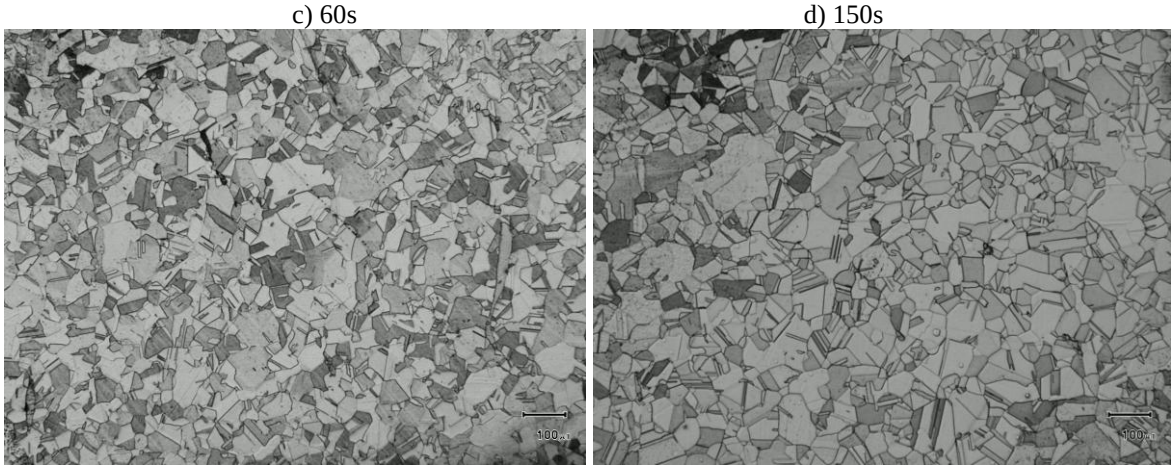

e) 300s f) 600s

Figure 6-18 Optical micrographs of samples deformed to a strain of 0.3 at 1000 ℃ and a strain rate of $0.1s^{-1}$, followed by holding at this temperature for a) 20s, b) 35s, c) 60s, d) 150s, e) 300s, f) 600s

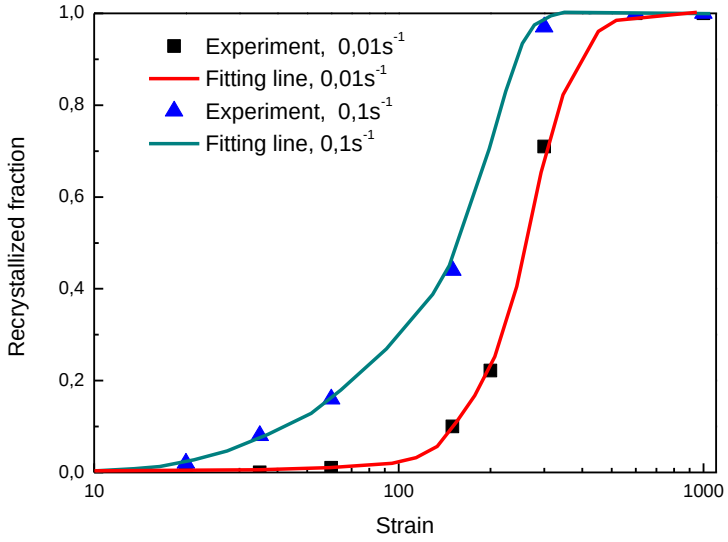

Figure 6-19 Effect of strain rate on the kinetics of SRX in 304L deformed to $\varepsilon = 0.3$ at 1000 ℃

Keeping the same deformation and strain rate ($\varepsilon = 0.3, \dot{\varepsilon} = 0.1/s$), when the deformation temperature is increased to 1100 ℃, SRX is found to be much faster than at 1000 ℃ (see Figure 6-21). After a short heating time of 20s, a relatively high fraction of small grains have appeared (Figure 6-20b), most of them containing annealing twins. As compared to the previous case (Figure 6-18a), the increase of temperature seems to have promoted nucleation, since most of the original grain boundaries are replaced by small grains (Figure 6-20b). The formation of small grains seems to be much less pronounced as heating time increases, and pre-existing old grains (examples are pointed out by black arrows in Figure 6-20) are consumed by the growing grains, exhibiting a concave shape. A nearly completely recrystallization structure is obtained after 60s' holding time, even though the microstructure is still quite heterogeneous with both small and big grains (Figure 6-20d). In Figure 6-20e, which corresponds to a heating time of 150s, equiaxed and more homogenous microstructure is obtained. These grains subsequently grow, and finally lead to a large grains microstructure, as shown in Figure 6-20f.

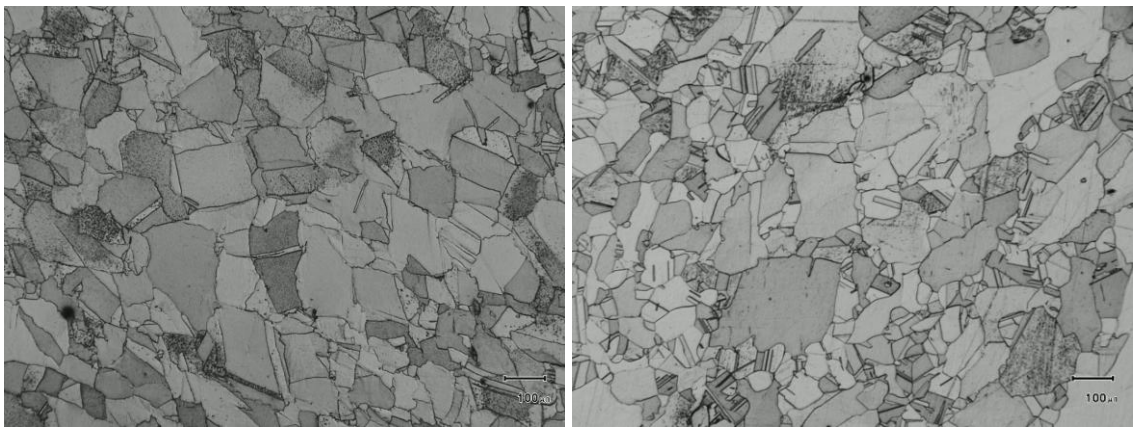

a) Quench after deformation b) 20s

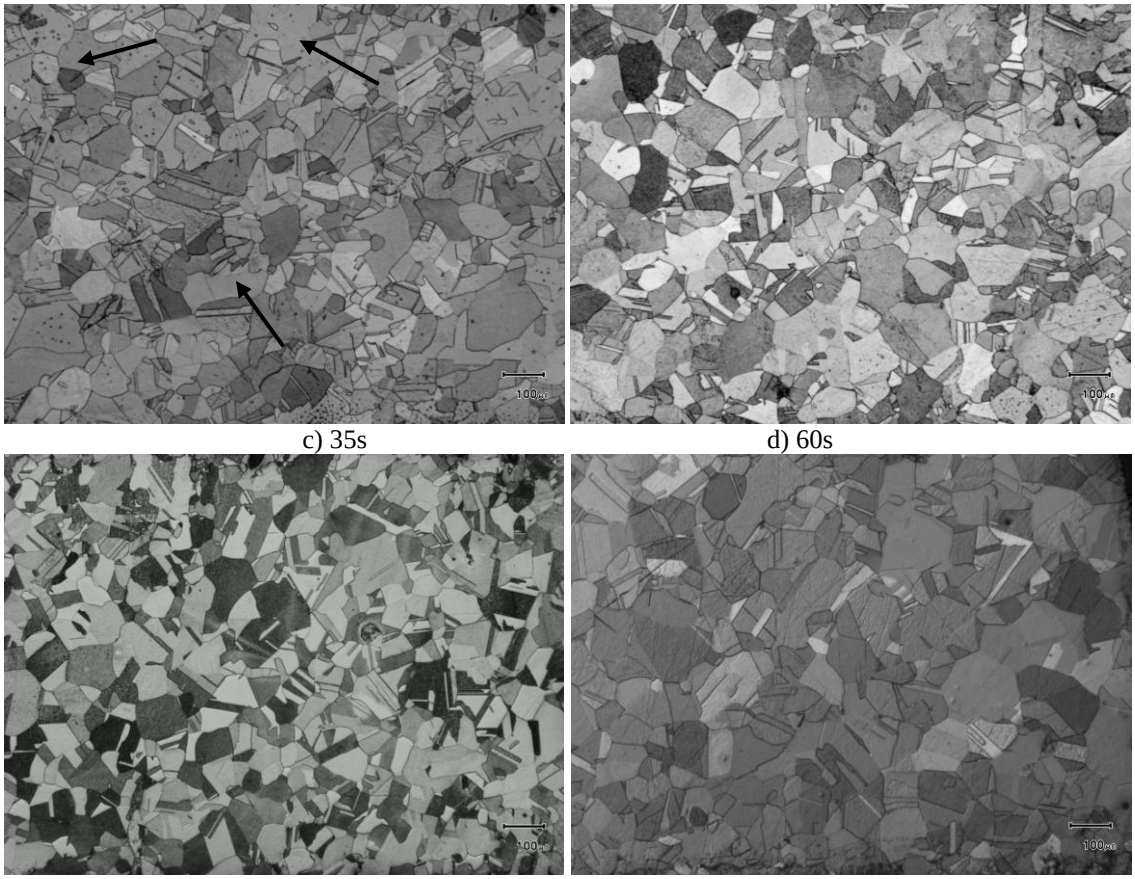

c) 35s d) 60s

e) 150s f) 600s

Figure 6-20 Optical microscope micrographs of samples deformed to a strain of 0.3 at 1100 ℃ and a strain rate of $0.1s^{-1}$, followed by holding at this temperature for a) 0s, b) 20s, c) 35s, d) 60s, e) 150s, f) 600s

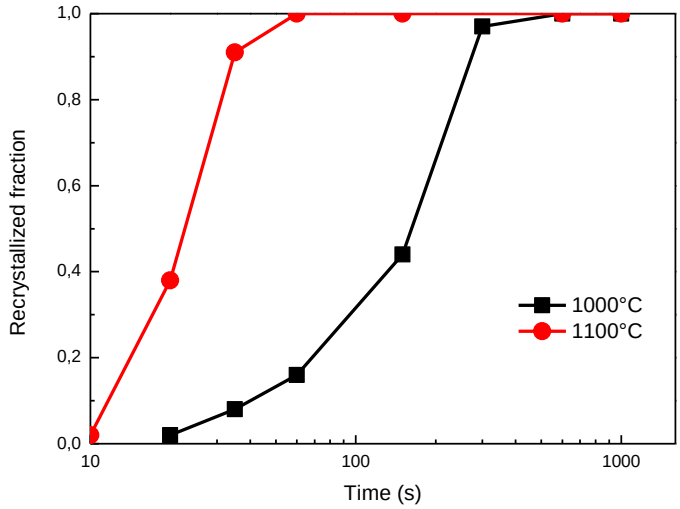

Figure 6-21 Effect of temperature on the kinetics of SRX in 304L deformed at 1000 ℃ to $\varepsilon = 0.3$ with strain rate of $\dot{\varepsilon} = 0.1s^{-1}$

6.3.3. Effect of applied strain

Besides the processing conditions, the amount of applied deformation also plays a role on SRX. By introducing more stored energy, larger strain can decrease the incubation time needed for SRX and at the same time accelerate recrystallization kinetics, the evidence is shown in Figure 6-22 considering T=1000°C and $\dot{\varepsilon} = 0.01s^{-1}$. When the deformation is interrupted at a larger deformation of 0.5 (as compared to 0.3 in Figure 6-17), it is very clear that small recrystallized grains appear on pre-existing grain boundaries (Figure 6-22b) after a shorter heating time of 30s (see Figure 6-23), with a size comparable to the wave length of the serrations, suggesting that bulging or SIBM is the mechanism of nucleation in this condition. An increased number of small grains (Figure 6-22c) are present when the heating time is increased to 60s. On the other hand, these earlier formed RX grains also started to grow. It is worth noticing that nucleation is not yet initiated after the same heating time when the sample is interrupted at a smaller strain (Figure 6-17c). These RX grains then keep growing, and gradually consume all of the original NR grains (Figure 6-17d and Figure 6-17e), grain growth then takes place with longer heating times (Figure 6-17f).

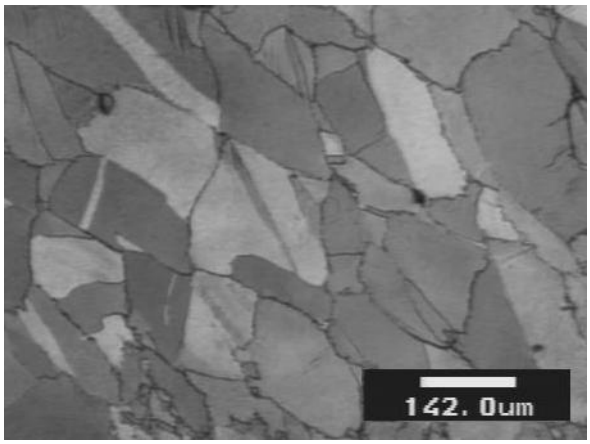

a) Quench after deformation

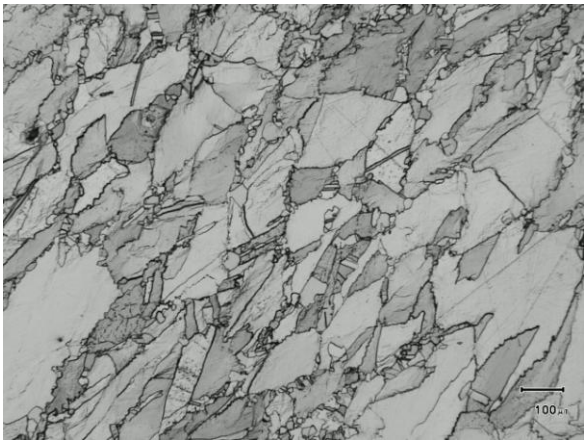

b) 30s

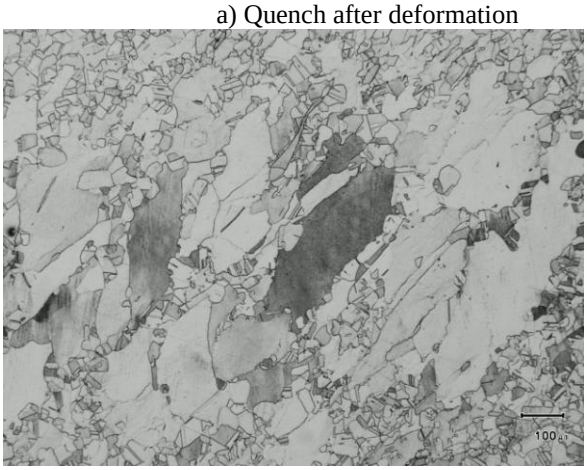

c) 60s

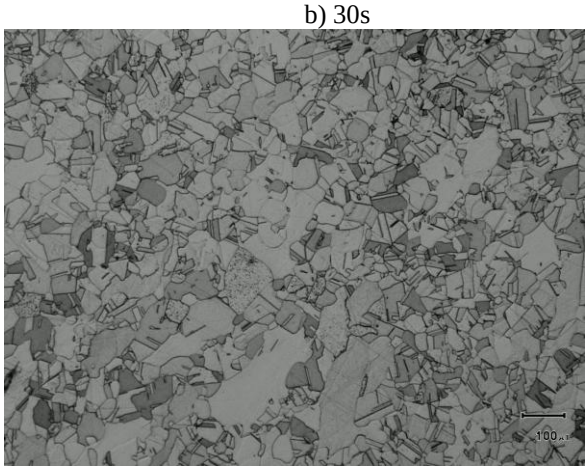

d) 120s

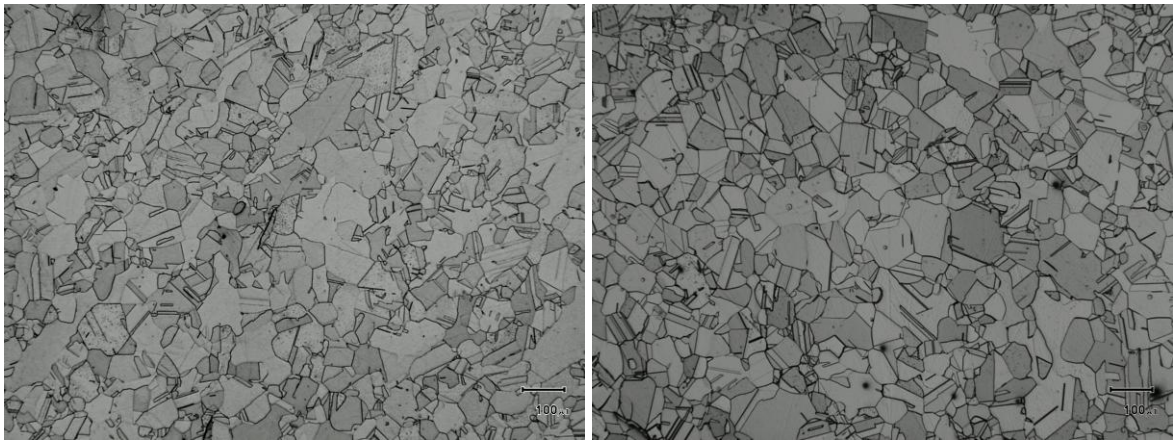

e) 180s f) 600s

Figure 6-22 Optical micrographs of samples deformed to a strain of 0.5 at 1000 ℃ and a strain rate of $0.01s^{-1}$, followed by holding at the same temperature for a) 0s, b) 30s, c) 60s, d) 120s, e) 600s, f) 1800s

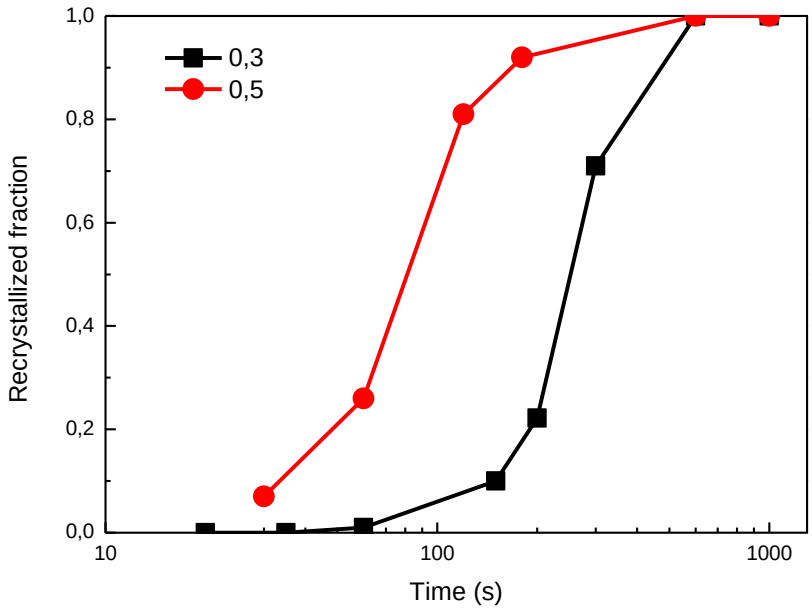

Figure 6-23 Effect of applied strain on the kinetics of SRX in 304L deformed at 1000 ℃ to $\varepsilon = 0.3$ and $\varepsilon = 0.5$ with a strain rate of $\dot{\varepsilon} = 0.1s^{-1}$

From the above investigation, it is clear that an incubation time is needed to initiate SRX, but high temperature, large strain rate and large applied strain tend to decrease incubation time, and thus accelerate SRX kinetics. The results will be discussed in more details in section 6.5.4 when comparing with numerical results.

6.4. Investigation of SRX/PDRX mechanisms by quasi in situ heating experiments

6.4.1. Experiment

Parallel to the traditional post-morten examinations, where a few samples deformed in the same conditions are examined with different annealing times, a few quasi in situ heating

experiments were also conducted to follow the microstructural evolution on a chosen area. A better understanding of the mechanisms of SRX, PDRX, as well as grain growth is thus possible by the complementary information obtained, which provides direct clues for numerical modelling. The full description of the quasi in situ test equipment and samples has been provided in Section 3.5.3.

Although observations of recrystallization are normally made on surface sections, it should be noted that the free surface itself could have an effect on the recrystallization process, since there is a tendency to form a groove at grain boundaries to satisfy the conditions for surface tension equilibrium [200]. The transitional time during heating and cooling steps might also play a role, even though it is known that recovery for 304L is slow. Kinetic data from surface observations of in situ heating experiments are compared with these obtained from bulk measurements, and are found to be close. So, the evolution of microstructure and the underlying mechanisms are assumed to be relevant and they are discussed here.

Quasi in situ experiments are conducted by heating the prepared thin samples for a short time in each of the heating steps. The procedures of thermal treatment sequences are schematically illustrated in Figure 3-9. The gradual evolutions of the microstructure of SRX, PDRX and grain growth are consequently obtained, analyses are conducted below on the mechanisms of these three processes.

6.4.2. Static recrystallization

The sample has been previously deformed at 1000 ℃ and $0.01s^{-1}$ to a very small strain ($\varepsilon = 0.3$), followed by water quench. The deformation is well below the critical strain, since no DRX was found even when it was deformed to a larger strain of 0.5, see Figure 5-4b. The results showing the full evolution under SRX is presented in Figure 6-24 and Figure 6-25.

After 150s' heating time, a few new grains appear on the pre-existing grain boundaries, mostly on the triple junctions and near the grains with high GOS value (more stored energy), as shown in Figure 6-24b and Figure 6-25b. All these new grains form annealing twins, and they have a typical GOS value of less than 1 °. Experimental evidence has been presented by Jones [201], which shows that annealing twins are formed at grain boundaries during the early stages of annealing in three different cold rolled, low stacking fault energy materials, including an AISI 310 stainless steel. It has been suggested that the formation of small twin segments at grain boundaries may occur sufficiently early to affect nucleation of recrystallization. It has been argued that such twinning events may stimulate nucleation of recrystallization.These earlier created new grains starte to grow at the expense of old grains with high GOS value after another heating step of 50s (Figure 6-24c). This growing process continues (Figure 6-24d and e), but there are almost no new grains created, suggesting that classic nucleation has stopped after a certain annealing time. A twin is usually found on the growing front of the RX grains, either parallel or perpendicular to the moving boundary. By forming a twin or a twin chain (indicated by the arrows), it seems the growth has been accelerated as compared to other RX grains (Figure 6-24d and e). However, this acceleration may stop later, when we follow the same grain as shown in Figure 6-24f. Example of nearly stagnant grain boundary (in principle free to grow (unimpinged)), marked by an arrow, is shown in Figure 6-24g, migration is resumed by forming a twin on the growing front as shown in Figure 6-24h and i. Filed *et al*. [202] observed the same phenomenon during annealing of pure copper at 155 ℃. From the GOS maps, it is also interesting to see that some of the deformed grains (Figure 6-25f) decrease their GOS value, either due to static recovery or because the most highly deformed parts of the grain have disappeared. However, it is almost sure that the left old grains with GOS value

higher than 1 °will finally disappear with longer heating time, meaning that an old grain (even if it is only slightly deformed) is usually consumed by other growing RX grains before they can decrease the dislocation density by static recovery to a very small value, as suggested by Hodgson *et al*. for austenitic Ni－30Fe alloy [117,118].

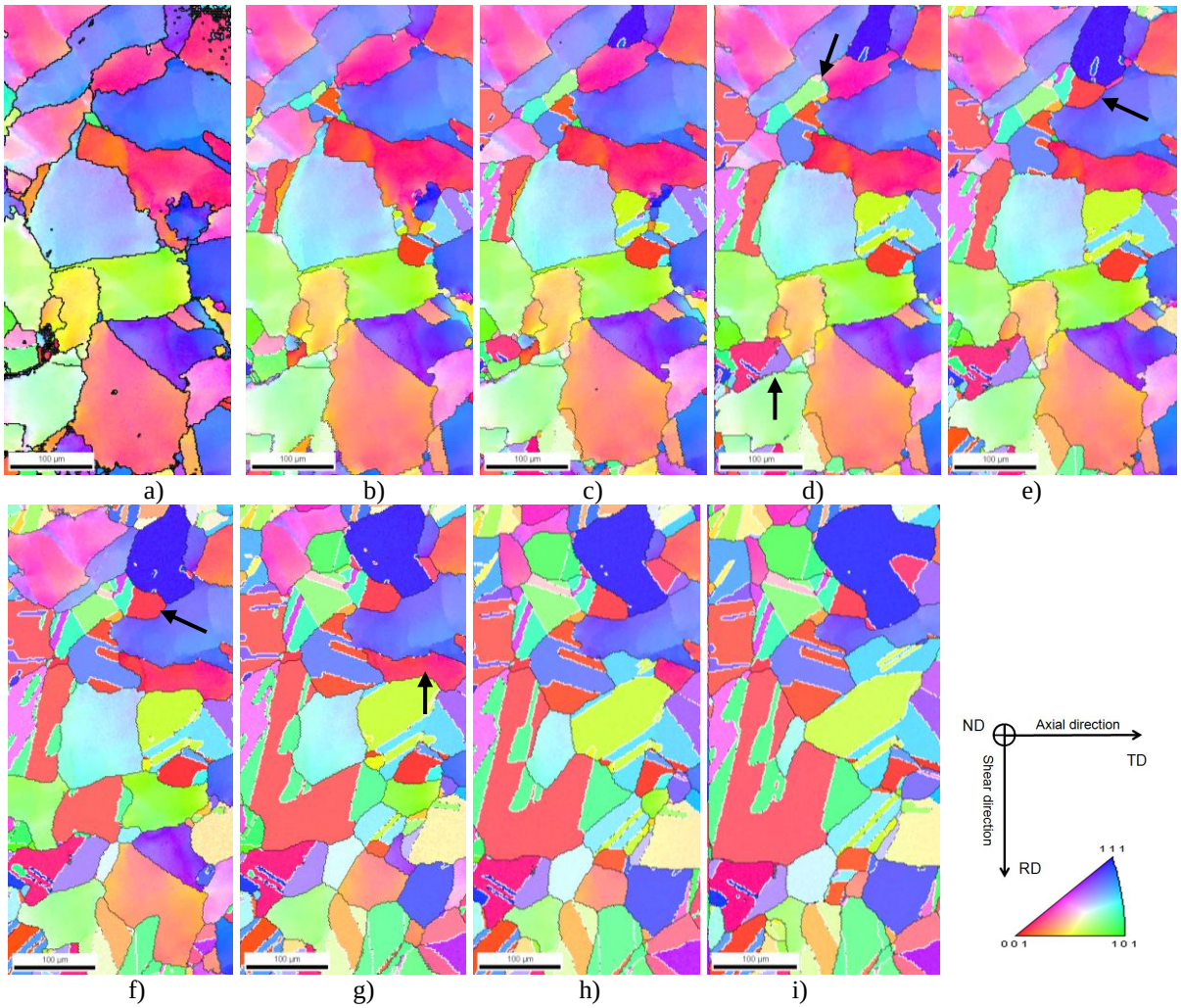

Figure 6-24 Inverse Pole Figure maps showing the gradual evolution of SRX process of the sample deformed to 0.3 at 1000 ℃ and 0.01s^{-1} , white lines represent twin boundary a) After deformation, b) 150s, c) 50s, d) 50s (arrows point to the formation of annealing twins on the growing front), e) 50s (arrow points to the fast growing annealing twin), f) 100s (the arrow points to the grain containing a twin slowing down its migration), g)100s (arrow indicts an almost stagnant boundary), h) 120s, i) 150s, all of them are times for each individual heating step

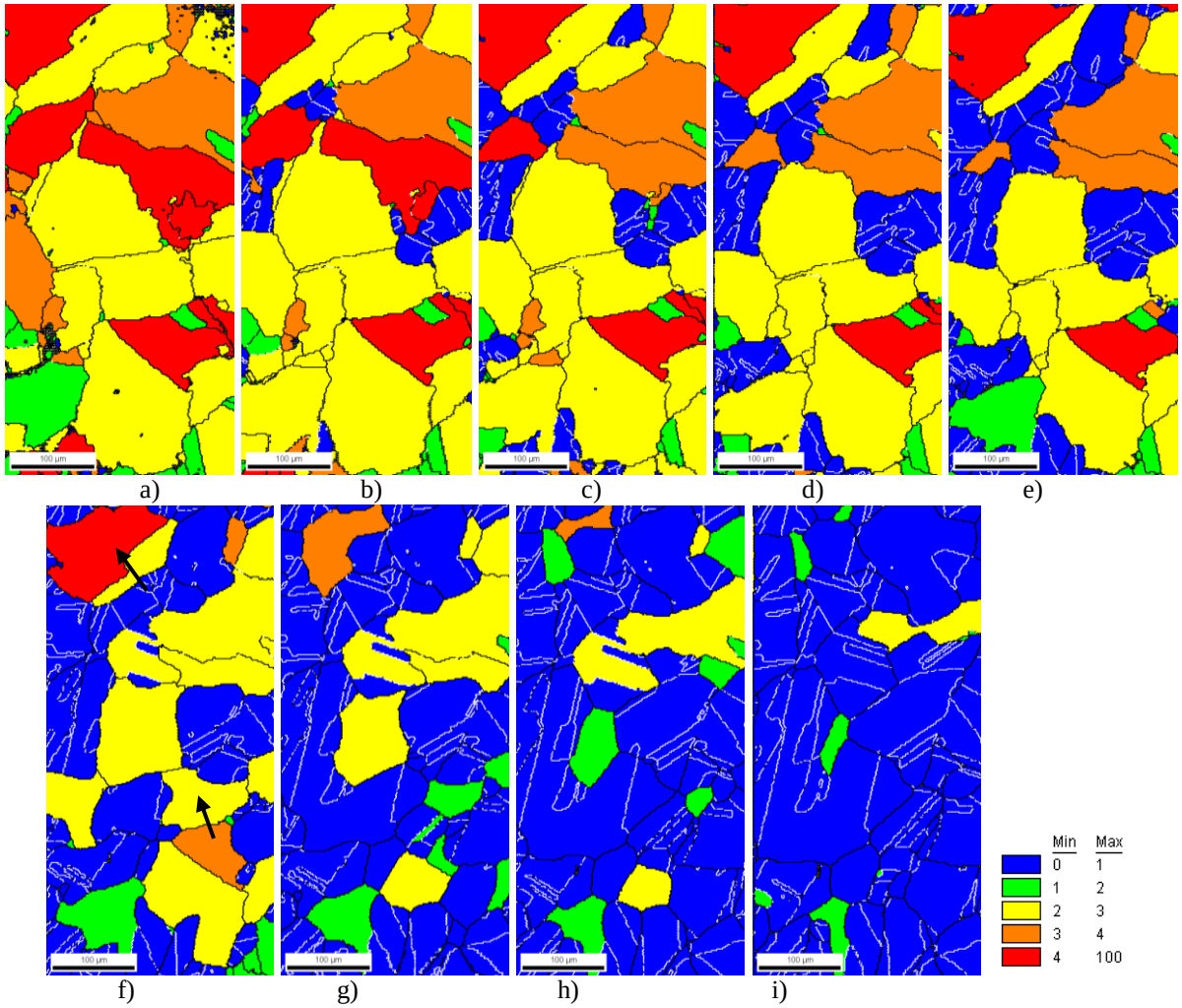

Figure 6-25 Grain orientation spread maps showing the gradual evolution of SRX process of the sample deformed to 0.3 at 1000 ℃ and $0.01s^{-1}$, white lines represent twin boundary, a) After deformation, b) 150s, c) 50s, d) 50s, e) 100s, f) 100s (Arrows point to the grains which decrease their GOS subsequently), g)100s, h) 120s, i) 150s, all of them are times for each individual heating step

6.4.3. Post dynamic recrystallization

When the sample was deformed at 1000 ℃ and $0.01s^{-1}$ to a large strain ($\varepsilon = 1.5$), which is well above the critical strain for DRX, PDRX will take place if the sample is subsequently kept at high temperature. The microstructural evolution during this process is captured by quasi in situ heating experiments and is presented in Figure 6-26.

After a short heating time of 20s, there is not only annealing twins formed at nucleation (indicated by circles), by also twins formed on the deformed DRX grains (pointed out by arrows), which is shown in Figure 6-26b. That is to say, the DRX grains help creating annealing twins and promote acceleration of the recrystallization kinetics, which is not seen in SRX. Growing processes associated with twinning continue at another heating step of 20s, as illustrated in Figure 6-26c. In Figure 6-26d, the new grains grow rapidly and consume the most part of the NR grains. A further heating step of 15s leads to an almost fully recrystallized structure (Figure 6-26e), the accumulated time is 70s which is comparable with the data from bulk measurement as shown in Figure 6-3.

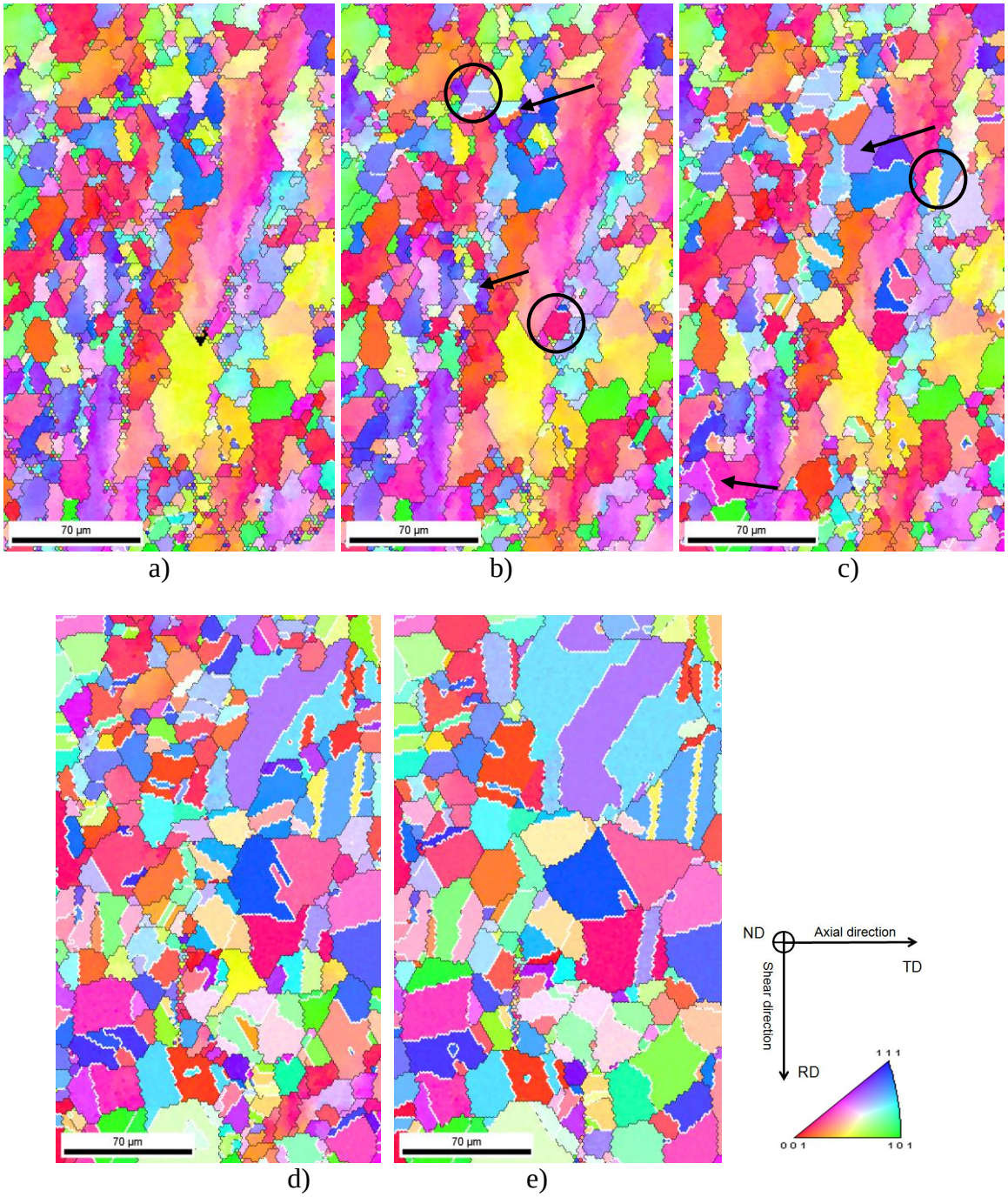

Figure 6-26 Inverse Pole Figure maps showing the gradual evolution of PDRX process of the sample deformed to 1.5 at 1000 ℃ and 0.01s^{-1}, white lines represent twin boundary, a) After deformation, b) 20s, c) 20s, d) 15s, e) 15s, all of them are times for each individual heating step and the white lines represent twin boundaries

Another sample was deformed in the same condition (ε=1.5 at 1000 ℃) but with a higher strain rate ($\dot{\varepsilon}$=0.1s^{-1}). For this experiment it is noted that the control of temperature was not as reliable as in the other experiments. The real temperature was most likely slightly above the pre-set temperature, since the observed PDRX kinetics is faster than that observed by bulk measurement is (in Figure 6-8). A larger amount of new grains is created as compared with Figure 6-26, most probably due to the increase in stored energy (see Figure 6-27a to Figure 6-27d), but the temperature may play a role as well.

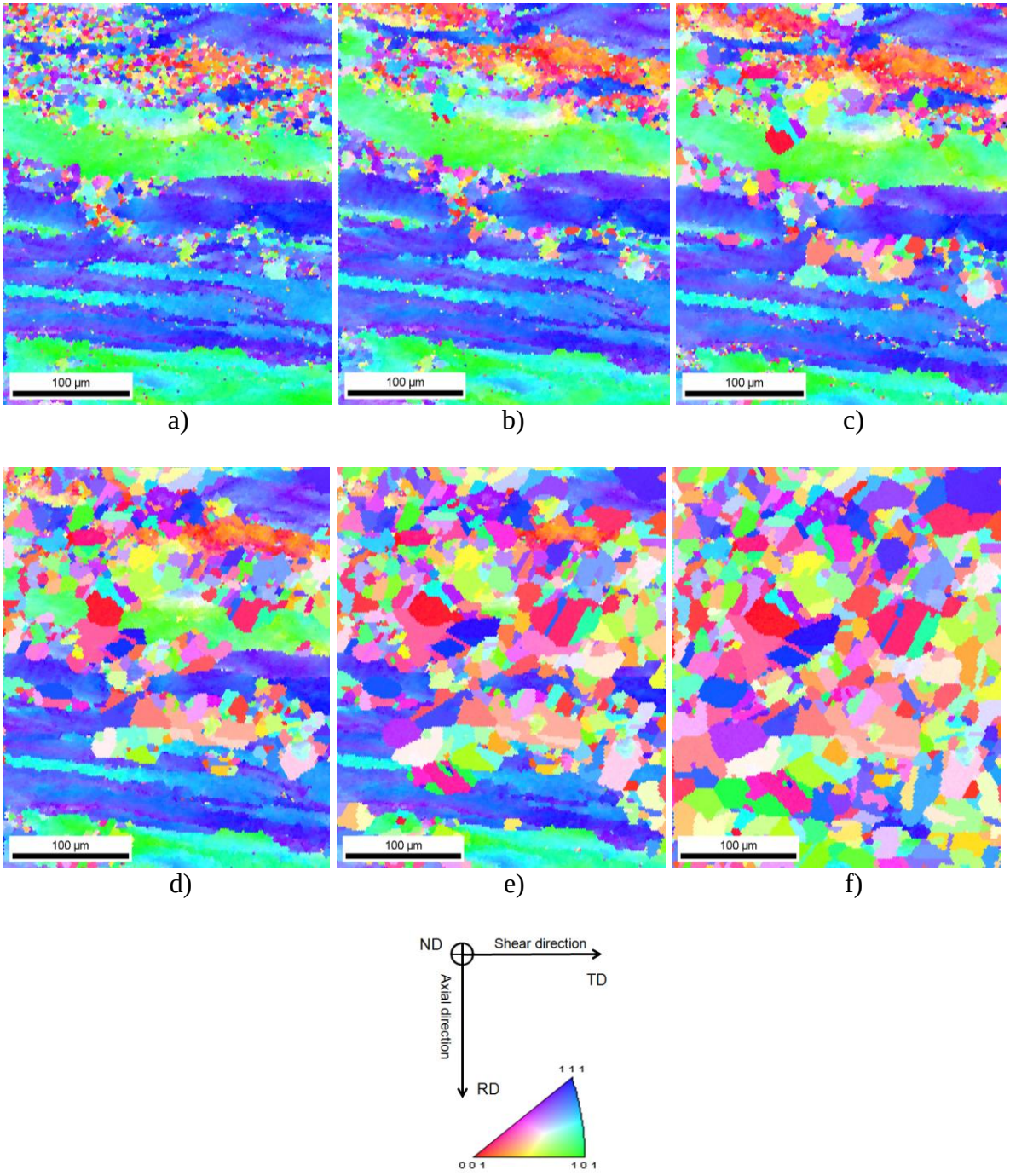

Figure 6-27 Inverse Pole Figure maps showing the gradual evolution of PDRX process of the sample deformed to 1.5 at 1000 ℃ and $0.1s^{-1}$ a) After deformation, b) 2s, c) 3s, d) 5s, e) 5s, all of them are times for each individual heating step.

6.4.4. Grain growth

After the examination of SRX and PDRX phenomena, the samples reach a nearly recrystallized state, and the subsequent grain growth is also investigated. The analyzed sample was deformed at 1000 ℃ and $\dot{\varepsilon} = 0.01s^{-1}$ to a strain of 0.5, and after the fully recrystallized microstructure is reached, another heating step of 180s is applied. A relatively big area was scanned and the results are shown below in Figure 6-28.

As expected the grains with small sizes tend to shrink or even disappear, as indicated by the numbers, while the big grains grow and tend to reach a stable configuration. Twinning is not so active, limited examples are shown by the arrows, which is consistent with the slow evolution of the structure.

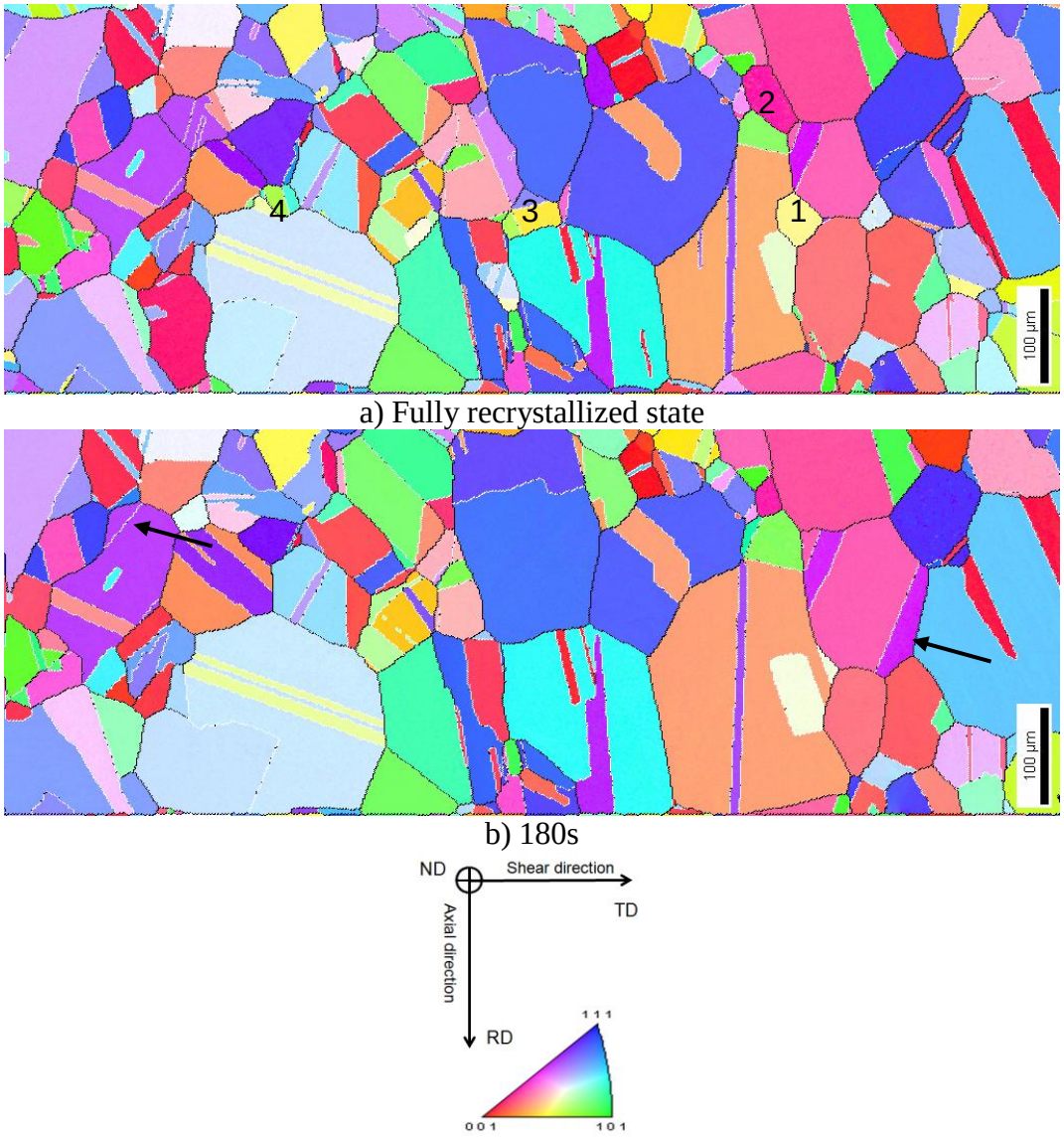

a) Fully recrystallized state

b) 180s

Figure 6-28 Inverse Pole Figure maps showing the microstructure evolution during grain growth of the sample deformed to 0.5 at 1000 ℃ and 0.01s^{-1}, white lines represent twin boundary, a) Fully recrystallized state, b) After a heating time of 180s

6.5. Application of the post deformation model to 304L steel

6.5.1. Annealing twins during DRX and SRX/PDRX

From the previous sections, it appears that annealing twins in 304L steel are more or less active depending on the regime (DRX, SRX, PDRX). As shown in Figure 3-7, the initial microstructure contains a large fraction of twin boundaries. During DRX, special boundaries boundaries lose their particularity due to crystallographic rotation of grains and serration of

boundaries. Therefore, the frequency of twin boundaries decreases by the progress of the deformation. However, as illustrated in 2.3.5, the formation of the first layer of the new DRX grains is subsequently followed by formation of new annealing twins, either formed during the growth of recrystallized grains on the recrystallization front or through formation of new grains at triple junctions. Therefore, at strains higher than the peak strain, where large numbers of new DRX grains have been formed, the frequency of annealing twins increases with strain. The concurrent deformation, on the other hand, tends to decrease the twin fraction. The evolution of twin fraction during DRX at high temperature was obtained quantitatively by Dehghan-Manshadi[96] and Gavard [158], as shown in Figure 6-29. A balanced twin fraction (about half of the initial value) can be found with deformation progress, more details can be found in the thesis works [96, 158].

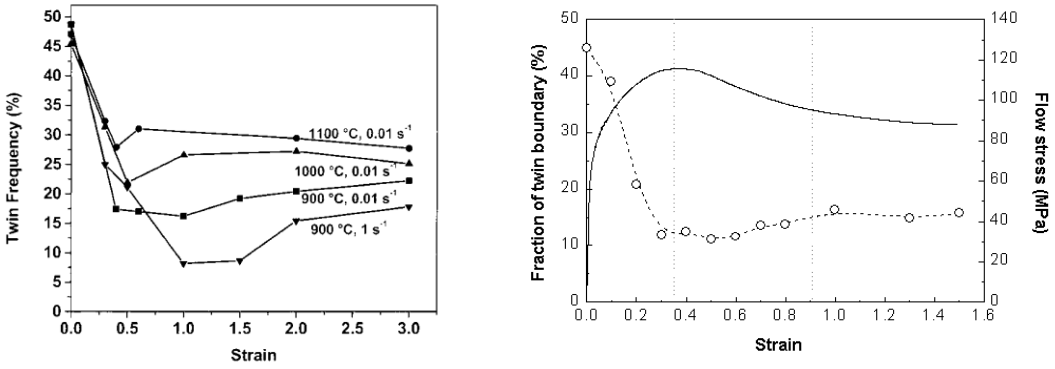

Figure 6-29 a) The frequency of twin boundaries as a function of strain, 304 stainless steel deformed at high temperature [96] b) The evolution of the twin boundary fraction during deformation of high purity 304 steel deformed by compression at 850 ℃ and 10^{-3} s^{-1} [158] (Both "twin frequency" and "fraction of twin boundary" are used to designate the ratio between the length of twin boundaries and the total length of high angle grain boundaries)

As compared to DRX, a dramatic increase in twin boundary frequency with increasing time was observed for both SRX and PDRX at all conditions as presented in section 6.2 to 6.4. The twins can either promote nucleation or affect the mobility of migrating boundaries. The increase of twin frequency continues until fully recrystallized structure is obtained, and tends to keep at constant during grain growth with both creation and disappear of twins.

The evolution of twin frequency during both DRX and PDRX at 900 ℃ is measured by Dehghan-Manshadi [96] using 304 stainless steel and it is presented in Figure 6-30. The twin frequency increases at the beginning of the post deformation process while the increase during hot deformation is negligible. It gradually increases to the same leave as the initial state (~50%) as shown in Figure 6-30 and Figure 6-29a.

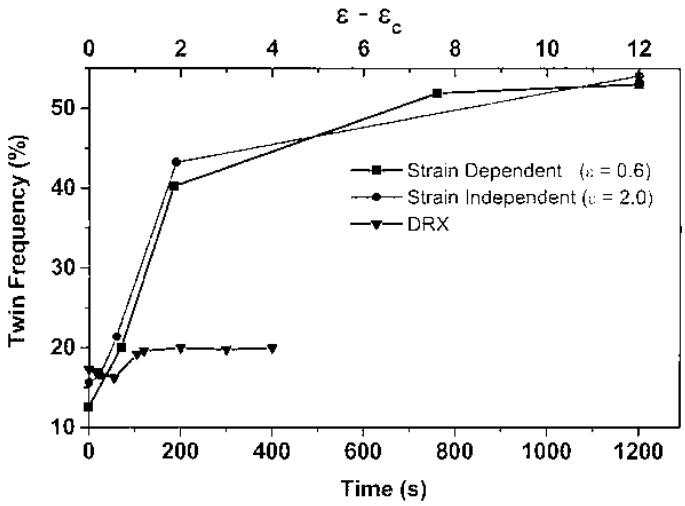

Figure 6-30 A comparison between twinning frequency in dynamic condition (at 900 ℃ and $0.01s^{-1}$) and in post deformation conditions (interrupted strain of 0.6 and 2.0 respectively) of 304 steel (at 900 ℃) [96] (P.S. The first point on the DRX curve must be wrong, as can be seen from Figure 6-29a)

The annealing twins, which affect the nucleation and growth of grain during SRX and PDRX shown in the previous sections, should be taken into account appropriately when modeling the recrystallization after deformation. Twinning can indeed create mobile high-angle grain boundaries. Frequently, even twin chains are observed [203]. In the model, this can (i) lead to apparent changes in the effective mobility, and (ii) influence the nucleation law.

6.5.2. Identification of fitting parameters for SRX/PDRX/GG model

6.5.2.1. From experimental results and literature data

Some of the model parameters are identical for both SRX and PDRX, they are first analyzed here. The static recovery constant K_s in (Equation 4-33), is one of these parameters. The steady state dislocation density of recovery ρ_{ss}^{SRV} (the minimal dislocation density static recovery can reach for deformed grains) is chosen as 5.0^{12} m^{-2}, higher than the dislocation density for fully recrystallized structure (~10^{11} m^{-2}), but lower than the typical critical dislocation density for SRX (~10^{14} m^{-2}). The constant relating critical dislocation density for SRX and DRX, ξ, in (Equation 4-35) is set to be 0.3 and parameter ω in (Equation 4-36) is 1.5. The drag and pinning effects due to alloying may control grain growth in commercial stainless steel and limit grain boundary migration capacity. This effect tends to disappear when temperature is increased [156]. The pinning effect term in (Equation 4-40) is thus set to be dependent on temperature, and the estimated value before optimization is calculated by considering a typical particle size and volume fraction.

For SRX, where no dynamically formed nuclei are present before the interruption of deformation as examined by micrographs, all grains are first deformed and recovered according to (Equation 4-1). The incubation time for SRX is approximately estimated as the time needed to observe the first nuclei in micrographs. Simulation of the SRX process is run use the SRX/PDRX/GG model presented in section 4.4.

As for PDRX, the calculation in dynamic condition is run by DRX model, after which all grains are re-defined according to (Equation 4-37), the constant β is set to be small (0.01) to define only the most recently recrystallized grains as RX grains. Incubation time is neglected

and set to 0 for PDRX, since the incubation time decreases with the applied strain. The PDRX process is then simulated using the SRX/PDRX/GG model.

There are two major parameters in the SRX/PDRX model which are $K_3 = m\tau$ related to the mobility, and the nucleation constant K_g in (Equation 4-8) respectively, which may evolve according to the type of driving force. It is easy to estimate K_3 in grain growth regime where the growth is solely driven by the surface energy, as in the case of DRX where the main driving force component is related to dislocation density. No indication can be found on K_g since it is a unique parameter in the present work and the estimated value before optimization is again taken to be the same as for DRX.

6.5.2.2. Inverse analysis

The two important parameters K_3 and K_g, together with the static recovery (K_s) and pinning effect (K_p) term were tuned using inverse analysis manually. K_3 is found to increase with temperature, applied strain rate, as well as applied strain, which is in accordance with the work done by Gavard [158]. The pinning effect was found to decrease with temperature as shown by El Wahabi *et al*. [156] for stainless steel, and almost regardless of strain rate and applied strain.

6.5.3. Post dynamic recrystallization

6.5.3.1. Calibration of the PDRX/GG model

Although a great deal is now known about the structure of grain boundaries, and models for grain boundary migration based on boundary structure have been formulated, there is as yet little evidence of quantitative agreement between the models and the experimental results [1].

In the present study, even though it is known that a perfect match between the experimental and numerical results is almost impossible due to many simplifications in the mean field model, much effort has been invested to get quantitatively reasonable agreement. Experimentally, it is found that nucleation still exists during PDRX, the assumption that PDRX is just the growth of existing RX grains is thus not adopted.

From some examinations by EBSD, it is observed that most of the dynamically formed RX grains are eventually consumed by the subsequent growth of the statically created nuclei due to their non negligible stored energy. These grains actually act the same as NR grains, a carful re-defining of all grains is conducted in the PDRX/GG model, which transfer some of the DRX grains into NR grains. Another important aspect is that the annealing twins, which are not very active during DRX, are found to play an important role during nucleation and growth of the RX grains. The value of K_3 is therefore allowed to increase during annealing as compared to the DRX case.

Two test runs have been conducted to show the reaction of the model based on the above improvements. They are which is given in Figure 6-31 where the modified PDRX model is the one proposed above. It will be shown later that this model gives relatively good agreement with experimental results. As illustrated in Figure 6-31a, the original un-improved model significantly underestimates the grain size. Without re-defining RX and NR grains, the recrystallized fraction starts from that obtained from DDRX as shown in Figure 6-31b, the consequence of this is that the mobile surface fraction of the RX grains (γ^{RX}) is very small ~0.1 (see Figure 6-32a) at the beginning of the PDRX process since $\gamma^{RX} = 1 - X^{2/3}$. The small

value of γ^{RX} is physically not true at the early stage of PDRX, both nucleation and growth of existing grains are observed near the deformed DRX grains. The evolution of both γ^{RX} and γ^{NR} calculated based on the improved model is shown in Figure 6-32b. Since the constant β in (Equation 4-37) is set to be very small (0.01), only the most recently recrystallized grains are re-defined as RX grains which results in an initially very small fraction of recrystallized grains.

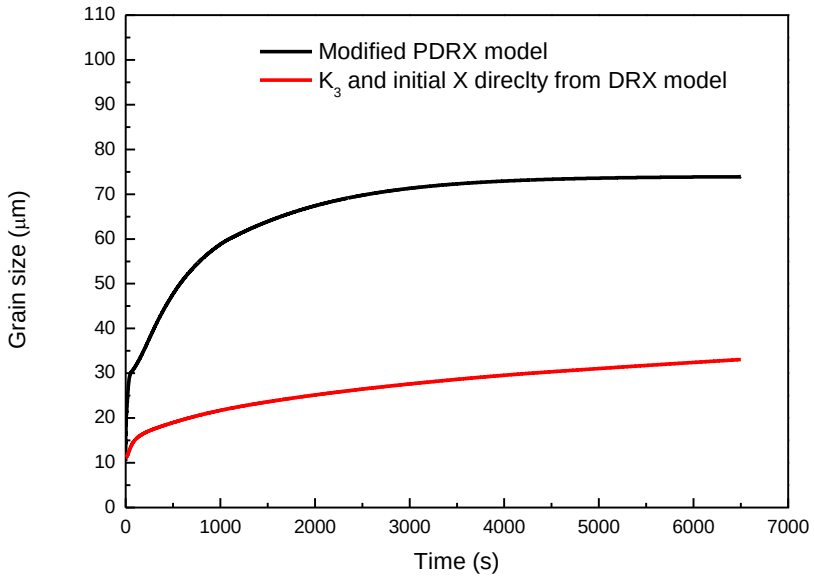

a)

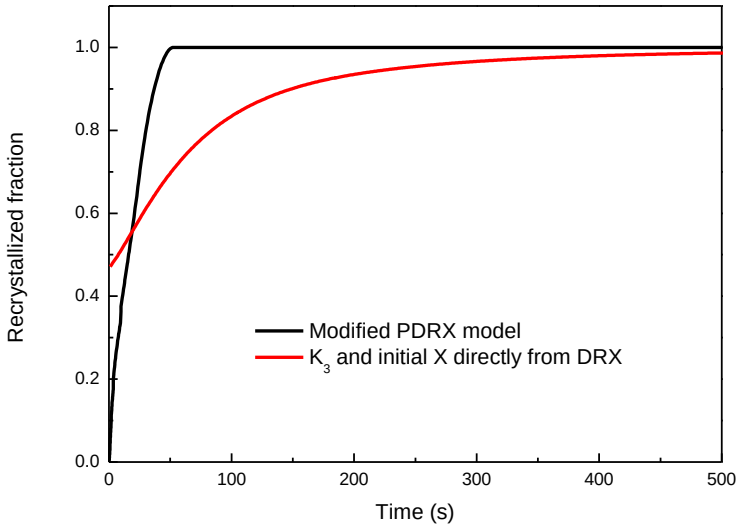

b)

Figure 6-31 Comparison between the PDRX model before improvements and the improved model (after deformation at 1000 ℃ and $\dot{\varepsilon} = 0.01s^{-1}$ to a deformation of 1.5) a) Recrystallized grain size b) Recrystallized fraction

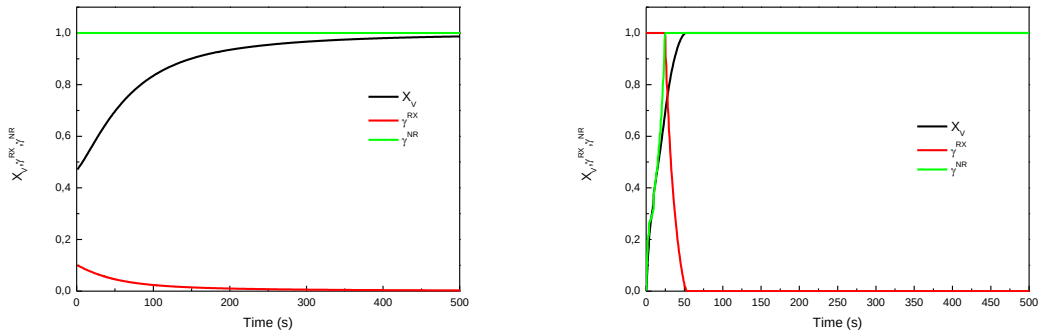

a) b)

Figure 6-32 Evolution of γ^{RX} and γ^{NR} surface factions, and of the recrystallized fraction X as a function of time with the two PDRX models (after deformation at 1000 ℃ and $\dot{\varepsilon} = 0.01s^{-1}$ to a deformation of 1.5). a) The model before improvements b) The improved PDRX model

It is known that during grain growth, where the driving force becomes small as compared to primary recrystallization , the growth usually ceases at a limiting value [1]. Grey and Higgins [129] suggested that the physical origin of the limiting value might be solute clusters which are unable to diffuse with the boundary. This effect is accounted in our model by introducing a term which is similar to the Zener pinning term, it is tested below. Its influence during the recrystallization process (nucleation + growth of grains) should be small due to the large dislocation density driving force, which is shown in Figure 6-33a. However, the pinning effect becomes apparent during GG, it decreases the grain growth rate in general and the limiting grain size is reached much earlier, as illustrated in Figure 6-33b.

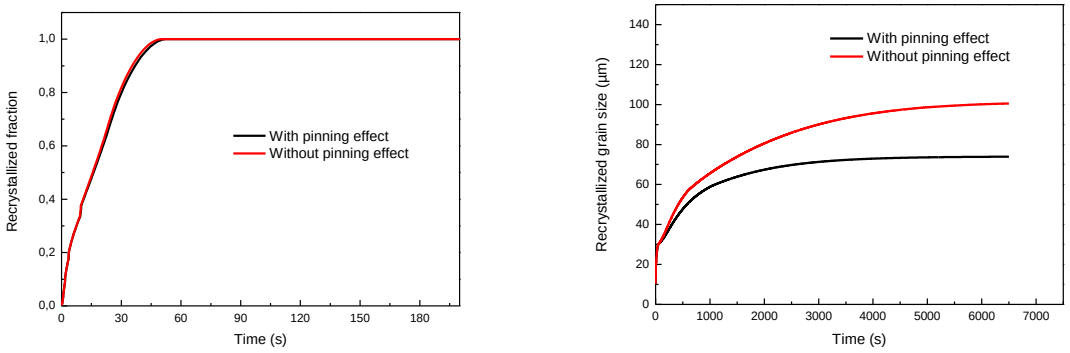

a) b)

Figure 6-33 Analysis of pinning effect in the PDRX model (after deformation at 1000 ℃ and $\dot{\varepsilon} = 0.01s^{-1}$ to a deformation of 1.5) a) Recrystallized grain size b) Recrystallized fraction

In PDRX regime, microstructural changes due to static recovery are assumed to be small [1]. This assumption is related to the fast kinetics of the PDRX process. In SRX conditions, where the kinetics is much slower, static recovery is no longer neglected (see section 6.5.4.1). Figure 6-34 confirms that with the adopted static recovery law, static recovery effect does not influence the PDRX model results.

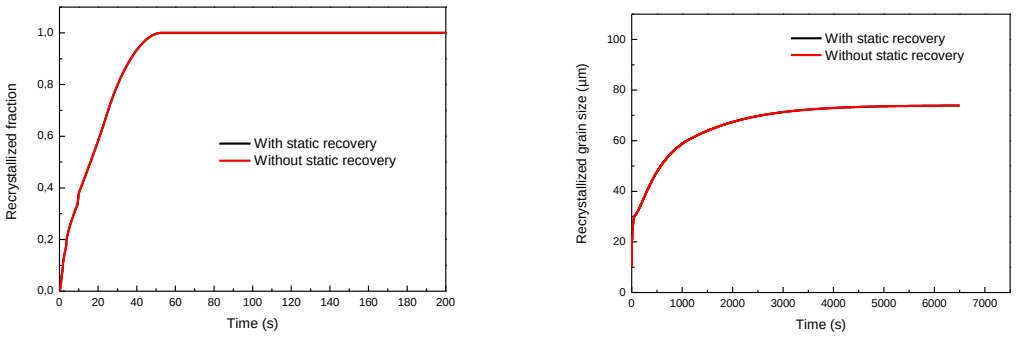

a) b)

Figure 6-34 Analysis of static recovery in the PDRX model (after deformation at 1000 ℃ and $\dot{\varepsilon} = 0.01s^{-1}$ to a deformation of 1.5) a) Recrystallized grain size b) Recrystallized fraction

A set of acceptable parameters values are found for the PDRX/GG model of 304L stainless steel, the trend of parameter values identified from comparison with experimental data (as detailed in the next sections) is presented in Figure 6-35. Parameters are expressed in a dimensionless form, relative changes due to value by both increasing strain rate and decreasing temperature is calculated according to the reference values obtained after deformation at 1000 ℃ and 0.01 s^{-1} to a strain of 1.5. K_3 increases with temperature, which is in accordance with the work done by Gavard [158], who developed an analytical model to identify grain boundary mobility (m) for low SFE materials, m was found to increase with temperature for recrystallization after deformation. K_g evolves similarly as K_3 , i.e. increasing with temperature, however, its dependence on temperature is less pronounced. The pinning effect parameter K_p decreases with temperature [156]. All of these three parameters are independent of strain rate.

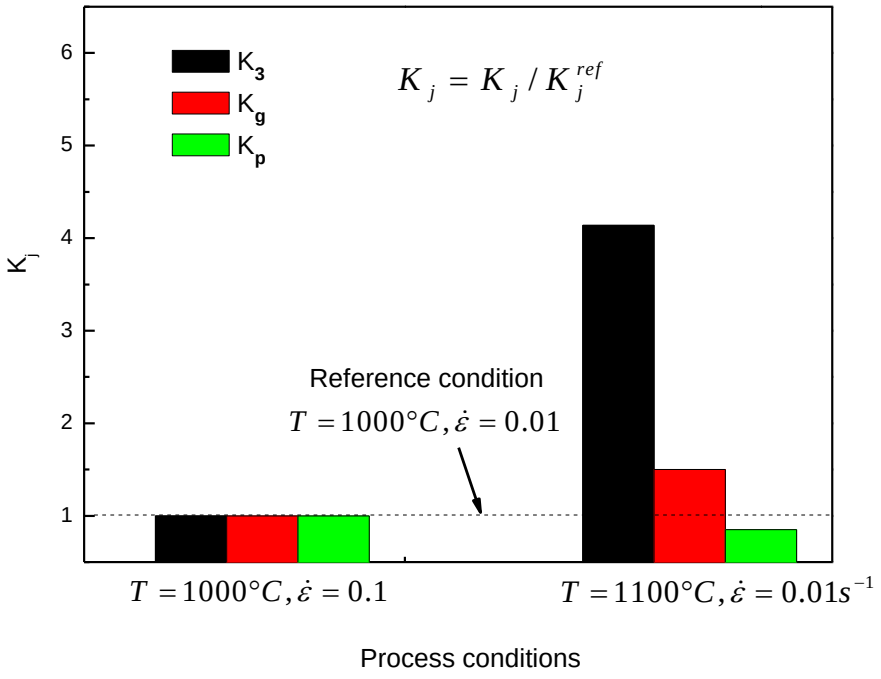

Figure 6-35 Relative evolution of K parameters for PDRX after a deformation of 1.5 as a function of temperature , with respect to the reference value (represented by the broken line) obtained after deformation at 1000 ℃ and $\dot{\varepsilon} = 0.01s^{-1}$

6.5.3.2. Effect of temperature

It has been clearly shown in Figure 6-3 and Figure 6-5 that high temperature promotes both faster recrystallization kinetics and increase in average grain size during PDRX. This is well captured by the PDRX/GG model as presented in Figure 6-36, a quantitative agreement is also obtained between the numerical and experimental results, even thought small discrepancies are found. At higher temperature, the grain size is underestimated (see Figure 6-36b) before a heating time of 1000s. This is probably caused by the fact that the grain boundary mobility during PDRX/GG process decreases with time because the magnitude of driving force decreases, while in the simulation an average value is used to get a general agreement with the experimental results for the whole process. The used grain boundary mobility seems to be underestimated in the early stage of the process, on the contrary, it is a little over estimated during the late stage of GG process, i.e. the real grain boundary mobility should decrease with annealing time instead of being constant throughout the whole process. It is also noted that the steady state grain size comes earlier when the temperature increases.

The reduction in the average boundary mobility may arise from at least two possibilities for the material analyzed. First, a mobility reduction could occur if the misorientation distribution function changed substantially, i.e., the environment of the migrating grain boundaries changes texturewise on average from a favorable to a less favorable one [204]. However, recent measurements of these misorientation relationships on partially recrystallized copper, aluminum and pure nickel by Juul Jensen and her co-workers [205,206] seem to suggest that the encountered misorientation distribution is not significantly affected by the annealing time.

Second, the role of annealing twins during recrystallization and early stages of the GG process seems to be different from that of late stages of the GG process. From our experimental investigation, it seems that annealing twins promote both nucleation and especially rate, which is also consistent with literature observation [201]. Inversely, high magnitudes of driving forces promote twinning [197]. This can explain the increased mobility at early states of PDRX. Similarly, when twinning does not operate, some grain boundaries become almost stagnant as illustrated in section 6.4.4, which results in a decrease of the average mobility.

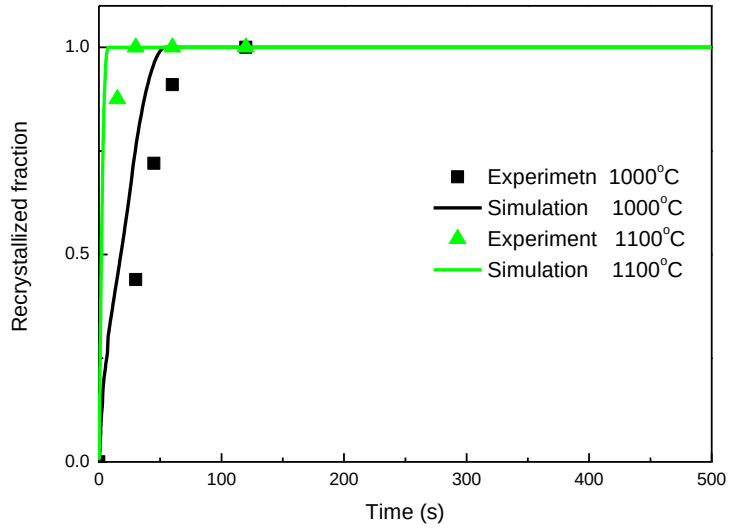

a)

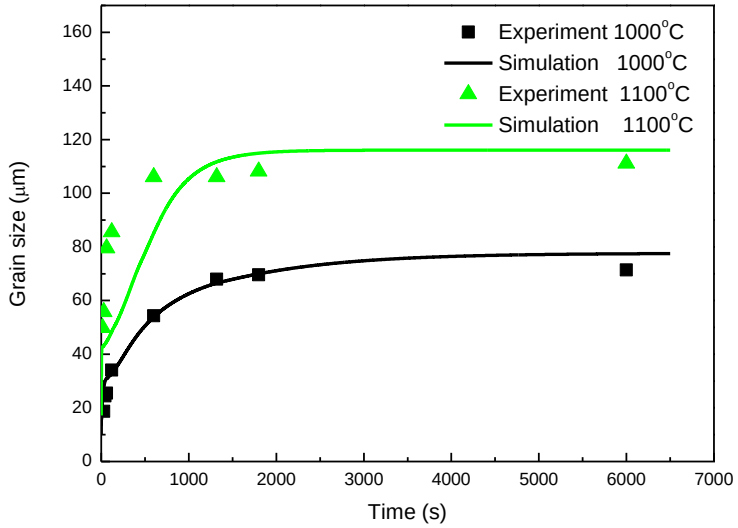

b)

Figure 6-36 Comparison between experimentally measured and numerically obtained for PDRX after deformation at $\dot{\varepsilon} = 0.01\text{s}^{-1}$ to $\varepsilon = 1.5$ a) Recrystallized fraction, and b) Recrystallized grain size of 304L steel. Results are shown for two different temperatures (1000 ℃ and 1100 ℃).

6.5.3.3. Effect of strain rate

The effect of strain rate on PDRX is introduced by the difference in stored energy. When the applied strain rate before annealing increases, more stored energy is created due to both shorter dynamic recovery time and increased work-hardening rate. The experimental data of PDRX after deformation at 1000 ℃ to $\varepsilon = 1.5$ with two strain rates, $\dot{\varepsilon} = 0.01s^{-1}$ and $\dot{\varepsilon} = 0.1s^{-1}$ is used here to validate the proposed model.

As illustrated in Figure 6-37a, the fact that larger strain rate promotes faster PDRX is reproduced qualitatively, but discrepancies exist. Even though very good agreements are obtained for DRX, it is still possible that some of the model parameters which are not sensitive in DRX but matter more in PDRX, and contributes to the overestimation of the recrystallized fraction. Using a mobility value which depends on driving force would probably help here again in improving the results.

Regarding the evolution of the recrystallized grain size during PDRX and GG process (Figure 6-37b), it is found that strain rate has a much smaller influence, as compared to temperature. At higher strain rate, the steady state in grain size is found earlier, a common steady state value is reached experimentally after longer annealing time, regardless of the applied strain rate. However, small discrepancy is observed for the numerical results, the assumption that pinning effect is strain rate independent might be too strong.

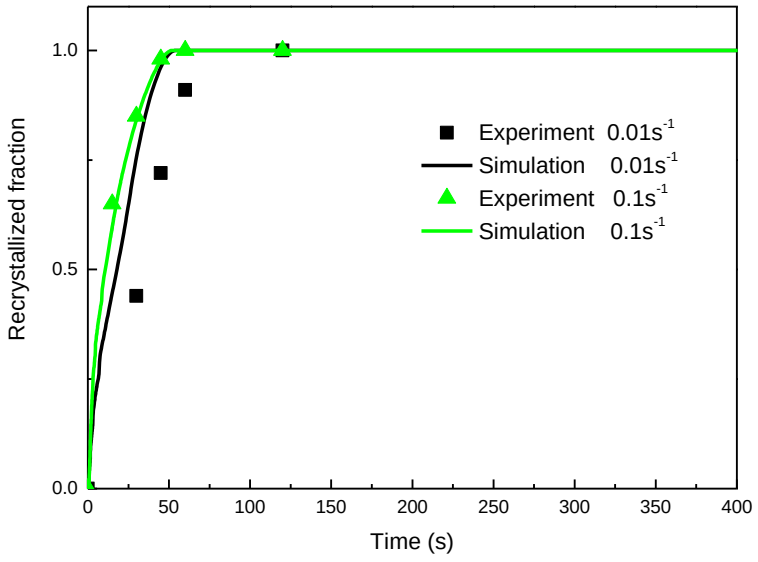

a)

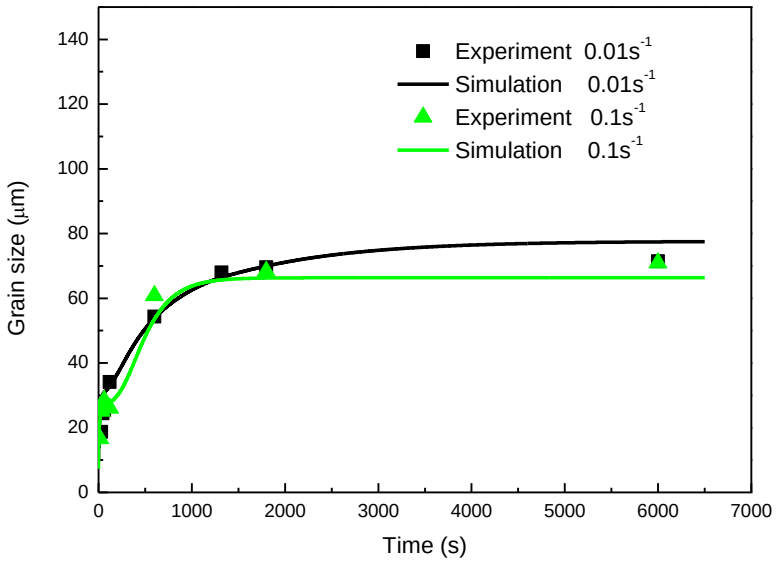

b)

Figure 6-37 Comparison between experimentally measured and numerically obtained results for PDRX after deformation at 1000 ℃ to $\varepsilon = 1.5$ a) Recrystallized fraction, and b) Recrystallized grain size of 304L steel. Results are shown for two different strain rates ($\dot{\varepsilon} = 0.01\text{s}^{-1}$ and $\dot{\varepsilon} = 0.1\text{s}^{-1}$).

6.5.3.4. Effect of applied strain

The effect of strain on PDRX after deformation at 1100 ℃ and $\dot{\varepsilon} = 0.01\text{s}^{-1}$ is analyzed for two different strains $\varepsilon = 1.5$ and $\varepsilon = 2.0$. The microstructural evolutions described by micrographs are presented in Figure 6-5 and Figure 6-15 respectively. In the current study, all the model parameters are kept the same for these two conditions. These interrupted strains correspond to the same level of flow stress, as shown in Figure 5-9.

The recrystallization process finishes in a very short time, the recrystallized fraction evolution was thus not measured experimentally, but it is predicted by the model, as shown in Figure 6-38a. It is found numerically that PDRX kinetics is faster after larger deformation. However, only a very small difference is observed when the interrupted strain increases from 1.5 to 2.0.

A similar evolution of recrystallized grain size is found at the early stage (<1000s), showing that the driving force for PDRX is similar for these two cases. When the steady state is reached, i.e. where the microstructure is stable due to a dynamic equilibrium between softening by dynamic nucleation and work-hardening, it is meaningful that the model predicts a unique grain size regardless of the applied strain.

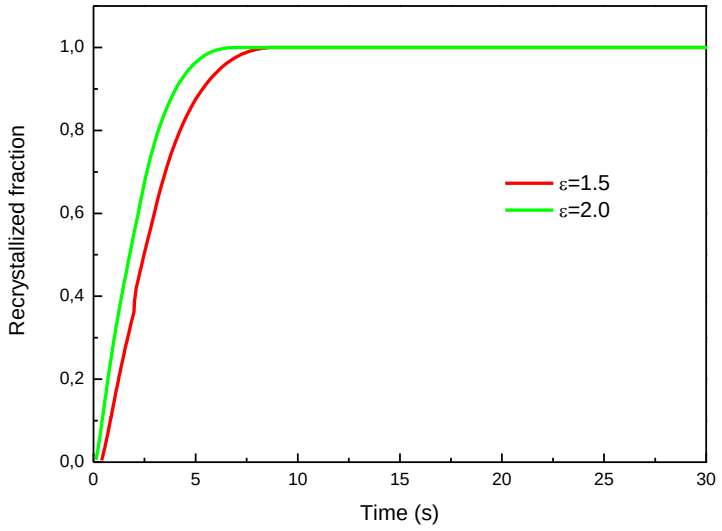

a)

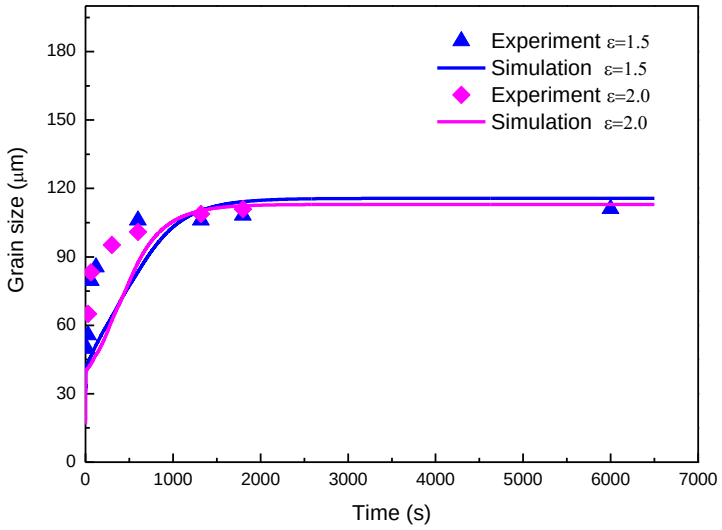

b)

Figure 6-38 Comparison between experimentally measured and numerically obtained results for PDRX after deformation at 1100 ℃ and $\dot{\varepsilon} = 0.01 s^{-1}$ a) Recrystallized fraction, and b) Recrystallized grain size of 304L steel. Results are shown for two different strains ($\varepsilon = 1.5$, $\varepsilon = 2.0$).

6.5.4. Static recrystallization

6.5.4.1. Calibration of the SRX model

Even though much similarity is found between SRX and PDRX models, there are at least three aspects which make the SRX model differ from the PDRX one. First, it is apparent both from literature review and the presented experimental data that an incubation time is needed to initiate SRX, this incubation time vary with the deformation conditions. Second, in the SRX

model, there is no need to re-define recrystallized volume fraction, since there are no DRX grains. The last aspect implies that the applied strain for SRX is usually very small, and in these conditions the match between experimental and numerical results is often not accurate (see the experimental and calculated flow stress in Figure 5-25a and Figure 5-26a). It is foreseeable that larger discrepancies might exist for the prediction of SRX.

Static recovery, which is time dependent and occurs both during SRX and PDRX, should be used with care especially for SRX, where the kinetics is much slower. Nucleation could be inhibited if static recovery is overestimated, with dislocation densities of the grains dropping to a value below ρ_{cr}^{SRX} . On the other hand, if no static recovery is considered, nucleation will be observed until the last NR grain disappears, which contradicts our experimental examination where it is found that nucleation mostly occurs after the incubation time and stops later. An example is given in Figure 6-39, where static recovery slightly changes both the kinetics and grain size of SRX. When static recovery is used, it is possible that the dislocation density of a few NR grains drops below ρ_{cr}^{SRX} , these grains are then consumed later by the growing RX grains. The consequences of these phenomena are is a gradual progress to the fully recrystallized structure as shown in Figure 6-39.

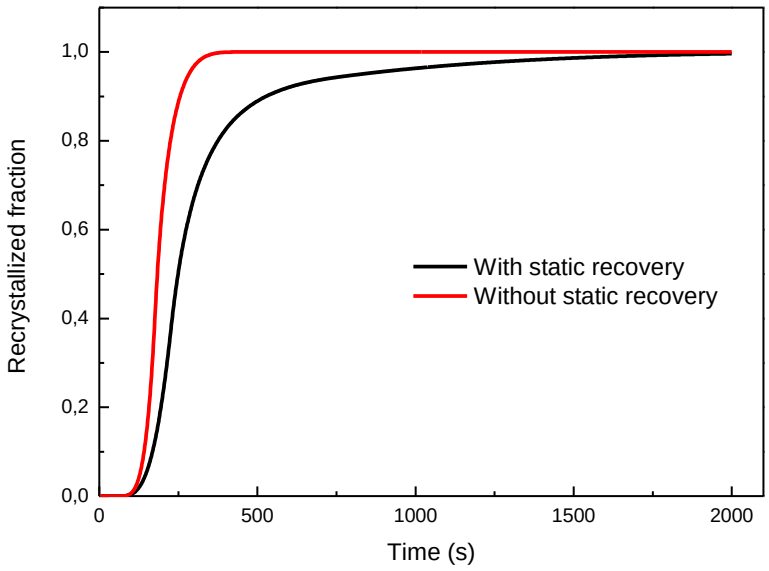

a)

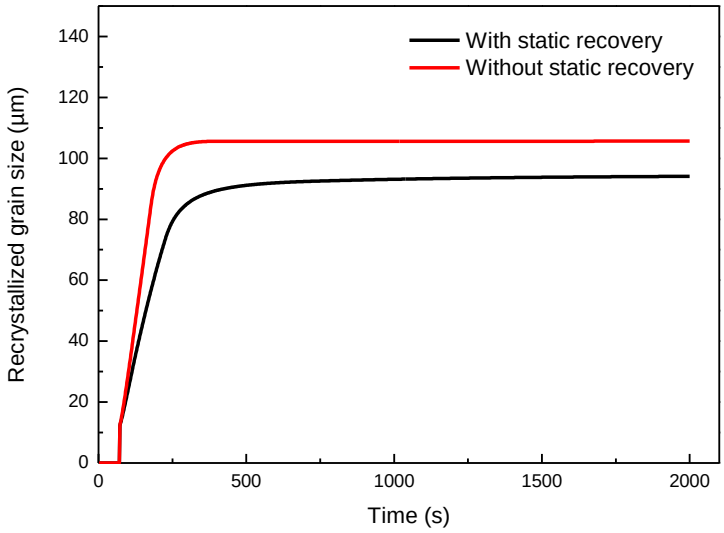

b)

Figure 6-39 Analysis of static recovery effect in the SRX model (after deformation at 1000 ℃ and $\dot{\varepsilon} = 0.01s^{-1}$ to a deformation of 0.3) a) Recrystallized fraction b) Recrystallized grain size

Example of the relative values of K_3, K_g and K_p used for modeling DRX (at 1000 ℃ and $\dot{\varepsilon} = 0.1s^{-1}$), SRX (annealing after deformation at 1000 ℃ and $\dot{\varepsilon} = 0.1s^{-1}$ to $\varepsilon = 0.3$), and PDRX (annealing after deformation at 1000 ℃ and $\dot{\varepsilon} = 0.1s^{-1}$ to $\varepsilon = 1.5$) is presented in Figure 6-40. It is found that K_3 increases in SRX and even more in PDRX, possibly due to the annealing twins which may promote both nucleation and growth of RX grains. The exact reason is not entirely clear. A possible explanation comes from the twinning activation related to the magnitude of driving forces. More twinning avoids grain boundary stagnation by changing crystallographic orientation, and promotes "special boundaries" which are less affected by impurity segregation than general boundaries [2].

A significant drop of K_g is found when switching from DRX to SRX and PDRX, while the pinning effect term keeps constant for all these types of recrystallization. Both K_3 and K_g decrease in SRX as compared to PDRX. Even though SRX is conducted at the same temperature, the decrease of K_3 seems to be linked once again to the magnitude of driving force. The decrease of K_g is apparent from the experimental observation, see for example Figure 6-11 and Figure 6-12 which correspond to SRX and PDRX at 1100 ℃, respectively. It seems both of these two parameters are dependent on the stored energy.

One can conclude, overall:

(i) that the nucleation law would need to account better for the accumulated strain;

(ii) that the mobility varies with the driving force magnitude.

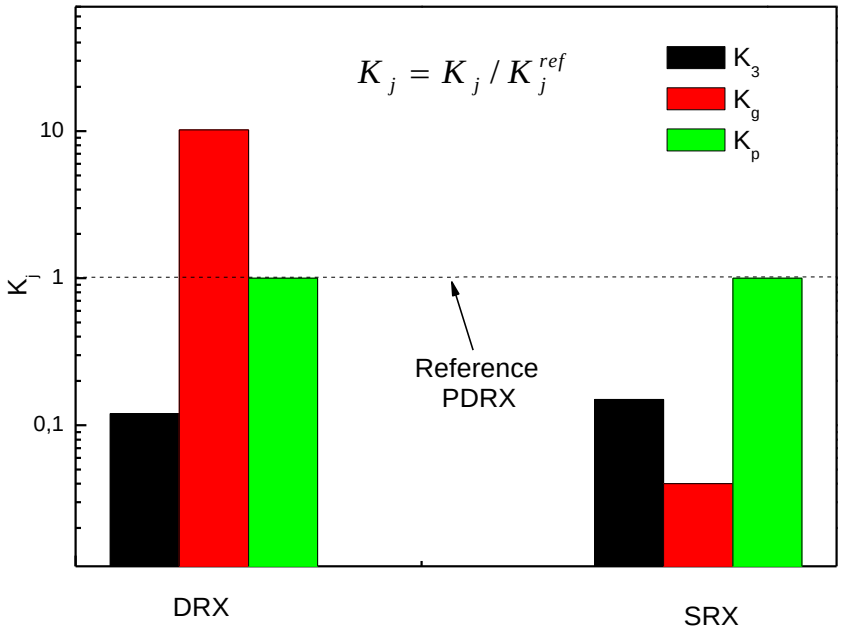

Figure 6-40 Evolution of common K parameters used for DRX, SRX and PDRX. (DRX corresponds to condition at $T = 1000°C, \dot{\varepsilon} = 0.1s^{-1}$, SRX corresponds to annealing after deformation at $T = 1000°C, \dot{\varepsilon} = 0.1s^{-1}, \varepsilon = 0.3$, PDRX corresponds to annealing after deformation at $T = 1000°C, \dot{\varepsilon} = 0.1s^{-1}, \varepsilon = 1.5$)

A set of acceptable parameters values are found for SRX/GG of 304L stainless steel, the trend of parameter values identified from comparison with experimental data (as detailed in the next sections) is presented in Figure 6-41. Parameters are expressed in a dimensionless form, showing changes by both increasing temperature and decreasing strain rate according to the reference values obtained for SRX after deformation at 1000 ℃ and 0.1 s^{-1} to a strain of 0.3. It is found that grain boundary migration constant K_3, nucleation constant K_g and static recovery constant K_s increase with temperature, while the pinning effect K_p decrease with temperature. All the model parameters are strain rate and applied strain independent, except the nucleation constant K_g. This dependence is actually a consequence of the increase in dislocation density when the strain rate increases. If one computes the inherited dislocation density from the deformation state, K_g is found to be linearly increase with this dislocation (see Figure 6-42). The nucleation constant is finally only dependent on temperature and current (computed) dislocation density. The incubation time (t_0), which can be directly identified from experiment, is also an input parameter of the model. Again, the dependence on strain rate and applied strain can be transformed into a dependence on calculated dislocation density. The relationship is found to be exponential as illustrated in Figure 6-43.

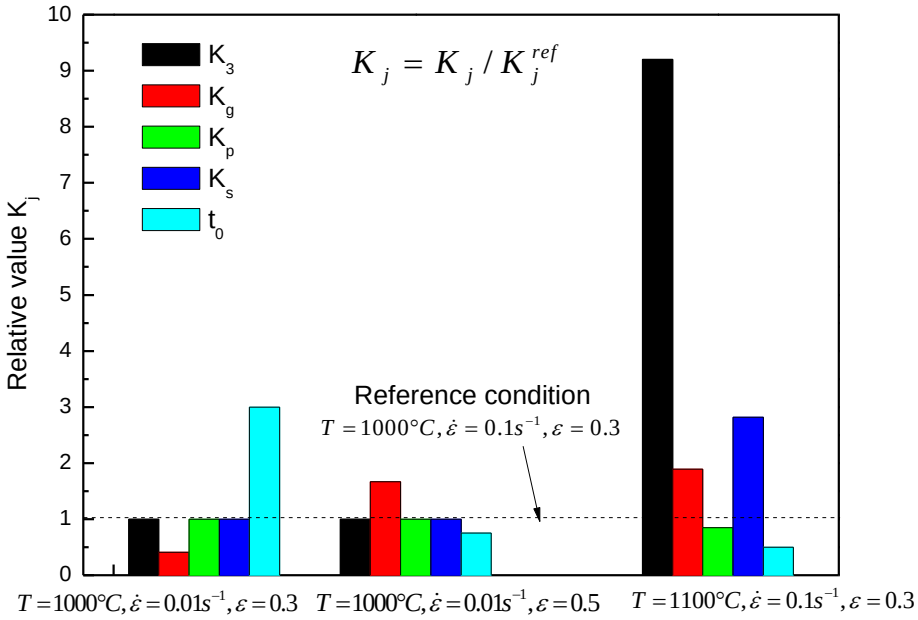

Figure 6-41 Relative evolution of K parameters for SRX as a function of temperature, strain rate and interrupted strain, with respect to the reference value (represented by the broken line) obtained after deformation at 1000 ℃ and $\dot{\varepsilon} = 0.1s^{-1}$ to a deformation of 0.3

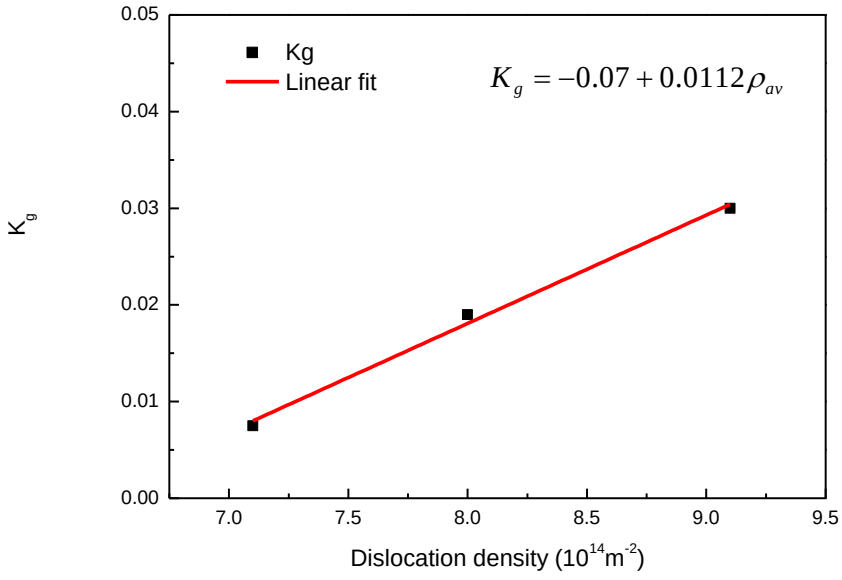

Figure 6-42 Evolution of nucleation constant K_g with the computed average dislocation density casued by the applied deformation.

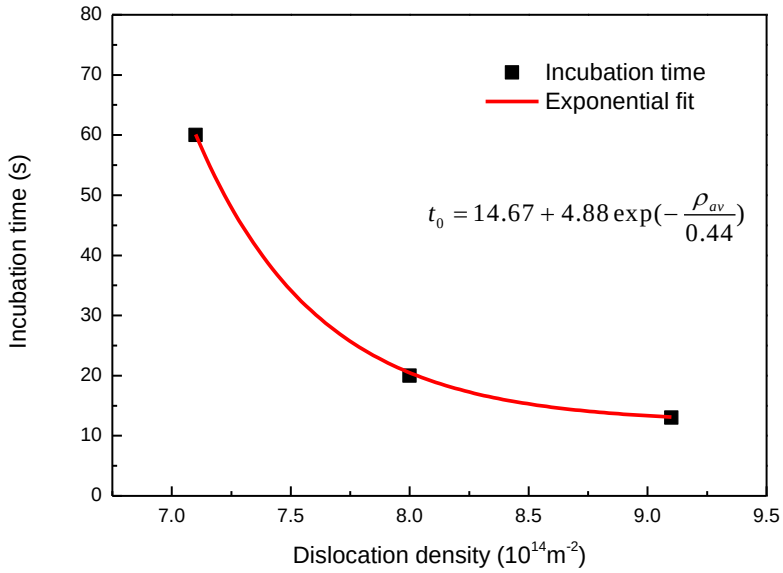

Figure 6-43 Evolution of incubation time (t_0) with the computed average dislocation density.

6.5.4.2. Effect of temperature

The influence of temperature on the evolution of SRX is examined by micrographs shown in Figure 6-18 and Figure 6-20, which correspond to SRX after deformation with $\dot{\varepsilon} = 0.1s^{-1}$ to $\varepsilon = 0.3$ at 1000 ℃ and 1100 ℃, respectively. The comparison between experimental and numerical results is presented in Figure 6-44. Although the model matches well at the beginning and late stages of the SRX/GG process, for both the recrystallization kinetics and recrystallized grain size, it predicts a faster growth rate in between. It was found in the quasi in situ heating experiments that the growth is quite complex, with boundaries moving, stopping and moving again by forming a twin on the growing front, which is a clear deviation from (Equation 4-5). This may explain in part the discrepancy in the current case, on the other hand, the nucleation law might also be of concern. In the current study, no nucleation is triggered unless the annealing time reaches the incubation time. In reality, the microstructure rearranges to a state where nucleation becomes possible after this incubation time. This rearrangement is not reflected in the model, since the main evolution during incubation time is the decrease of dislocation density, which actually reduces the possibility of nucleation. This is why the notion of incubation time must be added in the model when dealing with SRX, using a dislocation density dependence as that calibrated in Figure 6-43.

Considering all the issues mentioned above, the overall level of agreement obtained with the model looks encouraging.

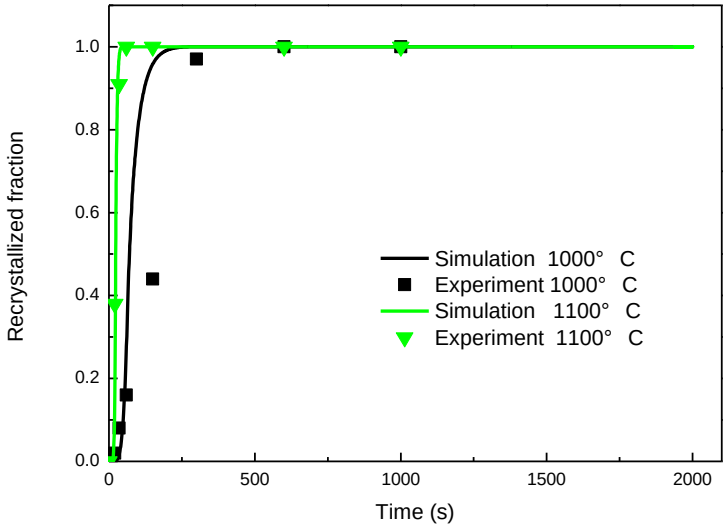

a)

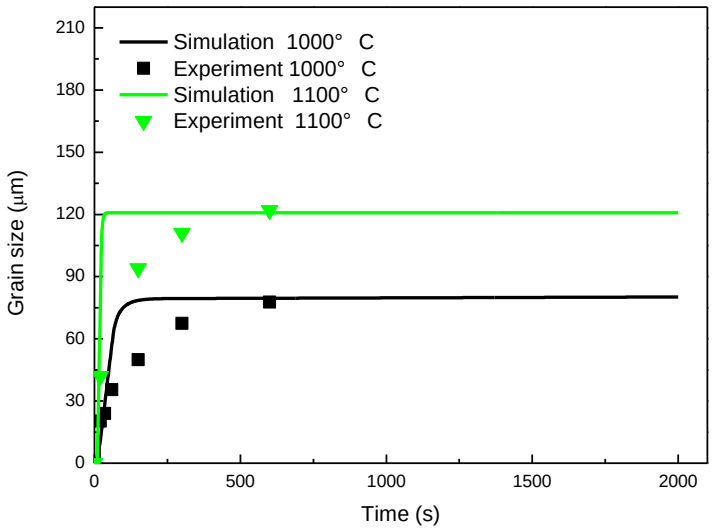

b)

Figure 6-44 Comparison between experimentally measured and numerically obtained for SRX after deformation at $\dot{\varepsilon} = 0.1s^{-1}$ to $\varepsilon = 0.3$ a) Recrystallized fraction, and b) Recrystallized grain size of 304L steel. Results are shown for two different temperatures (1000 ℃ and 1100 ℃).

6.5.4.3. Effect of strain rate

The dependence of the SRX evolution in the model on strain rate is evaluated by comparing the change of recrystallized fraction and recrystallized grain size during annealing after deformation at 1000 ℃ to a strain of 0.3 at two different strain rate $\dot{\varepsilon} = 0.01s^{-1}$ and $\dot{\varepsilon} = 0.1s^{-1}$. As illustrated in Figure 6-45, a better match has been obtained at lower strain rate. At high strain rate, both the kinetics and grain size are overestimated. The difference of recrystallized grain size comes from the number of nuclei created during SRX, clearly more nuclei are

created at higher strain rate (Figure 6-18) compared to (Figure 6-17). Again, it seems that the model does not use a totally appropriate nucleation law for SRX conditions.

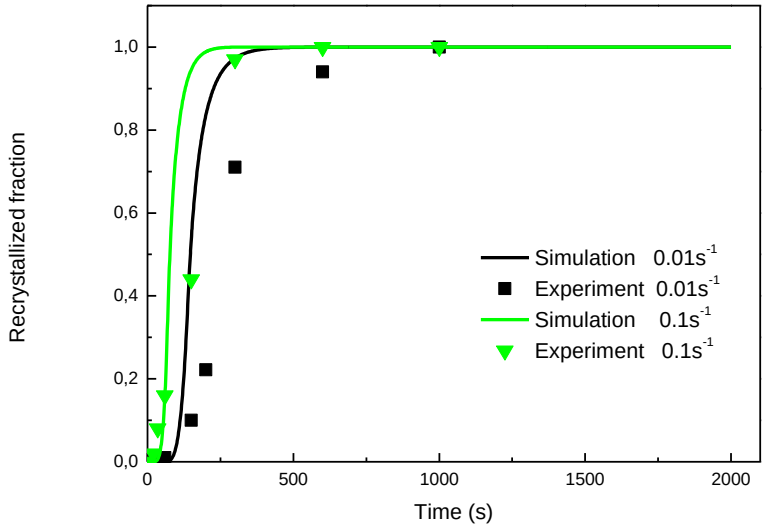

a)

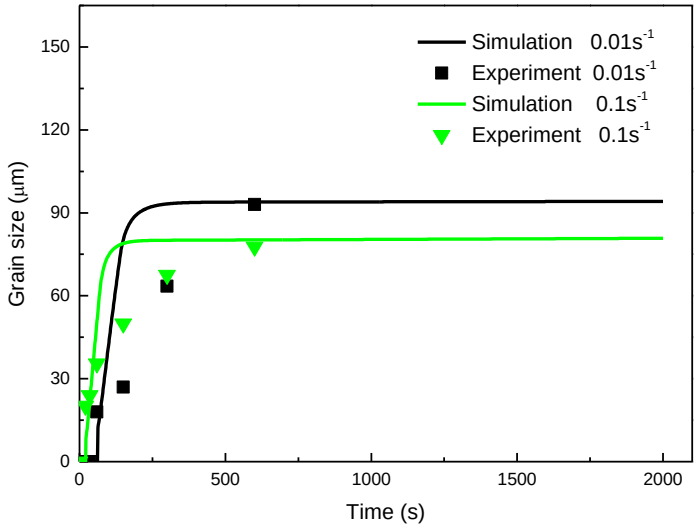

b)

Figure 6-45 Comparison between experimentally measured and numerically obtained results for PDRX after deformation at 1000 ℃ to $\varepsilon = 0.3$ a) Recrystallized fraction, and b) Recrystallized grain size of 304L steel. Results are shown for two different strain rates ($\dot{\varepsilon} = 0.01s^{-1}$ and $\dot{\varepsilon} = 0.1s^{-1}$).

6.5.4.4. Effect of applied strain

As the applied strain is increased, the time for 100% recrystallization decreases (Figure 6-46a) and the final recrystallized grain size decreases as well. The influence of increasing applied strain is similar to that observed by increasing strain rate, both of them increase the stored energy of the system before interrupting deformation. The grain size for SRX after the

smaller strain of 0.3 (~90 µm) is larger than that of DRX (~10 µm) and even PDRX (~70 µm, after a deformation of 1.5), conducted at the same temperature and strain rate.

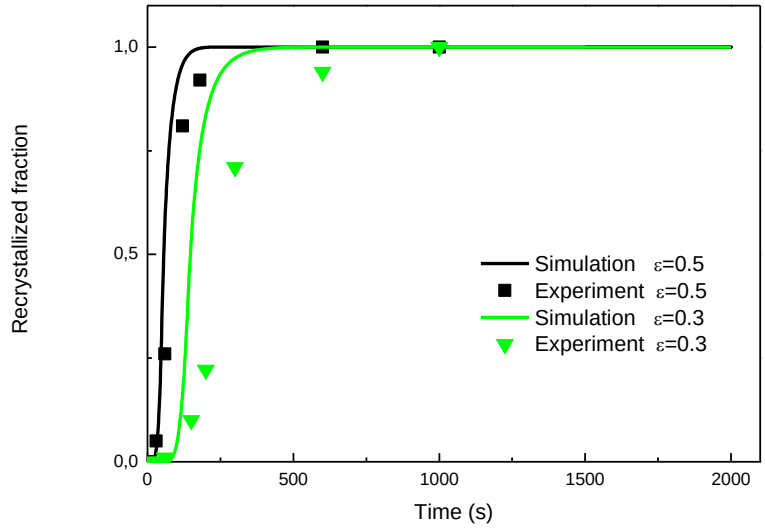

a)

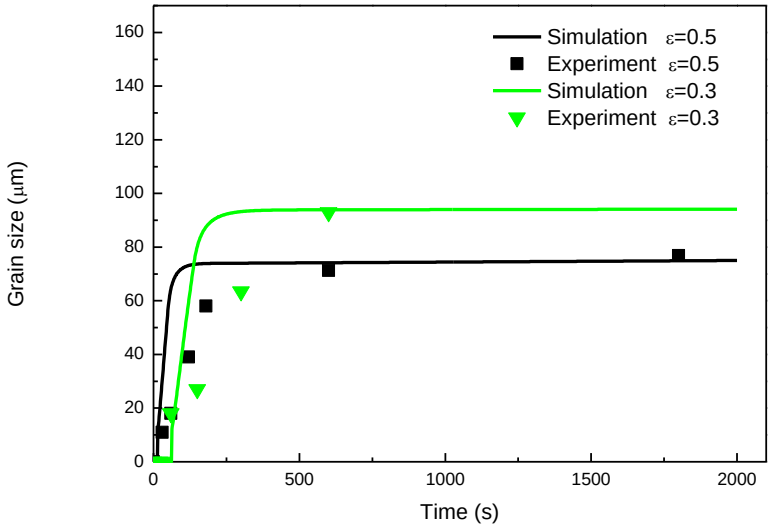

b)

Figure 6-46 Comparison between experimentally measured and numerically obtained results for PDRX after deformation at 1000 ℃ and $\dot{\varepsilon} = 0.01\text{s}^{-1}$ a) Recrystallized fraction, and b) Recrystallized grain size of 304L steel. Results are shown for two different stop strains ($\varepsilon = 0.3$, $\varepsilon = 0.5$).

It is important to notice that K_1 and K_2 are both optimized according to the whole DRX process, i.e. they are average values, not exactly the values we identified from flow stress curves as illustrated in section 5.6.1.1. That is why the match of flow stress between experimental and numerical results is not as good at the beginning of the deformation, as shown in section 5.6 in Figure 5-26a (DRX at 1100 ℃ and $\dot{\varepsilon} = 0.1s^{-1}$) and Figure 5-28a (DRX at 1000 ℃ and $\dot{\varepsilon} = 0.1s^{-1}$). So, it is likely that better match of SRX could be obtained with

experiment if K_1 and K_2 are kept the same as identified, i.e. with good match with the flow stress curve at early work-hardening stages. The accuracy obtained here remains acceptable however.

6.6. Conclusions

In this chapter, the two-site mean field SRX/PDRX/GG model has been successfully applied to 304L austenitic stainless steel, comparisons between experiment and model calculations in terms of recrystallized fraction and grain size show good agreement over a range of deformation conditions with different temperatures, strain rates and applied strains.

The effect of deformation temperature, strain rate, and strain on both SRX/PDRX are analyzed first. By examining the micrographs at different annealing times, the evolution of SRX, PDRX and GG are followed, and a full set of data for both recrystallized fraction and grain size are obtained. The differences between SRX and PDRX are also addressed in this chapter.

A few in situ heating experiments have been conducted to better understand the mechanisms for SRX/PDRX/GG. It is shown that annealing twins play an important role during both nucleation and grain boundary migration.

The identification of model parameters from existing data is described, three main parameters of the model are then tuned to match with experimental data on 304L stainless steel by inverse analysis. Reasonable data, i.e. physically consistent, are finally found. By re-defining RX and NR grains after DRX, and calibrating static recovery and pinning effects, the PDRX model is improved.

It is observed both numerically and experimentally that recrystallization kinetics is faster for both SRX and PDRX at high deformation temperature and large applied strain rate and strain. The recrystallized grain size for SRX is larger than that obtained through DRX and PDRX.

The good matches between the experimental results and predicted ones in terms of recrystallized fraction and grain size shows that the proposed model should be able to accurately describe microstructure evolution in multi-pass conditions, if:

(i) the mobility is properly calibrated as a function of the driving force magnitude;

(ii) the nucleation law in SRX/PDRX regimes is improved, in particular to account better for the accumulated strain.

6.7. French summary

Dans ce chapitre, le modèle à champs moyen 2-sites SRX/PDRX/GG a été appliqué avec succès à l'acier austénitique 304L. Les résultats numériques présentés sont en accord avec les résultats expérimentaux pour une large gamme de conditions de déformations, sous des valeurs de température, de vitesse de déformation et de taille initiale de grain différentes.

L'effet de la température de déformation, de la vitesse de déformation, et de la déformation pour SRX/PDRX sont analysés dans un premier temps. En analysant les micrographes pour différents temps de recuit, les évolution SRX, PDRX et GG sont observées, et un ensemble de données concernant la fraction recristallisé et la taille des grains est obtenu. Les différences entre SRX et PDRX sont aussi présentées dans ce chapitre.

Quelques essais en température *in situ* ont été réalisés afin de mieux comprendre les

mécanismes de SRX/PDRX/GG. Il est montré que les macles de recuit jouent un rôle important durant les phases de germination et de migration de joint de grain.

L'identification des paramètres du modèle à partir des données existantes est décrite. Trois principaux paramètres sont alors établis afin d'obtenir des résultats cohérents avec les données expérimentales pour l'acier 304L dans le cadre d'une analyse inverse. Des résultats convenables, i.e. physiquement cohérents, ont finalement été trouvés. En redéfinissant les grains RX et NR après DRX, et en calibrant la restauration statique et les effets d'ancrage, le modèle PDRX a pu être amélioré.

Il a pu être observé aussi bien numériquement qu'expérimentalement, que la cinétique de recristallisation est plus rapide pour SRX et PDRX à des hautes températures de déformation et sous des vitesses de déformation importantes. La taille des grains recristallisés pour SRX et plus grande que celle obtenue avec DRX ou avec PDRX.

La bonne cohérence des résultats expérimentaux et numériques concernant les valeurs de fraction recristallisée et de taille de grain, montre que le modèle proposé doit être capable de décrire l'évolution de la microstructure dans des conditions multi-passes de manière précise si :

i. La mobilité est correctement calibrée comme fonction de la valeur absolue de la force motrice.
ii. La loi de germination en régimes SRX/PDRX est améliorée, notamment pour mieux prendre en compte la déformation accumulée.

7. Conclusions and future work

7.1. Conclusions

The work presented in this thesis has described the recrystallization behavior of 304L austenitic stainless steel during and after hot deformation both experimentally and numerically. The focus of this work was to develop numerical models to predict microstructure evolution in 304L stainless steel, including phenomena like hardening, recovery and recrystallization.

Extensive research has been conducted on this subject, a review of which is presented in Chapter 2, focusing on the recrystallization in low SFE materials. It is found that there are still some issues that are not completely understood. This study is however not intended to clarify all these problems since some of them are neglected. Instead, the focus was to provide a physically based numerical model, which is computationally cheap thanks to some simplifications, but capable to predict microstructure evolution under multi-pass conditions with acceptable accuracy. Experiments were conducted to validate the model and identify the parameters: torsion tests plus heat treatments and analysis of the resulting microstructures in terms of recrystallized volume fraction and grain size. This study leads to the following conclusions.

In chapter 4, a two-site mean field recrystallization model has been developed and is based on the interaction between a set of representative grains and two HEMs having different properties. Representative grains are fully defined by their dislocation density, grain size, and volume fraction. HEM properties are derived as volume averages of the individual representative grains and influence themselves the evolution of the representative grains state variables. The respective influences of the two HEMs are linked to the values of mobile surface fractions which evolve with the microstructure, with explicit account of volume conservation. Comparing to the existing models in literature, this proposed model has the following outstanding features:

i) It provides data on recrystallization kinetics, stress-strain curves and recrystallized grain size together;

ii) It is able to simulate recrystallization under multi-pass conditions, including DRX, SRX, PDRX and GG;

iii) It takes into account the initial distribution of grain size and topology effects are partially introduced (necklace structure), parameters are not grain size dependent;

iv) It is not computationally demanding, since no explicit representation of microstructures is introduced, so it can readily be coupled to a FEM formulation describing standard forming processes.

In chapter 5, the two-site mean field DRX model has been successfully applied to 304L austenitic stainless steel, comparisons between experiment and model calculations show very good agreement over a range of deformation conditions with different temperature, strain rates and initial grain sizes. In the first part, the effects of material features & processing conditions on DRX are analyzed experimentally. The methods to calibrate the model are described, and the main four parameters are tuned to match with experimental data using a genetic algorithm. The most important results of this section can be summarized as:

v) It is found that the four parameters in the DDRX model evolve with physical meaning, and can be reasonably independent of initial grain size.

vi) The reaction of the model to different initial grain sizes is verified, the natural progress towards a steady-state in stress and in grain size with strain is observed.

vii) It is observed both numerically and experimentally that recrystallization kinetics is faster at conditions with low Zener-Hollomon (Z) value, and steady state values evolve in the expected way, i.e. smaller recrystallized grain sizes and increased flow stress for increased values of Z.

viii) It has been shown that an increase in initial grain size will slower the recrystallization kinetics while a unique steady state in grain size and flow stress is obtained, regardless of the initial microstructure, and only as a function of the thermomechanical conditions (represented by Z parameter).

ix) The initial grain size slightly affects the shape of the flow curves, with a decrease in the peak stress and steady state stress when decreasing the initial grain size.

x) The good match between experimental results and predicted ones in terms of flow stress, recrystallized fraction and grain size makes possible the extension of the DRX model to the post-dynamic or static recrystallization behavior.

The SRX/PDRX/GG phenomena are examined both numerically and experimentally in Chapter 6. The effects of deformation conditions on post deformation recrystallization are studied. The following key points can be highlighted from this chapter:

xi) A few in situ heating experiments have been conducted to better understand the mechanisms for SRX/PDRX/GG. It is shown that annealing twins play an important role during both nucleation and grain boundary migration.

xii) The identification of model parameters from existing data are described, four main parameters of the model are then tuned to match with experimental data on 304L stainless steel by inverse analysis. By re-defining RX and NR grains after DRX, plus the careful use of static recovery and pinning effects, the PDRX mode is improved.

xiii) It is observed both numerically and experimentally that recrystallization kinetics is faster for both SRX and PDRX at high deformation temperature and large applied strain rate and strain. The recrystallized grain size for SRX is larger than that obtained through DRX and PDRX.

xiv) The good matches between the experimental results and predicted ones in SRX/PDRX/GG conditions, in terms of recrystallized fraction and grain size, plus the excellent agreement during DRX, will lead to the modeling of multi-pass operations compatible with industrial applications.

7.2. Suggestions for the future work

According to the results for this study, the following suggestions are given for future work.

7.2.1. Experimental aspects

Even though experiments are conducted in various conditions of temperature, strain rate and applied strain, more investigations in a wider range of conditions would be useful. They should allow accurate prediction in variable conditions of strain rate and temperature, as the case in industrial applications.

The role of annealing twins during recrystallization, especially for SRX/PDRX is tentatively discussed in the present thesis, further investigation is clearly needed. For PDRX, more work on softening fractions can be conducted, which will make comparisons with recrystallized fractions examined by micrographs possible. Another important parameter, the transition strain (ε_T) which separates the strain dependent and strain independent area in PDRX regime should also be studied.

The multi-pass recrystallization (DRX+SRX+GG, DRX+PDRX+GG) has been investigated in this work, it would be interesting to extend to more complex multi-pass conditions (eg. DRX+SRX+DRX, DRX+PDRX+DRX…).

7.2.2. Numerical modeling aspects

The proposed recrystallization model provides reasonable results for many deformation conditions and even under multi-pass conditions. Some improvements are however foreseeable. The nucleation law, which is dependent on the dislocation density in the current study, should be modified as strain dependent, since the dislocation density of newly created RX grains becomes saturated soon after their appearance, no difference actually exists between these grains and those created earlier and which have accumulated more deformation. More precise equations for the surface fractions (γ^{RX} and γ^{NR}) evolution might also be needed, especially for conditions where necklace nucleation is not applicable.

Experimentally, it is found that the recrystallized fraction during DRX can be estimated from flow stress curves, since nucleation is the main softening mechanism during DRX. It would thus be interesting to compare the value of X_V calculated from our model with that predicted from stress-strain curve. For SRX/PDRX, it is possible to work in a similar way considering the softening fraction.

The proposed model identifies parameters values depending on the recrystallization regime (DRX, PDRX, SRX, GG). Ideally, one would look for a unified model, valid in all regimes. In that case, multi-pass conditions may easily be modeled. To reach such an objective, important steps must yet be taken:

- the design of nucleation laws must be improved, especially in static conditions

- the mobility should be calibrated as a function of the driving force magnitude

- hardening and recovery terms in evolution equations of dislocation density could be allow to vary with dislocation density. More advanced evolution equations could be considered as well, with possible extension to different types of dislocations.

7.3. French summary

Le travail présenté dans ce rapport de thèse décrit le comportement de l'acier 304L lorsqu'il est soumis à un traitement de recristallisation dynamique ou statique. L'objectif de ce travail était de développer un modèle numérique capable de prédire l'évolution de la microstructure de l'acier 304L en conditions multi passes de mise en forme en prenant en compte des phénomènes d'écrouissage, de restauration et de recristallisation. Les résultats numériques obtenus ont été analysés et les effets de la température et vitesse de déformation, ainsi que la déformation totale et la taille initiale de grain ont été étudiés. Finalement, les résultats numériques sont en bon accord avec les résultats expérimentaux pour tous les phénomènes étudiés, ouvrant ainsi la voie à la modélisation de la mise en forme en conditions multi passes compatibles avec des applications industrielles.

D'après les résultats obtenus dans cette étude, des suggestions pour des travaux futurs sont émises, portant aussi bien sur le modèle numérique que les essais expérimentaux, et concernant principalement le rôle des macles de recuit, la loi de germination et la calibration de la mobilité. L'approfondissement de ces thèmes permettrait l'extension du modèle à des conditions multi passes plus complexes que celles étudiées dans la thèse.

8. References

[1] F.J. Humphreys, M. Hatherly. Recrystallization and related annealing phenomena, second ed. Oxford: Elsevier. 2004.

[2] M. F. Ashby. Engineering Materials and Processes Desk Reference. Elsevier, U.S.A. 2009

[3] U.F.Kocks, H.Mecking, Physics and phenomenology of strain hardening: the FCC case. Progress in materials science. 48(2003), 171-273

[4] H.J.McQueen, S.Yue, N.D.Ryan, E.Fry, Hot working characteristics of steels in Austenitic state. Journal of material processing Technology 53(1995), 293-310

[5] H.J.McQueen, N.D.Ryan, Constitutive analysis in hot working. Materials science and Engineering A 2002, 322, 43-63.

[6] P.A. Beck, Annealing of cold worked metals.Adv. Phys. 3(1954) 245-324.

[7] M.B. Bever, Creep and Recovery, ASM, 14 (1957), Cleveland,.

[8] A.L. Titchener, M.B. Bever, Progress in metal physics. 7(1958), 247-338. Pergamon Press, London.

[9] E. Nes, Recovery revisited. Acta Metall. Mater. 43(1995) 2189-2207.

[10] U.F. Kocks. Laws for wrok-hardening and low-temperature creep. J.Eng.Mater.Technol. 98 (1976) 76-85

[11] H. Mecking, U.F. Kocks. Kinetics of flow and strain-hardening. Acta Metall. 29 (1981) 1865-1875

[12] Y.Estrin, H. Mecking. A unified phenomenological description of work hardening and creep based on one-parameter models. Acta Metall. 32 (1984) 57-70

[13] Y. Bergstrom. A dislocation model for the stress-strain behaviour of polycrystalline α - FE with special emphasis on the variation of the densities of mobile and immobile dislocations.Mater.Sci.Eng. 5 (1970) 193-200

[14]Y.Estrin, "Dislocation density-related constitutive modeling", Unified Constitutive Law of Plastic Deformation, Krausz A.S., Krausz K. (eds.), Academic Press, San Diego, CA, 1996, 69–106.

[15] P.A.Beck, P.R.Sperry. Strain induced boundary migration in high purity aluminum. Journal of Applied Physics. 21(1950) 150-152.

[16] M.C. Theyssier, J.H. Driver. Recrystallization nucleation mechanism along boundaries in hot deformed aluminum bicrystals. Mater. Sci. Eng. A272 (1999). 73-82

[17] W.B Hutchinson, H. Magnusson, J.M. Feppon, Proc. 4th Int. Conf. on Recrystallization, 1999. eds. Sakai and Suzuki, JIM, 49.

[18] W.B. Hutchinson: Recrystallisation textures in iron resulting from nucleation at grain boundaries, Acta Met, 37(1989), 1047-1056.

[19] P.A.Beck. The formation of recrystallization nuclei. Journal of Applied Physics. 20(1949)633-634.

[20] R.W.Cahn. A new theory of recrystallization nuclei. Proceedings of the Physical Society. ser.AI. 1950; 63(364):323-336.

[21] P.R.Riots et al., Nucleation and Growth During Recrystallization. Materials Research, 8(2005) 225-238

[22] A. Belyakov , H. Miura, T. Sakai. Dynamic recrystallization under warm deformation of a 304 type austenitic stainless steel. Materials Science and Engineering A255 (1998) 139–147

[23] T. Sakai. Microstructural development under dynamic recrystallization of polycrystalline materials, J.J. Jonas Symposium on thermomechanical processing of steel, S.Yue and E.Essadiqi Eds., Ottawa, Canada, 2000

[24] P. Karduck, G. Gottstein, H. Mecking. Deformation structure and nucleation of dynamic recrystallization in copper single crystals. Acta Mater. 31 (1983) 1525-1636

[25] E. Brunger, X. Wang, G. Gottstein. Nucleation mechanisms of dynamic recrystallization in austenitic steel alloy 800H. Scripta Mater 38 (1998) 1843-1849.

[26] X. Wang, E. Brunger, G. Gottste. The role of twinning during dynamic recrystallization in alloy 800H. Scripta Materialia 46 (2002) 875 – 880

[27] H. Beladi, P. Cizek and P.D. Hodgson, Dynamic recrystallization of austenite in Ni-30 Pct Fe model alloy: Microstructure and texture evolution Metall Mater Trans A 40 (2009), 1175.

[28] T. Sakai, J.J. Jonas, Overview no.35 Dynamic recrystallization: Mechanical and microstructural considerations. Acta Metall. 32 (1984) 189-209.

[29] C.Rossard, P. Blain. Evolution de la structure de l'acier sous l'effet de la déformation plastique àchaud, Mém. Sci. Rev. Métall. 56(1959) 285-300

[30] R.A. Petkovic, M.J .Luton, J.J. Jonas. Recovery and recrystallization of carbon steel between intervals of hot working. Can Metall Quart 14 (1975)137.

[31] J. P. Sah, G. J. Richardson,C. M. Sellars. Grain-size effect during dynamic recrystallization of Nickel. Metal Sci. 8 (1974) 325-331.

[32] M.J. Luton, C.M. Sellars, Dynamic recrystallization in nickel and nicke-iron alloys during high temperature deformation. Acta Metall. 17 (1969) 1033-1043.

[33] G. Glover, C. M. Sellars, Recovery and recrystallization during high temperature deformation of –Iron. Metall. Trans. A. 4 (1973) 765-775

[34] S. Sakui, T. Sakai, K. Takeishi. Hot deformation of austenite in plain carbon steel. Trans. Iron Steel Inst. Japan, 17(1977) 718.

[35] L. Blaz, T. Sakai and J.J. Jonas. Effect of initial grain size on dynamic recrystallization of copper. Metal Sci., 17 (1983) 609-616.

[36] M. Ueki, S. Horie, T. Nakamura. Critical condition for transition from multiple to single peak dynamic recrystallization . Scipta Metall. 19(1985) 547-549.

[37] L. Blaz. Proc. of 7th Riso International Symposium on Metallurgy and Materials Science ed. by N. Hansen, D. Jull Jensen, T. Leffers, B. Ralph, Riso National Laboratory, Denmark, (1986), 221.

[38] A. Dehghan-Manshadi, P.D. Hodgson. Dynamic Recrystallization of Austenitic Stainless Steel under Multiple Peak Flow Behaviours. ISIJ international. 47(2007) 1799-1803

[39] A. Dehghan-Manshadi, M.R. Barnett, P.D. Hodgson. Hot deformation and recrystallization of austenitic stainless steel: Part I. Dynamic Recrystallization. Metall. Mater. Trans. A, 39A (2008)1359-1370.

[40] C.Rossard, Proc.Int.Conf. Strength of metals and alloys, 3rd ed., Institute of Metals, London, 2(1973) 175-203

[41] N.D. Ryan, H.J. McQueen. Dynamic softening mechanisms in 304 austenitic stainless steel. Can. Metall. Quart. 29 (1990) 147-162.

[42] H. Miura , T. Sakai, S. Andiarwanto, J. J. Jonas. Nucleation of dynamic recrystallization at triple junctions in polycrystalline copper. Philosophical Magazine. Vol 85(2005) 2653 - 2669

[43] H. Miura , T. Sakai, H. Hamaji, J. J. Jonas. Preferential nucleation of dynamic recrystallization at triple junctions. Scripta Materialia. V 50 (2004) 65-69.

[44] S.-I. Kim, Y.-C. Yoo, Dynamic recrystallization behavior of AISI 304 stainless steelMaterials Science and Engineering A311 (2001) 108-113

[45] N.D. Ryan, H.J. McQueen. Dynamic recovery, strain hardening and flow stress in hot working of 316 steel. Czech J Phys 39(1989) 458–65.

[46] N.D. Ryan, H.J. McQueen. Dynamic softening mechanisms in 304 Austenitic stainless steel. Can Metall Q 29(1990) 147–62.

[47] N.D. Ryan, H.J. McQueen. Flow stress, dynamic restoration, strain hardening and ductility in hot working of 316 steel. J Mater Process Technol 21(1990) 177–99.

[48] P.J. Wray. Onset of recrystallization during the tensile deformation of austenitic iron at intermediate strain rates. Metallurgical Transactions A Vol 6 (1975) 1197-1203.

[49] E. I. Poliak, J. J. Jonas. A one-parmenter approach to determining the critical conditions for the initiation of dynamic recrystallization Acta mater. Vol. 44(1996) 127-136,

[50] C.M.Sellars, J.J.Jonas Symposium on thermomechanical processing of steel, S.Yue and E.Essadiqi Eds., Ottawa, Canada, 2000.

[51] C.Roucoules et al. Analysis of work hardening and recrystallization during the hot working of steel using a statistically based internal variable model. Materials science and engineering A339 (2003) 1-9.

[52] A. Najafizadeh, J.J. Jonas. Predicting the critical stress for initiation of dynamic recrystallization. ISIJ Int 46(2006) 1679–84.

[53] M.R. Barnett, G.L. Kelly, P.D. Hodgson. Predicting the critical strain for dynamic recrystallization using the kinetics of static recrystallization. Scripta Mater 43(2000) 365–369.

[54] M.R. Barnett, G.L. Kelly, P.D. Hodgson. Inferring dynamic recrystallization in ferrite using the kinetics of static recrystallization. Metall Mater Trans A 33(2002) 1892–900.

[55] G. Gottstein, Frommert M, Goerdeler M, Schäfer N. Prediction of the critical conditions for dynamic recrystallization in the austenitic steel 800H. Mater Sci Eng A 2004; 387–389:604–608.

[56] R.Sandstrom, R.Lagneborg. A controlling factor for dyanmic recrystallization. Scripta Met. 9 (1975) 59-65.

[57] W.Roberts, B.Ahlblom. A nucleation criterion for dynamic recrystallization during hot working. Acta Metall. 26 (1978) 801-813-209.

[58] B. Ahblom, A metallographic study of dynamic recrystallization in an 18/8 austenite stainless steel. Swedish Inst. für Metals Research, 1977

[59] M. El Wahabi, L. Gavard, F. Montheillet, J.M. Cabrera, J.M.Prado. Effect of initial grain size on dynamic recrystallization in high purity austenitic stainless steels. Acta Mater., 2005, vol. 53, pp. 4605–12.

[60] A. Dehghan-Manshadi and P.D. Hodgson. Dependency of Recrystallization Mechanism to the Initial Grain Size. Metall. Trans. A, 39A (2008) 2830-2840

[61] M. Ohashi, T. Sakai, T. Endo. Effect of initial grain size on dynamic recrystallization of pure nickel. J. Jpn Inst. Metals, 54 (1990), 435-441.

[62] P.J. Wray. Onset of Recrystallization During the Tensile Deformation of Austenitic Iron at Intermediate Strain Rates. Metall. Trans. A, 6A (1975). pp. 1197-1203.

[63] N.Fujita,R.Sahara,T.Narushima, C.Ouchi. Austenitic grain growth behavior immediately after dynamic recrystallization in HSLA steels and austenitic stainless steel.ISIJ International, V48(2008) 1419-1428.

[64] T. Sakai, Y. Nagao, M. Ohashi, J.J. Jonas. Flow stress and substructural change during transient dynamic recrystallization of nickel. Mater. Sci. Technol., 2 (1986), 659-665.

[65] T. Sakai and M. Ohashi. Dislocation Substnictures Developed during. Recrystallization in Polycrystalline Nickel.Mater. Sci. Technol., 6 (1990), 1251-1257.

[66] D.Sundararaman, R.Divakar, V.S.Raghunathan. Microstructural features of a type 304L stainless steel deformed at 1473K in the strain rate interval $10^{-3}s^{-1}$ to $10^{-2}s^{-1}$. Scripta Metall. Mater. 28 (1993) 1077-1082

[67] B. Derby, The dependence of grain size on stress during dynamic recrystallization.Acta Metall. 39 (1991), 955-962.

[68] M.C. Mataya, E.L. Brown, and M.P. Riendeau, Effect of Hot Working on Structure and Strength of Type 304L Austenitic Stainless Steel, Metall. Trans. A, 21A (July 1990), pp. 1969–1987.

[69] Y.C. Lin, X.M. Chen. A critical review of experimental results and constitutive descriptions for metals and alloys in hot working Materials and Design 32 (2011) 1733 – 1759

[70] M.Avrami, Kinetics of Phase Change I-III. J. Chem Physics. 7 (1939) 1103-1112.

[71] J.J. Jonas, X.Quelennec, L.Jiang, E.Martin, The Avrami kinetics of dynamic recrystallization. Acta Mater. 57

(2009) 2748-2756.

[72] S.Venugopal, S.L.Mannan, P.Rodriguez. Optimum design of hot extrusion process for AISI type 304L stainless steel using a model for the evolution of microstructure, Modelling and Simulation in Materials Science and Engineering. 10 (2002) 253-265

[73] H. P. Stüwe, B.Ortner, Recrystallization in Hot Working and Creep. Metal Science, Volume 8, Number 1, 1974 , pp. 161-167

[74] R.Sandstrom, R. Lagneborg. A Model for Hot Working Occurring by Recrystallization.Acta Metall 23(1975) 387-398.

[75] J.E.Bailey, P.B.Hirsch. The recrystallization process in some polycrystalline metals. Proc.R. Soc. London A 267 (1962) , 11-30

[76] F.Montheillet, O.Lurdos, G. Damamme, A grain scale approach for modeling steady-state discontinuous dynamic recrystallization. Acta Materialia 57 (2009) 1602 – 1612

[77] D.G.Cram, H.S.Zurob, Y.J.M.Brechet, C.R.Hutchinson. Modelling discontinuous dynamic recrystallization using a physically based model for nucleation. Acta Materialia 57 (2009) 5218 – 5228

[78] H.S.Zurob, Y.Brechet, J. Dunlop. Quantitative criterion for recrystallization nucleation in single-phase alloys: Prediction of critical strains and incubation times. Acta Mater 54(2006). 3983-3390.

[79] X.G. Fan, H. Yang, Z.C. Sun, D.W. Zhang. Quantitative analysis of dynamic recrystallization behavior using a grain boundary evolution based kinetic model Materials Science and Engineering A 527 (2010) 5368–5377

[80] Z.Jin, Z. Cui. Modelling the Effect of Initial Grain Size on Dynamic Recrystallization Using a Modified Cellular Automata and an Adaptive Response Surface Method. Journal of Materials Science and Technology, 26(2010), 1063-1070

[81] H. Frost, C. Thompson.The effect of nucleation conditions on the topology and geometry of two-dimensional grain structures.Acta Met. 35(1987), 529-540

[82] F.J. Humphreys. A network model for recovery and recrystallization.Scr. Meall. Mater. 27 (1992) 1557–1562.

[83] V.E. Fradkov, L.S. Shvindlerman, D. Udler. Computer simulation of grain growth in two dimension.Scr. Metall. 19 (1985) 1285–1290.

[84] A.D.Rollett, M.J.Luton, D.J.Srolovitz. Microstructural simulation of dynamic recrystallization . Acta Met. Mater. 40 (1992) 43-55.

[85] P. Peczak. A Monte Carlo study of influence of deformation temperature on dynamic recrystallization .Acta Metall. Mater. 43 (1995) 1279-1291.

[86] N. Yazdipour, C.H.J. Davies, P.D. Hodgson. Microstructural modeling of dynamic recrystallization using irregular cellular automata. Comput Mater Sci. 44 (2008) 566-576.

[87] H. Hallberg, M. Wallin, M. Ristinmaa. Simulation of discontinuous dynamic recrystallization in pure Cu using a probabilistic cellular automaton.Comput Mater Sci. 49 (2010) 25-34.

[88] N. Xiao, C. Zheng, D. Li, Y. Li. A simulation of dynamic recrystallization by coupling a cellular automaton method with a topology deformation technique.Comput. Mater. Sci. 44 (2008) 366-374.

[89] G. Kugler, R. Turk. Modeling the dynamic recrystallization under multi-stage hot deformation. Acta Materialia 52 (2004) 4659 – 4668

[90] T .Takaki, Y.Hisakuni, T.Hirouchi, A.Yamanaka, Y.Tomita. Multi-phase-field simulations for dynamic recrystallization. Comput Mater Sci. 45 (2009) 881-888.

[91] R.E.Logé, M.Bernacki, H. Resk, L. Delannay, H.Digonnet, Y.Chastel, T.Coupez. Linking plastic deformation to recrystallization in metals using digital microstructures. Phil Mag. 88 (2008) 3691-3712.

[92] M.Bernacki, Y.Chastel, T.Coupez, R.E.Logé, Scripta Mater. 58 (2008) 1129-1132.

[93] M.Bernacki, H. Resk, T.Coupez, R.E.Logé Finite element model of primary recrystallization in polycrystalline aggregates using a level set framework. Model Simul Mater Sci Eng 17 (2009) 064006.

[94] M.Bernacki, T.Coupez, R.E.Logé Level set framework for the finite-element modelling of recrystallization and grain growth in polycrystalline materials. Scripta Mater. 64 (2011) 525-528.

[95] A.D.Rollett, Overview of modelling and simulation of recrystallization. Prog. Mater. Sci. 42 (1997) 79-99.

[96] A.Dehghan-Manshadi. The evolution of recrystallization during and following hot deformation. Ph.D thesis, Deaking University, Australia, 2007

[97] G.A. Wilber, J.R. Bell, J.H. Bucher, W.J. Childs, The determination of rapid recristallization rates of austenite at the temperatures of hot deformationTrans. TMS-AIME 244 (1968) 2305–2308.

[98] R.A.P. Djaic, J.J. Jonas, Static recrystallozation of austenite between intervals of hot working. J. Iron Steel Inst. 210 (1972) 256–261.

[99] R.A.P. Djaic, J.J. Jonas, Recrystallization of High Carbon Steel Between Intervals of High Temperature Deformation. Met. Trans. 4 (1973) 621–624.

[100] Z.Xu, T.Sakai. Kinetics of recovery and recrystallization in dynamically recrystallized austenite. Materials transactions JIM. 32 (1991) 174-180

[101] H. L. Andrade, M. G. Akben, J. J. Jonas. Effect of molybdenum, niobium, and vanadium on static recovery and recrystallization and on solute strengthening in microalloyed steels. Metall. Trans. A. 14A(1983), 1967 -1977

[102] D.R. Barraclough, C.M. Sellars. Static Recrystallization and Restoration after Hot Deformation of Type 304 Stainless Steel. Met. Sci. 13 (1979) 257–267.

[103] I. Schindler, J. Kliber, J. Boruta. Mathematical description of static recovery of type C−Mn−Mo−Nb−V microalloyed steel.Steel Res. 62 (1991) 266–271.

[104] K.P. Rao, Y.K.D.V. Prasad, E.B. Hawbolt. Study of fractional softening in multi-stage hot deformation. Mater. Proccess. Technol. 77 (1998) 166–174.

[105] A. Yanagida, J. Yanagimoto. Formularization of softening fractions and related kinetics for static recrystallization using inverse analysis of double compression test. Materials Science and Engineering A 487 (2008) 510–517

[106] A.I. Fernandez, B. Lopez, J.M. Rodriguez-Ibabe, Relationship between the austenite recrystallized fraction and the softening measured from the interrupted torsion test technique. Scripta Mater. 40 (1999) 543–549.

[107] R.W. Cahn. Physical Metallurgy. North Holland Publishing Company, Amsterdam, 1965, p. 925.

[108] R.A.Petkovic, M.J.Luton, J.J.Jonas. Recovery and recrystallization of carbon steel between intervals of hot working. Can Metall Quart 14(1975) 137-145.

[109] J.J.Jonas, C.M. Sellars, W.J. McG. Tegart. Strength and structure under hot-working conditions. Metallurgical Reviews, 130(1969), 1-33.

[110] R.A.P. Djaic, J.J. Jonas. Static recrystallization of austenite between intervals of hot working. J. Iron and Steel Inst. 210(1972), 256-261.

[111] R.A. Petkovic, M.J. Luton, J.J. Jonas. Recovery and recrystallization of polycrystalline copper after hot working. Acta Metall 27(1979) 1633-1648.

[112] M.J. Luton, R.A. Petkovic, J.J. Jonas. Kinetics of recovery and recrystallization in polycrystalline copper . Acta Metall 28(1980) 729-743.

[113] T. Sakai, M. Ohashi, K. Chiba, J.J. Jonas. Recovery and recrystallization of polycrystalline nickel after hot working. Acta Mater 36(1988) 1781-1790.

[114] P. D. Hodgson R. K. Gibbs. A Mathematical Hot Rolled C-Mn Model to Predict and Microalloyed the Mechanical Properties of hot rolled C-Mn and Microalloyed Steels; ISIJ International, Vol. 32 (1992), 1329-1338

[115] C. Roucoules, P.D. Hodgson, S. Yue, J.J. Jonas. Softening qnd microstructural change following the dynamic recrystallization of austenite. Metall. Mater. Trans. A 25 (1994) 389-400.

[116] C. Roucoules, P.D. Hodgson, Post-dynamic recrystallisation after multiple peal dynamic recrystallisation in C-Mn steels. Materials Science and Technology. 11 (1995) 548-556

[117] H. Beladi, P. Cizek, P.D. Hodgson. The mechanism of metadynamic softening in austenite after complete dynamic recrystallization. Scripta Materialia 62 (2010) 191-194

[118] H. Beladi, P. Cizek, P.D. Hodgson. New insight into the mechanism of metadynamic softening in austenite. Acta Materialia 59 (2011) 1482-1492

[119] J.E. Burke. Some Factors Affecting the Rate of Grain Growth in Metals.Metall. Trans.Soc. A.I.M.E. 180(1949) 73-91.

[120] J.E. Burke, D. Turnbull. Recrystallization and grain growth. Prog. Metal Phys. 3(1952), 220-292.

[121] J. W. Christian, The Theory of Transformations in Metals and Alloys, 2002. 3d ed. Oxford ; New York : Pergamon Press PP 851

[122] W.W. Mullins. Estimation of the geometrical rate constant in idealized three dimensional grain growth. Acta Metallurgica, 37(1989),2979-2984.

[123] D.Weygand, Y. Brechet, J. Lepinoux,W. Gust.. Three dimensional grain growth: a vertex dynamics simulation. Philos.Mag. B, 79(1999) 703–716.

[124] M.Hillert. On the theory of normal and abnormal grain growth. Acta Materialia, 13(1965) 227-238

[125] P. Feltham. Grain growth in metals. Acta Metall. 5(1957) 97-105.

[126] P. A.Beck ,J.C.Kremer, L.J. Demer, M. L.Holzworth. Grain Growth in High-Purity Aluminum and in an Aluminum-Magnesium Alloy. Trans. Metall. Soc. AIME 175 (1948) 372-394.

[127] G. F. Boilling, W.C.Winegard. Grain growth in zone-refined lead. Acta Metall. 6(1958) 283-287

[128] E. L.Holmes, W. C.Winegard. Grain growth in zone-refined tin. Acta Metall. 7 (1959) 411- 414

[129] G.T. Higgins. Grain boundary migration and grain growth. Met. Sci. J. 8(1974) 143-150.

[130] R. L. Fullman, J. C. Fisher. Formation of Annealing Twins During Grain Growth. 22 (1951) J. Appl. Phys. 1350-1356.

[131] G. F. Boilling, W.C.Winegard. Some effects of impurities on grain growth in zone-refined lead . Acta Metall. 6(1958), 288-292

[132] D.P. Field, L.T. Bradford, M.M. Nowel, T.M. Lillo. The role of annealing twins during recrystallization of Cu. Acta Materialia 55 (2007) 4233-4241

[133] H. Hu, C.S. Smith. The formation of low-energy interfaces during grain growth in alpha and alpha-beta brasses. Acta Metall. 4 (1956) 638-646

[134] A. Dehghan-Manshadi, M.R. Barnett, P.D. Hodgson. Recrystallization in AISI 304 austenitic stainless steel during and after hot deformation Materials Science and Engineering A 485 (2008) 664–672

[135] A . Di Schino, J.M.Kenny, Analysis o f the recrystallization and grian growth processes in aisi 316 stainless steel. Journal of Materials Science. 37 (2002) 5291-5298

[136] C.Roucoules. Dynamic and metadynamic recrystallization in HSLA steels. PhD thesis, McGill University, Montreal, Canada,1992

[137] C.A.C. Imber, H.J. McQueen. Static Recrystallization of Tool Steels. Materials Science Forum 539-543 (2007) 4458-4463

[138] C.M.Sellars. Deformation, processing and structure. ASM Materials Science Seminar, 1982, St. Louis, Missouri 245-257

[139] A.R.Morgridge. Metadyanmic recrystallization in C steel. Bull. Mater. Sci. 25(2002) 291-299

[140] A.M.Elwazri, P.Wanjara, S.Yue. Metadynamic recrystallization and static recrystallization of hypereutectoid steel. ISIS International. 43(2003) 1080-1088

[141] S.H. Cho, Y.C. Yoo. Hot rolling simulations of austenitic stainless steel. Journal of Materials Science. 36 (2001) 4267 – 4272

[142] Y.C. Lin, Ming-Song Chen . Study of microstructural evolution during metadynamic recrystallization in a low-alloy steel. Materials Science and Engineering A 501 (2009) 229–234

[143] G.Li, T.M.Maccagno, D.Q.Bai, J.J.Jonas. Effect of initial grain size on the static recrystallization kinetics on Nb Microalloyed steel. ISIS International. 52(2004) 1475-1478

[144] D.R Barraclough, C.M.Sellars. Static recrystallization and restauration after hot deformation of type 304 stanlees steel. Metal Science 13 (1979), pp. 257–267.

[145] C. M. Sellars. The kinetics of softening processes during hot working of austenite. Czech, J. Phys. B 35 (1985) 239-248

[146] S.Cho, K.Kang, J.J.Jonas. The dynamic, static,and metadynamic recrystallization of Nb microalloyed steels. ISIJ International. 41(2001) 63-69

[147] D.J.Towle, T.Gladman Recristallization of austenitic stainless steels after hot rolling Metal Science 13 (1979), pp. 246–256

[148] S.Cho, K.Kang, J.J.Jonas. Mathematical modelling of the recrystallization kinetics of Nb microalloyed steels. ISIJ International. 41(2001) 766-773

[149] A.Kirihata, F.Siciliano,T.M.Maccagno, J.J.Jonas. Mathematical modelling of mean flow stress during the hot strip rolling of multiply-alloyed medium carbon steel. 38(1998), 187-195

[150] S.H. Cho, Y.C. Yoo. Metadynamic recrystallization of austenitic stainless steel. Journal of Materials Science 36 (2001) 4279 – 4284

[151] P.Uranga et al. Transition between static and metadynamic recrystallization kinetics in coarse Nb microalloyed austenite Materials Science and Engineering A345 (2003) 319-327

[152] B.Radhakrishnan, G. B. Sarma, T. Zacharia, Modeling the kinetics and microstructural evolution during static recrystallization-Monte Carlo simulation of recrystallization, Acta Materialia. Vol. 46 (1998) 4415-4433

[153] K.N. Melton. The deformation models needed by the steel industry. Phil. Trans. R. Soc. Lond. A357 (1999), 1531-1547.

[154] R.Sandstrom, R. Lagneborg. A model for static recrystallization after hot deformation. Acta Metall 23(1975) 481-488.

[155] O.Lurdos. Lois de comportement et recristallisation dynamique: approche empirique. PhD thesis, Ecole Nationale Superieure des Mines de Saint-Etienne, France; 2008.

[156] M. El Wahabi, L. Gavard, J.M. Cabrera, J.M. Parado, F. Montheillet, EBSD study of purity effects during hot working in austenitic stainless steels. Materials Science and Engineering A 393 (2005) 83–90

[157] M. El Wahabi, J.M. Cabrera, J.M. Parado, Materials Science and Engineering A 393 (2003) 116–125

[158] L.Gavard. Recristallisation dynamique d'aciers inoxydables austénitiques de haute pureté. PhD thesis, Ecole Nationale Superieure des Mines de Saint-Etienne, France; 2001.

[159] K.C. Mills. Recommended values of thermophysical properties for selected commercial alloys. Woodhead, Cambridge, 2002.

[160] J.Spiznagel, R. Stickler. Correlation between precipitation reactions and bulk density changes in type 18-12 austenitic stainless steels. Met. Trans., 5, 1363–1371, 1974.

[161] ASM, Materials and process engineering bookshelf: selection of stainless steels, ASM, Ohio, 1982

[162] H.J.Frost, M.F. Ashby. Deformation mechanism maps, Pergamon Press, 1982

[163] G.E. Dieter, H.A. Kuhn, S.L.Semiatin. Handbook of workability and process design. ASM international. 2003 pp 89

[164] D.S.Fields. W.A.Backofen. Determination of strain hardening characteristics by torsion testing. Proc.Am.Soc.Test. Mater., 57(1957), pp.1259-1272.

[165] M.C. Mataya and V.E. Sackschewsky, "Effect of Internal Heating during Hot Compression Testing on the Stress-Strain Behavior and Hot Working Characteristics of Alloy 304L," Metall. Trans. A, 25A (1994), pp. 2737–2752.

[166] R.L. Fullman. Measurement of particle sizes in opaque bodies. Trans. AIME. 197(1953), 447-452.

[167] E.E. Underwood, Quantative Stereology, Addison-Wesley Publishing Company,1981

[168] P.L.Orsetti Rossi, C.M.Sellars. Quantitative metallography of recrystallization. Acta Mate.V45(1996) 137-148

[169] F. N. Rhines. Microstructology, Behavior and Microstructure of Materials. Rieder-Verlag, Stuttgart (1986).

[170] J. Byskzycki, W. Przetakiewicz, K. J. Kurzydlowski. Study of annealing twins and island grains in F.C.C. alloy. Acta Metall. Mater. 41(1993) 2639-2649.

[171] A.W. Thompson,W.A. Backofen. The effect of grain size on fatigue. Acta Met., 19(1971) 597-606.

[172] C.M.Young, O.D. Sherby. Subgrain formation and subgrain strengthening in iron-based materials. J. lron Steel lnst. 2l I (1973), 640-647.

[173] W. Roberts, H.Benden, B.Ahlbom. Dynamic recrystallization kinetics. Metal science. 13(1979) 195-203

[174] R.L.Fullman. Measurement of particle sizes in opaque bodies. Trans.AIME. 197(1953) 447; 1267

[175] T.Wejrzanowski, K. Batorski, K.J. Kurzydłowski. Grain growth modelling: 3D and 2D correlation. Materials Characterization. 56(2006) 336-339

[176] A.Delesse. Pour determiner la composition des roches. Ann. Des Mines. 13(1848), fourth series, 379-388

[177] S.F. Nielsen , S. Schmidt. Growth kinetics of individual grains during recrystallization with an intermediate cooling cycle. Scripta Materialia 48 (2003) 513–518

[178] S.I. Wright, M. Nowell, A Review of In Situ EBSD Studies, in Electron Backscatter Diffraction in Materials Science, Eds. A.J.Schwartz et al., Springer, 2009,329-337,

[179] B.Gaudout. Mod élisation des évolutions microstructurales et étude de la lubrification par film solide lors du filage à chaud d'alliages de zirconium. PhD thesis, Ecole Nationale Superieure des Mines de Paris, France; 2009.

[180] K. Deb, A. Pratap, S. Agarwal, T. Meyarivan. A fast and elitist multi-objective genetic algorithm: NSGA-II. IEEE Trans. Evol. Comput. 6 (2002) 182–197.

[181] R.D. Doherty , D.A. Hughes , F.J. Humphreys , J.J. Jonas , D. Juul Jensen , M.E. Kassner , W.E. King , T.R. McNelley, H.J. McQueen , A.D. Rollett.Current issues in recrystallization: a review. Materials Science and Engineering A238 (1997) 219–274

[182] J.C.M. Li, in: J.B. Newkirk, J.H. Wernick (Eds.), Direct Observation of Imperfections in Crystals, Interscience, New York, 1962, p. 234.

[183] W.B.Morrison. Recrystallization of a low-carbon steel in austenite range.J. Iron Steel Inst., 210(1972),618.

[184] S.-H.Cho, Y.-C.Yoo,Static recrystallization kinetics of 304 stainless steels. Journal of Materials science. 36 (2001) 4273 - 4278

[185] M.H. Alvi, S.Cheong, H.Weiland, A.D. Rollett. Recrystallization and Texture Development in Hot Rolled 1050 Aluminum. Mater.Sci.Forum, Vol.467-470(2004), Part 1, 357-362,

[186] R.Ding, Z.X.Guo. Coupled quantitative simulation of microstructural evolution and plastic flow during dynamic recrystallization. Acta mater. 49 (2001) 3163–3175.

[187] J. J. Jonas, X. Quelennec, L.Jiang, É.Martin. The Avrami kinetics of dynamic recrystallization . Acta Materialia, 57(2009) 2748-2756

[188] R.E.Smallman,A.H.W. Ngan. Physical metallurgy and advanced material. Seventh ed. Oxford: Elsevier, 2007.

[189] W.J.Poole, M.F.Ashby, N.A.Fleck. Micro-hardness of annealed and work-hardened copper polycrystals. Scripta Materialia. 34 (1996) 559-564

[190] S.C. Wang, Z. Zhu, M.J. Starink. Estimation of dislocation densities in cold rolled Al-Mg-Cu-Mn alloys by combination of yield strength data, EBSD and strength models. Journal of Microscopy, 217 (2005) 174-178.

[191] S. J.Basinski, Z. S. Basinski, 1979, Dislocation in Solids, Vol. 4, edited by F. R. N. Nabarro (Amsterdam: North-Holland), 261.

[192] E.V. Kozlov, N.A. Koneva. Internal fields and other contributions to flow stress. Materials Science and Engineering. A234-236 (1997) 982-985

[193] L. Bäcke. Modeling the Microstructural Evolution during Hot Deformation of Microalloyed Steels. Ph.D thesis, Royal Institute of Technology (KTH), Sweden, 2009

[194] P.J. Wray. Onset of recrystallization during the tensile deformation of austenitic iron at intermediate strain rates. Metall. Trans. A, 6(1975) 1197-1203.

[195] T. Maki, K. Akasaka, K. Okuna, k Tamura. Dynamic recrystallization of austenite in 18-8 stainless steel and 18-Ni maraging-steel. Trans. Iron Steel Inst.Jpn. 22 (1982) 253-61.

[196] C. S. Pande, M. A. Imam. Grain growth and twin formation in boron-doped nickel polycrystals. Materials Science and Engineering: A, 512(2009), 82-86

[197] N.Soua ï, N.Bozzolo, L.Naz é, Y.Chastel, R.E.Log éAbout the possibility of grain boundary engineering via hot-working in a nickel-base superalloy. Scripta Materialia 62 (2010) 851-854

[198] K.T.Aust, J.W. Rutter. Grain boundary migration in high-purity lead and dilute lead-tin alloys. Transactions of the Metallurgical Society of AIME. 215 (1959) 119-127.

[199] K.T.Aust, J.W. Rutter. Kinetics of grain boundary migration in high-purity lead containing very small additions of silver and of gold. Transactions of the Metallurgical Society of AIME. 218(1960) 682-688.

[200] J.W. Christian. The theory of transformations in metals and alloys. Pergamon, 2002.

[201] A.R.Jones. Annealing twinning and nucleation of recrystallization at grain boundaries. Journal of meterials science. 16(1981) 1374-1380

[202] D.P. Field, L.T. Bradford, M.M. Nowell, T.M. Lillo. The role of annealing twins during recrystallization of Cu.Acta Materialia 55 (2007) 4233 – 4241

[203] G. Gottstein. Physical Foundation of Materials Science. Springer, 2005

[204] R.A.Vandermeer, D. Juul Jensen. The Migration of High Angle Grain Boundaries during Recrystallization. Interface Science. 6(1998) 95-104.

[205] D. Juul Jensen. Growth rates and misorientation relationships between growing nuclei/grains and the surrounding deformed matrix during recrystallization. Acta Metall. et Mater. 43(1995) 4117-4129

[206] Y.B. Zhang , A. Godfrey, Q. Liu, W. Liu, D. Juul Jensen. Analysis of the growth of individual grains during recrystallization in pure nickel. Acta Materialia. 57 (2009) 2631-2639

Appendix A Evaluation of the critical dislocation density in DRX conditions

The condition for growth of a dynamically recrystallized grain has been studied by [56] and is based on Figure.A-1.

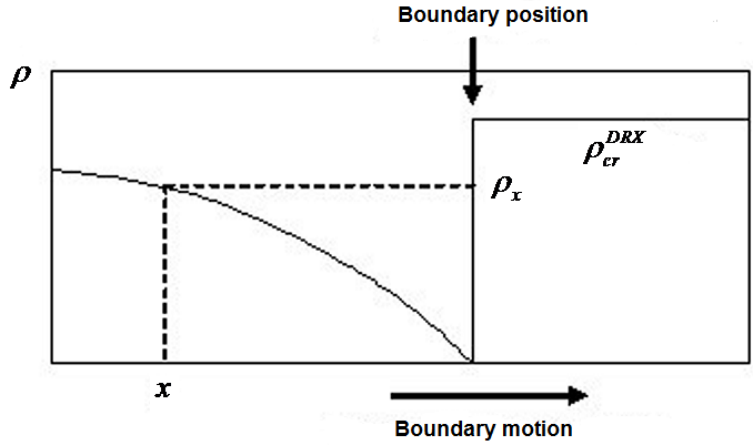

Figure A-1 Dislocation density evolution near a dynamic recrystallization front.

As the boundary moves from left to right into NR material with dislocation density ρ_{cr}^{DRX}, the dislocation density is reduced in its wake to around zero. The continued deformation rises however the dislocation density in the new grain, building up behind the moving boundary and reaching ρ_x at a distance x behind the boundary.

The approximate analysis given by [56] and described in [1] ignored dynamic recovery. It was therefore adapted below. The dislocation density variation within the grain is expressed from (Equation 4-1) as

$$\frac{d\rho}{dt} = (K_1 - K_2\rho)\dot{\varepsilon} \qquad \text{(Equation A-1)}$$

From (Equation 4-4) and (Equation 4-5), the grain boundary velocity is given by

$$\frac{dx}{dt} = m\rho_{cr}^{DRX}\tau \qquad \text{(Equation A-2)}$$

Where the capillarity term has been neglected, compared to the dislocation density term. Combining (Equation A-1) and (Equation A-2) leads to

$$\frac{d\rho}{dx} = \frac{K_1 - K_2\rho}{m\rho_{cr}^{DRX}\tau}\dot{\varepsilon} \qquad \text{(Equation A-3)}$$

It is assumed that when the grain size reaches a critical value (x_{cr}), the dislocation density also reaches the critical value (ρ_{cr}^{DRX}). Integrating (Equation A-3) and replacing x_{cr} by (Equation 4-12) yields,

$$\ln\left(1 - \frac{K_2}{K_1}\rho_{cr}^{DRX}\right) = -K_2\frac{2\gamma_b\dot{\varepsilon}}{m(\rho_{cr}^{DRX})^2\tau^2} \qquad \text{(Equation A-3)}$$

which can be write in the following form,

$$\rho_{cr}^{DRX} = \left[-2\gamma_b \dot{\varepsilon} \frac{K_2}{K_3 \tau} \Big/ \ln\left(1 - \frac{K_2}{K_1}\rho_{cr}^{DRX}\right) \right]^{1/2} \qquad \text{(Equation A-4)}$$

By iterative calculation of (Equation A-4), the critical dislocation density for dynamic recrystallization ρ_{cr}^{DRX} can be found.

Vers la modélisation des phénomènes de recristallisation en conditions multi-passes - Application à l'acier 304L

RESUME : La recristallisation, qui peut se produire de façon dynamique ou statique, est un important phénomène qui transforme la microstructure des matériaux métalliques déformés modifiant ainsi ses propriétés mécaniques. Malgré l'existence de travaux approfondis sur la modélisation numérique du phénomène de recristallisation, la littérature scientifique manque de modèles précis capables de prédire l'évolution microstructurale dans des conditions de mise en forme multi passes. Bien que des efforts aient été réalisés dans cette direction, la plupart des modèles existants dans la littérature présentent soit un manque de validation expérimentale, soit ne fournissent que des accords qualitatifs entre les résultats numériques et expérimentaux dans des conditions de déformations connues et sélectionnées. De plus, les relations entre la recristallisation statique (SRX), la recristallisation dynamique (DRX), la recristallisation post-dynamique (PDRX) et la croissance de grains (GG) sont généralement trop simplistes. Par ailleurs, la plupart de ces modèles ne sont pas conçus pour la réalisation de simulations avec des conditions thermiques et/ou mécaniques variables, ce qui limite par conséquent leur utilisation pour des applications industrielles.

Pour cette étude, un modèle à champ moyen à 2 sites a été développé afin de décrire l'évolution microstructurale de l'acier 304L. L'originalité de ce modèle réside dans : (a) l'interaction de chaque grain avec deux milieux homogènes équivalents, avec respectivement une densité de dislocation élevée et faible; (b) le poids relatif de chaque milieu est lié à leur fraction volumique ; (c) la germination et la disparition des grains rendent la microstructure variable au cours du temps ; (d) les paramètres dépendent de la température et de la vitesse de déformation mais pas de la taille des grains dans les conditions DRX, et uniquement de la témpérature dans les conditions statiques (SRX/PDRX/GG); (e) des accords quantitatifs avec les résultats expérimentaux sont obtenus en fonction de (i) la cinétique de recristallisation, (ii) la courbe contrainte-déformation, (iii) taille de grain après recristallisation, et (f) le modèle a été développé pour être utilisé en conditions multi- passes, avec des valeurs variables de température et de vitesse de déformation.

Afin de vérifier et valider le modèle, plusieurs essais de traction ont été réalisés sous de nombreuses conditions différentes de température et de vitesse de déformation, afin de caractériser le mode DRX. Pour la validation des modèles de SRX et PDRX, des traitements de recuit ont été réalisés après la déformation plastique. Les paramètres du modèle ont premièrement été estimés à partir des donnés expérimentales ou présentes dans la littérature, et ont ensuite été établis par analyse inverse. Il a été constaté que tous les paramètres du modèle évoluent de manières physiquement cohérentes en fonction de la température et de la vitesse de déformation.

Les résultats obtenus à partir de la simulation de la DRX, SRX/PDRX/GG ont été analysés, en prenant en compte les effets de la température de déformation, la vitesse de déformation, la déformation appliquée ainsi que la taille de grain initiale. Un bon accord entre les résultats numériques et expérimentaux a été observé pour les différents types de recristallisation, ce qui ouvre la voie à la modélisation de la mise en forme en conditions multi passes pour des applications industrielles.

Finalement, des traitements thermiques avec analyse in situ ont été réalisés afin d'obtenir une meilleure compréhension des mécanismes de SRX/PDRX/GG. Le rôle du maclage pendant le traitement de recuit a été discuté : il semble favoriser à la fois la germination et la migration des joints de grains.

Mots clés : Modélisation numérique, recristallisation dynamique, recristallisation post-dynamique, recristallisation statique, croissance des grains, conditions multi passes, acier austénitique inoxydable 304L, évolution microstructurale, déformation à chaud, maclage thermique.

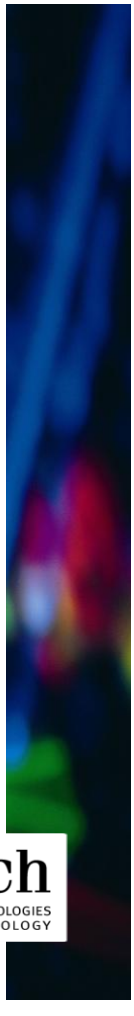

MINES ParisTech

ParisTech
INSTITUT DES SCIENCES ET TECHNOLOGIES
PARIS INSTITUTE OF TECHNOLOGY

Towards the modeling of recrystallization phenomena in multi-pass conditions - Application to 304L steel

ABSTRACT : Recrystallization, which can occur dynamically or statically, is an important phenomenon causing microstructure changes in deformed metals and therefore affecting the properties of the material. Even though extensive investigations have been carried out on the numerical modeling of recrystallization, the literature lacks accurate recrystallization models which are able to predict microstructure evolution under multi-pass conditions. Although some efforts have been reported in this direction, most of them either lack experimental validation or only provide qualitative agreement in selected deformation conditions. The connections between static recrystallization (SRX), dynamic recrystallization (DRX), post-dynamic recrystallization (PDRX) and grain growth (GG) are usually oversimplified. Furthermore, most of them are not designed for variable thermal and/or mechanical conditions and are therefore difficult to use for industrial applications.

In this work a physically-based two-site mean field model has been developed to describe the microstructural evolution of 304L austenitic stainless steels. The originality of the model lies in: (a) the interaction of each representative grain with two homogeneous equivalent media, with high and low dislocation density, respectively; (b) the relative weight of the two media is functionally related to their volume fractions; (c) nucleation and disappearance of grains make the data structure variable in time; (d) the model parameters vary with temperature and strain rate but do not depend on grain size in DRX conditions, and become only temperature dependent in static conditions (SRX/PDRX/GG); (e) quantitative agreement with experimental results is obtained in terms of (i) recrystallization kinetics, (ii) stress-strain curves, (iii) recrystallized grain size, and (f) it is designed to be used in multi-pass conditions, with variable temperature and strain rate.

To verify and validate the model, torsion tests were conducted over a wide range of conditions for investigation of DRX. Subsequent annealing after termination of deformation, which led to SRX or PDRX depending on the applied strain, was also carried out. The model parameters were first estimated from experimental and literature data, and were further tuned by inverse analysis. It is found that all identified model parameters evolve with temperature and strain rate in a physically consistent way.

The application of this proposed model to DRX, SRX/PDRX/GG is then analyzed, taking into account the effects of deformation temperature, strain rate, applied strain, as well as initial grain size. Good quantitative agreements with measured data are obtained in the different recrystallization regimes, which opens the possibility of modeling multi-pass operations compatible with industrial applications.

A few in situ heating experiments were carried out to provide a better understanding of the SRX/PDRX/GG mechanisms. The role of annealing twins is tentatively discussed: it seems to promote both nucleation and grain boundary migration.

Keywords : numerical modeling, dynamic recrystallization, post-dynamic recrystallization, static recrystallization, grain growth, multi-pass conditions, 304L austenitic stainless steel, microstructure evolution, hot deformation, annealing twins

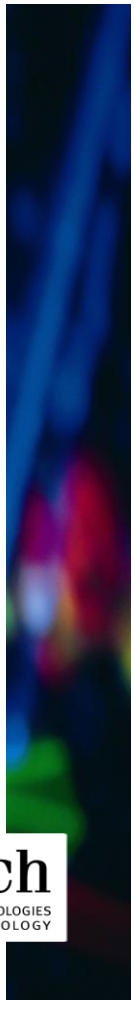

MINES ParisTech

ParisTech
INSTITUT DES SCIENCES ET TECHNOLOGIES
PARIS INSTITUTE OF TECHNOLOGY